Diffusion tensor imaging and resting state functional connectivity as advanced imaging biomarkers of outcome in infants with hypoxic-ischaemic encephalopathy treated with hypothermia

Dr Nora Tusor

A thesis submitted in partial fulfiment of the requirements for the degree of

Doctor of Philosophy

Imperial College London 2014

Centre for the Developing Brain

Abstract

Therapeutic hypothermia confers significant benefit in term neonates with hypoxic-ischaemic encephalopathy (HIE). However, despite the treatment nearly half of the infants develop an unfavourable outcome. Intensive bench-based and early phase clinical research is focused on identifying treatments that augment hypothermic neuroprotection. Qualified biomarkers are required to test these promising therapies efficiently.

This thesis aims to assess advanced magnetic resonance imaging (MRI) techniques, including diffusion tensor imaging (DTI) and resting state functional MRI (fMRI) as imaging biomarkers of outcome in infants with HIE who underwent hypothermic neuroprotection.

FA values in the white matter (WM), obtained in the neonatal period and assessed by tract-based spatial statistics (TBSS), correlated with subsequent developmental quotient (DQ). However, TBSS is not suitable to study grey matter (GM), which is the primary site of injury following an acute hypoxic-ischaemic event. Therefore, a neonatal atlas-based automated tissue labelling approach was applied to segment central and cortical grey and whole brain WM. Mean diffusivity (MD) in GM structures, obtained in the neonatal period correlated with subsequent DQ. Although the central GM is the primary site of injury on conventional MRI following HIE; FA within WM tissue labels also correlated to neurodevelopmental performance scores. As DTI does not provide information on functional consequences of brain injury functional sequel of HIE was studied with resting state fMRI. Diminished functional connectivity was demonstrated in infants who suffered HIE, which associated with an unfavourable outcome.

The results of this thesis suggest that MD in GM tissue labels and FA either determined within WM tissue labels or analysed with TBSS correlate to subsequent neurodevelopmental performance scores in infants who suffered HIE treated with hypothermia and may be applied as imaging biomarkers of outcome in this population. Although functional connectivity was diminished in infants with HIE, resting state fMRI needs further study to assess its utility as an imaging biomarker following a hypoxic-ischaemic brain injury.

Declaration of Originality

This thesis and the work presented herein are my own and were conducted at Imperial College London between September 2009 and May 2014. All sources are appropriately referenced.

This work has not been submitted to obtain any other degree at this University or any other institution.

Dr Nora Tusor

Copyright Declaration

Acknowledgements

Statement of publications

Journal papers

Groves AM, Durighel G, Finnemore A, **Tusor N**, Merchant N, Razavi R, Hajnal JV, Edwards AD. Disruption of intracardiac flow patterns in the newborn infant. Pediatr Res. 2012;71(4-1):380-385.

Tusor N, Wusthoff C, Smee N, Merchant N, Arichi T, Allsop JM, Cowan FM, Azzopardi D, David Edwards A, Counsell SJ. Prediction of neurodevelopmental outcome after hypoxic-ischemic encephalopathy treated with hypothermia by diffusion tensor imaging analysed using tract-based spatial statistics. Pediatr Res. 2012;72(1):63-9.

Arichi T, Fagiolo G, Varela M, Melendez-Calderon M, Allievi A, Merchant N, **Tusor N**, Counsell SJ, Burdet E, Beckmann CF, Edwards AD. Development of BOLD signal Hemodynamic Responses in the Human Brain. Neuroimage. 2012;1;63(2):663-73.

Finnemore A, Toulmin H, Merchant N, Arichi T, **Tusor N**, Cox D, Ederies A, Nongena P, Ko C, Dias R, Edwards AD, Groves AM. Chloral hydrate sedation for magnetic resonance imaging in newborn infants. Paediatr Anaesth. 2014;24(2):190-5.

Tusor N, Arichi T, Counsell SJ, Edwards AD. Brain development in preterm infants assessed using advanced MRI techniques. Clin Perinatol. 2014;41(1):25-45.

Ball G, Aljabar P, Zebari S, **Tusor N**, Arichi T, Merchant N, Robinson EC, Ogundipe E, Rueckert D, Edwards AD, Counsell SJ. Rich-club organization of the newborn human brain. Proc Natl Acad Sci U S A. 2014 May 5. [Epub ahead of print]

Book chapter

Tusor N, Counsell SJ, Rutherford MA, Diffusion MRI techniques to study the neonatal brain. New diagnostic and therapeutic tools in child neurology. Mariani Foundation Paediatric Neurology: 24. John Libbey Eurotext. 2011;33-54.

Conference abstracts

Durighel G, **Tusor N,** Razavi R, Hajnal J, Edwards AD, Groves A. Four-dimensional phase contrast imaging demonstrates variability of intra-cardiac flow patterns in newborn infants. Euro-CRM 2010

Arichi T, Fagiolo G, Melendez A, Merchant N, **Tusor N**, Counsell SJ, Burdet E, Beckmann C, Edwards AD. Characterisation of the BOLD signal Haemodynamic Response Function (HRF) in the neonatal somatosensory cortex. International Society for Magnetic Resonance in Medicine 2011

Arichi T, Counsell SJ, Merchant N, **Tusor N,** Cowan F, Rutherford M, Beckmann CF, Burdet E, Edwards AD. Characterisation of early somatosensory functional and structural cerebral organisation following neonatal unilateral haemorrhagic parenchymal infarction (HPI) with functional MRI and probabilistic tractography. British Paediatric Neurology Association annual meeting 2011

Finnemore A, Toulmin H, Arichi T, Cox D, Dias R, Ederies A, Ko C, Merchant N, Nongena P, **Tusor N**, Groves A, Edwards AD. Safety profile of chloral hydrate sedation for MRI in term and preterm neonates. European Society for Paediatric Research 2011

McGuinness AK, Malamateniou C, Allsop JM, Counsell SJ, Nunes RG, **Tusor N**, Wu ZQ, Ederies A, Hajnal JV, Rutherford MA. Evaluation of neonatal pathology using T1 weighted techniques, SNAPIR and gradient echo. International Society for Magnetic Resonance in Medicine 2011

Tusor N, Smee N, Arichi T, Counsell SJ, Cowan F, Azzopardi D, Edwards AD. Diffusion Tensor Imaging analyzed by Tract-Based Spatial Statistics as a biomarker of adverse outcome after hypoxic-ischaemic encephalopathy treated with hypothermia. Neonatal Societies' Spring Meeting 2011

Tusor N, Smee N, Arichi T, Counsell SJ, Azzopardi D, Edwards AD. Neurodevelopmental outcome and white matter microstructure in infants treated with

hypothermia for perinatal hypoxic-ischemic encephalopathy. Pediatric Academic Societies 2011

Arichi T, Counsell SJ, Chew A, Allievi A, Melendez A, Merchant N, **Tusor N**, Burdet E, Beckmann CF, Cowan FM, Edwards AD. Characterization of structural and functional connectivity in the developing somatosensory system following focal neonatal brain injury. Pediatric Academic Societies 2012

Ederies A, Malamateniou C, Kyriakopoulou V, Allsop JM, Counsell SJ, **Tusor N**, Arichi T, Merchant N, Hayat T, Hajnal JV, Edwards AD, Rutherford M. Thalamic volumetric growth in utero and the effect of preterm birth. International Society for Magnetic Resonance in Medicine 2012

Huening B, Pazderova L, Ball G, **Tusor N**, Merchant N, Arichi T, Allsop J, Felderhoff-Mueser U, Rutherford M, Edwards AD, Counsell SJ. Serial diffusion tensor imaging demonstrates that the degree of prematurity at birth is associated with white matter microstructure at term equivalent age but not to white matter microstructure in the early neonatal period. Pediatric Academic Societies 2012

Tusor N, Arichi T, Fagiolo G, Doria V, Allsop J, Wusthoff C, Azzopardi D, Beckmann C, Counsell SJ, Edwards AD. Altered Resting State Functional Networks In Infants With Hypoxic-Ischemic Encephalopathy Assessed By Model-Driven Functional Connectivity Analysis. Pediatric Academic Societies 2012

Arichi T, Allievi A, Melendez-Calderon A, **Tusor N**, Pazderova L, Toulmin H, Counsell, Burdet E, Edwards AD. Development of somatosensory cortical responses in the preterm period characterized with fMRI and a novel robotic device. International Society for Magnetic Resonance in Medicine 2013

Counsell SJ, Tournier D, Ball G, **Tusor N,** Wurie J, Nongena P, Ederies A, Allsop J, Fox M, Ogundipe E, Edwards AD, Hajnal J. Constrained Spherical Deconvolution Based Tractography in the Neonatal Brain Performed Using High b Value High Angular Resolution Diffusion Imaging. International Society for Magnetic Resonance in Medicine 2013

Table of contents

4. Mean diffusivity in cortical and deep grey matter correlates to neurodevelopmental performance in infants with hypoxic-ischaemic encephalopathy treated with hypothermia 178

List of figures

List of tables

List of equations

List of abbreviations

AA – ascorbic acid

ADC – apparent diffusion coefficient

aEEG – amplitude integrated electroencephalogram

ALIC – anterior limb of the internal capsule

AMPA – amino-3-hydroxy-5-methyl-4 isoxazole propionate

ATP – adenosine triphosphate

ATPase – adenosine triphosphatase

AUC – area under the curve

b – degree of diffusion weighting

B_0 – external magnetic field

BET – Brain Extraction Tool

BGT – basal ganglia and thalami

BOLD – blood oxygen level dependent

C – particle concentration

CBF - cerebral blood flow

CBV – cerebral blood volume

CI – confidence intervals

$CMRO_2$ – cerebral metabolic rate of oxygen

CPP – cerebral perfusion pressure

CSD – constrained spherical deconvolution

CSF – cerebrospinal fluid

CSO – centrum semiovale

CST – corticospinal tract

CVR – cerebral vascular resistance

CytOx – cytochrome oxidase

D – diffusion coefficient

DHA – dehydroascorbic acid

DMN – default mode network

DNA – deoxyribonucleic acid

DOF – degrees of freedom

DQ – developmental quotient

DTI – diffusion tensor imaging

DWI – diffusion weighted imaging

EAA – excitatory amino acid

EEG – electroencephalogram

EPI – echo planar imaging

EPP – exchangeable phosphate pool

FAST – FMRIB's Automated Segmentation Tool

FDT – FMRIB's Diffusion Toolkit

FFD – free form deformation

FLIRT – FMRIB's Linear Image Registration Tool

fMRI – functional magnetic resonance imaging

FMRIB – Functional Magnetic Resonance Imaging of the Brain

FNIRT – FMRIB's Nonlinear Image Registration Tool

FSL – FMRB's Software Library

FWHM – Full Width at Half Maximum

G – amplitude of diffusion gradient

GABA – gamma-aminobutyric acid

GLM – general linear model

GMDS – Griffiths Mental Development Scales (Revised)

GMFCS – Gross Motor Function Classification System

HIE – hypoxic-ischaemic encephalopathy

IC – independent component

ICA – independent component analysis

IL – interleukin

ILF – inferior longitudinal fasciculus

IRTK – Image Registration Toolkit

J – net particle flux

kB – Boltzmann constant

lCMRglc – local cerebral metabolic rate of glucose

MCFLIRT – Motion Correction using FMRIB's Linear Image Registration Tool

MD – mean diffusivity

MELODIC – Multivariate Exploratory Linear Optimised Decomposition into
Independent Components

MI – mutual information

mm – millimetre

mmHg – millimetre of mercury

MPRAGE – magnetisation-prepared rapid acquisition with gradient echo

MR – magnetic resonance

MRI – magnetic resonance imaging

MRS – magnetic resonance spectroscopy

ms – millisecond

NAC – N-acetyl cystein

NE – neonatal encephalopathy

NIRS – near infrared spectroscopy

NMDA – N-methyl-D-aspartate

NMR – nuclear magnetic resonance

NMV – net magnetisation vector

nNOS – neural nitric oxide synthase

NNT – number needed to treat

NO – nitric oxide

NODDI – neurite orientation dispersion and density imaging

NOS – nitric oxide synthase

NPV – negative predictive value

NTP – nucleotide triphosphate

PGSE – pulsed field gradient diffusion weighted spin echo

PLIC – posterior limb of the internal capsule

PMA – postmenstrual age

ppm – parts per million

PPV – positive predictive value

r – radius

RA – relative anisotropy

RF – radio frequency

ROC – receiver operating characteristic

ROI – region of interest

RSN – resting state network

S – signal measured with diffusion weighting

S_0 – signal measured without diffusion weighting

SBCA – seed-based correlation analysis

SCPE – Surveillance of Cerebral Palsy in Europe

SD – standard deviation

SRSS – square root of sum of squares

t – time

T – temperature

TBSS – tract-based spatial statistics

TE – echo time

TR – repetition time

WM – white matter

ΔC – concentration gradient

Chapter 1

Introduction

1.1 Motivation

Hypoxic-ischaemic encephalopathy (HIE) is a significant cause of brain injury in term infants. The outcome may be devastating and permanent, making this condition a major burden for the infant, family and society.

Although brain injury occurs during a sufficiently severe period of hypoxia and ischaemia, neuronal loss continues to evolve for hours after resuscitation offering the potential for providing treatment to reduce brain injury (Gunn and Bennet 2008; Bennet et al. 2009). Trials of hypothermia have proved the concept that neuroprotection following delivery is possible (Jacobs et al. 2007; Edwards et al. 2010; Jacobs et al. 2013). Therapeutic hypothermia reduces the rate of unfavourable outcome in infants who suffered HIE. However, hypothermic neuroprotection is partial as despite the treatment nearly half of the subjects have an unfavourable outcome (Edwards et al. 2010). Approximately 20% of the affected infants die in the neonatal period. Survivors are at a higher risk of developing epilepsy, feeding, cognitive, behavioural, fine and gross motor problems. Even subjects, who develop appropriately initially, may have cognitive difficulties at school age (Gonzalez and Miller 2006).

Intensive bench-based and early phase clinical research is focused on developing novel therapies to provide additional neuroprotection in combination with hypothermia. Biomarkers are needed to accelerate translation of potential treatments

and assess their efficacy in rapid early phase clinical trials (Azzopardi and Edwards 2010; Bennet et al. 2010). Although candidate therapies must be shown to improve long-term outcome in adequately sized randomised clinical studies, surrogate endpoints are important to select interventions that are likely to succeed and study only those further in larger clinical trials.

Neuroimaging studies are increasingly employed in the development of biomarkers (Ment et al. 2009; Azzopardi and Edwards 2010; Thayyil et al. 2010). Conventional magnetic resonance imaging (MRI) and magnetic resonance spectroscopy (MRS) are suitable surrogate endpoints in studies of novel neuroprotective therapies for HIE. However, these techniques are relatively inefficient for early evaluation of treatment effect as a substantial number of subjects is needed to detect significant differences between treatment groups. Statistically robust voxelwise comparison of imaging data in small groups of infants would enable more efficient preliminary assessment of putative neuroprotective therapies.

Tract-based spatial statistics (TBSS) is an observer-independent research tool to evaluate whole-brain white matter (WM) across multi-subject diffusion tensor imaging (DTI) data (Smith et al. 2006). The TBSS pipeline has been optimised for the neonatal brain (Ball et al. 2010). DTI data analysed using this approach proved to be a biomarker of brain injury following HIE and a biomarker of therapy after hypothermia (Porter et al. 2010). It is possible therefore that TBSS could be used to accelerate translation of potential additional neuroprotective therapies. Further studies, correlating TBSS findings in the early neonatal period with subsequent

neurodevelopmental performance are required to qualify this tool as an imaging biomarker following HIE.

However, a disadvantage of TBSS is that it assesses diffusion measures within the centre of the WM tracts, therefore it is not suitable for studying grey matter (Smith et al. 2006), which is the primary site of injury following a hypoxic-ischaemic insult (Black et al. 1996). Determining diffusion parameters within grey matter is a feasible approach to study structural changes in the cortex and basal ganglia and thalami (BGT). Although manual placement of regions of interest (ROI) is time consuming and prone to observer bias, many of these limitations are circumvented when ROIs are defined by mapping tissue label information from a neonatal atlas to the individual subject's brain (Xue et al. 2007; Kuklisova-Murgasova et al. 2011; Serag et al. 2012; Makropoulos et al. 2012).

Diffusion MRI does not provide information on functional consequences of a hypoxic-ischaemic insult. In absence of a task or stimulation coherent spontaneous fluctuations of the blood oxygen dependent (BOLD) signal between distinct brain regions form resting state networks (RSN) (Beckmann et al. 2005; Fox et al. 2005; Fransson et al. 2005; Damoiseaux et al. 2008). Functional connectivity refers to the strength of coherence of the BOLD signal between distinct brain regions (Greicius et al. 2003). Estimating functional connectivity within RSNs is a suitable approach to assess brain function and dysfunction. Resting state fMRI has been used to study functional changes related to neuropathology in adult and paediatric populations (Fox et al. 2010; Smyser et al. 2013). Although structural and metabolic changes associated with a hypoxic-ischaemic brain injury have been studied extensively, alterations in

functional connectivity associated with a hypoxic-ischaemic event have not been explored.

1.2 Aims and hypothesises

The aim of this thesis was to assess advanced magnetic resonance imaging techniques as imaging biomarkers of outcome following hypoxic-ischaemic encephalopathy in infants who underwent therapeutic hypothermia.

The following hypotheses were tested:

Structural and functional changes associated with a hypoxic-ischaemic event, as assessed with diffusion tensor imaging and resting state functional magnetic resonance imaging, correlate to early neurodevelopmental outcome in infants with hypoxic-ischaemic encephalopathy who received therapeutic hypothermia.

Functional connectivity as assessed by resting state functional magnetic resonance imaging is altered in infants with hypoxic-ischaemic encephalopathy who received therapeutic hypothermia.

This is conducted with the following aims:

Apply tract-based spatial statistics on multi-subject diffusion tensor imaging data to assess the correlation between fractional anisotropy in the white matter obtained in the neonatal period and early neurodevelopmental performance scores in infants with hypoxic-ischaemic encephalopathy treated with hypothermia.

Apply neonatal atlas-based automated tissue segmentation to define grey matter tissue labels within which diffusion parameters are determined and correlate these measures to early neurodevelopmental performance scores in infants with hypoxic-ischaemic encephalopathy treated with hypothermia.

Apply hypothesis-free and hypothesis-driven methods to explore the effect a perinatal hypoxic-ischaemic insult on resting state connectivity compared to healthy controls.

Apply voxelwise and region of interest approaches to investigate the correlation between changes in functional connectivity and early neurodevelopmental performance in infants who suffered hypoxic-ischaemic encephalopathy treated with hypothermia.

Chapter 2

Background

2.1 Magnetic Resonance Imaging

MRI is a non-invasive, non-ionising technique, primarily used in medical settings to visualise internal structures of the body using nuclear magnetic resonance (NMR) (Bloch 1946; Purcell et al. 1946). The image is generated by placing a subject into a powerful magnet, applying energy to the system and observing how the energy is released. MRI provides good contrast between different soft tissue types of the body. Two and 3 dimensional anatomical as well as functional images can be obtained. These advantages have made MRI an important clinical and research tool. This chapter provides a brief summary of MRI and the NMR phenomenon. The references used for this chapter are McRobbie et al. 2007 and Westbrook et al. 2008.

2.1.1 Nuclear magnetic resonance

The NMR phenomenon relies on the interaction of the nuclei of NMR active atomic isotopes with a static magnetic field. NMR active atomic isotopes have nuclei with a nonzero spin number, and are characterised by their tendency to align their axis of rotation to an applied external magnetic field. The magnetic field makes the possible spin states of the nucleus differ in energy, and using NMR techniques the spins can be made to create observable transitions between the spin states.

Hydrogen nucleus is the NMR active nucleus used in clinical MRI as it is abundant in the human body. It contains a single proton, which gives it a relatively large magnetic

moment. In absence of a magnetic field the magnetic moments of the hydrogen nuclei are randomly oriented. When placed in a strong static external magnetic field, the B_0, the magnetic moments of the hydrogen nuclei align longitudinally with this magnetic field. Hydrogen nuclei exist in two energy states low and high. Low energy hydrogen nuclei do not possess enough energy to oppose the magnetic field hence align parallel with it (spin up); whereas a smaller number of the nuclei with high energy state do possess enough energy to oppose the magnetic field and are able to align anti-parallel to it (spin down). The vector sum of all the magnetic moments in a sample is its net magnetisation vector (NMV) (Figure 2.1.1). The NMV is created by two components 90° to each other, magnetisation in the longitudinal and in the transverse planes.
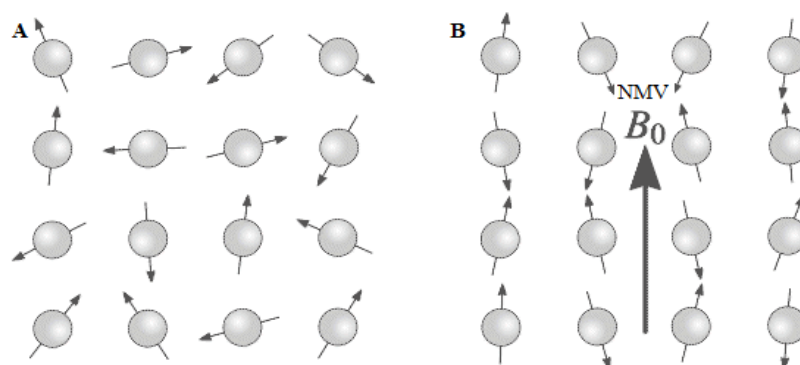
Figure 2.1.1: The effect of an external magnetic field on hydrogen nuclei. A*: In absence of an external magnetic field (B_0=0) the nuclear magnetic moments are arranged randomly. B: In presence of an external magnetic field (B_0) the nuclear moments align either parallel or antiparallel to it; and net magnetisation vector (NMV) develops parallel to the B_0.*

2.1.2 The magnetic resonance signal

When a patient is placed in the bore of a magnet, the hydrogen nuclei within the patient align parallel and antiparallel to the B_0. A small excess of hydrogen nuclei line up parallel to the B_0 and constitute to the magnetic moment of the hydrogen. The difference between the two populations of nuclei increases as B_0 increases resulting in improved signal.

The influence of B_0 results in each hydrogen nucleus that makes up the NMV spinning on its axis around the B_0. This secondary spin is called precession and causes the magnetic moments to follow a circular path, called precessional path around the B_0. The speed at which the NMV spins around B_0 is called the precessional frequency (ω). Its value is determined by the Larmor equation [2.1.1]:

$$\omega = \gamma\, B_0 \qquad\qquad [2.1.1]$$

where γ is the gyro-magnetic ratio, a constant expressing the relationship between the angular momentum and the magnetic moment of each NMR active nucleus. It is expressed as precessional frequency of a given NMR active nucleus at 1 Tesla. As γ is a constant of proportionality, B_0 is proportional to ω.

Resonance is a phenomenon that occurs when an object is exposed to an oscillating perturbation that has a frequency close to its own natural frequency of oscillation. In such case the nucleus gains energy from the external force. Energy at the precessional frequency of hydrogen at all field strength in clinical MRI corresponds to the radio frequency (RF) band of the electromagnetic spectrum. The application of an RF pulse that causes resonance is called excitation. It results in absorption of energy and an increase in the number of high energy (spin down) hydrogen nuclei population.

Before resonance there is a full longitudinal magnetisation parallel to the B_0. Resonance results in two phenomena. First, the NMV moves out of alignment away from the B_0. The angle to which the NMV moves out of alignment is called the flip angle. Its magnitude depends on the amplitude and duration of the RF pulse. Second, the magnetic moments of the hydrogen nuclei within the transverse NMV move into phase with each other, and will be in the same place on the precessional path around the B_0.

Faraday's law of electromagnetic induction states that if a receiver coil is placed in the area of a moving magnetic field, a voltage is induced in the receiver coil. Signal is produced when coherent, in phase magnetisation cuts across the coil. Therefore the moving NMV produces magnetic field fluctuations inside the coil. As the NMV precesses at the Larmor frequency in the transverse plane, a voltage is induced in the coil. This voltage constitutes the magnetic resonance (MR) signal.

2.1.3 Relaxation

After the RF pulse is switched off, the NMV is again influenced by the B_0 and tries to realign with it. To do so, a process called relaxation happens by which the NMV loses its energy given to it by the RF pulse. At the same time, but independently, the magnetic moments of the NMV lose transverse magnetisation due to dephasing. Relaxation results in recovery of magnetisation in the longitudinal phase (T1 recovery) by the nuclei giving up their energy to the surrounding lattice (spin-lattice relaxation). A decay of transverse magnetisation (T2 decay) is caused by the magnetic field of each nucleus interacting and exchanging energy with its neighbour (spin-spin relaxation). Both relaxation processes are well modelled by exponential curves. If 90°

RF pulse has been applied, T1 is the time (t) taken for the magnetisation in the longitudinal plane (M_z) to return to approximately sixty-three percent of its value prior to the RF pulse (M_{0z}) [2.1.2]; and T2 is the time taken for the magnetisation in the transverse plane (M_T) to fall to approximately thirty-seven percent of its original (maximum) value (M_{0T}) after the RF pulse has been applied [2.1.3] (Figure 2.1.2).

$$M_z = M_{0z} (1 - \exp(-t/T1)) \qquad [2.1.2]$$

$$M_T = M_{0T} \exp(-t/T2) \qquad [2.1.3]$$
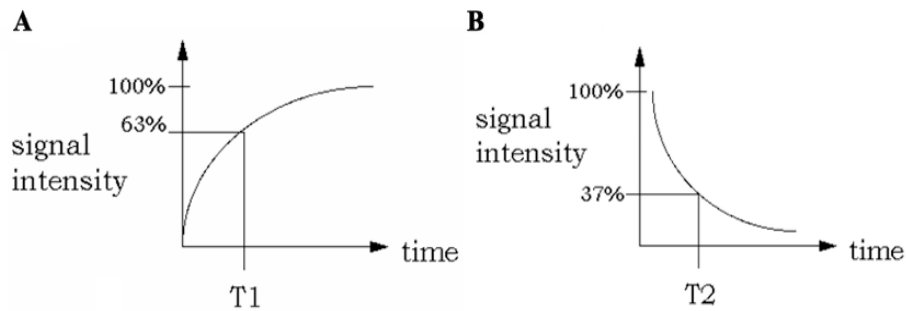
Figure 2.1.2: T1 relaxation and T2 decay. *A: T1 relaxation. The longitudinal magnetisation recovers towards equilibrium with a tissue dependent recovery constant T1. B: T2 decay. The transverse magnetisation decays towards zero with a tissue dependent decay constant T2.*

The magnitude and timing of the RF pulses form part of the pulse sequences, the basis of contrast generation in MRI. A simplified pulse sequence is a combination of RF pulses, signals and intervening periods of recovery. Repetition time (TR) is the time between application of one RF pulse to the next, that determines the amount of T1 relaxation to occur between two RF pulses. Echo time (TE) is the time from the application of the RF pulse to the peak of the signal induced in the coil, which controls the amount of T2 decay to occur before the signal is read.

2.1.4 Image contrast

Image contrast in medical imaging depends on extrinsic contrast parameters, which can be set by the operator, such as TE, TR and flip angle; and intrinsic contrast parameters which are inherent to the tissue, such as T1 recovery, T2 decay, and proton density.

A tissue has high signal if it has a large transverse component of coherent magnetisation at time TE, when the amplitude of the signal received by the coil is large, resulting in a bright area on the image. A tissue returns low signal if it has a small component of transverse coherent magnetisation, the amplitude of the signal received by the coil is small, resulting in a dark area on the image. Images obtain contrast mainly through T1 recovery, T2 decay and proton density, which is the number of protons per unit volume of that tissue.

Fat molecules consist of closely packed lipid molecules, whose molecular tumbling rate is relatively slow and matches the Larmor frequency, which allows the recovery process to be relatively rapid and an efficient energy exchange from hydrogen nuclei to the surrounding molecular lattice is possible. The NMV of fat realigns rapidly with B_0 so the T1 time of fat is short. Spins dephase quickly and the loss of transverse magnetisation is rapid. The T2 time of fat is short.

Water molecules are spaced apart; they only contain one oxygen and two hydrogen molecules and their molecular tumbling rate is relatively fast. Due to the high molecular mobility in water, the T1 recovery is less efficient because the molecular tumbling rate does not match the Larmor frequency. The NMV of water takes longer

to relax, regain the longitudinal magnetisation and realign with B_0. The T1 time of the water is long. Spins dephase slowly and the loss of transverse magnetisation is gradual. T2 time of water is therefore long (Figure 2.1.3).
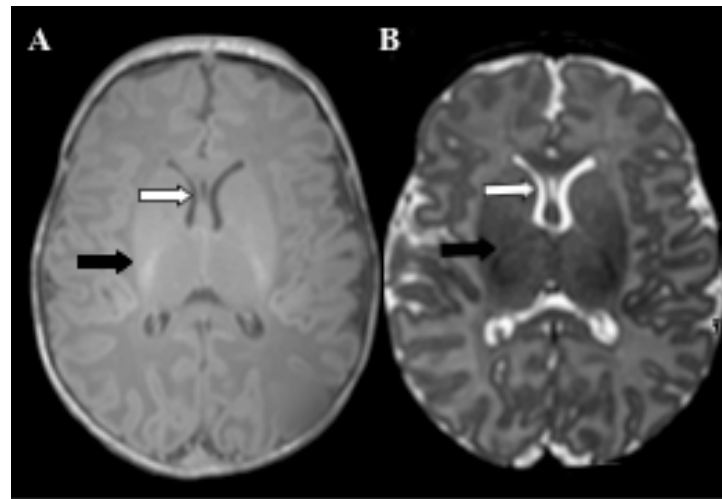
Figure 2.1.3: Image contrast. *T1 (A) and T2 (B) weighted images of a healthy term infant. A: Lipid has high (black arrow) and water has low (white arrow) signal on a T1 weighted image. B: Lipid has low (black arrow) and water has high (white arrow) signal on a T2 weighted image.*

The proton density of a tissue is the number of protons per unit volume of that tissue. The higher the proton density of a given tissue the more signal is available. To produce contrast due to the differences in the proton densities, the transverse component of magnetisation must reflect these differences. Tissues with a high proton density have a large transverse component of magnetisation and therefore high signal; tissues with low proton density have a small transverse component of magnetisation and therefore a low signal on a proton density contrast image.

In any image, the contrast due to the inherent proton density together with T1 and T2 mechanisms occur simultaneously and contribute to the image contrast. Image contrast needs to be weighted towards one of the parameters and away from the others using specific values of TR and TE for a given pulse sequence. To achieve T1 weighting the TR must be short enough so that tissues have no sufficient time to fully recover to the B_0 before the next RF pulse is applied. As TE controls the amount of T2 decay that is allowed to occur before the signal is received; to achieve T2 decay, the TE must be long enough. Proton density weighting is always present for some extent. To achieve proton density weighting, the effects of T1 and T2 contrast must be diminished, so that proton density weighting can dominate.

The relaxation and decay processes occur immediately, once RF pulse is removed. T2* decay is the decay of the free induction decay following the RF excitation pulse, which is faster than the T2 decay and is a combination of two effects: (i) the T2 decay itself and (ii) dephasing due to magnetic field inhomogeneities, which are areas within the magnetic field that do not exactly match the external magnetic field strength. Dephasing due to inhomogeneities is an exponential process, which produces a rapid loss of coherent magnetisation and therefore signal. There are two ways of compensating for T2* dephasing by using (i) gradients (gradient echo sequence) or (ii) an additional 180° RF pulse (spin echo sequence).

The gradient echo sequence is the simplest MRI sequence. It consists of a series of excitation pulses; each separated by a given TR. Data is acquired at characteristic time points after the application of the excitation pulses. A gradient echo pulse sequence uses an RF excitation pulse that is variable and therefore flips the NMV

through any angle. A transverse component of magnetisation is created, the magnitude of which is less than that in a spin echo sequence. A gradient causes a change in the magnetic field strength within the magnet, which rephases the magnetic moments so that a signal is received by the coil. The signal is called gradient echo. Although gradient echo sequences are fast, they are sensitive to susceptibility artefacts and B_0 inhomogeneities.

The spin echo pulse sequence uses a 90° RF pulse to flip the NMV into the transverse plane. The NMV precesses in the transverse plane inducing a voltage in the receiver coil. When the 90° RF pulse is removed free induction decay is produced. T2* dephasing occurs immediately, and the signal decays. An 180° RF pulse that has sufficient energy to move the NMV through 180° is then applied to compensate for dephasing. As a consequence the magnetic moments are momentarily in transverse phase again because they are at the same place of the precessional path, and so maximum signal is induced in the coil. This signal is called spin echo that contains T1 and T2 information as T2* dephasing has been reduced. Spin echo sequences result in high signal to noise ratio and are able to generate true T2 contrast, however they require relatively long scanning time.

2.1.5 Image formation

The created signal has a frequency equal to the Larmor frequency of the hydrogen regardless of the origin of the signal in the subject. To obtain an image from the NMR signal, it is necessary to locate the signal spatially in three dimensions. It is accomplished by applying spatially varying magnetic field gradients.

When a gradient coil is switched on, the magnetic field strength and therefore the precessional frequency of a spin along its axis is altered in a linear fashion. To give each slice a thickness, a 'band' of nuclei must be excited by the excitation pulse. Selective excitation of a single slice (slice select) is achieved by applying a linear field gradient perpendicularly to the plane of the desired slice at the same time as a narrow band RF pulse. In this way, only the spins with resonance frequencies centred around the transmitting frequency and within the bandwidth (range of frequencies) of the RF pulse will be excited. If a gradient is applied along the z axis, the excited spins will be located within a transverse slice, perpendicular to this axis.

The differences in phase acquired after the application of a gradient can also be used to spatially encode the signal. In 2 dimensional imaging, frequency encoding is used along one direction (x) and phase encoding along the other (y). Slice selection is usually used along the z direction. Three-dimensional volumetric images are generated by applying phase encoding along a third (z) direction.

The application of all the gradients selects individual slices and produces a frequency shift along one axis of the slice and a phase shift along the other. Individual signal can be located within the image by measuring the number of times the magnetic moments cross the receiver (frequency) and their position around their precessional path (phase). When data of each signal position are collected, the information is stored as data points in K-space. In MR physics, the K-space is the 2 or 3 dimensional Fourier transform of the MR image measured. It is rectangular in shape and has two axes perpendicular to each other (frequency axis - horizontal; phase axis - vertical). K-space is a temporary image matrix, where information of frequencies in space or

distance is stored during data acquisition. Frequency is defined as phase change over distance or over time. K-space has the same number of rows and columns as the final image and is filled with raw data during the scan, usually one line per TR. When it is full at the end of the scan, the data is processed to produce the final image.

The Fourier transform decomposes a complicated signal into frequencies and relative amplitudes of its simple component waves and so allows studying the frequency content of a variety of complicated signals. An approximation of a complicated wave is achieved by adding together very simple sine and cosine waves with varying combinations of frequencies and amplitudes (Gallagher et al. 2008).

An MR image consists of a matrix of pixels, the number of which is determined by the number of lines filled in K-space (phase matrix) and the number of data points in each line (frequency matrix). As a result of Fourier transform, each pixel is allocated a colour on a grey scale corresponding to the amplitude of specific frequencies coming from the same spatial location as represented by that pixel.

2.1.6 Echo planar imaging

Echo planar imaging (EPI) requires specific MR scanner hardware that is able to produce fast gradient oscillations to capture whole brain images in less than 100 milliseconds (ms) through switching off the gradients. Each oscillation fills a row of the K-space. A single-shot EPI is commonly of poorer contrast and lower resolution than other forms of EPI. However, it captures the rapidly changing dynamic processes of neuronal firing in fMRI, and diffusion of water molecules in diffusion MRI (Mansfield 1977; Ordidge et al. 1981; Jezzard et al. 1998).

2.2 Diffusion Magnetic Resonance Imaging

2.2.1 Diffusion

Diffusion, a mass transport process, was described by Robert Brown when observing pollen grains suspended in water constantly moving about. This observation led to the description of the constant random thermal motion that all molecules above zero degrees kelvin undergo. The physical law that explains this phenomenon is called the Fick's law [2.2.1]:

$$J = - D\Delta C$$ [2.2.1]

where J is the net particle flux, D is the diffusion coefficient and C is the particle concentration. Fick's law embodies the idea of particles diffusing from regions of high concentration to low concentration. Diffusion is proportional to the concentration gradient (ΔC) and to the D. The D is an intrinsic property of the medium. Its value depends on factors, such as the size of the molecules, viscosity, temperature and microstructural features of the environment. According to the Stokes-Einstein equation [2.2.2], for spherical particles of radius (r), D increases with temperature (T), due to the increased thermal energy of molecules, and decreases with viscosity (η) as the resistance to motion becomes greater:

$$D = \frac{k_B T}{6\pi \eta r}$$ [2.2.2]

where k_B is the Boltzmann constant.

The sensitivity of D on the local microstructure enables its use as a probe of physical properties of biological tissues.

The diffusion process can be described statistically as a Gaussian process. The displacement distribution quantifies the fraction of particles that will traverse a certain distance within a particular timeframe. The Einstein equation for 3 dimensional isotropic diffusion is [2.2.3]:

$$\lambda = \sqrt{6Dt}$$

[2.2.3]

where λ is root mean square distance travelled by a molecule in time t (Jones 2009 in Johansen-Berg et al. 2009).

2.2.2 Pulsed field gradient diffusion weighted spin echo sequence

MRI provides the opportunity to quantify the diffusional characteristics of biological specimens. The diffusional processes of a molecule are influenced by the structure of the environment, therefore MRI can be used to probe the microstructure of the environment non-invasively.

To sensitise the MR signal to the magnitude of diffusion within the brain, a pulsed field gradient diffusion weighted spin echo sequence (PGSE) is commonly used (Stejskal and Tanner 1965). PGSE induces diffusion weighting through two pulsed gradients applied either side of an 180˚ RF pulse (Figure 2.2.1). During the first diffusion gradient, spins accumulate a position dependent phase shift, the RF pulse inverts the spins before the second diffusion gradient, equal in amplitude and duration to the first, rephases the spins to bring them into coherence and produce the MR signal. Spins those remain stationary between the applications of the two gradients refocus completely. The two phase shifts cancel each other out with no loss of signal. Conversely, the random motion of spins induced by water diffusion results in the

application of unequal phase shifts, intravoxel spin dephasing and a loss in signal amplitude.
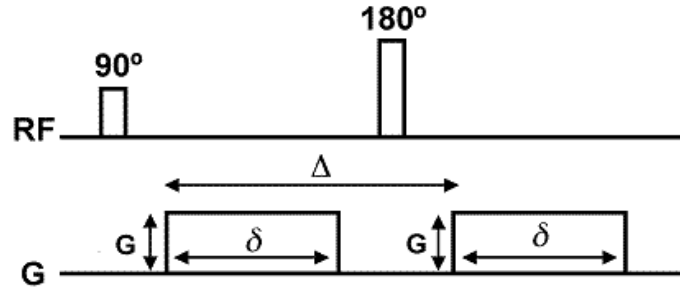
Figure 2.2.1: Pulse diagram for the pulse gradient diffusion weighted spin echo sequence. *Abbreviations: G = amplitude of diffusion gradients, δ = duration of the pulsed gradient; Δ = time interval between the leading edges of the two pulsed gradients.*

The b value characterises the level of the induced sensitivity on diffusion and is proportional to the square of the gradient strength [2.2.4]:

$$b = \gamma^2 G^2 \delta^2 (\Delta - \delta/3) \qquad [2.2.4]$$

where G is the amplitude of diffusion gradients, δ is the duration of the pulsed gradient; Δ is the time interval between the leading edges of the two pulsed gradients.

2.2.3 Diffusion weighted imaging

With diffusion MRI the D is not measured directly, rather it is inferred from observations of molecular displacement over a given time [2.2.2]. If diffusing water molecules encounter any hindrances along their random walk, the mean square displacement per unit time will be lower than that observed in free water. The diffusion obtained in tissue depends on the local microstructure of the environment and the choice of diffusion weighting; hence D acquired in a tissue is termed the apparent diffusion coefficient (ADC). ADC is a scalar representation of total net

diffusion in a voxel. A minimum of two signal measurements needed to quantify diffusion: one with diffusion weighting and one without. ADC then can be calculated from (Le Bihan et al. 1986) [2.2.5]:

$$\frac{S}{S_0} = \exp(-b \cdot ADC)$$ [2.2.5]

where and S and S_0 are the signals measured with and without diffusion weighting respectively and b reflects the degree of diffusion weighting applied [2.2.4].

In certain brain regions, where diffusion is isotropic, the diffusion weighted signal intensity, and so ADC is the same in all directions. However, diffusion of water molecules in a tissue with ordered microstructure is directional dependent; it is termed anisotropic diffusion (Moseley et al. 1990). ADC is dependent on the direction of the underlying alignment of axons relative to the applied diffusion gradients. ADC is therefore a rotationally variant measurement; it is maximally sensitive to diffusion occurring in the direction of the applied gradient (Pierapoli and Basser 1996).

2.2.4 Diffusion tensor imaging

Diffusion tensor is a mathematical model that can be used to characterise diffusion in which the displacements per unit time are not equal in all directions. DTI provides a measurement of diffusion in tissues, which is independent of the direction of the applied diffusion gradients and the choice of laboratory frame of reference. To examine diffusivity in a tissue with ordered microstructure, a minimum of six non-collinear directions of diffusion sensitisation are obtained, and one without any diffusion weighting. However, to construct the diffusion tensor usually 15 or more directions are acquired.

The diffusion tensor is a 3x3 matrix of numbers that characterises displacements in 3 dimensions in a given voxel [2.2.6]:

$$D = \begin{bmatrix} D_{xx} & D_{xy} & D_{xz} \\ D_{xy} & D_{yy} & D_{yz} \\ D_{xz} & D_{yz} & D_{zz} \end{bmatrix}$$

[2.2.6]

The diagonal elements of this matrix correspond to diffusivities along three orthogonal axes, while the off-diagonal elements correspond to the correlation between molecular displacements along those orthogonal axes.

In an isotropic medium the diffusion is isotropic, and the diffusion profile resembles a sphere. However in an anisotropic medium, molecules diffuse further along the principal axis of the medium than in perpendicular orientation. The displacement profile can be described with an ellipsoid with the long axis parallel to the long axis of the anisotropic medium.

The diffusion tensor system provides an internal reference frame, the eigen-system. The orientation of the principal axes of the ellipsoid is given by the eigenvectors (ε_1, ε_2 ε_3), which are mutually orthogonal. The three eigenvalues (λ_1, λ_2, λ_3) correspond to the diffusivities along the principal axes of the diffusion tensor. The orientation of the tensor is taken to be parallel to the principal eigenvector, which is the eigenvector associated with the largest eigenvalue and is assumed to be collinear with the dominant fibre orientation within the voxel (Figure 2.2.2).

$$\begin{bmatrix} D & 0 & 0 \\ 0 & D & 0 \\ 0 & 0 & D \end{bmatrix} \qquad \begin{bmatrix} \lambda_3 & 0 & 0 \\ 0 & \lambda_2 & 0 \\ 0 & 0 & \lambda_1 \end{bmatrix} \qquad \begin{bmatrix} D_{xx} & D_{xy} & D_{xz} \\ D_{yx} & D_{yy} & D_{yz} \\ D_{zx} & D_{zy} & D_{zz} \end{bmatrix}$$
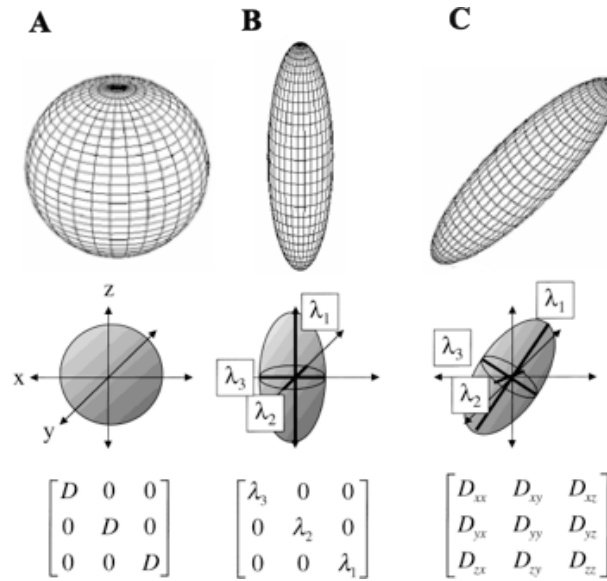
Figure 2.2.2: The diffusion ellipsoids. *A: In an isotropic medium diffusion is equal in all directions, the surface is spherical. The tensor is diagonal with all diffusivities equal to the scalar diffusion coefficient (D); B and C: In an anisotropic medium diffusion along one direction (λ_1) is preferred over others (λ_2, λ_3). The surface is an ellipsoid. B: If the laboratory frame coincides with the principal directions of the ellipsoid, the tensor will be diagonal with diffusivities λ_1, λ_2 and λ_3 along each of the three axes. C: In general the principal axis of the ellipsoid will not coincide with the laboratory frame and all elements will be necessary to characterise the tensor.*

2.2.5 Preprocessing of diffusion data

Preprocessing of diffusion MR data refers to manipulation of the raw images performed prior to fitting the model. Preprocessing aims to minimise the effects of motion, susceptibility artefacts and eddy currents (Smith et al. 2004; Gavrilescu et al. 2008; Weissenbacher et al. 2009; Dijk et al. 2010; Jones et al. 2010; Pannek et al. 2012).

Distortions due to susceptibility inhomogeneities caused by susceptibility at air-tissue boundaries are potentially less severe in neonates compared with children or adults due to the smaller size of air-filled cavities and a lower degree of bone calcification.

However, eddy currents, which are due to the relatively low bandwidth in the phase-encoding direction and the large changes in diffusion gradients, induce stretches and shears that cause distortions and blur the boundaries between grey and WM in. Distortions due to eddy currents lead to misregistration between individual images and miscalculation of diffusion tensors. Implementing post-acquisition algorithms distortions are estimated by cross-correlating the diffusion weighted images with an undistorted baseline image in terms of scaling, shear, and translation along the phase-encoding direction. The estimated distortion parameters are then applied to correct the distorted images (Haselgrove et al. 1996; Horsfield et al. 1999; Bastin et al. 2000; Bodammer et al. 2004). In Functional Magnetic Resonance Imaging of the Brain (FMRIB) Software Library (FSL) the diffusion weighted images are registered to the image acquired without diffusion weighting to minimise the effect of eddy currents (Smith et al. 2004; Jenkinson et al. 2012).

2.2.6 Fitting the tensor

After preprocessing of diffusion data the tensor in each voxel is estimated. Most software packages estimate the diffusion tensor by using ordinary least squares.

2.2.7 Parameters derived from the diffusion tensor

Although the assumption of Gaussianity is not always valid throughout the brain, it is possible to extract parameters to estimate diffusion properties from the tensor. The

advantage of invariant scalar parameters is that they do not depend on the reference frame used.

Independent of the direction of the underlying tracts λ_1 represents the estimated magnitude of diffusion parallel to fibre direction, described as axial diffusivity. λ_2 and λ_3 represent the magnitude of diffusion perpendicular to λ_1. Radial diffusivity, the average of λ_2 and λ_3, provides an estimate of diffusion across the direction of the fibres.

A measurement of the average diffusivity may be obtained by using the trace of the tensor [2.2.7]:

$$\text{Trace} = \lambda_1 + \lambda_2 + \lambda_3 \qquad \text{[2.2.7].}$$

The trace/3 is equal to the averaged mean diffusivity (MD) [2.2.8], which represents the directionally averaged diffusivity in each voxel:

$$MD = \bar{\lambda} = \frac{\lambda_1 + \lambda_2 + \lambda_3}{3}$$

$$\text{[2.2.8].}$$

In the b value range used in clinical studies MD is uniform throughout the parenchyma. Although it makes distinguishing anatomical details difficult, it has the advantage that the effects of anisotropy do not confound detection of diffusion abnormalities.

Besides describing the amount of diffusion, it is often important to describe the relative degree of anisotropy in a voxel. The simplest measure is the ratio of the longest (λ_1) and the shortest axes of the ellipsoid (λ_3). However, sorting the eigenvalues according to their magnitude introduces bias at low signal to noise ratio

(Pierpaoli et al. 1996). To overcome this problem, rotationally invariant, scale- and sorting-independent indices have been proposed. Fractional anisotropy (FA) is the square root of sum of squares (SRSS) of the diffusivity differences, divided by the SRSS of the diffusivities [2.2.9]:

$$FA = \sqrt{\frac{3}{2}} \frac{\sqrt{(\lambda_1 - \bar{\lambda})^2 + (\lambda_2 - \bar{\lambda})^2 + (\lambda_3 - \bar{\lambda})^2}}{\sqrt{(\lambda_1)^2 + (\lambda_2)^2 + (\lambda_3)^2}}$$

[2.2.9].

FA measures the fraction of the tensor that is assigned to anisotropic diffusion. FA normalises the variance by the magnitude of the tensor as a whole, hence it takes values from 0 to 1. An FA close to 0 suggests an isotropic spherical tensor ellipsoid. An FA close to 1 corresponds to diffusion constrained along one axis.

Relative anisotropy (RA) is a normalised standard deviation, which represents the ratio of the anisotropic part of the diffusion tensor to its isotropic part [2.2.10] (Jones 2009 in Johansen-Berg et al. 2009).

$$RA = \sqrt{\frac{1}{3}} \frac{\sqrt{(\lambda_1 - \bar{\lambda})^2 + (\lambda_2 - \bar{\lambda})^2 + (\lambda_3 - \bar{\lambda})^2}}{\bar{\lambda}}$$

[2.2.10].

2.2.8 Microstructural basis of anisotropy in white matter

Biological tissues are highly heterogeneous media that consist of various compartments and barriers of different diffusivities. In biological tissues, the movement of water molecules during diffusion driven random displacement is impeded by compartmental boundaries in such a way that the actual diffusion distance is reduced compared with unrestricted diffusion.

The WM of the central nervous system contains tightly packed and coherently aligned axons, their myelin sheath and glial cells. Axons are the core nerve fibres extending from neuronal cell body. They carry signal from one neurone to another. Within a tract, the majority of axons lie parallel (optic nerve); however distant populations of axons may traverse the tract in different directions (corpus callosum). The majority of the axons in a healthy adult are surrounded by a lipid-rich myelin sheath that renders the tracts white. Myelin sheath acts to insulate the fibres and promote efficient electrical conduction. Glial cells can be divided into two broad classes: (i) macroglia and (ii) microglia. Of the macroglia populations, oligodendrocytes produce the lipid-rich myelin sheath, while astrocytes play supporting roles including regulating extracellular ion concentration, maintaining blood-brain barrier and providing structural and trophic support for neurons and oligodendrocytes. The third macroglia population consists of precursor cells of oligodendrocytes and astrocytes. Microglia cells are small phagocytic immune cells engulfing waste products and dying cells. Unlike other cell types of the central nervous system microglia are of mesodermal origin (Johansen-Berg et al. 2009).

As a result of the ordered arrangement of neural fibres in the WM, the movement of water molecules are hindered to a greater extent in the direction perpendicular to the axonal orientation than parallel to it. Consequently molecular displacement parallel to the fibre is greater than perpendicular to it, it is anisotropic. As discussed before, in such case the displacement distribution is not Gaussian, but cigar shaped or even more complicated if the underlying tissue contains fibres with various orientations (Hagmann et al. 2006). Anisotropy is influenced by many non-axonal and axonal membrane factors. The axonal membrane, the myelin sheath around axons and the

neurofibrils (microtubules, neurofilaments) are the three longitudinally oriented axonal structures that impart non-random barriers to diffusion (Figure 2.2.3).
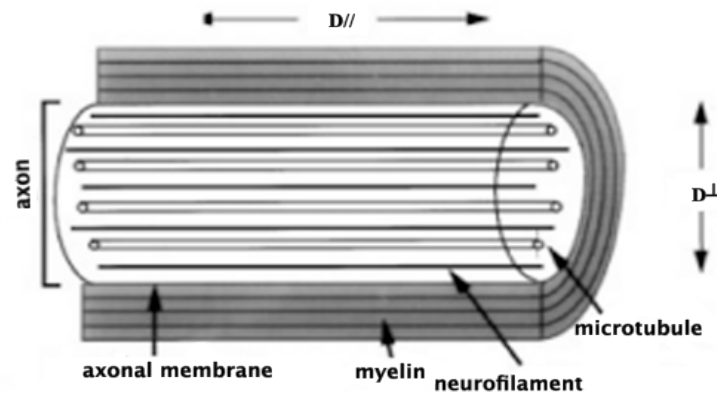
Figure 2.2.3: Longitudinal view of a myelinated axon. *The longitudinally oriented structures (microtubules, neurofilaments, axonal membrane, myelin sheath) hinder diffusion perpendicular to the axon and cause the perpendicular diffusion coefficient ($D\perp$) to be smaller than the parallel diffusion coefficient (D//) (From Beaulieu 2002)*

The hypothesis of myelin being the main structure hindering water diffusion perpendicular to the axons was disproved when anisotropic water diffusion was demonstrated in an intact, non-myelinated olfactory nerve of a garfish. A similar degree of anisotropy was observed in the non-myelinated olfactory nerve as in the myelinated trigeminal and optic nerves of the garfish (Beaulieu et al. 1994a, 1994b; 1996; 1998). Subsequently, anisotropic water diffusion was observed in several animal models of normally non-myelinated WM tracts, including the walking leg nerve of the lobster, vagus nerve of the rat and the spinal cord of the lamprey (Seo et al. 1999; Beaulieu et al. 2002; Takahashi et al. 2002).

Besides animal studies, in vivo measurements in the developing brain of human infants have shown anisotropic diffusion in fibres not yet myelinated (corpus callosum, anterior limb of the internal capsule (ALIC), optic radiation) (Toft et al. 1996; Huppi et al. 1998; Neil et al. 1998). The degree of anisotropy in non-myelinated tracts in preterm and term infants has been shown to be sufficient to permit DTI tractography (Partridge et al. 2005; Counsell et al. 2007; Bassi et al. 2012). The aforementioned studies of non-myelinated WM proved that the axonal membranes themselves are sufficient barriers alone to hinder water diffusion perpendicular to the WM fibres relative to diffusion along the fibres. A single plasma membrane of an axon is permeable to water via processes such as simple diffusion, ion co-transport and water channels, yet hinders the distances travelled by diffusing water molecules (Beaulieu 2009 in Johansen-Berg et al. 2009).

However, genetically modified animal models of dysmyelination (Ono et al. 1995; Gulani et al. 2001; Song et al. 2002; Nair et al. 2005; Tyszka et al. 2006; Harsan et al. 2007) and DTI histology correlation studies (DeBoy et al. 2007; Mi et al. 2007 Wu et al. 2007) have shown that myelin modulates the degree of anisotropy, albeit in a smaller degree, than the axonal membranes. In the developing brain a gradual increase in anisotropy, which may take place over years, can be observed as myelin matures.

Alternatively, it has been proposed that diffusion parallel to the axons could be accentuated by axonal transport. The 3 dimensional cytoskeleton of axons is posed of microtubules and neurofilaments, which are interconnected by small microfilaments. Studies performed to determine the importance of neurofilaments; microtubules and

fast axonal transport in anisotropy have concluded that these factors do not have a significant role in producing anisotropy in the WM (Beaulieu et al. 1994).

2.2.9 Diffusion weighted imaging of the neonatal brain

Diffusion weighted imaging (DWI) techniques have been used to study brain development in healthy infants (Tanner et al. 2000; Miller et al. 2003; Boichot et al. 2006; Bartha et al. 2007).

The diffusion of water is less restricted in all tissues of the neonatal brain than it is in the adult brain. ADC values in both grey and WM are higher in term infants than those found in adults. Unlike in the adult brain (Pierpaoli et al. 1996), ADCs are higher in the WM than in grey matter. The foetal and neonatal brain contains more water than that of older children and adults (Dobbing and Sands 1973). The water content reduces rapidly towards full term gestational age and in early infancy. It is reflected in rapid reduction in ADC. However, localised restriction to diffusion due to increasing oligodendrocytes, more tightly packed axons, thickening myelin sheath and its reduced permeability to water contribute to the reduction in ADC. ADC values of grey and hemispheric WM decrease and become closer to each other towards term age despite fibres in these regions are not myelinated yet (Nomura et al. 1994; Oatridge et al. 1995; Huppi et al. 1998). These developmental changes are greater frontally than occipitally and are most marked when measured perpendicular to tracts (Oatridge et al. 1995; Takeda et al. 1997).

ADC maps of the normal neonatal brain show the corpus callosum, the optic radiation and the posterior limb of the internal capsule (PLIC) to be of low signal intensity

before they are seen to be myelinated on conventional imaging at term age. At term age a lower ADC in the PLIC compared to the ALIC reflects more advanced myelination. ADC values within non-myelinated WM show a rapid decrease over the first 6 months post-term (Toft et al. 1996; Morris et al. 1999). On T2 weighted images the PLIC is fully myelinated by 6 months, optic radiations by 7 months and corpus callosum by 8 months (Van der Knaap et al. 1991). ADC values are close to mature adult values by about 2 years, although further decreases may still be observed until early adulthood.

2.2.10 Diffusion tensor imaging of the neonatal brain

Anisotropy values also differ between the adult and the neonatal brain (Hermoye et al. 2006). In the WM, anisotropy values are relatively low in infants and increase with increasing age (Klinberg et al. 1999). The increase in WM FA during development takes place in two steps. The first increase happens before the histological appearance of myelin (Huppi et al. 1998; Neil et al. 1998). It is attributed to changes in WM structure, which accompany the premyelinating state (Wimberger et al. 1995) and is characterised by a number of histological changes, including an increase in microtubule-associated proteins in axons, a change in axon calibre, and a significant increase in the number of oligodendrocytes. It is also associated with changes in the axonal membrane, such as an increase in conduction velocity and changes in sodium/potassium adenosine triphosphatase (ATPase) activity. The second increase in FA is associated with the histological appearance of myelin and its maturation. Similar to brain maturation, the two-stage increase in WM anisotropy takes place at different rates for different brain regions (Brody et al. 1987).

Although they are largely non-myelinated in the newborn period, the commissural fibres in the splenium and the genu of corpus callosum have the highest FA values in neonates. Their high anisotropy is in part due to a high degree of parallel organisation of the fibres. The earliest signs of the second stage changes in FA are observed in the projection fibres of the PLIC in the newborn period (Kinney et al. 1988).

2.2.11 Approaches to analyse diffusion magnetic resonance imaging data

2.2.11.1 Region of interest analysis

The most frequently employed technique in neonatal diffusion imaging studies is the manual delineation of ROIs (Mukherjee et al. 2002; Partridge et al. 2004; Deipolyi et al. 2005; Bartha et al. 2007; Rose et al. 2008; Thompson et al. 2011). ROI analysis, however, requires expert knowledge for accurate placement of ROIs. Colour coded FA maps can improve identification of WM structures. The technique is time consuming when a large number of regions and/or subjects are assessed. As the approach is operator dependent, ideally ROIs are drawn several times by the same operator, as well as by different operators to assess intra- and inter-rater reproducibility of results. FA might change with pathology; and this approach is prone to operator-dependent bias when extracting FA values from ROIs affected by pathology (Pannek et al. 2012).

2.2.11.2 Voxel-based whole brain analysis

Although the ROI approach is still the standard method to study diffusion metrics across neonatal subjects, a voxel-based technique, TBSS has several advantages. TBSS aims to improve the sensitivity, objectivity and interpretability of analysis of

multi-subject diffusion imaging studies (Smith et al. 2006). TBSS is an automated, observer independent method for assessing FA in major WM tracts.

The method will be discussed in details in Chapter 3. Briefly, to perform TBSS a WM skeleton, representing the centre of the WM tracts of all subjects, is derived from the group FA image, and values of individual FA maps are projected onto this skeleton. Then multivariate voxel-wise statistics across subjects is carried out on the voxels within the skeleton. While voxel-based techniques are fully automated, thus removing operator dependence, and are therefore more objective and less time consuming than ROI approaches, they rely on the alignment of all participants' images to a common space using nonlinear registration, which is challenging particularly when brain anatomy is distorted due to pathology. Because of the large number of voxels assessed, it is essential to apply methods to correct for multiple comparisons, such as threshold free cluster enhancement, to distinguish statistically significant clusters from chance events (Smith et al. 2009).

The TBSS protocol has been optimised for use in the neonatal brain (Ball et al. 2010). TBSS has been used in neonatal populations to investigate the effect of prematurity (Anjari et al. 2007), and preterm birth associated pathologies on WM microstructure (Anjari et al. 2008; Ball et al. 2010; Bassi et al. 2011; Lepomaki et al. 2013). Using TBSS specific changes of WM structure have also been correlated with outcome scores in ex preterm infants (Bassi et al. 2008; Counsell et al. 2008; Van Kooij et al. 2012).

2.2.11.3 Region of interest versus voxel-wise analysis

The decision on which method to use depends on several factors. Studies that require quantitative assessment of tensor metrics in a clinically relevant timeframe are best done using the ROI approach to avoid the extensive computer-based manipulation of DTI data required by TBSS. Longitudinal studies of large number of subjects are best performed using TBSS, because manual ROI analysis is time consuming and subject to intra- and inter-observer variability. However, TBSS presents problems of registration of images when the age range of the subjects is broad, or when the brain is affected by pathology. ROI analysis is ideal to study of a particular region of WM while TBSS is better suited to whole brain analysis. Furthermore, diffusion tensor metrics derived from manual ROI analysis were found not to be consistently comparable to those derived using TBSS (Seo et al. 2013).

2.3 Functional Magnetic Resonance Imaging

2.3.1 Functional magnetic resonance imaging

To infer information about brain activity MRI signals can be sensitised to cerebral oxygenation using deoxyhaemoglobin as an endogenous susceptibility contrast agent (Ogawa et al. 1990).

Neural activity is closely related to cerebral blood flow (CBF). CBF is the rate of delivery of arterial blood to the capillary beds of a particular mass of tissue. CBF is determined by two factors (i) the cerebrovascular resistance (CVR) and (ii) the cerebral perfusion pressure (CPP) (Pryds et al. 1996). These are related such that [2.3.1]:

$$CBF = \frac{CPP}{CVR}$$

[2.3.1].

Relatively low neuronal activity in the newborn brain means that metabolism can be maintained by a global CBF of 10-20 millilitre/100milligram tissue per minute (Pryds et al. 1996). Cerebral blood volume (CBV), the fraction of the tissue volume occupied by blood vessels, was estimated as 2 millilitre/100gram tissue in term infants (Wyatt et al. 1990).

2.3.2 Brain metabolism

Energy metabolism in the brain maintains basic processes of cellular work (biosynthesis of nucleic acids, proteins, lipids, axonal transport) and high energy demand processes of neuronal signalling.

The development of the ^{14}C deoxyglucose method made it possible to measure local rates of glucose utilisation during neuronal activation (Sokoloff et al. 1977). It was shown that increased functional activity stimulates and decreased functional activity diminishes local cerebral metabolic rate of glucose in activated neural pathways (Sokoloff et al. 1981). The increases in glucose consumption evoked by functional activation are confined to synapse-rich regions (Kadekaro et al. 1985; Sokoloff et al. 1999) and the magnitude of these increases is directly and linearly related to the frequency of action potentials in the afferent pathways (Yarowsky et al. 1983; Kadekaro et al. 1985; Sokoloff et al. 1999). The local cerebral metabolic rate of glucose of regions rich in neuronal cell bodies is unaffected by functional activation as glucose metabolised in cell bodies is mainly to support cellular processes.

Studies with ^{14}C deoxyglucose in neural tissue slices showed that the activation of energy metabolism by neuronal firing is mainly due to sodium/potassium ATPase activity (Mata et al. 1980). Action potentials reflect the depolarisation of the cells by the uptake of sodium into and the extrusion of potassium from the cells. The ion shift stimulates sodium/potassium ATPase that pumps the sodium back out and the potassium back into the cells. This process depends on the energy derived from breakdown of adenosine triphosphate (ATP). The breakdown of ATP stimulates glucose metabolism to restore the ATP that had been consumed (Sokoloff 2008).

The main sources of energy for the brain are high-energy phosphates, predominantly ATP. Brain energy metabolism normally maintains a constant concentration of ATP, as the processes that restore this metabolite are sensitive to increased ATP utilisation (Gjedde et al. 2001). Even rapid variations in cellular work are sustained with

minimal changes in ATP concentration via short- and longer-term regulatory mechanisms (Wyss et al. 1992). ATP is produced almost entirely through oxidative metabolism, which results in high ATP yield (38 molecules of ATP per 1 molecule of glucose) and carbon dioxide, an end product easily eliminated through the blood-brain barrier. In a non-steady state, ATP is produced by hydrolysis of phosphocreatine. More sustained increases in rates of ATP utilisation are balanced by increases in rates of non-oxidative glycolysis. Although, in the latter cases the yield of ATP is small (2 molecules of ATP per 1 molecule of glucose), the rate of production is fast. However, lactate, the end product of anaerobic glycolysis, is toxic to neurons, hence needs to be eliminated by export from the cells or via conversion into pyruvate in the mitochondria and subsequent oxidative catabolism (Gjedde et al. 2001).

2.3.3 Neurovascular coupling

Cerebral metabolism depends on a constant supply of both glucose and oxygen, which is maintained by the CBF. The close spatial and temporal relationship between neural activity and CBF is termed neurovascular coupling. However, the mechanisms linking increased metabolic demand of neural activity with correlated changes in CBF are still a matter of debate. It is likely that multiple mechanisms, both feedback and feed forward, function to mediate neurovascular coupling (Attwell et al. 2002; Uludag et al. 2004; Lauritzen 2005).

Local CBF is controlled by feed forward mechanisms involving neuronal signalling via neurotransmitters (Attwell et al. 2002; Lauritzen 2005). Evidence for this suggests that astrocytes play an important role in linking neurotransmitter activity to vascular responses (Harder et al. 1998; Pellerin et al. 2004). Glutamate, released by neural

activity, activates glutamate receptors in cortical astrocytes, leading to an increase in intracellular calcium, which then activates cyclooxygenase that produces local vasodilation through prostaglandins (Zonta et al. 2003). In addition, arterioles at rest exhibit periodic contractions and relaxations, called vasomotion resulting from calcium oscillations in smooth muscle cells. Calcium waves induced by electric stimulation in astrocytes propagate to arterioles and inhibit vasomotion, which eventually allow arterioles to be more relaxed and increase flow. Furthermore, neurovascular coupling might be mediated by diffusion of products of neuronal activity without the involvement of glial cells (Attwell et al. 2002).

Regional CBF is also controlled by feedback mechanisms that are sensitive to variations in concentration of vasoactive ions, metabolic by-products and other vasoactive factors produced by neural activity. Potassium and hydrogen are generated by extracellular ionic currents induced by action potentials and synaptic transmission. High concentrations of extracellular potassium and hydrogen and activity-induced reduction of extracellular calcium result in vasodilation (Kuschinsky et al. 1972; Faraci et al. 1998; Nguyen et al. 2000). Vasoactive factors increase the intracellular calcium concentration, which activates calcium dependent enzymes that produce potent vasodilators. Neuronal isoform of nitric oxide synthase (nNOS) activated by increased calcium concentration leads to production of vasodilator nitric oxide (NO) (Yang et al. 1996; 1997; 2003). Elevation of intracellular calcium also activates phospholipase A2, leading to production of arachnoid acid, which is then metabolised by the cyclooxygenase pathway producing vasodilator prostaglandins (Garavito et al. 2003).

Adenosine, generated during ATP catabolism (Ko et al. 1990; Li et al. 1994), lactate, produced through glycolysis, dopamine, gamma aminobutyric acid (GABA), acetylcholine and vasoactive intestinal peptide, released during neural activity, contribute to vasodilation (Atwell et al. 2002).

Finally, there is evidence that direct neuronal innervation of smooth muscle cells controls blood flow (Hamel 2004; Iadecola 2004).

Neurovascular coupling must provide energy for continuous brain function, which requires metabolic nutrients and the elimination of waste products. The fact that this process occurs on a fine spatiotemporal scale provides the basis for many powerful neuroimaging techniques.

2.3.4 Blood oxygen level dependent signal

Functional MRI relies on two basic assumptions. First, neuronal activation induces an increase in glucose metabolism, and second, this increased demand is met by an increase in local CBF.

Functional MRI measures neural activity by detecting associated changes in CBF, cerebral metabolic rate of oxygen ($CMRO_2$) and CBV using the BOLD signal. The BOLD arises due to two distinct phenomena. When diamagnetic oxyhaemoglobin loses oxygen to become deoxyhaemoglobin, its magnetic properties change in a subtle way. MR signal increases when the blood becomes more oxygenated. When an area of the brain is activated, the blood flow increases more than the $CMRO_2$. It leads to a reduction of the oxygen extraction fraction, a seemingly paradoxical scenario in that

the venous blood is more oxygenated despite the increase in $CMRO_2$, because the blood flow has increased more. The two phenomena together produce the BOLD signal, a local increase of the MR signal due to relative reduced oxygen extraction fraction during increased neural activity (Figure 2.3.1).
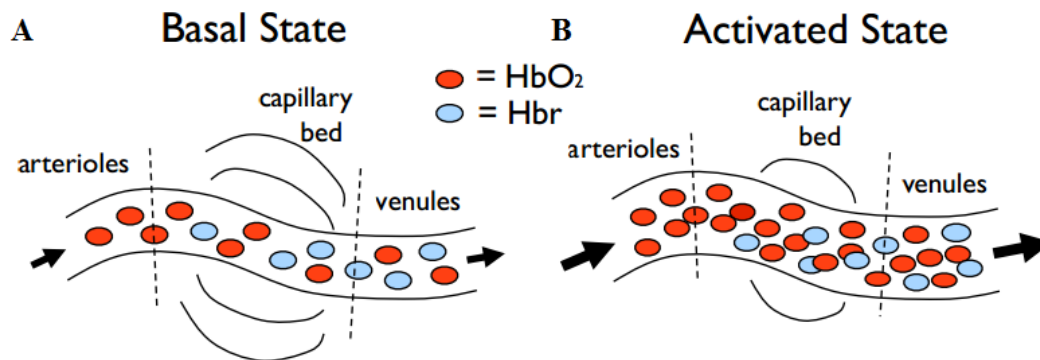
Figure 2.3.1: The blood oxygen level dependent (BOLD) signal. *A: Cerebral blood flow (CBF) in a non-activated brain region. B: Due to increased neural activity CBF increases more than the cerebral metabolic rate of oxygen, which results in more diamagnetic oxyhaemoglobin (HbO_2), which is the basis of the BOLD signal HbO_2=oxyhemoglobin; Hbr=deoxyhemoglobin (Source: http://fsl.fmrib.ox.ac.uk)*

However, BOLD signal does not measure the neuronal activity directly. Neuronal activity is a complex process of action potential and synaptic activity. BOLD is sensitive to changes in CBF, CBV and $CMRO_2$, a set of physiological responses that are referred to as the haemodynamic response to activation. Instead of a simple chain of events, where neuronal activity triggers energy metabolism and eventually the change in CBF, CBV and $CMRO_2$, they are driven in parallel by neural activity. The change in CBF responds specifically to synaptic signalling, while the $CMRO_2$ is increased by the overall energy cost of neural activity. BOLD response is primarily

reflecting the change in CBF, however it is strongly affected by two other factors: (i) the ratio of the fractional change in CBF to the fractional change in $CMRO_2$ (the mismatch of CBF and $CMRO_2$ changes) and (ii) a local scaling factor that depends on the amount of deoxyhaemoglobin present in the baseline state, that characterises the maximum BOLD response that could occur in a brain region (Buxton et al. 2009).

Given that much of the BOLD signal comes from the draining veins, away from the site of neuronal activity, and the CBF changes are more widespread than the underlying neuronal activity, the spatial resolution of fMRI is limited to within few millimetres (mm) of the neural activity. Temporal resolution of fMRI is determined by the scanning parameters and intrinsic temporal resolution of the CBF response and is in the range of ms. A single voxel's response signal over time is called its timeseries.

2.3.5 Functional magnetic resonance imaging of the neonatal brain

Functional MRI provides powerful means to identify and trace the evolution and development of cognitive neural networks, as well as neural network alterations due to disease and other adverse factors from the neonatal period through childhood and beyond.

Beyond the general issues of brain MRI of this population, such as smaller brain size, shorter neck, more difficulties in controlling motion artefacts; there are factors specifically influencing fMRI in neonates and children (Gaillard et al. 2000). Paediatric subjects have higher heart and respiratory rates and more dynamic

cardiorespiratory cycle resulting in greater pulsatility transmitted to the cortex (Poncelet et al. 1992).

The BOLD signal is directly affected by the oxygen carrying capacity of blood, hence it is important to note that the oxygen binding capacity of foetal haemoglobin is greater. However, the amount of foetal haemoglobin gradually declines to less than 2% by 12 months (Garby et al. 1962). Similar to myelination that occurs at different rates in different brain regions (Yakovlev et al. 1967), glucose utilisation of the brain shows regional differences during maturation reflecting changes in synaptic density in the grey matter. First primary sensory cortex, then motor cortex and finally the association areas reach the adult levels of glucose consumption and CBF (Chugani et al. 1987; Chiron et al. 1992; Bentourkia et al. 1998; Van Bogaert et al. 1998).

Furthermore, synaptic connections may be less well formed, less efficient, and more diffusely spread in cortical regions as neural networks and cortical areas may not be completely consolidated resulting in a more widespread and lower signal. Although the relationship between structural immaturity and the physiology of the BOLD is not precisely known, it likely diminishes its magnitude and limits detection (Gaillard et al. 2000). As a result, neonates may exhibit different vascular responses than older children or adults (Yamanda et al. 1997; Born et al. 1998; Martin et al. 1999) hence it is essential to apply age-appropriate haemodynamic response function models when analysing fMRI data of the neonatal population (Arichi et al. 2012).

2.3.6 Task-driven and resting state functional magnetic resonance imaging

2.3.6.1 Task-driven functional magnetic resonance imaging

In task-driven fMRI acquisition is carried out continuously while the subject performs tasks or is stimulated in the scanner. Tasks or stimulations are arranged in a block design where periods of activity are interspersed with periods of rest that gives an epoch. Some brain events, such as hallucinations, are transient and unpredictable in nature. In such cases event related fMRI scanning is carried out continuously at high image acquisition rate and when that event occurs the corresponding changes in the signal are detected (McRobbie at al 2010).

Task-driven fMRI studies with a passive task are feasible in neonates. For the first time in 1996 Born et al. showed brain activation in healthy newborns using visual stimulation (Born et al. 1996). Since then, several task-driven fMRI studies have been performed to investigate the development and organisation of different cortical functions in preterm and term infants. These studies were carried out using visual, somatosensory and auditory stimulations (Yamada et al. 1997; 2000; Born et al. 1998; 2000; 2002; Martin et al. 1999; Souweidane et al. 1999; Morita et al. 2000; Altman et al. 2001; Anderson et al. 2001; Dehaene-Lambertz et al. 2002; Konishi et al. 2002; Muramoto et al. 2002; Erberich et al. 2003; 2006; Marcar et al. 2004; Arichi et al. 2010).

Functional MRI has also been used to study brain function in infants with neuropathology. Abnormal activation might be used as a marker of altered brain function, including absence of activity in the injured cortex or abnormal functional laterality (Born et al. 2000; Sie et al. 2001). Also, the nature of the response might be

different from the response detected in healthy subjects. However, using altered BOLD signal as a marker of altered brain function should be considered with caution, given that both positive and negative responses have been observed in healthy infants. Functional MRI provides the opportunity to perform longitudinal studies for monitoring plasticity and evolution of functional response (Seghier et al. 2004, 2005, 2010; Heep et al. 2009).

2.3.6.2 Resting state functional magnetic resonance imaging

The importance of intrinsic brain activity in absence of an external task or stimulation can be evaluated by examining its cost in terms of energy consumption of the brain. In an average adult, the brain represents about 2% of the total body weight, however it receives 15% of the cardiac output and accounts for 20% of all the energy consumed (Clarke et al. 1999). The energy used by the brain is ten times larger than expected from its weight alone in adults. Relative to the high rate of basal energy utilisation, the additional energy consumption associated with evoked changes in brain activity required to respond to changes in the environment is small, often less than 5% (Raichle et al. 2006). These observations led to the conclusion that much of the energy consumed by the brain is unaccounted for by its responses to external stimuli. It implies that intrinsic activity may be more important than evoked activity in terms of whole brain function (Sokoloff et al. 1955; Raichle 2006). However, the full accounting of the components of the cost of intrinsic activity, the 'dark energy' of the brain, awaits further exploration (Raichle 2006). Nevertheless, these findings stimulated the extensive research of intrinsic functional connectivity (Biswal et al. 1995).

The idea of resting state functional connectivity suggests that the brain is spontaneously active even in absence of a goal-driven task, showing rich intrinsic dynamics, which can be modulated by external stimuli. Intrinsic neuronal activity can be detected as low frequency, spontaneous fluctuations of the BOLD signal. RSNs replicate a set of functional networks exhibited by the brain over its range of possible tasks (Smith et al. 2009), encompassing spatially distinct neural systems, including medial, lateral and dorsal visual, auditory, somatomotor, executive control and default mode networks (DMN) (Beckmann et al. 2005, Fox et al. 2007) (Figure 2.3.2).
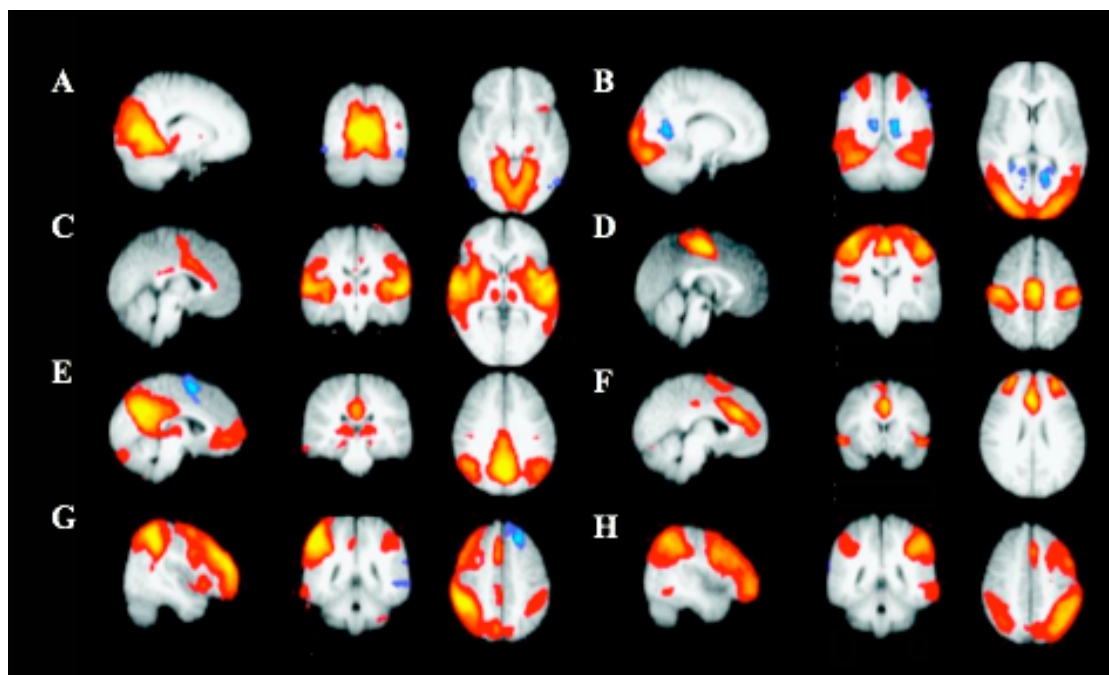
Figure 2.3.2: Functional resting state networks in healthy adults. *A: Medial visual; B: Lateral visual; C: Auditory; D: Sensory-motor; E: Default mode; F: Executive control; G: Right dorsal visual; H: Left dorsal visual networks (From Beckmann et al. 2005)*

Although the research of intrinsic activity is still a work in progress, several general observations have been made about patterns of RSNs. They transcend levels of

consciousness, are detected under anaesthesia both in humans (Greicius et al. 2008), and animals (Lu et al. 2007; Vincent et al. 2007), and during early stages of sleep in humans (Fukunaga et al. 2006; Larson-Prior et al. 2009). Although RSNs respect patterns of structural connectivity, they are not constrained by these anatomical connections. Therefore absence of anatomical connections between brain regions does not preclude the existence of functional connectivity (Vincent et al. 2007; Zhang et al. 2008; Raichle 2009, 2011).

Functional connectivity describes the correlation between patterns of neuronal activation in anatomically separated brain regions, reflecting the level of functional communication between regions (van den Heuvel et al. 2010). Thus, relationship exists not only within systems, but also among systems even in the resting state (Fox et al. 2005, 2009).

2.3.6.2.1 Development of resting state networks

Simplicity of resting state fMRI and the possibility of powerful segregation of several networks in the same acquisition provide a unique opportunity to study functional organisation of the brain in infants with and without brain injury (Tau and Peterson 2010).

The strength of coherence between nodes within systems shows a developmental trend in infants and increases with age (Fair et al. 2007; 2008). Experience and spontaneous activity itself may play a role in developing increasing strength of coherence (Jiang et al. 2004; Bartels et al. 2005; Sun et al. 2007; Lewis et al. 2009).

The full repertoire of RSNs was identified in healthy full term infants within two weeks of birth. RSNs were localised in the occipital, sensorimotor, temporal, parietal, and prefrontal cortices and the basal ganglia (Fransson et al. 2009; Uddin et al. 2010). In term infants cortical hubs were found within or adjacent to the primary sensorimotor and sensory systems, including the auditory and visual systems. In the developing brain higher-level association cortices, such as the insula, precuneus, and ventromedial prefrontal cortex were found to be of less importance as cortical hubs (Fransson et al. 2011).

RSNs are present in infants born preterm (Fransson et al. 2007). Bilateral networks were identified with strong inter-hemispheric connections, localised in the occipital, somatomotor, temporal, parietal and anterior prefrontal cortices. In a longitudinal analysis of RSNs in a cohort of preterm infants, functional connections between spatially more distant regions did not to appear until later in development. The connections gradually become more focused with advanced age (Smyser et al. 2010). RSNs demonstrate a network-specific rate of development, exhibiting increasingly coherent inter-hemispheric activity with advancing postmenstrual age (PMA). Functional connectivity in preterm infants at term equivalent age is similar to that seen in term infants (Figure 2.3.3) (Doria et al. 2010). Comparing healthy term and preterm infants at term age, the spatial properties between preterm and term infants were comparable, however discrepancies in power spectrum and connection strength of RSNs were identified (Damaraju et al. 2010).
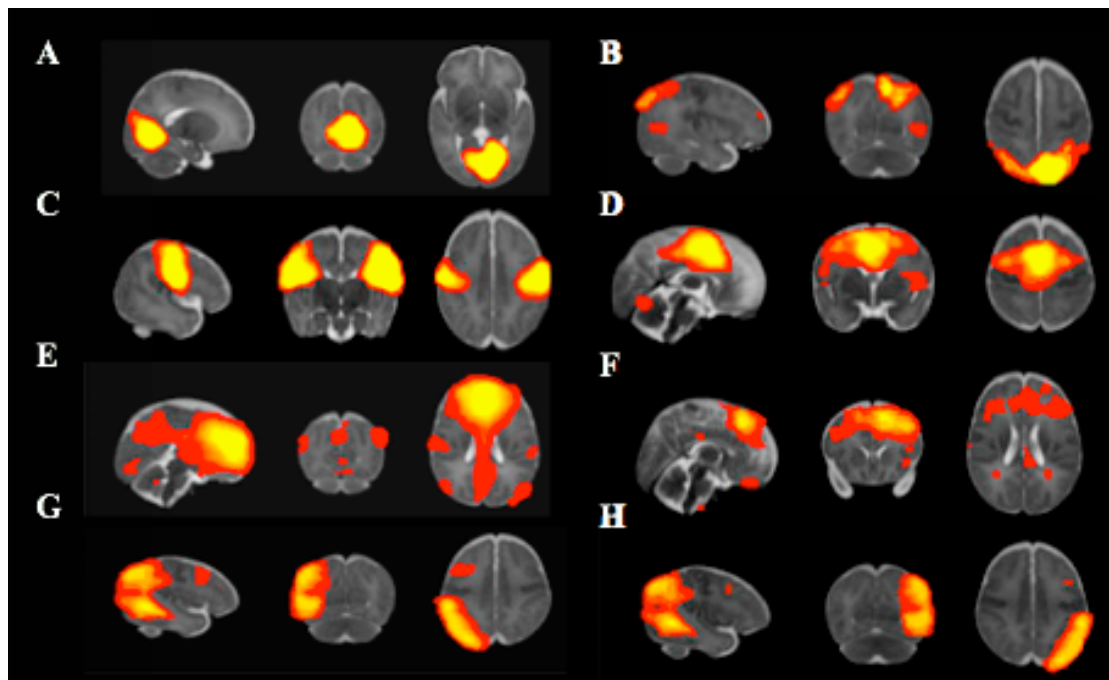
Figure 2.3.3: Functional resting state networks in healthy term infants. *A: Medial visual; B: Lateral visual; C: Auditory; D: Sensory-motor; E: Default mode; F: Executive control; G: Right dorsal visual; H: Left dorsal visual networks (From Doria et al. 2010)*

Longitudinal development of resting state functional connectivity during infancy and early childhood was investigated within the sensorimotor (Lin et al. 2008; Liu et al. 2008), visual (Lin et al. 2008) and default mode networks (Gao et al. 2009) in preterm and term infants as well as in healthy one and two year old children. RSNs were identified in each age category. Functional correlation within homotopic counterparts of the brain demonstrated increasing size and strength with increasing age. The number of regions connected and the strength of connection between regions increased by one year to become similar to that identified in adults by 2 years of age (Gao et al. 2009).

2.3.6.2.2 Resting state networks in brain injury

Although functional connectivity has been initially used as a research tool to investigate the functional architecture of the brain in healthy subjects potential clinical applications emerged (Seeley et al. 2009; Fox et al. 2010; Zhang et al. 2010). Resting state functional connectivity is now applied to study various neurological and psychiatric disorders (Lowe et al. 2002; Greicius et al. 2008; Mohammadi et al. 2009; Tedeschi et al. 2012; Rocca et al. 2010; Bonavita et al. 2011; Sharp et al. 2011; Carter et al. 2012; Dijkhuizen et al. 2012; Hunter et al. 2012; Karbasforoushan et al. 2012; Smits et al. 2012; Vemuri et al. 2012; Zhou et al. 2012; Yamasaki et al. 2012; Yu et al. 2012; Marchetti et al. 2012; Sheline et al. 2013).

There are both theoretical and practical considerations for using resting state fMRI for clinical applications (Fox et al. 2010). As discussed earlier, task related increases in neuronal metabolism are usually small compared to the large baseline energy consumption (Raichle et al. 2006). Therefore studying task-related changes allows studying a small fraction of the brain's overall activity. In addition, with resting state fMRI it is possible to study multiple cortical systems at the same time. Imaging functional connectivity also allows a broader sampling of patient populations, including non-cooperative infants, and impaired patients who may not be capable of performing tasks accurately in the scanner.

There are many clinical areas where resting state fMRI could be valuable. By far the largest application is comparing patterns of resting state connectivity between patients and healthy controls (Sharp et al. 2011; Hunter et al. 2012; Karbasforoushan et al. 2012; Vemuri et al. 2012; Yamasaki et al. 2012; Yu et al. 2012, Zhou et al. 2012;

Sheline et al. 2013). Through identification of differences, functional abnormalities of different disease states can ultimately be interpreted at a single subject level, which in turn could lead to identification of new treatments or drug targets. Functional connectivity analysis may segregate patients within a disease category by applying an algorithm that clusters patients into groups with similar resting state abnormalities. Differences seen between two groups of subjects can also be related to relevant clinical variables, such as severity of the disease (Greicius et al. 2007; Bluhm et al. 2007) or cognitive outcome (Bonnelle et al. 2011). Resting state fMRI is suited to perform longitudinal studies to follow disease progression or the effect of an intervention. Normalisation of resting state abnormalities with therapy may prove to be a suitable surrogate outcome in clinical trials (Anand et al. 2005; He et al. 2007). Preoperative planning, especially in patients who lack the ability to perform tasks, is another promising clinical area to utilize resting state fMRI (Liu et al. 2009; Shimony et al. 2009; Zhang et al. 2009).

However, several hundreds of papers have been published across different diseases with inconsistent results. To improve translation of resting state fMRI, it is essential to improve the ability to replicate and compare results from different resting state studies (Fox and Greicius 2010).

Resting state fMRI has been also used to investigate changes in functional connectivity in several cerebral disorders in paediatric populations (Church et al. 2009; Fair et al. 2010; Jones et al. 2010).

2.3.6.2.3 The effect of sedation on resting state networks

MRI of preterm and term infants provides a new insight into brain development and pathology. However, to achieve good quality images for diagnostic or research purposes infants are required to be still during scanning. To avoid movement artefact sedative medications are commonly used in the neonatal population.

Studying different stages of wakefulness in humans without medication, persistent DMN activity was demonstrated during early stages of sleep (Horovitz et al. 2008), meanwhile increased BOLD signal oscillations were found in the sensory networks of those subjects who reported to fall asleep during the scan compared to those who stayed awake throughout (Fukunaga et al. 2006).

Although the effect of sedation on functional connectivity has been widely investigated in both animal (Vincent et al. 2007; Pawela et al. 2009) and human studies using different drugs, the results are controversial. RSNs were present in anaesthetised macaques (Vincent et al. 2007). In humans midazolam induced conscious sedation caused an increase in functional connectivity in the somatomotor network (Grecious et al. 2008), the auditory and visual cortices (Kiviniemi et al. 2006), and a significant focal decrease in connectivity of the posterior cingulate cortex (Grecious et al. 2008) using independent component analysis (ICA) (Grecious et al. 2008) and seed-based correlation analysis (SBCA) (Kiviniemi et al. 2005). Decreasing levels of consciousness induced by propofol resulted in decreasing cortico-cortical connectivity in the default mode and executive control networks (Boveroux et al. 2010). However, propofol sedation increased functional connectivity in several other cortical and subcortical areas (Stamatakis 2010). Sevoflurane induced

anaesthesia altered functional connectivity in the motor cortex (Peltier et al. 2005) and in high order cognitive regions of pain and memory (Martuzzi et al. 2010).

Meanwhile neonatal resting state fMRI studies were mainly performed during natural sleep (Lin et al. 2008; Liu et al. 2008; Gao et al. 2009; Fransson et al. 2009; Smyser et al. 2010; Fransson et al. 2010) few studies involved infants who were sedated with oral (Damaraju et al. 2010; Doria et al. 2010) or rectal (Fransson et al. 2007) chloral hydrate. Although no dedicated study was conducted to investigate the effect of sedation on RSNs in infants, there are few studies that included both naturally sleeping and sedated subjects (Damaraju et al. 2010; Doria et al. 2010). No significant difference was found in correlation coefficients of any networks between the two sedated and unsedated groups (Doria et al. 2010).

Electrophysiological studies have shown that the amplitude and character of neural responses are not affected by mild or moderate sedation (Sisson et al. 1989; Avlonitou et al. 2011). Although some studies also suggested that sedative medication may alter baseline CBF (Lindauer et al. 1993; Rivkin et al. 2004; Seghier et al. 2006), CBF was unaffected by sedation with chloral hydrate in infants (Arichi et al. 2012).

2.3.7 Acquisition of functional magnetic resonance imaging data

During an fMRI experiment a series of dynamic images is collected using an EPI pulse sequence (Howseman et al. 1999; Jezzard et al. 1999), which gives excellent T2* contrast, making it sensitive to the BOLD effect. Rapidly acquired image slices make the resulting single image robust against motion artefact, and motion between images can be corrected with post-acquisition algorithms to some extent. However,

EPI is also vulnerable to image artefacts, such as geometrical distortion and Nyquist ghosts that need to be adequately corrected before statistical analysis is performed (Jezzard et al. 1999; Schapiro et al. 2002; Wilke et al. 2003).

2.3.8 Preprocessing of functional magnetic resonance imaging data

2.3.8.1 Temporal filtering

If signal and noise are present in the data at separable frequencies by using filtering in time and/or space, the noise can be attenuated and thus the signal to noise ratio increased.

By using 'high pass filtering', frequencies that are lower than the expected frequency of the data are filtered out. When 'low pass filter' is applied the frequencies that are too high to correspond to the signal are filtered out. In this way high frequencies are removed and low frequencies are passed through. A combination of high and low pass filtering, so called 'band pass filtering', constricts the detected signal to a specific band of frequencies, preserving only oscillations faster and slower than a certain speed to minimise the effects of low-frequency drifts and high-frequency noise.

2.3.8.2 Slice-timing correction

In multi-shot EPI image, slices are acquired throughout the TR, therefore the BOLD signal is sampled at different locations in the brain at different time points. Slice-timing correction corrects for differences in acquisition time within the TR. With slice-timing correction the timeseries is shifted by a small amount, interpolating between points that were actually sampled to provide a timeseries that would have been created in case all voxels had been sampled at the same time point. By this, the

assumption is made that every point in a given functional image is the actual signal from the same point in time.

2.3.8.3 Motion correction

Analysis of fMRI data assumes that the location of a given voxel does not change during acquisition. As typical fMRI sequences are several minutes long, and infants may move during acquisition, it is common to have some degree of changes of head position between volume acquisitions. Head motion in the scanner can generate artefacts that are estimated and corrected for. It is a multiple image registration task. A motion correction target is chosen, which can be either one original volume, mean of several or a standard space image. Then each fMRI volume is registered to the target, usually using six degrees of freedom (DOF) rigid body registration.

2.3.8.4 Spatial normalisation

Individual brains vary in size and shape. Spatial normalisation is the process of transforming an individual subject's image to match a standard brain to ensure that the same brain regions are compared across subjects. It allows generalisation of results to a larger population, comparison with other studies and enables averaging across subjects. However, it also reduces spatial resolution and it may reduce activation strength.

2.3.8.5 Spatial smoothing

In spatial smoothing data points are averaged with their neighbours. It has the effect of a low pass filter as high frequencies of the signal are removed from the data while enhancing low frequencies. Spatial smoothing results in blurring of sharp edges and a

more pronounced spatial correlation within the data. Convolving the fMRI signal with a Gaussian function of a specific width is a standard procedure of spatial. This is a Gaussian kernel with the shape of a normal distribution curve. The size of the Gaussian kernel defines the width of the curve, which in turn determines how much the data is smoothed. The width is expressed with the Full Width at Half Maximum (FWHM). There are several benefits from applying spatial smoothing, such as improved signal to noise ratio, improved validity of the statistical tests by making the error distribution more normal and increased overlap of activated brain regions across subjects in multi-subject studies. However, there are also drawbacks, including reduction of spatial resolution, edge artefacts, and attenuation of meaningful activations and mislocalisation of activation peaks.

2.3.8.6 Intensity normalisation

The process of global normalisation is designed to remove whole-brain signal changes that act as confounds in studies designed to evaluate regional signal changes. It results in the timeseries from different runs or subjects being centred around the same mean. However, intensity normalisation is controversial and is not performed in most studies as it may create spurious artefacts (Laurinetti 2004), such as signal changes in the WM and cerebrospinal fluid (CSF), where little or no BOLD signal changes should occur. It might be because many normalisation procedures assume that the global signal change is distributed across all regions with no spatial variation in magnitude (Macey et al. 2004).

2.3.9 Statistical analysis of functional magnetic resonance imaging data

A number of statistical approaches are available for resting state data and each has advantages and pitfalls. The methods used in this thesis for resting state fMRI analysis are discussed in the next paragraph (Smith 2004a; Cole et al. 2010; Marguiles et al. 2010).

2.3.9.1 Data-driven method

Assuming the brain is organised into a number of functionally discrete networks, an optimal analytic technique determines the signals unique to each network from the data alone. Single-session probabilistic ICA finds independent components (IC) by maximising the statistical independence of the estimated components (Beckmann et al. 2005). However, estimation of maximum spatial independence does not preclude spatial overlap between components. In the model, data variables are assumed to be linear mixtures of some unknown latent variables. The latent variables are assumed to be non-Gaussian and mutually independent, they are called ICs of the observed data (Hyvarinen et al. 2001). Probabilistic ICA decomposes 4 dimensional data into a linear mixture of spatially ICs plus non-neural origin of noise, such as physiologic noises of cardiac and respiratory cycles, motion artefacts and corresponding variance normalised timeseries. A set of spatial maps and associated timeseries jointly describe the spatial and temporal characteristics of the underlying components. ICA has several advantages as it requires no a priori assumptions of spatial localisation of RSNs, detects interacting networks by taking account of multiple simultaneous voxel-voxel relationships and it automatically denoises the dataset (Zuo et al. 2010). Using ICA, RSNs comparable to sensory and cognitive processing systems were identified.

However, the true number of components present in the data is not known. The process of dimensionality reduction and model order selection are empirically chosen or automatically estimated. Although approaches exist to optimally select the number of ICs for a given dataset according to statistical criteria, there is no single best solution for model order or dimensionality of multiple distributed systems (Kiviniemi et al. 2009; Smith et al. 2009). Furthermore, ICA may 'split' an IC into a number of sub-networks. The reproducibility of ICA is another challenge as it may produce results that are variable across analyses (Marguiles et al. 2010). Although ICA does not require initial assumptions about spatial localization of the networks, it does require a posteriori selection of valid ICs (Beckmann et al. 2005).

2.3.9.2 Hypothesis-driven method

SBCA has a historical relevance, as Biswal and colleagues first identified low-frequency, coherent, spontaneous activation in the somatomotor cortex to derive timeseries models of functional connectivity using this technique (Biswal et al. 1995).

SBCA involves two steps: (i) extraction of a model timeseries from a specified area (seed) and (ii) quantification the similarity between the model timeseries with the timeseries from other voxels. A priori selection of the ROI (a voxel, cluster or atlas region) from where the timeseries is extracted is usually based on previous studies. Timeseries is then used as a regressor in a linear correlation analysis to calculate whole-brain, voxel-wise functional connectivity maps of covariance with the seed region. The major advantage of the technique is its straightforward interpretability. It shows the network of regions most strongly functionally connected with the ROI.

Functional connectivity can be identified by SBCA with moderate to high reliability (Shehzad et al. 2009).

One of the potential weaknesses of SBCA is the influence of structured spatial confounds, such as other RSNs and structured noise. Although some of these effects are removed by preprocessing steps, the presence of residual confounds in reference timeseries can negatively influence correlation maps if the estimated networks also include voxels which describe the spatial extent of an artefact. The univariate approach disregards the richness of information available within the statistical relationships of multiple data points. A priori selection of the timeseries of one seed region imposes anatomical restrictions on the measurement of network connectivity. Fundamentally there are as many possible networks as there are possible seeds. Consequently discussing and interpreting one resulting spatial map as a distinct and meaningful neurobiological system is an under-representation of the data. Biologically, the choice of seed may bias connectivity findings towards specific, smaller overlapping sub-systems, rather than larger, distinct networks. SBCA is also biased by investigator (location and size of the seed) and subject specific factors (spatial normalisation, functional localisation). Biases inherent in the seed selection process can result in a large amount of variability in the results and subsequent interpretations (Cole et al. 2010; Marguiles et al. 2010).

2.3.9.3. Group analysis

Methodologies discussed above are also used for group analysis. The advantages and disadvantages of the techniques still apply on a group level, along with additional caveats common to all attempts to combine functional imaging datasets this way.

Gross variability in cortical thickness, folding and functional localisation between individuals may cause problems for group inferences.

2.3.9.3.1 Group independent component analysis

Recently coherent methods have been proposed and validated for comparing activity patterns across subjects and/or sessions within an ICA-based framework. Group-level ICA supports a higher dimensional, and therefore more finely detailed, decomposition than single-session ICA. On the other hand, single subject ICA has a greater power to model session-level structured noise than group-level ICA approaches.

In group-level ICA first data from all subjects are spatially normalised and the dimensionality is reduced via principal component analysis for each subject. These reduced datasets are then assumed to contain the most important source of signals that have been 'mixed' into the measurements. All reduced datasets are temporally concatenated before application of group ICA that identifies voxels with common temporal patterns within and between subjects. By means of temporal concatenation of multiple datasets (Calhoun et al. 2001), group-ICA can thereby estimate group-level ICs (Beckmann et al. 2005).

A more recent approach (Beckmann et al. 2009; Filippini et al. 2009) estimates subject-specific RSNs from information within the original functional data by dual regression. This approach uses regression of the group ICA spatial maps onto the original, individual fMRI datasets. The spatial maps from group ICA decomposition are first used as a set of spatial regressors in the general linear model (GLM) in a multiple regression analysis. It generates individualised, session-specific timeseries

for each IC for each subject. The subject-specific timeseries are then normalised and used as temporal regressors in a multiple linear regression resulting in subject-specific spatial maps for each group-level component. The analysis is carried out in the standard space to perform cross-subject voxel-wise nonparametric permutation testing. Estimated timeseries and spatial maps form unbiased least squares approximations to the original ICA maps at the individual subject level. Dual regression has been validated to estimate session-level RSNs from group ICA spatial maps consistently and more reliably than single-session template matching approaches (Zuo et al. 2010).

2.3.9.3.2 Group seed-based correlation analysis

In most group SBCA, correlation coefficients are identified from an initial, whole-brain analysis of functional connectivity with the timeseries extracted from a given seed region. At higher level, these values are then converted into Z scores and averaged across subjects in a GLM, followed by standard hypothesis testing.

2.4 Image registration in medical imaging

Computational post-acquisition MR analysis tools provide the means to quantify differences between MR images objectively, automatically with reproducible measurements. Image registration is the process of determining a spatial transformation or mapping that relates the coordinates in the source image to the corresponding coordinates in a target image to achieve precise spatial correspondence (Hajnal et al. 2001). Correspondence may mean structural, functional or structural-functional similarity. In broad terms registration includes transformation estimation and/or applying the transformation, thus creating a new, modified image. A common way of formulating the registration process as a mathematical problem is to construct a cost function, which quantifies the dissimilarity between the two images, and then search for a transformation which gives the minimum cost.

In medical imaging, registration has been developed for almost all anatomical parts or organs of the human body. In terms of neuroimaging, commonly used applications of image registration include combining images across individuals in order to quantify structural changes associated with development (Anjari et al. 2007), aging (Barrick et al. 2010; Burzynska et al. 2010) or pathology (Porter et al. 2010), characterising shape and size variations amongst subjects or groups (Aljabar et al. 2008, Hughes et al. 2012) and correcting for motion (Liao et al. 2006).

There are a number of image registration methodologies and several criteria have been proposed to classify them (Elsen et al. 1993; Maintz and Viergever 1998;

Hawkes 2001). Registration methods can be classified based on data dimensionality: (i) spatial dimensions only or (ii) time series with spatial dimensions. Registration allows different brain images from either the same subject (intra-subject), or from different subjects (inter-subject) to be aligned into a common space. An image acquired from a single subject that is aligned to an image constructed from a database obtained using imaging from many subjects is called atlas registration (Serag et al. 2012). Registration can be carried out using different (inter-modality registration; e.g. structural-functional) or same imaging modalities (intra-modality registration; e.g. diffusion-diffusion). Considering the amount of image information used in the registration process, registration is classified as (i) global, if all the voxels presented in the ROI are used; or (ii) local if only a part of the voxels in a ROI is used. Concerning image registration methodologies three levels of interaction are recognised depending on the input of the user in the registration process: (i) interactive, where the user does the registration assisted by a software; (ii) semiautomatic, where the user has to initiate the algorithm or (iii) automatic, where the user only supplies the algorithm with the image data. The two main groups of image registration algorithms based on the nature of registration basis are (i) voxel-based/intensity-based, which aims to estimate and improve anatomical correspondence between images based on intensity values in both images; and (ii) feature-based or geometrical-based, whereby the same features are extracted in each image and the registration is driven by attempting to bring these into spatial correspondence. In neuroimaging, voxel-based methods were proved to be more reliable than feature-based approaches (Maintz and Viergever 1998).

Transformation models can be divided into linear (rigid and affine) and nonlinear, based on the number and types of deformation models applied (Figure 2.4.1). Any non-rigid transformation can be described by three components. A transformation, which relates the target and the source images by finding the best geometric alignment to maximise the similarity between the two images; a similarity measurement, which describes the similarity between the target and the source images; and an optimisation, which varies the parameters of the transformation model to maximise the matching criterion as a function of the similarity measure.

2.4.1 Transformation models

2.4.1.1 Linear transformation

Rigid transformation is defined by 6 DOF in 3 dimensions, 3 translational and 3 rotational parameters. Rigid transformations preserve size and shape of the image. It is commonly used for within subject registrations, where anatomy is the same but positional differences may exist due to movement during image acquisition, or for a starting point for subsequent non-rigid alignment.

Affine transformation is defined by 12 DOF, 3 translational, 3 rotational and 3 scaling (shear and skew) parameters over 3 dimensions (Figure 2.4.1). It compensates for additional global size changes and shears. Linear registration is usually used to correct for scanner-induced geometric distortions, most commonly due to eddy current effects in EPI data, to account for the scale and size differences in inter-subject brain registration, to provide an approximate alignment of images from different subjects before more precise registration.

2.4.1.2 Nonlinear registration

Nonlinear transformation includes local transforms along with global affine transform; hence always more than 12 DOF are used. Two types of nonlinear registrations have been used in medical imaging: (i) guided deformations, in which the deformation is controlled by a physical model that has taken into account the material properties, such as tissue elasticity or fluid flow (Bajcsy et al. 1989; Christensen et al. 1996), and (ii) freeform deformation (FFD), in which any deformation is allowed. Such registration techniques are based on the assumption that a set of corresponding points of landmarks can be identified in the source and the target images. In FFD models, a grid of control points is defined to determine the deformation involved (Figure 2.4.1).

A

$$A = \begin{pmatrix} a_{11} & a_{12} & a_{13} & a_{14} \\ a_{21} & a_{22} & a_{23} & a_{24} \\ a_{31} & a_{32} & a_{33} & a_{34} \\ 0 & 0 & 0 & 1 \end{pmatrix}$$

B
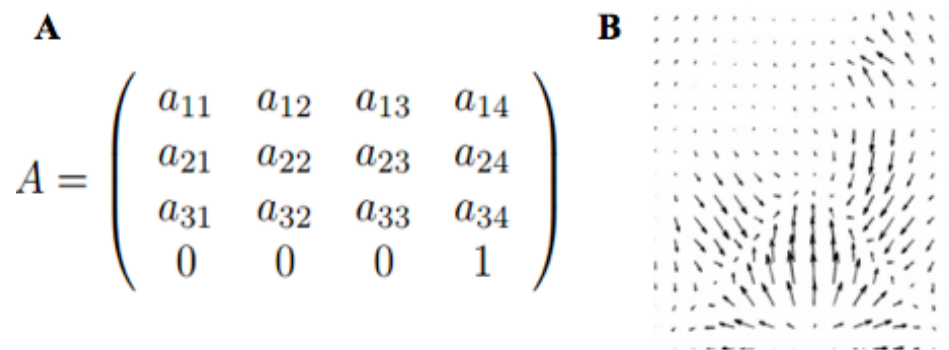
Figure 2.4.1: Transformation matrix for affine (A) and nonlinear (B) registration. *A: Affine transformation is represented by 12 parameters. B: A nonlinear transformation is represented by a deformation field. (Source: http://www.fmrib.ox.ac.uk)*

The points of such a grid are moved individually in the direction that optimises the similarity measure, defining local translations. The translation required to bring one image into the space of another is described by a vector. Vectors at each control point

are blended using a B-spline kernel to produce a smooth deformation field. Transformation between control points is propagated by interpolation. The most popular interpolator used for FFD is B-spline (Rueckert et al. 1999; Rohlfing et al. 2003). Spline-based registration algorithms use corresponding points, in the source and target images and a spline function to define correspondences away from these points. Anatomical or geometrical landmarks are identified in both images to determine the control points (Bookstein 1991). The location of control points can be updated by optimisation of a voxel similarity measure, such as mutual information (MI) (Meyer et al. 1997). Alternatively, control points can be arranged with equidistant spacing across the image forming a regular mesh (Davis et al. 1997). In this case the control points are only used as a parameterisation of the transformation and do not correspond to anatomical or geometrical landmarks. Therefore they are often referred to as pseudo- or quasi-landmarks (Hajnal et al. 2001).

2.4.3 Similarity measure

A similarity measure describes the similarity between the target and the source images. It is composed of at least two terms, one related to the voxel intensity or structure/feature similarity and the other to the deformation field (Rueckert et al. 1999; Rohlfing et al. 2006; Lu et al. 2004).

Intensity approaches match intensity patterns in each image using mathematical or statistical criteria. They define a measure of intensity similarity between the source and the target and adjust the transformation until the similarity measure is maximised (Crum et al. 2004). The most commonly used similarity measures are based on intensity difference, intensity cross correlation and information theory. The measures

based on the intensity difference assume that the corresponding structures in both images have identical intensities. Cross correlation and its derived measures are based on the assumption that there is a linear relationship between the signal intensities of the corresponding structures on both images. These similarity measures are appropriate for mono-modal image registration. When performing registrations between different image modalities, or between images with different contrasts, entropy-based metrics are more suitable (Pluim et al. 2003). Information theory similarity measures are based on mutual information (MI) or derived measures. MI measures how well one image explains the other based on the assumption that there is a functional between the variables involved (Wells et al. 1996, Maes et al. 1997).

Geometric approaches build explicit models of identifiable anatomical elements in each image. These elements typically include functionally important surfaces, curves and points of landmarks that can be matched with their counterparts in the second image (Bookstein 1989, Rohr et al. 2001, Johnson and Christensen 2002). The use of structural information ensures that the mapping has biological validity and allows the transformation to be interpreted for the underlying anatomy or physiology. Similarity measure used in feature-based registration is often computed as the sum of the 'distances' associated to each correspondence established. These distances can be related to the spatial position of the corresponding structures (Oliveira et al. 2012). Other approaches use anatomical surfaces, such as the ventricular borders or cortical surfaces (Thompson and Toga 1996, Yeo et al. 2010) or features such as sulcal and gyral ridges (Subsol et al. 1997, Joshi et al. 2010).

2.4.4 Optimisation

Optimisation refers to the method in which the transformation is adjusted to improve the image similarity. The similarity measure is an n dimensional function, where n is the number of DOF of the transformation involved. Once a cost function has been chosen it is necessary to search for the transformation, which yields the minimum cost value. To do this, an optimisation method is implemented to search through the parameter space of allowable transformations (Jenkinson et al. 2002). Parameters that make up the registration can be computed directly, or can be searched for. Of the optimisation methods the iterative algorithms use a coarse-to-fine approach. The process starts by identifying a pair of image pyramids that are used to down-sample the images. Then the registration starts by registering the images from the lower to the higher resolution. In each step, the transformation found in the previous step is used as the new initial registration. The transformation is updated according to the parameter change that results in the largest increase in similarity and the process continues stepping along the direction of maximum increase until no more increases are achieved, or a convergence criterion is reached. By altering the step size to become progressively smaller and sub-sampling the data onto lower resolution voxel grids, it is possible to perform registration through several resolution levels, optimising the alignment first according to gross image features and progressing to finer anatomical details. An advantage of this approach is that the initial transformations at low resolution is calculated relatively quickly and used to inform higher resolution transformations (Hajnal et al. 2001).

2.4.5 Interpolation

In the registration process, when a point is mapped from one space into another by transformation, it is generally allocated a non-grid position. Due to the discrete nature of MR images, data are sampled in a grid of voxels and it is unlikely that the corresponding points lie on the same voxel grid after transformation. To compare the images it is necessary to interpolate between points, resampling the transformed source image onto the same grid as the intended target (Lehmann et al. 1999, Hill et al. 2001). The goal of interpolation is to evaluate the image intensity in that new position. The interpolation solution can affect the accuracy and speed of registration. To increase the speed, a simple interpolation algorithm is usually used in the optimisation step, such as ones that are based on the nearest neighbour or trilinear interpolations, and then higher quality interpolation is used to obtain the final registered image, as the ones based on cubic B-spline or sinc interpolation (Hill et al. 2001).

2.4.6 Validation

Validation usually means showing that a registration algorithm applied to a typical dataset in a given application consistently succeeds (Crum et al. 2004). A number of possible solutions exist for any given registration problem, and often the decision to use a particular transformation is a qualitative one based on visual inspection (Good et al. 2002). For geometric approaches an error can be computed, which for landmark methods expresses the distance between corresponding landmarks post-registration (Collins et al. 1997; Woods et al. 1998). For intensity-based approaches it is common to identify corresponding landmarks or regions independently of the registration process and establish how well the registration brings them into alignment. Another

solution is to establish whether the registration of source to target produces the same alignment as from target to source (Christensen et al. 2003).

2.4.7 Registration software

In this thesis image registration has been carried using tools implemented in FSL (Smith et al. 2004b; Jenkinson et al. 2004) and Image Registration Toolkit (IRTK) (Rueckert et al. 1999; Studholme et al. 1999; Schnabel et al. 2001).

2.4.7.1 Functional Magnetic Resonance Imaging of the Brain Software Library

FSL has been developed by the FMRIB Analysis Group. It is freely available as a single integrated software package, including tools for analysis of functional, structural and diffusion brain MRI data. FMRIB's Linear Image Registration Tool (FLIRT) is a fully automated tool for linear intra- and inter-modal image registration. FLIRT performs translation, rotation, zoom and shear to match the source image to the target. For inter-subject registration purposes FMRIB's Nonlinear Image Registration Tool (FNIRT) is more suitable. FNIRT allows a more fine transformation by permitting local deformations to perform inter-subject alignment (Jenkinson and Smith 2001; Jenkinson et al. 2002).

2.4.7.2 Image Registration Toolkit

IRTK is a comprehensive library of tools for medical image registration. It implements a variety of algorithms for 2 and 3 dimensional image registration including rigid, affine and nonlinear. The software also includes tools for transforming and resampling images using a variety of geometric transformations and interpolation methods (Denton et al. 1999; Rueckert et al. 1999; Schnabel et al. 2001).

2.5 Human brain development

2.5.1 Neurulation

Neurulation refers to the inductive events that occur on the dorsal aspect of the embryo and results in formation of the brain and the spinal cord. Primary neurulation refers to formation of the brain and spinal cord excluding segments caudal to the lumbar region. Secondary neurulation or caudal neural tube formation is related to the formation of the lower sacral segments of the spinal cord.

Primary neurulation (Figure 2.5.1) occurs during third and fourth weeks of gestation. The nervous system begins to form on the dorsal aspect of the embryo as a plate of tissue differentiating in the middle of the ectoderm. The underlying notochord and mesoderm induce formation of the neural plate at approximately 18 days (Lemire et al. 1975; Monsoro-Burq et al. 1995). Under the continuing inductive influence of the dorsal mesoderm, the neural plate invaginates along its central axis to form the neural groove, with neural folds on each side. The neural folds gradually approach each other in the midline and fuse there, converting the neural groove into a neural tube. As the neural tube separates from the surface ectoderm, the neural crest cells migrate to the sides of the neural tube. The neural crest separates into the right and left part and migrates to dorsolateral aspects of the neural tube, giving rise to the sensory ganglia of the spinal and cranial nerves. The first fusion of neural folds occurs in the region of the lower medulla around 22 days and it proceeds caudally and rostrally (Golden et al. 1995; Seller et al. 1995; Manning et al. 2000; Copp et al. 2003). The anterior end closes at 24 and the posterior end closes at 26 days at the upper sacral level. Deformation of the developing neural plate required to form the neural folds, and

subsequently the neural tube depend on cellular and molecular mechanisms (Manning et al. 2000; Copp et al. 2003; Detrait et al. 2005). Under the influence of vertically oriented microtubules, cells of the developing neural plate elongate, and their basal portions widen. Under the influence of microfilaments oriented parallel to the apical surface, the apical surface of the cells constricts. These deformations produce the stresses that lead to the formation of the neural folds and then the neural tube. Cell-cell recognition and adhesive interactions with extracellular matrix are led by cell adhesion glycoproteins (Volpe 2008).
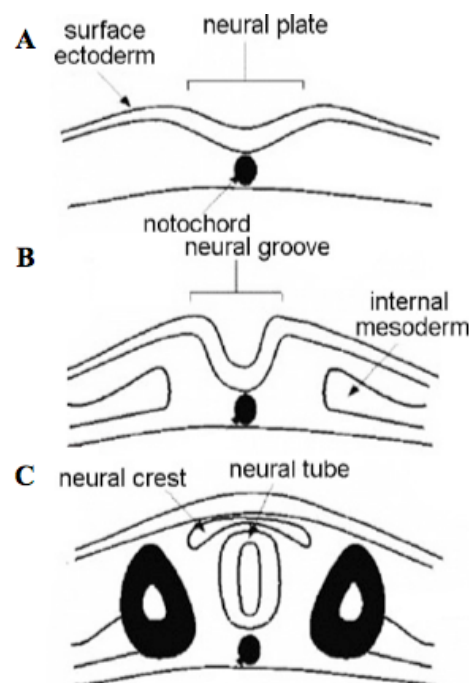
Figure 2.5.1: S**cheme of the embryo's transverse sections during primary neurulation process.** *A: Neural plate formation, B: Neural groove stage, C: Neural tube formation. (From Alfarra et al. 2011)*

2.5.2 Development of prosencephalon

Prosencephalic development occurs by inductive interactions under the primary influence of the prechordal mesoderm during the second and third months of gestation

(Yakovlev 1959; Lemire et al. 1975; Leech 1986). The interaction of the prechordal mesoderm and the forebrain that occurs ventrally at the rostral end of the embryo results in formation of the face and the forebrain. Prosencephalic formation begins at the rostral end of the neural tube at the end of the first month. Prosencephalic cleavage occurs most actively during the fifth and sixth weeks of gestation and includes three basic cleavages: (1) horizontally to form the paired optic vesicles, olfactory bulbs and tracts; (2) transversely to separate the telencephalon from diencephalon; (3) sagittally to form, from the telencephalon, the paired cerebral hemispheres, lateral ventricles, and basal ganglia. The midline prosencephalic development occurs from 6 weeks to the third month, when three crucial plates of tissue become apparent. From dorsally to ventrally these are the commissural, chiasmatic and hypothalamic plates. These structures are important in the formation of the corpus callosum and the septum pellucidum, the optic chiasm, and the hypothalamic structures respectively. The most important molecular pathways in prosencephalic development are the sonic hedgehog signalling pathways (Muenke et al. 2000; Nanni et al. 2000; Roessler et al. 2003; Sarnat et al. 2005).

2.5.3 Neuronal proliferation

All neuron and glia are derived from the ventricular and subventricular zones, present in the subependymal region of the developing nervous system (Samuelsen et al. 2003). Quantitative information on cellular proliferation is derived from studies of deposition of brain deoxyribonucleic acid (DNA), the chemical correlate of cell number. Proliferation occurs in two phases. The first, occurring 2 to 4 months, is associated primarily with radial glia and neuronal proliferation; the second, occurring

from approximately 5 months of gestation until 1 year of birth, is associated with glial

multiplication (Figure 2.5.2) (Dobbing and Sands 1973).
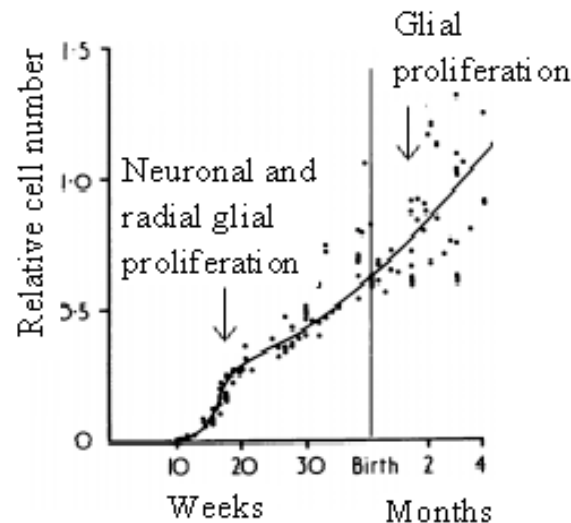
Figure 2.5.2: The two phases of prenatal neuronal proliferation. *Y axis: total*

forebrain deoxyribonucleic acid, equivalent to total cell number. X axis: gestational

age in weeks until birth, then in months until fourth postnatal month (From Dobbing

and Sands)

At least two types of neuronal progenitors are present in the ventricular zone (i) short

neural precursors that have a ventricular end-foot and a leading process of variable

length; and (ii) radial glial cells which are progenitors for cortical neurons, astrocytes

and oligodendrocytes and guide neuronal migration. When the radial glial cell

functions as a neuronal progenitor, the clonally related neurons migrate along the

parent radial glial fibre (Ever et al. 2003; Mo et al. 2007; Noctor et al. 2007).

Cells in the periphery of the ventricular zone replicate their DNA, migrate toward the

luminal surface and divide. The two daughter cells then migrate back to the periphery

of the ventricular zone. This to-and-fro migration or inter-kinetic nuclear migration is

repeated each time DNA replication and mitosis occur in the ventricular zone. In some regions of the forebrain a subventricular zone of proliferation can also be identified. In the monkey cerebrum, the ventricular zone gives birth to most neurons, and the subventricular zone is the point of origin of some late appearing neurons, such as upper layers of cerebral cortex and later subplate neurons, and most glia (Rakic 1975, 1988, 1995, 2005).

In the earliest days of proliferation progenitor cells divide symmetrically into two cells. Around the second half of the second month the progenitor cells begin to divide asymmetrically, when each division results in a stem cell and a post-mitotic neuronal cell. As the proliferative phase progresses, proportionately more neuronal cells and less stem cells are produced (Rakic 1975, 1988, 2005). When cells withdraw from the mitotic cycle and cease proliferative activity, they migrate into the intermediate zone on their way to forming the cortical plate (Caviness et al. 2000, 2003).

The signalling pathways that modulate neuronal proliferation include the Notch, ErbB and fibroblast growth factor receptor, connexin channels and beta-catenin (Ever et al. 2005; Lasky et al. 2005).

2.5.4 Neuronal migration

Neuronal migration refers to the series of events whereby millions of neurons move from their sites of origin in the ventricular and subventricular zones to the loci within the central nervous system, where they will reside for life. The peak period for this is between the third and fifth months of gestation.

The earliest mode of migration to the cerebral cortex is movement by translocation of the cell body that results in formation of the preplate. This layer of neurons is split later by the arrival of the cortical plate neurons into a superficial layer nearest the pial surface, which produces the Cajal-Retzius and related neurons of the marginal zone, and a deeper layer, which forms the subplate neurons (Nadarajah et al. 2001; Bielas et al. 2004).

Radial migration is the primary mechanism of formation of the cortical projection neurons and deep nuclear structures. Projection neurons, generated by radial glial progenitors, proceed primarily from the dorsal subependymal germinative zones. The clonally related neurons migrate along the parental radial glia, which extends to the pial surface (Volpe 2008). Cells migrate first take the deepest positions, meanwhile those migrate later take more superficial positions (Rakic 1975, 1988).

Tangential migration of the neurons from the ventral aspect of the subependymal germinative zones results in GABA expressing interneurons of the cortex. These neuronal precursors migrate parallel to the surface of the cortex and proceed in one of three streams through the subventricular, intermediate zone or marginal zones arriving in the cortical plate (Komuro et al. 1998; Pearlman et al. 1998; Walsh et al. 2000; Bielas et al. 2004; Kriegstein et al. 2004; McManus et al. 2005).

By 20-24 weeks of gestation, the human cerebral cortex has its full complement of neurons. The cerebral cortex consists of six parallel layers (Figure 2.5.3). However, some areas of the cortex differ from this six layer configuration, for example the Limbic-system has only three layers and the insular cortex and cingulate gyri have six

indistinct layers. Layer I contains intracortical fibres and some small cells. Layer II contains small, mainly stellate cells, which are connected in local circuits. Layer III contains mainly pyramidal cells, which give rise to commissural and projections fibres. Layer IV contains granular cells and receives projection fibres from thalamic nuclei. Layer V contains granular cells and receives projection fibres to the basal ganglia, brain stem and spinal cord. Layer VI contains cells that send fibres to the thalamus.
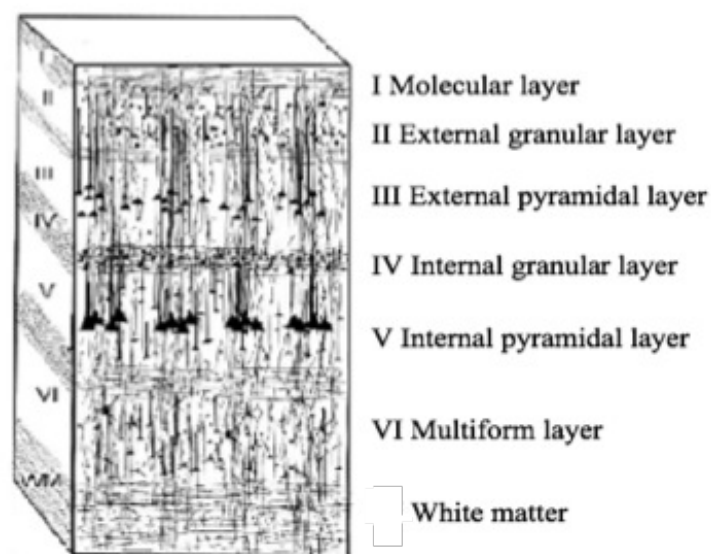
Figure 2.5.3: Layers of the cerebral cortex. (From Bentivoglio et al. 2003)

Molecular determinants of migration of radial glia include three signalling pathways, ErbB4 and Notch receptors and brain lipid-binding proteins (Anton et al. 1997; Rio et al. 1997; Pearlman et al. 1998; Hatten et al. 1999; Walsh et al. 2000). Several other proteins are involved in regulating migration of the preplate, such as fibronectin, integrins, laminin, reelin, and the migrating neurons, such as neuregulin, astrotactin, doublecortin, filamin-1 (Volpe 2008).

2.5.5 Neuronal organisation

Neuronal organisation continues from fifth months of gestation to several years after birth. There are six major developmental features including the (1) establishment and differentiation of the subplate, (2) attainment of proper alignment, orientation and layering of the cortical neurons, (3) elaboration of dendritic and axonal ramifications, (4) establishment of synaptic contacts, (5) cell death and selective elimination of neuronal processes and synapses, (6) proliferation and differentiation of glia (Volpe 2008).

Subplate neurons are generated from the preplate. They differentiate rapidly and express a variety of receptors for neurotransmitters, neuropeptides and growth factors. The subplate neurons elaborate a dendritic arbor with spines. They receive synaptic inputs from ascending afferents and provide a site for synaptic contact for 'waiting' axons from thalamus and other cortical sites. Subplate neurons extend axonal collaterals to overlying cortical and subcortical sites and establish a functional synaptic link between waiting afferents and cortical targets. They provide axonal guidance to the cerebral cortex for ascending afferents, and to subcortical targets for descending axonal collaterals from the cortex (Volpe et al. 1996; Bystron et al. 2005; Kostovic et al. 2006; Ohshiro et al. 2006; Volpe 2008).

Attainment of proper alignment, orientation and layering of the cortical neurons occurs as neuronal migration ceases. The first steps in cortical organisation accompanying the axonal ramification are the appearance of synaptic elements, the development of neurofibrils, and an increase in size of the endoplasmatic reticulum within the cytoplasm (Evrard et al. 1992; Marina-Pallida 1998). The biochemical

correlates of these changes are increasing cerebral content of ribonucleic acid and protein relative to DNA. The maturational changes happen relatively rapidly in the hippocampus compared to supra-limbic areas. Dendritic development occurs earlier in the thalamus and brainstem than in cerebral cortical regions (Takashima et al. 1990; Mojsilovic et al. 1991).

Strikingly active axonal development in the cerebrum over the last trimester and early postnatal period was demonstrated by immunostaining with GAP-43, a protein expressed on growing axons. Exuberant expression of GAP-43 was demonstrated in the cerebral WM to the subplate region at 20 weeks reflecting the growth of axons from the thalamus to the subplate; to the cortex at 27 weeks showing axons growing from the subplate to the cerebral cortex. GAP-43 positive staining in the cortex from 37 weeks until the end of the first year of birth may reflect the increase in cortical penetration of thalamo-cortical afferents, cortico-cortical fibres and descending cortical fibres, initially pioneered in the subplate axons (Haynes et al. 2005).

The progress of dendritic differentiation depends on the establishment of afferent inputs and synaptic activity. Initial axonal growth is facilitated by neural cell adhesion molecule and neuronal cadherin, which are glycoproteins located on the cell surface (Takeichi et al. 1988). An extracellular matrix protein, laminin, stimulates axonal extension and guidance. Laminin interacts with axonal surface glycoproteins, integrins, which guide axons through the developing brain to specific sites (Dodd and Jessell 1988). Neuronal activity initiates its effects on dendritic development by inducing calcium influx that will result in a direct effect on the actin, microtubular components of the cytoskeleton and adhesion molecules, and in an indirect effect of

activating multiple signalling pathways (Volpe 2008). These developmental changes are accompanied by a fourfold increase in cerebral cortical volume between 28 and 40 weeks gestation as shown by quantitative MRI measurements (Kapellou et al. 2006).

Synaptic formation differs among regions in the human brain. From fifth month of gestation dendrites appear as thick processes with only a few fine spicules. As development progresses a great number and variety of dendritic spines appear. Synapse elimination then begins and approximately 40% of the synapses will be lost. The synaptic formation is stimulated by activity-independent factors, such as molecular mechanisms involved in targeting, followed by activity-dependent events occurring after the development of receptors on target neurons and the generation of electrical activity (Goodman et al. 1993; Johnston et al. 1995; Flint et al. 1998; Ethell et al. 2005).

After formation of synapses by 'progressive processes' of proliferation and migration, a programmed cell death occurs (Huttenlocher et al. 1982; Narayanan 1997; Rakic and Zecevic 2000; Kinney et al. 2002) initiated by caspases (Bergeron et al. 1998). Although variable in degree among regions, typically about half of the neurons in a given area die before final maturation. This loss of neurons happens to quantitatively match the interconnecting populations of neurons and eliminate the aberrant or otherwise incorrect populations (Cowan et al. 1984; Oppenheim 1991; Ferrer et al. 1992; Allsopp et al. 1993). Neural organisation is refined further by a second regressive event, the selective elimination of neuronal processes and synapses to remove terminal axons and their synapses; however larger-scale elimination of total pathways also occurs (Volpe 2008). Apoptosis and selective synaptic elimination are

determined by activation of the N-methyl-D-aspartate (NMDA) type glutamate receptors (Rabacchi et al. 1992).

Astrocyte and oligodendroglia progenitors are principally subventricular cells and radial glial progenitors. Their proliferation occurs at their sites of origin and locally during and after migration. Astrocytes are generated before oligodendrocytes. The progression of oligodendroglia lineage proceeds through four stages: oligodendroglia progenitor, preoligodendrocyte, immature and mature oligodendrocyte (Back et al. 1997, 2001, 2002; Porter et al. 2000; Nguyen 2006; Yue et al. 2006). The preoligodendrocyte is the predominant oligodendroglia before term age and it accounts for ninety percent of total oligodendroglia population until twenty-eighth week of gestation. The preoligodendrocyte differentiates into post-mitotic immature oligodendrocyte. The ratio of immature oligodendrocytes gradually increases to about 50% at term age. In the third trimester the immature cells develop linear extensions as they wrap around axons in preparation for myelination. This process is followed by differentiation to the mature oligodendrocyte, which becomes the predominant oligodendroglia stage in months following term and gives rise to myelination (Volpe 2008).

Microglia originates from bone marrow-derived monocytes (Kinney et al. 2002). Microglial cells entry from the circulation to the ventricular and subventricular zones. Migration of microglia progenitors proceeds through the cerebral WM during middle to late gestation and then to cortex near term. The cerebral WM is heavily populated with activated microglia during a period when developmental events are active and a variety of insults can lead to WM injury (Gould et al. 1991; Rezaie et al. 2002, 2005).

2.5.6 Myelination

Myelin is a specialisation of the plasma membrane of glial cells (Volpe 2008). Myelin is organised as multiple spiral and compacted layers. It is composed of 40% water, 40% lipid bilayer, primarily galactocerebrozid, as well as cholesterol and phospholipids, and 20% of proteins, including myelin basic protein, myelin oligodendrocyte glycoprotein, and proteolipid protein. Sphingomyelin chain serves to strengthen the myelin sheath (Arroyo 2000). Myelin is essential for normal brain function. It increases the nerve pulse transmission rate, promotes saltatory action potential conduction and protects axons from damage. Fast signal propagation requires the restriction of action potentials to short axonal segments, termed the nodes of Ranvier.

Myelination is characterised by the acquisition of highly specialised myelin membrane around the axons. This process begins during the second trimester and continues into adulthood (Bunge 1968; Gilles et al. 1983; Kinney et al. 1988, 2002).

Myelination is considered as a two-phase process. First oligodendroglia proliferation and differentiation; then myelin deposition occur around axons. Myelination begins in the peripheral nervous system, where motor roots myelinate before the sensory roots. From around term age myelination of the central nervous system begins in the brainstem and cerebellum. Myelination in central sensory systems precedes that in central motor systems. Myelination within the cerebral hemispheres, particularly those regions involved in higher-level associative and sensory functions, occurs well after birth and progresses over decades. Generally, proximal pathways myelinate before distal, projection pathways before associative, central cerebral sites before

cerebral poles and occipital areas before fronto-temporal regions (Yakovlev et al. 1967; Brody et al. 1987; Kinney et al. 1988, 2002). As myelination progresses the amount of water in the brain reduces, which might be due to the development of the hydrophobic inner lipid layer of the myelin sheath (Dobbing and Sands1973).

The central fibres of the vestibular and cochlear systems myelinate first. At 20 weeks myelin is evident in the medial longitudinal fasciculus, the tectospinal tract, the trapezoid body, the lateral lemniscus and the inferior colliculi. The medial lemniscus myelinates at 22 weeks. Myelination of the vestibulocochlear portion of the inferior cerebellar peduncles takes place between 20 and 26 weeks. The spino-, olivo-, and reticulo-cerebellar fibres begin to myelinate at 28 weeks and complete the myelination cycle by around 3 months post-term. In the superior cerebellar peduncles the cerebello-reticular and bulbar fibres myelinate first followed by fibres of the mesencephalon and red nuclei from 26 to 28 weeks. Myelination of these fibres continues until about 8 months. The middle cerebellar peduncles myelinate between term and 4 years of age. Of the sensory fibres the medial geniculate nuclei begin to myelinate around 24 to 28 weeks and complete myelination about 4 months post-term. The optic nerve and tracts of the superior colliculi and lateral geniculate nuclei begins at 36 weeks and is complete by 3 months. The inner segment of the globus pallidus starts myelinating before the outer segment at 28 weeks. The PLIC does not begin to myelinate until 32 to 36 weeks, followed by the ALIC. Myelination is evident in the corticospinal tracts (CST) of the pre- and post-central gyri between 36 and 40 weeks. The corpus callosum and optic radiations start myelinating at 6 and 8 weeks post-term respectively (Yakovlev et al. 1967; Gilles 1976; Brody et al. 1987; Kinney et al. 1988, 2002).

2.6. Hypoxic-Ischaemic Encephalopathy

2.6.1 Neonatal encephalopathy

Neonatal encephalopathy (NE) is a heterogeneous syndrome characterised by signs of central nervous system dysfunction, affecting mainly term infants. The terminology does not imply a specific underlying aetiology, rather it is a clinically defined syndrome manifested by difficulty with initiating and maintaining respiration, abnormal tone, reflexes and level of consciousness, feeding difficulties and often seizures (Nelson et al. 1991; Badawi et al. 1998). NE occurs in approximately 3-6 infants in every 1000 live births. Earlier, NE was automatically attributed to a hypoxic-ischaemic insult (Ferriero 2004). However, it is not always possible to document significant perinatal hypoxia and it is now known that hypoxia-ischaemia is only one of the many possible contributors to NE. Therefore, it is important to exclude intracranial and intracerebral haemorrhage, focal cerebral infarction, vascular abnormality, metabolic disorder, hyperbilirubinaemia, cerebral tumor, drug exposure, central nervous system infection and malformation as other possible causes of NE.

In a large cohort of infants with a history of NE, pre-labour maternal conditions that might have contributed to the risk of NE were identified in one-third of the cases. Pre-labour foetal conditions, such as small for gestational age or congenital malformations, were present in 25% of the infants. Two-thirds of the subjects with NE were delivered by surgical delivery, which was associated with over a twofold increased risk of NE, whereas there was an inverse relation with elective caesarean section. The foetal heart rate monitoring was described as abnormal in two-thirds of the infants with NE compared with one-third of the control neonates. In about 25% of

the cases both ante- and intrapartum risk factors could be identified. Postnatal complications, such as respiratory distress, sepsis or shock were present in less than 10% of the infants with NE (Badawi et al. 1998; Nelson et al. 2012; Pfister et al. 2012).

2.6.2 Hypoxic-ischaemic encephalopathy of the newborn

Only a small proportion of infants with a history of NE have documented exposure to an acute intrapartum hypoxic-ischaemic sentinel event (Higgins et al. 2006; Volpe 2008; Pfister et al. 2012). In a study of infants with HIE documented sentinel events included uterine rupture, placental abruption, prolapsed cord and ante-partum haemorrhage due to placenta praevia (Okereafor et al. 2008).

HIE occurs in 1 of every 1000 live full-term births in the developed countries (Pierrat et al. 2005; Vanucci et al. 1997), however the incidence is much higher in the developing world. It is estimated by the World Health Organisation that about 4 million newborns suffer moderate or severe asphyxia each year in the developing countries (Lawn et al. 2005). There is a trend towards a higher prevalence of asphyxia in Africa than in Asia (Ellis and Manandhar 1999).

2.6.3 Pathophysiology of perinatal asphyxia

Hypoxia refers to reduction of oxygen supply of a tissue below physiological levels, despite adequate perfusion of that tissue. Ischaemia refers to insufficient blood supply to the tissue which compromises both oxygen and substrate delivery. The term asphyxia describes the pathological changes of compromised or ceased placental or pulmonary gas exchange resulting in both hypoxia and hypercarbia with metabolic

acidosis. HIE is the abnormal neurological behaviour of the neonate arising as a result of a perinatal hypoxic-ischaemic event.

The primary pathophysiological causes of HIE are brain hypoxia and ischaemia. With prolonged systemic hypoxia cardiac hypoxia occurs, leading to diminished cardiac output and, ultimately to reduced CBF and brain ischaemia (Grow and Barks 2002; Ferriero 2004; Perlman 2004). Thus, brain injury resulting from asphyxia is the consequence of ischaemia superimposed on hypoxia. A hypoxic-ischaemic event initially causes an increase in blood flow to certain organs, such as the brain, heart and adrenal glands. This is accompanied by redistribution of the cardiac output and an increase in the blood pressure due to increased release of adrenaline.

In adults, cerebral autoregulation ensures that CBF is maintained at a constant level despite wide range of changes in blood pressure. Limited data in the human foetus and newborn suggest that CBF is stable over a much narrower range of blood pressure (Papile et al. 1985; Rosenkrantz et al. 1988). In the perinatal period once the early compensatory mechanism fails, the CBF becomes pressure-passive and brain perfusion will be dependent on the systemic blood pressure. As the blood pressure falls, the CBF falls below a critical level, and brain injury secondary to diminished blood supply and lack of sufficient oxygen occurs. Depletion of oxygen leads to a switch to anaerobic metabolism resulting in depletion of high energy phosphate reserves, accumulation of lactic acid and the inability to maintain cellular functions (Perlman et al. 2004). This leads to intracellular energy failure (Figure 2.6.1). The magnitude of the final neuronal damage depends on the duration and the severity of the initial insult combined with the effects of reperfusion and cell death.
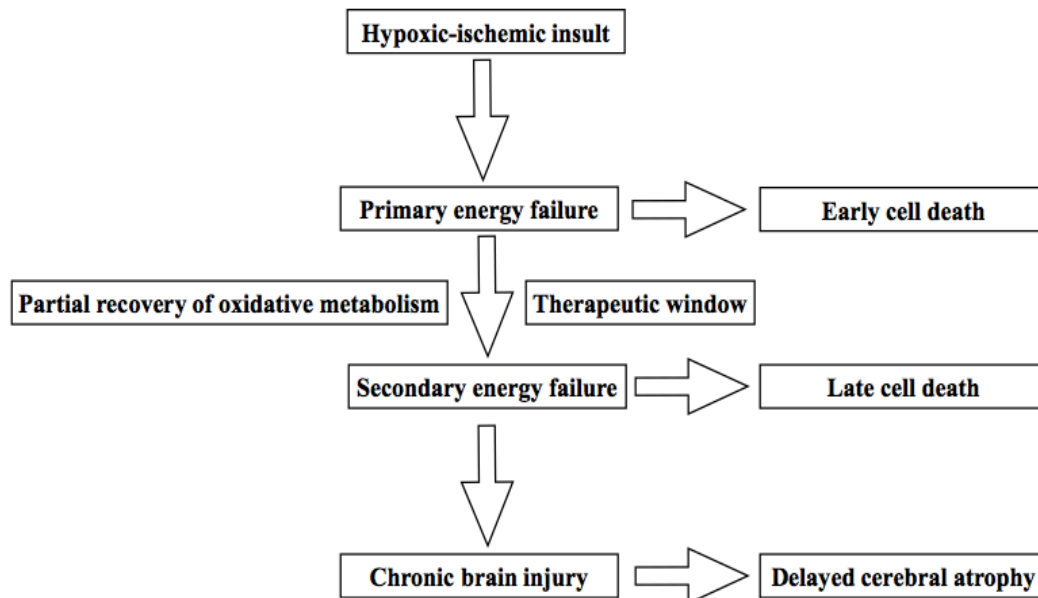
Figure 2.6.1: Schematic representation of sequence of events following a hypoxic-ischaemic insult.

2.6.3.1 The primary phase

At the biochemical level cerebral hypoxia-ischaemia leads to an impaired uptake of the major excitatory neurotransmitter, glutamate. It results in high synaptic levels of glutamate and eventually excitatory amino acid (EAA) receptor, such as NMDA, amino-3-hydroxy-5-methyl-4 isoxazole propionate (AMPA) and kainate, over-activation. NMDA receptors are permeable to calcium and sodium, while AMPA and kainate receptors are permeable to sodium. Accumulation of sodium and failure of energy dependent enzymes, such as sodium/potassium ATPase, lead to cytotoxic oedema and necrotic cell death. Activation of NMDA receptors, along with release of calcium from the intracellular stores and failure of the calcium efflux mechanisms lead to intracellular calcium accumulation and contribute to the escalating pace and extent of programmed cell death through secondary calcium intake into the cells. Consequences of increased intracellular calcium concentration include activation of

phospholipases, endonucleases, proteases and nitric oxide synthase (NOS). Activation of phospholipase A2 leads to release of calcium from the endoplasmatic reticulum through activation of phospholipase C. Activation of proteases and endonucleases results in cytoskeletal and DNA damage. During reperfusion enzymes, such as cyclooxygenase, xanthine oxidase, and lipoxygenase are activated resulting in free radical production. Immature antioxidant defences of the neonate exacerbate free radical damage. Free radicals cause lipid peroxidation, DNA and protein damage and trigger apoptosis. They also combine with NO to form a highly toxic oxidant, peroxynitrite (Fellman and Raivio 1997).

Inflammatory mediators have been implicated in the pathogenesis of HIE and may represent a final common pathway of brain injury. Inflammatory cytokines are significantly elevated in term infants who later develop cerebral palsy (Damman et al. 2008). High levels of interleukin (IL) 6 and IL-8 in the CSF of term neonates have been correlated with a more severe encephalopathy and adverse neurodevelopmental outcome (Savman et al. 1998).

2.6.3.2 The delayed phase

Experimental and clinical observations suggest that perinatal asphyxia is not a single event, but rather an evolving process. Although neurons may die during the actual hypoxic-ischaemic event (primary cell death), many neurons initially recover at least partially from the primary insult, only to die later secondary to delayed cell death (Gunn and Thoresen 2006). The longer and more severe the insult, generally the greater proportion of neurons dies due to primary cell death. Following reperfusion the initial hypoxia-induced cytotoxic oedema and accumulation of EAAs typically

resolve over 30 to 60 minutes, with at least partial recovery of cerebral oxidative metabolism, in the latent phase (Vanucci et al. 1997) (Figure 2.6.2).
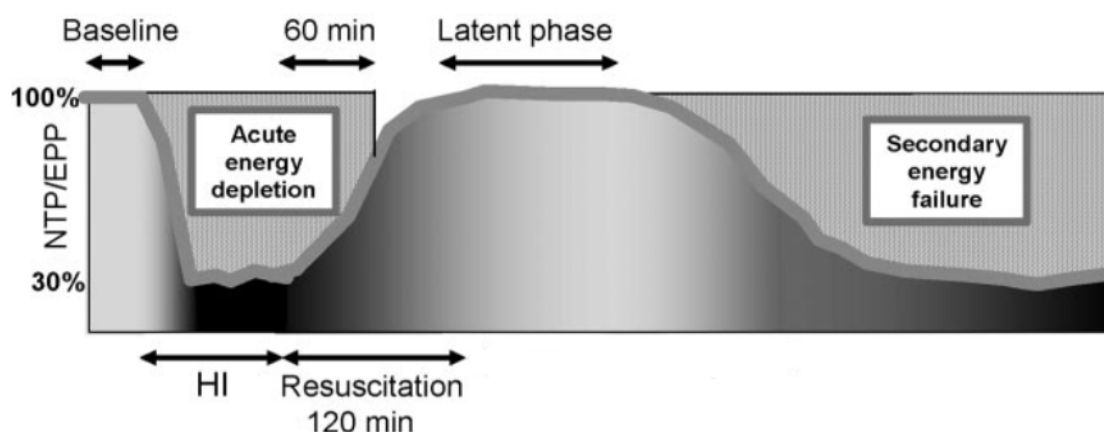
Figure 2.6.2: Schematic diagram of energy failure associated with a transient hypoxic–ischaemic insult visualised using [31]Phosphorus MR spectroscopy. *Y axis: nucleotide triphosphate (NTP)/exchangeable phosphate pool (EPP) (EPP = Inorganic Phosphate + Phosphocreatine + NTP); X axis: time. The change in NTP/EPP during transient hypoxia–ischaemia (HI), resuscitation, the latent phase and secondary energy failure are shown (From Kelen and Robertson 2010).*

Despite adequate oxygenation and circulation, a secondary phase of impaired cerebral energy generation ensued 8 to 24 hours after the hypoxic-ischaemic event, characterised by progressive decline in phosphocreatine and nucleotide triphosphate and increased inorganic phosphate levels (Hope et al. 1984). This sequence of events was modelled experimentally and termed 'secondary energy failure' (Lorek et al. 1994) (Figure 2.6.2). This phase is marked by secondary cytotoxic oedema, accumulation of cytokines, mitochondrial failure and the onset of seizures. Mitochondrial failure is a key step leading to delayed cell death. Microglia was

110

suggested to contribute to the secondary neuronal injury through the production of pro-inflammatory cytokines, proteases, reactive oxygen species, NO and complement factors.

It was demonstrated in a piglet model of perinatal asphyxia that more severe cerebral energy depletion during transient hypoxic-ischaemia leads to shorter latent phase, worse secondary energy failure and more extensive neuronal death. Latent phase duration showed significant correlation with secondary energy failure severity and the eventual extent of neuronal injury. Latent phase duration was proved to be shorter for more severe insults (Iwata et al. 2007). Latent phase provides a window of opportunity to initiate neuroprotective treatments to reduce brain injury.

Two morphologic patterns of delayed cell death have been described: necrosis and apoptosis. Necrosis is defined by the loss of plasma membrane integrity associated with a random pattern of DNA degradation accompanied by swelling of the cytoplasm and organelles. Apoptosis is the form of active cell death, involving a cascade of 'suicide' processes. It is defined by shrinkage of the cell, 'karyohexis', associated with DNA degradation. Eventually the shrunken cell breaks into small fragments. Both types of neuronal death were identified in infants with perinatal asphyxia (Edwards et al. 1997; Scott and Hegyi 1997).

2.6.4 Investigations

The diagnosis of HIE depends principally on information gained from a careful history and a thorough neurological examination. Certain metabolic parameters and evaluations, such as EEG and imaging studies help the diagnosis (Volpe 2008).

2.6.4.1 Perinatal history

Recognition of HIE requires awareness of those perinatal risk factors that may lead to perinatal asphyxia (Okereafor et al. 2008). Certain maternal disorders, foetal factors, and disturbances of labour and/or delivery that could potentially lead to utero-placental insufficiency, impair placental respiratory gas exchange or blood flow should be sought for (Nelson et al. 2012).

2.6.4.2 Biochemical markers

A cascade of biochemical reactions occurs during and after a hypoxic-ischaemic event. Changes in biochemical markers are useful methods for monitoring the progress of HIE. However, the majority of these markers assess the total body effects of asphyxia rather than just those affecting the brain. Biochemical markers reported in the literature focus on changes in energy states (foetal scalp or cord blood pH, lactate, base excess), hormonal responses (vasopressine, erythropoietin, insulin) or brain-based proteins (neuron specific enolase, myelin basic protein) (Volpe 2008).

2.6.4.3 Clinical symptoms

Recognition of clinical signs provides critical information regarding the presence, site, and extent of a hypoxic-ischaemic brain injury. Term infants exposed to a perinatal hypoxic-ischaemic event usually show a definite and often predictable sequence of neurological symptoms and signs. HIE was originally described by Amiel-Tison (Amiel-Tison 1969) and numerous scoring systems have been developed since, such as the post-asphyxia score (Lipper et al. 1986) and the neonatal behavioural neurological assessment (Bao et al. 1993). Sarnat and Sarnat devised a method for detailed description of progression of symptoms combined with EEG

(Sarnat and Sarnat 1976). However, administration of the Sarnat and Sarnat scoring system takes time and requires training, therefore a simplified version, the Thompson Score was developed, which correlates well with the Sarnat and Sarnat score, but is easier to administer (Thompson et al. 1997).

2.6.4.4 Electroencephalography

Amplitude-integrated electroencephalography (aEEG) is a method for continuous monitoring of brain function. The method is based on filtered and compressed EEG that enables evaluation of long-term changes and trends in electro-cortical background activity by relatively simple pattern recognition. Cerebral function monitor is a portable electronic device that records bipolar cortical electrical signals derived from two parietal scalp electrodes. During the first few hours of birth, continuous aEEG monitoring recorded bedside is a suitable method to assess the severity of HIE in newborns (van Rooij et al. 2005; de Vries et al. 2006 a; Hellstrom-Westas et al. 2006).

Two classification systems have been developed to interpret aEEG. The semi-quantitative method defines three categories of normal, moderately and severely abnormal patterns in term infants (Al Naqeeb et al. 1999). The classification is based on the amplitude assessed by measuring the upper and lower margins of the trace (Al Naqeeb et al. 1999). The other classification system is based on pattern recognition relative to normative data for different gestational ages (Viniker et al. 1984; Verma et al. 1984; Thornberg et al. 1990; Burdjalov et al. 2003; Tekgul et al. 2005). It describes the dominating type of background activity, the presence or absence of sleep-wake cycling as well as the presence of seizures (Hellstrom-Westas et al. 2006).

In many centres aEEG is part of the clinical evaluation to assess eligibility of infants for hypothermic neuroprotection (Shankaran et al. 2005; Azzopardi et al. 2010), as well as eligibility for clinical studies of additional neuroprotective therapies after a hypoxic-ischaemic insult.

Amplitude-integrated EEG has a high specificity, sensitivity, positive (PPV) and negative predictive value (NPV) for predicting outcome in infants with HIE (Leijster et al. 2007b; El-Ayonty et al. 2008; Thoresen et al. 2010; Vasiljevic et al. 2012). However, the predictive value of an abnormal aEEG background is reduced in infants who received therapeutic hypothermia (Thoresen et al. 2010). Amplitude-integrated EEG background activity correlates with conventional MRI findings (Leijster et al. 2007b; El-Aytony et al. 2008).

Multichannel EEG is part of the clinical evaluation of infants with HIE. In some cases serial EEGs are obtained to assess seizure control and evolution of background abnormalities. Multichannel EEG and aEEG correlate well, especially for normal and severely abnormal traces (Murray et al. 2010). Although prediction of outcome with aEEG is reliable, it is less accurate than multichannel EEG (Murray et al. 2010).

2.6.4.5 Neuroimaging

2.6.4.5.1 Cranial ultrasound

Cranial ultrasound scan has several advantages in evaluating infants with HIE. It is a bedside tool that can be performed even on clinically unstable neonates. A cranial ultrasound scan performed on admission is useful to document that there are no other

changes that may account for the symptoms (de Vries et al. 2006 b; Leijser et al. 2007a).

Cerebral oedema, intraparenchymal, intraventricular haemorrhage and cystic lesions may be identified with cranial ultrasound scan. Using appropriate transducers, echo densities within the basal ganglia and thalami (BGT), cortical highlighting and infarction in the subcortical WM may be visualised (Eken et al. 1994; 1995; Leijser and Cowan 2007). Lesions identified with ultrasound scan in the thalamus, cortex and periventricular WM correlate to histological findings (Eken et al. 1994).

Doppler ultrasonography is a non-invasive method, which allows repeated and safe assessment of neonatal cerebral hemodynamics by measuring the Pourcelot's resistance index (Archer et al. 1986). The resistance index is usually measured in the anterior cerebral artery and is calculated from the measurement of peak systolic and end-diastolic velocity. A resistance index of < 0.55 has a high PPV and NPV for death or disability (Archer et al. 1986). An abnormally low resistance index in infants with severe HIE reflects cerebral vasodilatation and is suggested to be due to vasoparalysis or release of vasodilators (Pryds et al. 1990; Meek et al. 1999).

2.6.4.5.2 Magnetic resonance imaging
2.6.4.5.2.1 Conventional magnetic resonance imaging
Conventional MRI provides excellent details of the lesions characteristic of a perinatal hypoxic-ischaemic brain injury. The abnormalities identified on conventional MR images vary with sequence parameters used, postnatal age of the infant and the type

and severity of the insult (Rutherford et al. 1991, 1994, 1995; 2010, Mercuri et al. 2002, Cowan et al. 2003, Miller et al. 2005, de Vries et al. 2009).

A global hypoxic-ischaemic insult does not affect brain structures uniformly. The concept 'selective vulnerability' describes the phenomenon that certain cerebral tissues are more likely to be injured and injure earlier than others. Gestational age is important in terms of susceptibility of different cerebral structures. Below 20 weeks a hypoxic-ischaemic insult leads to neuronal heterotopia or polymicrogyria. An injury occurring between 26 and 36 weeks primarily affects the WM, leading to periventricular leukomalacia as the oligodendroglia, developing during this period, is uniquely susceptible to excitatory and free radical damage which lead to WM involvement. In term infants a hypoxic-ischaemic even most often results in grey matter damage, however the pattern of injury depends on the duration and severity of the insult. The deep grey matter has the highest concentrations of EAA receptors and is more susceptible to excitotoxic injury. Furthermore, the thalamo- and cortico-cortical excitatory circuitries are developing (Huang and Castillo 2008), and WM tracts are myelinating at this age, which explain the regional susceptibility of such brain areas. Because of the fundamental differences in the definition and neuropathological consequences of a hypoxic-ischaemic insult between preterm and term infants, this thesis discusses HIE concerning term infants.

2.6.4.5.2.1.1 Acute hypoxic-ischaemic insult

A short intense hypoxic-ischaemic episode, typically occurring during labour and/or delivery, results in a primarily central pattern of injury involving the deep grey matter. This pattern of injury can be explained by developmental aspects (active myelination

and developing thalamo-cortical, cortico-cortical circuitries), and by biochemical aspects (high concentration of EAA receptors). Central grey matter injury is usually accompanied by abnormalities in the PLIC. In severe cases there may also be brainstem involvement. In term born neonates with history of an acute hypoxic-ischaemic insult specific cortical regions may also be affected accompanied by involvement of the adjacent subcortical WM. This has been termed as central cortico-subcortical involvement (Roland et al. 1988; Barkovich et al. 1992; Rademaker et al. 1995; Mercuri et al. 2002; Cowan et al. 2003; Miller et al. 2005; de Vries et al. 2009).

Basal ganglia and thalami

Neuropathological consequence of an acute hypoxic-ischaemic insult is diffuse necrosis in the BGT. When the thalamus is selectively affected, the injury is usually frank infarction with or without haemorrhage (Pasternak and Gorey 1998).

The severity of BGT lesions as assessed on conventional MRI can be graded. Mild lesions are focal, typically in posterior position with normal signal intensity of the PLIC. Moderate lesions are focal involving the posterior and lateral lentiform nucleus and lateral thalamus with an equivocal or abnormal PLIC. In severe injury the involvement is diffuse, extending into the midbrain and the mesencephalon. In such cases the signal intensity in the PLIC is always abnormal. On conventional MRI abnormal signal intensity within the BGT is the most obvious by 2 weeks. In cases of severe injury, a focal or diffuse atrophy with or without cyst formation can be observed. Infants with multifocal or diffuse lesions within the BGT also have progressive WM atrophy (Rutherford 2002). However, in mild to moderate cases signal intensity in the BGT normalises by 3 to 9 months.

The BGT are key areas of cognition, behaviour, locomotion, motor and postural control. Bilateral BGT lesions are associated with motor impairment and the extent of lesions is closely related to the severity of that impairment (Rutherford et al. 1996). Severe BGT injury is predictive of severe motor impairment at 2 years (Martinez-Biarge et al. 2011). In addition to motor problems, difficulties with feeding, speech, vision and cognition also occur in children with BGT lesions, as well as seizures (Martinez-Biarge et al. 2010).

Posterior limb of the internal capsule

The PLIC is often affected by an acute hypoxic-ischaemic insult. In those infants who died the PLIC was infarcted or oedematous on histological examination (Rutherford 2002).

On conventional MR images the signal intensity of the PLIC may apparently be normal if the scan is done early, as it takes few days to evolve following an acute insult. The signal may be abnormally high on T1 and abnormally low on T2 weighted images. The signal intensity may be equivocal (diminished or asymmetrical) before its loss. In association with the loss of normal signal intensity, abnormality in the lentiform nucleus is often observed. However, the normal signal intensity from myelin may return after few weeks depending on the severity of the injury. In presence of atrophy of the BGT, the tracts appear to be irreversibly damaged; the myelin looks irregular and discontinuous (Rutherford 2002).

Whilst lesions in the BGT are predictive of cerebral palsy, appearance of the PLIC predicts the ability of walking independently by 2 years (Rutherford et al. 1994; Martinez-Biarge et al. 2010; Martinez-Biarge et al. 2011).

Brainstem

Injuries to the brainstem are usually associated with concomitant lesions to the BGT. Brainstem involvement is more frequent with more severe BGT lesions. The most vulnerable structure is the inferior colliculus, due to its high metabolic rate. The reticular formation, lateral geniculate bodies, and pontine nuclei may also be involved (Levene 2002; Rutherford 2002).

Lesions in the brainstem, consistent with infarction are of low signal intensity on T1, and high signal intensity on T2 weighted images. Diffuse changes appear as abnormal widespread high signal on T1 and low on T2 weighted images with marked asymmetries and/or atrophy on later scans. Moderate changes are sometimes transient; including loss of anatomical details, excessive differentiation between the anterior and posterior pons, focal areas of abnormality and mild asymmetries (Rutherford 2002; Martinez-Biarge et al. 2010). The presence and severity of the brainstem injury is a good predictor of death in the neonatal period and later (Martinez-Biarge et al. 2010).

Cortex

In acute stages of HIE, the cerebral cortex may appear normal, however within a week it may show grey-brown discoloration, gyral sclerosis with widening of the sulci. Due to differences in metabolic rate (Farkas-Bargeton and Diebler 1978),

microscopically layers III and V are preferentially involved; with II being relatively preserved (Larroche 1984). The pyramid cells of the hippocampus are particularly vulnerable (Larroche 1977). Other areas, such as somatomotor and visual cortices are also often involved (Larroche 1984).

Following a perinatal hypoxic-ischaemic insult, the cortex around the central sulci, the interhemispheric fissure and the insula may show abnormal highlighting as abnormal high signal on T1, and abnormal low signal on T2 weighted images. The depth of the sulci is more often affected. Cortical highlighting may take several days to develop, with maximum intensity during the second week after the insult, when abnormal signal intensity in the adjacent subcortical WM may also appear consistent with ischaemic damage, which then proceeds to break down and atrophy (Rutherford et al. 2010).

Cortical highlighting is usually associated with other cerebral lesions in the brain and therefore it is difficult to identify specific neurodevelopmental sequel. Widespread highlighting has been associated with the development of a spastic diplegia, microcephaly and intellectual deficit, partly due to the associated WM involvement (Rutherford 2002).

Cerebral oedema

Brain oedema has been classified into two types: cytotoxic and vasogenic. Cytotoxic oedema is due to the failure of cellular membrane pumps allowing entry of sodium into the cells resulting in swelling. In the case of vasogenic oedema the blood-brain barrier is leaking, allowing entry of serum proteins into the cerebral parenchyma.

Osmotic pressure results in accumulation of fluid within the extracellular compartment of the brain. Cytotoxic oedema occurs earlier and may affect the grey matter in preference to the WM (Klatzo 1985). Later, the blood-brain barrier opens to proteins and vasogenic oedema develops. Although, brain swelling does not reach its maximum until about 48 hours following the sentinel event (Anderson and Belton 1974), even if severe, usually disappears by the second week (Rutherford 2002).

The signs of brain swelling are best identified on T1 weighted images. Loss of extra-cerebral space and sulcal markings, closure of the Sylvian fissures, narrow interhemispheric fissure and slit-like anterior horns of the lateral ventricles suggest brain swelling. It may be accompanied by loss of anatomical details, especially loss of grey WM differentiation. Swelling is likely to represent oedema, however it is not easy to differentiate between the two types, vasogenic and cytotoxic on conventional images. Areas of cytotoxic oedema with impending tissue breakdown appear on diffusion weighted images during the first week of birth.

Although cerebral oedema makes assessment of the brain more difficult, if the brain is otherwise normal in appearance once the swelling disappeared, the outcome is good (Rutherford 2002).

2.6.4.5.2.1.2 Partial hypoxic-ischaemic insult

Episodes of prolonged foetal hypoxia result in shunting of the blood to vital brain structures, such as the brainstem, BGT, hippocampus and cerebellum, meanwhile metabolically less active structures, such as the cerebral cortex and WM, are more likely to be affected. Prolonged, partial asphyxia with repetitive insults causes injury

to the inter-vascular boundary resulting in 'watershed-predominant' pattern, sometimes with parasagittal distribution. If the hypoxic-ischaemic insult is more severe the overlying cortex in the vascular watershed zones is also affected (Levene 2002; Leijser et al. 2007b; Huang and Castillo 2008). The lesions can be uni- or bilateral, predominantly posteriorly or anteriorly located with loss of grey WM differentiation on conventional images (Leijser et al. 2007b). Follow-up scans often reveal cystic evolution, atrophy or gliosis (Rutherford et al. 1994). WM injury is often triggered by other risk factors, such as cardiovascular instability, hypoglycaemia or infection (Barkovich 1998; Traill et al. 1998; Yokochi et al. 1998; Kinnala et al. 1999; Murakam et al. 1999; Back et al. 2006; Li et al. 2009). Neonates with HIE and history of decreased foetal movements tend to sustain WM injury either in isolation or in combination with BGT lesions (Martinez-Biarge et al. 2012). The injured WM may subsequently atrophy leading to microcephaly. WM injury due to a hypoxic-ischaemic insult also affects thalamo-cortical connectivity and leads to atrophy of grey matter (Govaert et al. 2008).

Moderate WM abnormalities are associated with relatively good outcome. However, severe WM infarction leads to cognitive delay communication, behavioural problems, visual impairment and seizures (Mercuri et al. 2000; Cowan et al. 2003; Martinez-Biarge et al. 2012). However, cognitive and memory problems may not be apparent until school age (Gonzalez et al. 2006; de Vries and Jongmans 2010).

2.6.4.5.2.2 Diffusion magnetic resonance imaging

Diffusion MRI is an excellent tool to study brain injury early following a hypoxic-ischaemic event. Visual assessment of diffusion MRI may be inconclusive (Forbes et

al. 2000); however, early detection of brain injury is improved by calculating objective measures to verify diminished diffusion.

Compared to healthy term controls significantly lower ADC values were found in the PLIC, corona radiata, posterior-frontal and parietal WM within 12 days of birth in subjects with HIE (Wolf et al. 2001). ADC values in the PLIC and putamen, regions often affected by a perinatal hypoxic-ischaemic event, correlated with perinatal clinical data as assessed by the Apgar score at 5 minutes (Brissaud et al. 2010).

Several studies investigated the predictive value of DWI for subsequent outcome following HIE. The presence of normal findings on both DWI and conventional MRI was predictive of a normal neuromotor outcome (Khong et al. 2004). Visual appearances of the BGT (Liauw et al. 2009; Twomey et al. 2010), WM (Twomey et al. 2010) and brainstem (Liauw et al. 2009) on diffusion weighted images associated with outcome at 2 years (Twomey et al. 2010) and at school age (Liauw et al. 2009). Furthermore ADC values measured in the PLIC and BGT correlated to neurodevelopmental performance scores at 1 and 2 years of age (Hunt et al. 2004; Vermulen et al. 2008; Twomey et al. 2010).

However, ADC may underestimate the eventual lesion load within the BGT as visualized on later conventional imaging (Rutherford et al. 2004). Furthermore the utility of ADC measurements in HIE is limited due to pseudonormalisation. Pseudonormalisation was first described in adult patients with stroke (Sotak et al. 2002) and it was also observed in infants with perinatal stroke (Rutherford et al. 2004) and HIE. ADC is typically reduced during the first week of the injury, then returns to

normal and increases further after about 2 weeks; hence postnatal age at scanning must be taken into account when evaluating ADC values (Wolf et al. 2001; McKinstry et al. 2002; Hunt et al. 2004; Rutherford et al. 2004; Winter et al. 2007; Liauw et al. 2009). In infants with HIE pseudonormalisation occurs around 8-10 days (McKinstry et al. 2002; Rutherford et al. 2004; Boichot et al. 2006; Winter et al. 2007). Therefore abnormally decreased ADC values may be evident to almost 7 days, however abnormally elevated values may not be apparent until late in the second week of birth. Pseudonormalisation limits the absolute sensitivity of ADC; however by the time it occurs, lesions are usually more obvious on conventional images (Ward et al. 2006).

Unlike ADC, FA values do not pseudonormalise. In infants with moderate and severe BGT and WM lesions as assessed by visual inspection of conventional MRI, FA values decreased throughout the first and continued to decrease during the second week of birth (Ward et al. 2006). On serial diffusion tensor images at 1 and 12 weeks of age, a significant difference was demonstrated in age-related FA increase and MD decrease in WM and subcortical grey matter between infants with HIE and healthy term controls (Malik et al. 2006). Such alterations in WM structure as assessed with FA persist into adolescence (Nagy et al. 2005).

FA is also predictive of outcome. FA in the PLIC and cerebral peduncles correlated to early neurological function as assessed by the Amiel-Tison scores (Amiel-Tison 1986; Brissaud et al. 2010), meanwhile FA values measured in the CST correlated to motor scores as assessed by the Bayley Scales of Infant Development test (Bayley 1966) at 3 months (Malik et al. 2006).

As therapeutic hypothermia is now the standard care for infants with HIE, it is important to evaluate how hypothermia affects diffusion parameters. As it was discussed in 2.2.1 the diffusion coefficient of a medium depends on several factors including the temperature of the environment. As per the Stokes-Einstein equation [2.2.2] the diffusion coefficient increases with temperature, due to the increased thermal energy of the molecules. Diffusion measurements during the cooling period are expected to be lower, than those obtained at normal body temperature (Le Bihan et al. 1989). However, in most of the studies as well as in clinical settings infants are imaged following rewarming, under normothermic conditions.

Therapeutic cooling does not influence the predictive value of diffusion MRI for subsequent outcome. FA in infants who underwent hypothermia was predictive of conventional MRI findings (Lee et al. 2012). Visual appearance of the PLIC and BGT on diffusion MRI, and MD in the putamen following hypothermia correlated with outcome at 2 years (Artzi et al. 2011; Cheong et al. 2012). In neonates, who received selective brain cooling as part of the Coolcap trial (Gluckmann et al. 2005), the volume of acute injury in the corpus callosum on diffusion weighted images was associated with developing epilepsy (Mulkey et al. 2012).

However, therapeutic hypothermia alters diffusion parameters. Infants who received therapeutic hypothermia were less likely to have abnormal diffusion parameters in cerebral regions that are often affected by a hypoxic-ischaemic insult (Artzi et al. 2011; Cheong et al. 2012). Furthermore, hypothermia delays the timecourse of evolution of MD. Pseudonormalisation takes place at approximately 12 days in

infants who underwent cooling compared 8 to 10 days in infants treated with normothermia (Figure 2.6.3) (Bednarek et al. 2012).
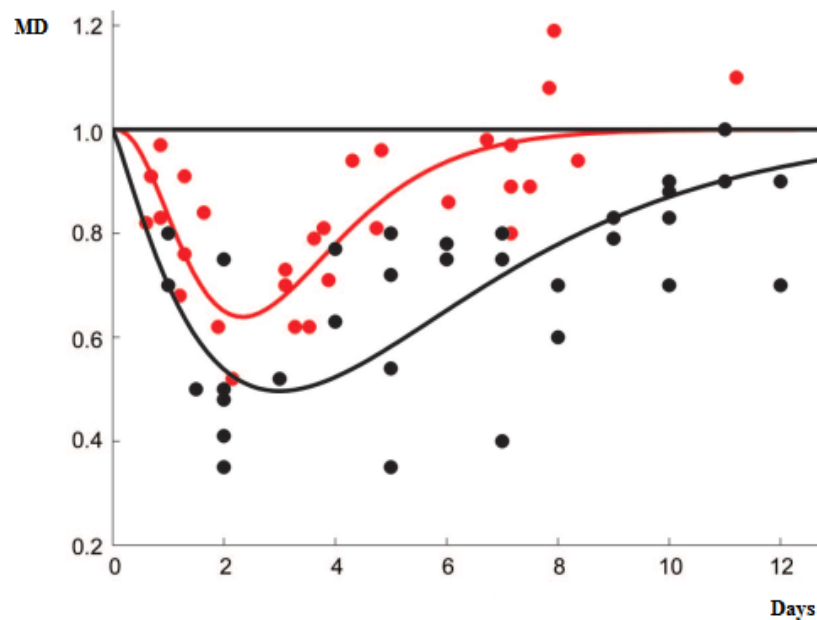
Figure 2.6.3: Pseudonormalisation of mean diffusivity (MD) values following a perinatal hypoxic-ischaemic event in infants treated with normothermia (red) and hypothermia (black). *X-axis: time after birth in days; Y-axis: MD ratio. (From Bednarek et al. 2012)*

2.6.4.5.2.3 Magnetic resonance spectroscopy

MRS enables *in vivo* quantitative analysis of cerebral metabolites. MRS extracts information about chemicals that reside on the frequency scale between water and fat, in both qualitative and quantitative manner, using principles of MRI. However, instead of generating an image, a plot representing chemical composition of a region is produced. Chemical information is displayed as the 'position' of the peaks on the x axis in parts per million (ppm). The ppm is calculated by dividing the difference of two peaks in frequency by the operating frequency of the scanner.

126

Following perinatal asphyxia [31]Phosphorus and proton MRS have been used to study cerebral metabolism, including the biphasic pattern of impaired cerebral energy metabolism (Figure 2.6.2) (Hope et al. 1984; Hamilton et al. 1986; Azzopardi et al. 1989). A close relationship was observed between the severity of cerebral energy impairment assessed by [31]Phosphorus MRS during the first week of birth and brain growth and short-term neurological outcome in infants (Azzopardi et al. 1989; Roth et al. 1992; 1997).

Most MRS studies use proton MRS, as the greater sensitivity of the hydrogen nucleus allows more accurate regional measurements (Azzopardi and Edwards 2010). Within the proton MR spectrum, peaks can be assigned using appropriate scanning parameters to N-acetyl aspartate, choline-containing compounds, creatine plus phosphocreatine, lactate, myoinositol, alanine, glutamine and glutamate. N-acetyl aspartate is a marker of neuronal integrity. Its level decreases with loss or damage to neuronal tissue. Choline is associated with membrane turnover. Its level increases in both cell division and membrane breakdown. Creatine and phosphocreatine are markers of brain energy metabolism that decrease with major neuronal cell death. The presence of lactate as a doublet indicates anaerobic glycolysis that might be due to hypoxic-ischaemia, mitochondrial disorder or tumor. Myoinositol, a glia cell marker, is a product of myelin breakdown. Glutamine and glutamate are excitatory neurotransmitters.

Characteristic changes in peaks of proton spectra observed in infants with HIE are consistent with cerebral metabolic changes that occur in perinatal asphyxia. Elevation of lactate indicates tissue ischaemia and hypoxia. A fall in N-acetyl aspartate reflects

neuronal injury (Hanrahan et al. 1996, 1998; Penrice et al. 1996; Barkovich et al. 1999; Robertson et al. 1999, 2002; Khong et al. 2004; L'Abbe et al. 2005; Cheong et al. 2006). A rise in myoinositol and glutamate may also be observed with scanning parameters optimised to demonstrate these peaks (Groenendaal et al. 2001; Robertson et al. 2001).

Metabolites detected by proton MRS correlated to the clinical condition of infants at risk of perinatal asphyxia as assessed by the Apgar score (Pavlakis et al. 1999). Significant correlation was also demonstrated between certain metabolite ratios and neurological outcome following HIE. A meta-analysis found the lactate/N-acetyl aspartate and lactate/creatine ratios to be the most accurate predictors of outcome in infants with HIE (Thayyil et al. 2010). Unlike diffusion MRI, MRS results are not influenced by the age at scanning during the first 30 days after birth.

Furthermore, MRS is a bridging biomarker of treatment effect (Robertson and Iwata 2007; Cady et al. 2008; Azzopardi and Edwards 2010; Faulkner et al. 2011; Robertson et al. 2013 a, b). Lactate/N-acetyl aspartate ratio is a suitable surrogate endpoint in the neonatal period for use in early phase neuroprotective studies in infants with HIE (Azzopardi and Edwards 2010; Thayyil et al. 2010). Hypothermia treatment results in reduced lactate levels in cortical and subcortical brain regions (Corbo et al. 2012).

2.6.4.5.4 Near-infrared spectroscopy

Cerebral near-infrared spectroscopy (NIRS) uses light in the near-infrared region of the spectrum. The relatively low absorption of near-infrared light in biological tissues

allows the light to penetrate the skin and skull layers to sample brain tissue. Near-infrared light is absorbed by oxygenated and deoxygenated haemoglobin and cytochrome oxidase (CytOx). Total haemoglobin is an index of CBV; meanwhile CytOx is the terminal complex of the mitochondrial respiratory chain and generator of ATP (Cooper et al. 1999; van Bel et al. 2008). NIRS can be used to study brain perfusion and oxygen consumption non-invasively (Peebles et al. 1992). It has limitations, as the measurements are qualitative and are prone to movement artefacts (Toet et al. 2006).

NIRS has been used to show that during recovery from severe asphyxia there is a brisk restoration of CBV, oxygenation and oxidative metabolism (Bennet et al. 2007). In the early recovery, CytOx activity returns to normal followed by a progressive loss, accompanied by a relative reduction in brain oxygenation consistent with mitochondrial failure (Bennet et al. 2006). However, loss of CytOx activity may not be possible to detect until the secondary deterioration is already in progress (Peeters-Scholte et al. 2004). By contrast with mitochondrial failure, suppression of $CMRO_2$ in the latent phase occurs rapidly after reperfusion (Jensen et al. 2006). Studies combining NIRS with MRS in newborn piglets after hypoxic-ischaemia found that reduction of $CMRO_2$ in the latent phase was mediated by impaired mitochondrial function and reduced energy demand (Winter et al. 2009). Whereas suppression of $CMRO_2$ and EEG both correlated with duration of cerebral ischaemia, the reduction in $CMRO_2$ was more sensitive to milder injuries (Tichauer et al. 2009). Thus, the combination of EEG and NIRS monitoring may improve early detection of injury.

In human studies of HIE regional oxygen saturation and fractional tissue oxygen extraction reflected secondary energy failure (Toet et al. 2006). An increased tissue oxygenation index correlated to abnormal neurological outcome at 1 year (Ioroi et al. 2002). In infants undergoing selective brain cooling with mild systemic hypothermia, NIRS identified a reduction in CBV during hypothermia that recovered in the rewarming period. As brain cooling reduces delayed hyperaemia meanwhile maintains neuronal metabolism after a cerebral hypoxic-ischaemic insult, cerebral oxygenation monitoring may be useful during hypothermia treatment to monitor changes in CBV and brain oxygenation as possible indicators of efficacy of the treatment (Bennet et al. 2006).

2.6.5 Treatment of hypoxic-ischaemic encephalopathy

2.6.5.1 Hypothermia

Until recently intensive care, including correction of acidosis, respiratory and cardiovascular support, fluid restriction and anticonvulsants, was the only available treatment for infants with HIE.

Studies of hypothermia for neural rescue began when experimental studies showed that mild hypothermia initiated soon after the hypoxic-ischaemic insult decreased pathophysiological changes and improved functional outcome (Busto et al. 1989; Thoresen et al. 1995; 1996; Sirimanne et al. 1996; Gunn et al. 1997). Hypothermic neuroprotection ameliorates the pathophysiological processes following a hypoxic-ischaemic insult and has beneficial effects on cerebral metabolism (Busto et al. 1989; Globus et al. 1995; Nakashima et al. 1996; Smith et al. 1996; Amess et al. 1997; Thoresen et al. 1997; Akisu et al. 2003; Qing et al. 2003). Hypothermia reduces the

number of apoptotic neurons by influencing intracellular mechanisms (Edwards et al. 1995; Xu et al. 2002; Zhu et al. 2004).

Therapeutic hypothermia for infants with HIE has been studied in several randomised clinical trials. Despite the heterogeneity of asphyxia and the use of different cooling methods, there are consistent findings that hypothermia reduces the extent of neurological damage. The meta-analyses of the cooling trials based on 18 months follow-up indicate that 72 hours of moderate hypothermia started within 6 hours of birth is beneficial in term infants with HIE (Jacobs et al. 2007; Schulzke et al. 2007; Edwards et al. 2010; Tagin et al. 2012; Jacobs et al. 2013), resulting in a significant reduction in the combined rate of mortality or major neurodevelopmental disability at 18 months. Although there might be adverse effects associated with cooling, such as sinus bradycardia, thrombocytopenia and subcutan fat necrosis (Zifman et al. 2010; Strohm et al. 2011); the long-term benefits outweigh short-term adverse effects. Importantly, therapeutic hypothermia reduces mortality without increasing major disability in survivors (Jacobs et al. 2013).

In many countries cooling is already the standard of care for term infants with HIE. Therapeutic cooling is achieved by using either selective head (Gluckmann et al. 2005; Gunn and Gluckman 2007) or whole body cooling (Shankaran et al. 2005; Azzopardi et al. 2010; Jacobs et al. 2011). Selective head cooling provides cooling of the surface of the head while the rest of the body is actively warmed, whereas whole-body cooling reduces the body temperature achieving a minimal difference between core body and overall brain temperatures (Tolley et al. 2005; Iwata et al. 2006).

Despite the promising results of the cooling trials, the effect of moderate whole-body hypothermia is modest as half of the infants who underwent hypothermia still have an abnormal outcome. However, experimental data suggest that hypothermia extends the duration of the therapeutic window (O'Brien et al. 2006) and certain interventions initiated during this time may augment neuroprotection (Robertson et al. 2012).

2.6.5.2 Potential additional therapies

Due to the complex mechanisms of a hypoxic-ischaemic brain injury intervening at a particular pathway may not be sufficient to prevent brain injury and combination of therapies may result in a more prominent reduction of brain injury. Drugs added during or after hypothermia may improve neuroprotection, by extending the therapeutic window or providing long-lasting additive or synergistic effect. The timing of administration of treatments is critical to attain maximum benefit and avoid neurotoxicity. Intervening early on in the cascade is more likely to achieve optimal neuroprotection (Carroll et al. 1992; Gunn et al. 1998).

Intensive research is focused on preclinical and early phase clinical studies of agents, which in combination with hypothermia may increase the rate of intact survival following HIE (Cillio and Ferriero 2010; Fan and Van Bel 2010; Kelen and Robertson 2010; Robertson et al. 2012). These potential additional therapies are classified based on time of administration (antenatal/postnatal, early or later treatments), or their point of action in the cascade (ion channel blockade; inhibition of free radicals, NOS production, anti-inflammatory, anti-apoptotic) (Cillio and Ferriero 2010; Fan and Van Bel 2010).

Based on consensus of investigators with special interest in neonatal neuroprotection the most promising agents are: (i) antenatal – tetrahydrobiopterin (BH4), melatonin, neural nitric oxide synthase (nNOS) inhibitors, xenon, allopurinol, vitamins C and E; (ii) postnatal – melatonin, erythropoietin (Epo), N-acetyl-cysteine (NAC), Epo mimics, allopurinol, xenon (Robertson et al. 2012).

2.6.5.2.1 Tetrahydrobiopterin

BH4 is a cofactor for a number of enzymes, including aromatic amino acid hydroxilase and NOS. BH4 levels increase during foetal life (Vasquez-Vivar 2009). It is crucial for brain development as it determines the vulnerability of the foetal brain to hypoxia-ischaemia. Deficiency of BH4 exacerbates oxidative injury (Madsen et al. 2003). Experimental evidence suggests that neonatal hypoxia-ischaemia causes relative BH4 deficiency (Fabian et al. 2010). Maternal treatment increased foetal levels of BH4 in basal ganglia and significantly ameliorated motor deficit and decreased stillbirth in a rabbit model of neonatal asphyxia (Vasquez-Vivar 2009). Although, there have been no studies of combination of BH4 with hypothermia, the safety profile make BH4 supplementation a candidate for further study (Gizewska et al. 2009; Robertson et al. 2012).

2.6.5.2.2 Melatonin

Melatonin is a natural neuroprotectant with potent antioxidant and anti-apoptotic effects (Hardeland et al. 2005; Luchetti et al. 2010). It is mainly produced by the pineal gland, allowing the entrainment of circadian rhythms of several biological functions (Altun et al. 2007). Due to its lipophilic properties, it easily crosses biological membranes, such as the placenta (Sadowsky et al. 1991; Reppert et al.

1997; Okatanai et al. 1998) and the blood-brain barrier (Vitte et al. 1988). Melatonin is used in children with sleep abnormalities related to neurological diseases (Jan et al. 1996).

Neuroprotective effect of melatonin, administered either before or after a hypoxic-ischaemic insult, has been demonstrated in animal models (Husson et al. 2002; Pei et al. 2002, 2003). Maternal administration reduced signs of cerebral inflammation and apoptosis (Hutton et al. 2009) and prevented free radical production in experimental models of birth asphyxia (Miller et al. 2006). Administered directly to foetal sheep after umbilical cord occlusion, melatonin decreased the number of activated microglia and apoptotic cells in the brain (Welin et al. 2007). It has been shown to protect the WM following excitotoxic and hypoxic injury in small animals (Husson et al. 2002; Kaur et al. 2010). In a piglet model of HIE melatonin combined with hypothermia was associated with improved energy metabolism as assessed by [31]Phosphorus MRS and reduced apoptotic cells (Robertson et al. 2013a).

Melatonin can be administered intravenously (Merchant et al. 2013) and oral doses show good uptake, even in patients who are critically ill (Mistraletti et al. 2010). However, the optimal dose and mode of delivery still need to be defined in critically ill human infants (Robertson et al. 2012a).

2.6.5.2.3 Neural nitric oxide synthase inhibitors

NO is a ubiquitous intercellular messenger and signalling molecule (Bolanos et al. 1994) and is important for neuronal survival, differentiation, and precursor proliferation (Chen et al. 2004). All isoforms of NOS are up-regulated in a hypoxic-

ischaemic injury. NO is produced in excessive amount early in the reoxygenation/reperfusion phase and is involved in the early phase of injury and secondary energy failure (Perlman et al. 2006). The toxic effect of NO is produced by its reaction with superoxide to form peroxynitrite and other reactive nitrogen species, although NO also has a direct effect on the mitochondria. The higher the nNOS activity is, the more likely the given brain region would be infarcted (Chen et al. 2004).

Seven-nitroindazole, a nNOS inhibitor, decreased caspase immunoreactivity and DNA fragmentation when administered before hypoxic-ischemia to 4 day old piglets (Parikh et al. 2003) and protected against brain injury in 7 day old rats following carotid artery ligation (Castillo et al. 2000; Ji et al. 2008, 2009a,b).

2.6.5.2.4 Xenon

Xenon is a noble, chemically inert gas that has been used safely in adults as an anaesthetic (Cullen et al. 1951) and in neonates to assess CBF (Greisen et al. 1988). Inhalational anaesthetics cross the placenta (Steffenson et al. 1970). Xenon has no teratogenic effects (Lane et al. 1980). It rapidly crosses the blood-brain barrier, due to its low blood-gas partition coefficient.

Xenon reduces excitotoxicity via non-competitive antagonism of the NMDA subtype of the glutamate receptor (Franks et al. 1998) and activation of the TREK-1 two-pore-domain potassium channels (Gruss et al. 2004). At higher glutamate concentrations, as occur during a hypoxic-ischaemic injury, xenon blocks kainate and AMPA receptors, thereby preventing depolarisation (Dinse et al. 2005) and inhibits

calcium/calmodulin dependent protein kinase II (Ma et al. 2007). Xenon also induces the expression of hypoxia inducible factor 1-alfa and its downstream effectors Epo and vascular endothelial growth factor both of which interrupt apoptotic pathway (Kilic et al. 2009).

In a rat model of intrauterine asphyxia, the combination of sevoflurane and xenon reduced the number apoptotic neurons in the hippocampus, and improved long-term cognitive function (Ma et al. 2005, Dingley et al. 2006). Xenon combined with hypothermia was neuroprotective following hypoxic-ischemia in a neonatal piglet model (Faulkner et al. 2011). A synergic effect was demonstrated (Ma et al. 2005) even when the administration of xenon and hypothermia occurred asynchronously (Martin et al. 2007).

Early phase clinical studies of xenon in human infants with HIE are in progress (Azzopardi et al. 2013; Dingley et al. 2014).

2.6.5.2.5 Allopurinol

Delayed neuronal death following a perinatal hypoxic insult is due partly to xanthine oxidase-mediated production of cytotoxic free radicals. Allopurinol, an inhibitor of xanthine oxidase and xanthine dehydrogenase, acts as an antioxidant reduces delayed cell death in experimental models of perinatal asphyxia. In high concentrations allopurinol scavenges hydroxyl radicals and prevents free radical formation by chelating their catalyst non-protein bound iron.

Allopurinol crosses the placenta (Robertson et al. 2012). Antenatal administration of allopurinol was associated with preservation of ^{31}Phosphorus MRS energetics (Williams et al. 1992) and reduced brain oedema in an animal model of HIE (Palmer et al. 1993). However, high doses are needed for antenatal neuroprotection. Maternal allopurinol reduced cord blood levels of S-100B in human pregnancies when foetal hypoxia was suspected (Torrance et al. 2009). The antenatal allopurinol for reduction of birth asphyxia induced damage (ALLO) determined a safe dose for administration during labour (Kaandorp et al. 2010, 2014). A randomised study of administration of allopurinol to infants with perinatal asphyxia demonstrated a reduction in the rate of adverse outcome (Kaandorp et al. 2012).

2.6.5.2.6 Vitamin C

Although ascorbic acid (AA) (vitamin C) does not penetrate the blood-brain barrier, it scavenges free radicals at supra-physiological concentrations (Jackson et al. 1997). Its oxidised form, dehydroascorbic acid (DHA) passes through cell membranes, enters the brain and diffuses across the placenta. The placenta also transports AA by a sodium-dependent mechanism (Rybakowsky et al. 1995). Intravenous administration of DHA allows supra-physiological concentrations of AA to be achieved in the brain. Teratological and adverse effects have not been documented.

DHA administered either before or after ischemia decreased infarct volume with a reduction in neurological deficit and mortality in an animal model (Huang et al. 2001). A randomised controlled clinical study in asphyxiated term infants found that the combination of AA with ibuprofen has no effect on outcome at 6 months of age (Aly et al. 2009).

2.6.5.2.7 N-acetyl-cysteine

NAC is a precursor of glutathione and therefore acts as an antioxidant, anti-apoptotic, and anti-inflammatory agent. It can be administered orally, intraperitoneally, or intravenously. However, adverse reactions in humans, such as anaphylaxis, limit its intravenous use (Heard 2007). Although NAC crosses the placenta, its transport across the blood-brain barrier is poor. Therefore NAC is likely to act as a neuroprotectant at the level of the vascular bed (Schaper et al. 2002).

In small animal studies NAC administered during pregnancy was protective against inflammatory insult (Paintlia et al. 2004; Lante et al. 2007). Experimental post-insult treatment resulted in inhibition of accumulation of lactate, a marked reduction of brain injury with improved cerebral perfusion, redox state, (Wang et al. 2007) and functional outcome (Lante et al. 2008; Lee et al. 2008). Combined with hypothermia, NAC decreased infarct volume, improved myelin expression and outcome in rats (Jatana et al. 2006).

Teratogenic effects are not known and NAC is thought to be safe in human pregnancy (Riggs et al. 1989). However, in animal studies pregnancy related adverse effects were reported, including augmentation of lipopolysaccharide (LPS)-induced preterm labour, and exacerbation of LPS-induced foetal hypoxaemia, hypotension and polycythaemia (Probyn et al. 2010).

2.6.5.2.8 Erythropoietin

Epo is a glycoprotein hormone that controls erythropoiesis. In vitro, the Epo receptor is expressed in hippocampal and cerebral cortical neurons (Morishita et al. 1997). The

safety of recombinant human Epo has been demonstrated in clinical studies of anaemia of prematurity (Ohls et al. 2004; Fauchere et al. 2008; Juul et al. 2008). Epo has not known teratogenic effects.

Neuronal apoptosis is prolonged after brain injury, and neurogenesis and angiogenesis play a part in repair. Epo is up-regulated in umbilical cord blood of infants who have suffered perinatal asphyxia (Ruth et al. 1990; Juul et al. 1998). Neuroprotective effects of Epo have been associated with Janus kinase/Stat5 activation and nuclear factor kappa B phosphorylation (Digicaylioglu et al. 2001). Epo also stimulates growth factors, including vascular endothelial growth (Wang et al. 2008) and brain-derived neurotrophic factor secretion (Viviani et al. 2005). Its effects include decreased neuronal apoptosis, increased neurogenesis and angiogenesis.

After hypoxic-ischaemia in neonatal rodents, Epo facilitated the recovery of sensorimotor function (Spandou et al. 2005), improved behavioural and cognitive performances (Demers et al. 2005), and preserved the integrity of cerebral tissue (Matsushita et al. 2003; Kellert et al. 2007; Gonzales et al. 2009).

A randomised controlled clinical study reported that repeated low doses of recombinant Epo were safe and resulted in improved neurological outcome in infants with moderate to severe HIE (Zhu et al. 2009; Elmahdy et al. 2010). However, clearance of Epo was slower when was administered in combination with hypothermia (Wu et al. 2012).

2.6.5.2.9 Epo-mimetics

Epo-mimetic peptides have specific subsets of Epo and might circumvent unwanted clinical effects of Epo, such as haematopoiesis and provide improved permeability with the ability to cross the placenta or the blood-brain barrier. However, the safety and efficacy of novel Epo-mimetics have not been determined (Robertson et al. 2012).

2.6.6 Outcome of perinatal asphyxia

The spectrum of outcome following perinatal asphyxia in human infants varies from mild cognitive or motor impairment to severe cerebral palsy, mental retardation or death. Outcome of subjects with mild HIE has been reported to be comparable to that of healthy term neonates (Finer et al. 1981; Pin et al. 2009). Infants who suffer moderate HIE tend to have a more variable prognosis and about one-third of them develop an unfavourable outcome (Pin et al. 2009). Those infants with severe HIE either die or develop cerebral palsy and/or cognitive delay (Finer et al. 1981; Robertson et al. 1989; Barnett et al. 2002).

2.6.6.1 Death

About one-third of the infants with HIE die. Meanwhile the majority of them die during the neonatal period (Jacobs et al. 2013), 20% of children die within the first 3 years. In these children death is often preceded by epilepsy, motor and feeding problems (Martinez-Biarge et al. 2010). However, the meta-analysis of the hypothermia trials found that the rate of mortality is reduced in infants who undewent therapeutic cooling (Edwards et al. 2010; Jacobs et al. 2013).

2.6.6.2 Motor impairment

Children with mild HIE have normal or mildly delayed motor development. However about one-third of those with a history of moderate HIE have delayed motor development at 1 year (Van Schie et al. 2006). BGT injury on early MRI scan is a good predictor for developing cerebral palsy at 24 months (Martinez-Biarge et al. 2010).

Cerebral palsy is an "umbrella term" to describe non-progressive conditions where there is primarily a disorder of movements, posture and coordination; however it is often accompanied by cognitive delay, visual, hearing and communication problems. Unlike earlier views on aetiology of cerebral palsy, evidence available from epidemiological studies suggests that in the developed countries about 10% of all cerebral palsy cases are associated with a perinatal hypoxic-ischaemic sentinel event (Nelson and Ellenberg 1986; Ellenberg and Nelson 2013). The type of cerebral palsy largely depends on the site of injury. While dyskinetic cerebral palsy or quadriplegia is more commonly seen following an acute, near total event with MRI abnormalities present in the BGT and perirolandic region, milder forms of cerebral palsy, such as spastic diplegia, are more common among those subjects with subacute, partial asphyxia with MRI abnormalities in the watershed areas (van Handel et al. 2007).

The meta-analysis of the cooling trials demonstrated a significant reduction in cerebral palsy in the group of infants who received therapeutic hypothermia (Edwards et al. 2010; Jacobs et al. 2013).

2.6.6.3 Cognitive impairment

Children with history of HIE may develop cognitive and behavioural problems. Lesions involving the BGT may result in a reduction in WM volume by disrupting thalamo-cortical connections and WM growth, resulting in suboptimal head growth, which is related to abnormal neurodevelopment (Mercuri et al. 2000). As the thalamus is important for executive functioning, lesions in this region affect subsequent cognitive performance (Radanovic et al. 2003). The hippocampus and striatum may also be affected by a hypoxic-ischaemic insult (Barkovich 1992; Rademakers et al. 1995; Toft et al. 1995; Maneru et al. 2003). These structures are associated with specific cognitive functions such as memory and attention, and play a role in the pathogenesis of later cognitive and behavioural problems in this population (DeLong 1992; Lou 1996; Dilenge et al. 2001; van Petten 2004; de Haan et al. 2006).

At 2 years of age children with mild HIE demonstrate average general intellectual abilities, similar to those of healthy controls (Robertson et al. 1985; 1988; Shankaran et al. 1991; Barnett et al. 2002; 2004). Children with moderate HIE perform in the low average range, and their abilities are generally below of those with mild HIE and healthy controls. They may develop cognitive deficits, such as memory problems, visual-motor or visual-perceptive dysfunction (Gadian et al. 1989; Robertson et al. 1989; Maneru et al. 2001; Moster et al. 2002; Barnett et al. 2002; Dixon et al. 2002; Marlow et al. 2005). Such cognitive deficits often result in delayed school-readiness. Children with severe HIE show very low level of cognitive functioning at two years (van Handel et al. 2007).

Cognitive deficits may occur even in absence of motor impairment following HIE (Gonzalez and Miller 2006; deVries and Jongman 2010). Survivors of HIE without motor impairment had lower scores for quantitative language, auditory memory, letter recognition, visual-motor integration and developmental quotient (DQ) at 5 years. By 8 years these children had marked delay in reading, spelling and arithmetic, and were more likely to be at least one grade level behind their peers (Robertson et al. 1988; Marlow et al. 2005).

Meta-analysis of the hypothermia trials reported significant reduction in the rate of developmental delay and intellectual impairment in the hypothermia group (Jacobs et al. 2013).

2.6.6.4 Behaviour problems

A Dutch cohort of children with mild to moderate NE showed more problematic behaviour, attention problems and hyperacivity compared to controls (Robertson et al. 1988; Moster et al. 2002; Marlow et al. 2005; van Handel et al. 2010). In addition, problems related to tractability, aggression, passivity and anxiety were reported in children with NE compared to healthy controls (Moster et al. 2002).

2.6.6.5 Visual impairment

Visual problems occur in about 10% of the children with history of HIE, however it rarely occurs as an isolated impairment (Rennie et al. 2007). Meta-analysis of the cooling trials showed a lower rate of visual impairment in infants who received hypothermia (Jacobs et al. 2013).

2.7 Biomarkers

A biomarker is an objectively measured characteristic to evaluate a biological or pathogenic process, or a response to a therapeutic intervention. Although biomarkers are used in many fields, in medicine they facilitate screening, detection of a pathological condition, monitoring its progression, and predicting prognosis. Biomarkers also accelerate development of novel therapeutic interventions. Importantly, they detect the response early in a relatively small number of patients making short and cost-effective pragmatic trials possible (Atkinson et al. 2001). Chemical, physical or biological parameters and characteristic structural changes as detected by imaging can serve as biomarkers.

2.7.1 Classification of biomarkers

Although the term biomarker is relatively new, they have been used in preclinical and clinical research and clinical care. Examples include body temperature as a marker of fever, blood pressure as a marker of risk of stroke, and cholesterol as a marker of risk of cardiovascular diseases. These "classic" biomarkers are usually physical or laboratory parameters that can be obtained at the bedside to ascertain a diagnosis and choose the most appropriate treatment.

Currently, intensive work is taking place to develop innovative more efficient biomarkers (Figure 2.7.1). These "new" biomarkers are the basis for preventive medicine that identifies the risk of a disease early to take specific actions for prevention of its progression. Biomarkers are key to personalize medical care to an individual patient. By tailoring treatment individually, therapeutic response rate

144

improves, side effects are limited and associated costs of treating side effects and testing various therapies ultimately decrease (Baker et al. 2005). Biomarkers are classified based on their application. A diagnostic biomarker indicates whether a disease already exists and identifies high risk populations reliably in a symptom-free state to start treatment early. Staging biomarkers identify where an individual patient is in a disease process. Predictive biomarkers help to assess the most likely response to a particular treatment type, while prognostic markers indicate the progression of a disease with and without treatment. In contrast, treatment biomarkers indicate whether a therapeutic intervention is likely to be effective in a specific patient.

Biomarkers also have an important role in development of novel therapies, especially early development, safety and proof of concept studies. Using a biomarker the financial and opportunity costs of research are reduced by selecting interventions with a high chance of success and studying those further in large clinical trials (Baker et al. 2005). A surrogate endpoint substitutes for a clinical endpoint. The advantage of such a tool is that it provides information months or years before a meaningful clinical endpoint. However, biomarkers are experimental tools to triage early phase clinical studies efficiently and are not substitutes for proof of clinical benefit (Baker et al. 2005).

A biomarker needs to be qualified by firm evidence that it detects a particular effect. Qualification is not necessarily transferable between diseases or subject groups. However, bridging biomarkers detect a particular effect in both animal and human studies. Such biomarkers are particularly valuable because they allow the transfer of information from experimental to human studies.

Biomarkers are further classified based on their characteristics, such as molecular and imaging biomarkers. A number of imaging modalities are amenable for use as biomarkers. Imaging has the capacity to produce multidimensional results with both qualitative and quantitative aspects non-invasively. Ultrasound, computed tomography, or positron emission tomography as well as MRI can be used this way.

2.7.2 Neuroprotection following hypoxic-ischaemic encephalopathy

Although hypoxic-ischaemic brain injury occurs during a sufficiently severe and/or prolonged episode of hypoxia and ischaemia in many cases neuronal loss continues to evolve for hours after resuscitation (Gunn and Bennet 2008; Bennet et al. 2009). This period of evolution, the latent phase, offers a window of opportunity to provide treatment to reduce or prevent injury. Meanwhile hypothermia trials proved the concept that neuroprotection during this period is possible, they also highlighted that hypothermic neuroprotection is only partial as only about one-third of the subjects survive with normal neurological function to 18 months (Edwards et al. 2010; Jacobs et al. 2013). Therefore additional neuroprotective therapies are needed.

Although a number of potential additional neuroprotective therapies are being studied in both pre-clinical and early phase clinical studies, there is little consensus on which treatments have a chance to succeed for either antenatal or postnatal treatment (Robertson et al. 2012). Furthermore, with hypothermia several years needed before efficacy of the treatment could be evaluated by early neurodevelopmental outcome (Bennet et al. 2010).

Biomarkers are needed in HIE to ascertain the timing and severity of the initial hypoxic-ischaemic insult, determine prognosis rapidly before treatment (risk of adverse outcome), after treatment (early surrogates for long term neurodevelopmental outcome), and accelerate translation of potential additional neuroprotective interventions into clinical trials (Azzopardi and Edwards 2010; Bennet et al. 2010).

2.7.3 Biomarkers of hypoxic-ischaemic encephalopathy

Classic biomarkers of HIE are those that detect the exposure to a hypoxic-ischaemic injury. Exposure around the time of birth may be inferred from a combination of the presence of an abnormal foetal heart rate as assessed by cardiotocogram, an oxygen debt, as indicated by increased base deficit and lactate in the cord blood, and need for resuscitation as assessed by the Apgar scores. However, these measures have low PPV for presence of HIE and subsequent outcome and their utility is limited in selecting infants for trials of neuroprotective treatments (Low et al. 1997; Bennet et al. 2009; Laptook et al. 2009; Murray et al. 2009).

Several serum, urine, and CSF markers have been investigated as potential biomarkers. However, to identify infants who would benefit from neuroprotection the time of sampling is crucial. In majority of the studies samples were taken after 24 hours of birth, following the latent phase, when selection of infants for neuroprotective interventions is over. In other studies, where samples were taken early, the apparent timecourse of changes of metabolites was variable (Nagdyman et al. 2009). In a meta-analysis four markers were predictive of an unfavourable outcome: serum interleukin-6, CSF neuron-specific enolase, and serum and CSF interleukin-1b when measured within 96 hours of birth (Ramaswamy et al. 2009).

However, these markers are not specific for hypoxic-ischaemia and there have been only few long-term follow-up studies. Furthermore the effect of hypothermia on these markers is uncertain (Massaro et al. 2012)

Electrophysiology measures are already applied in assessing eligibility for hypothermic neuroprotection (Azzopardi et al. 2009, Shankaran et al. 2005). Assessment of amplitude or pattern of aEEG combined with neurological assessment has high specificity for adverse outcome (Shalak et al. 2003). In the CoolCap trial, infants with the most severe aEEG pattern demonstrated no improvement after cooling (Gluckman et al. 2005), offering the opportunity to identify infants who would not benefit from neuroprotective interventions. However, severe suppression of aEEG activity within the first 6 hours of birth may occur in both subjects with favourable and unfavourable outcome (George et al. 2004; Pezzani et al. 2006; Murray et al. 2009). During this early period it is not known whether brain activity is suppressed by increased release of neuroinhibitors that help to improve recovery and the amplitude will return to normal as in cases with a favourable outcome; or brain activity is suppressed by an injury-induced impairment and only improves transiently as in infants with severe outcome (Bennet et al. 2010). Although the sensitivity, specificity, PPV and NPV of aEEG are high, they vary between studies (El-Ayonty et al. 2008; Thoresen et al. 2010 Vasiljevic et al. 2012). Furthermore, hypothermia influences the predictive value of aEEG (Thoresen et al. 2010).

Neuroimaging offers the potential to assess brain injury non-invasively. Although visual analysis of conventional MR images might be subjective, hypoxic-ischaemic changes detected on conventional MRI correlate closely with pathology and

neurodevelopmental outcome in a single patient (Rutherford et al. 2005; Barkovich et al. 2006). The timing of imaging is important, since characteristic abnormalities on conventional MRI occur progressively over several days and the severity of injury may be underestimated during the first few days of birth. However its predictive value is not affected by hypothermia (Rutherford et al. 2010). Furthermore, visual assessment of conventional MR images is a biomarker of injury and is a suitable surrogate endpoint in studies of neuroprotective therapies (Rutherford et al. 2010). Although, the required sample size to detect treatment effect is considerably smaller than in pragmatic trials, it is substantial.

MRS has been used to define the biphasic pattern of impairment of cerebral energy metabolism and characterize cerebral biochemical changes in infants with HIE. MRS is a bridging biomarker that demonstrated the preservation of high-energy phosphates and reduction of cerebral lactate levels during 72 hours of mild hypothermia in experimental models of asphyxia (Thoresen et al. 1995; Amess et al. 1997; Laptook et al. 1997; Robertson and Iwata 2007; Cady et al. 2008; Faulkner et al. 2011). Furthermore, lactate/N-acetylaspartate peak and lactate/creatine ratios measured in the deep grey matter correlate to outcome in infants with HIE and are qualified biomarkers of outcome with a strong physiological evidence base (Thayyil et al. 2010). Importantly, hypothermia does not affect the predictive value of MRS (Ancora et al. 2013). Meanwhile continuous variables, such as metabolite ratios, are generally efficient outcome measures as the number patients required to detect significant differences between treatment groups is smaller, it is still substantial. Therefore, MRS is a relatively inefficient method for rapid preliminary evaluation of potential therapies in early phase, first in human studies (Azzopardi and Edwards 2010).

Although diffusion measures, such as ADC, provide the potential for early and objective detection of brain injury, in a meta-analysis of MR biomarkers it was shown to have poor specificity and sensitivity for predicting outcome (Thayyil et al. 2010). This might be due to pseudonormalisation (Wolf et al. 2001; McKinstry et al. 2002; Sotak et al. 2002; Hunt et al. 2004; Rutherford et al. 2004; Winter et al. 2007; Liauw et al. 2009), which is delayed by hypothermic neuroprotection. FA was proved to be more accurate in predicting subsequent abnormality on conventional MRI (Ward et al. 2006) and early outcome (Malik et al. 2006; Brissaud et al. 2010). However, diffusion parameters were determined within *a priori* selected manually defined ROIs in most of these studies. This approach is time consuming and may introduce errors due to observer bias and partial volume effects.

TBSS, an observer-independent research tool for voxel-wise assessment of whole brain WM across multi-subject DTI data (Smith et al. 2006), overcomes some of these limitations. Using TBSS, widespread WM abnormalities were revealed in a small group of infants who had suffered perinatal asphyxia when compared to normal term control neonates. Infants treated with therapeutic hypothermia exhibited significantly less extensive WM injury when compared to infants with HIE who received intensive care only (Figure 2.7.1) (Porter et al. 2010). These results suggest that TBSS could be used as an imaging biomarker in infants who suffered HIE. However, further studies, correlating TBSS findings in the early neonatal period and subsequent neurodevelopmental performance, are required before this imaging tool can be considered a qualified early imaging biomarker following HIE.
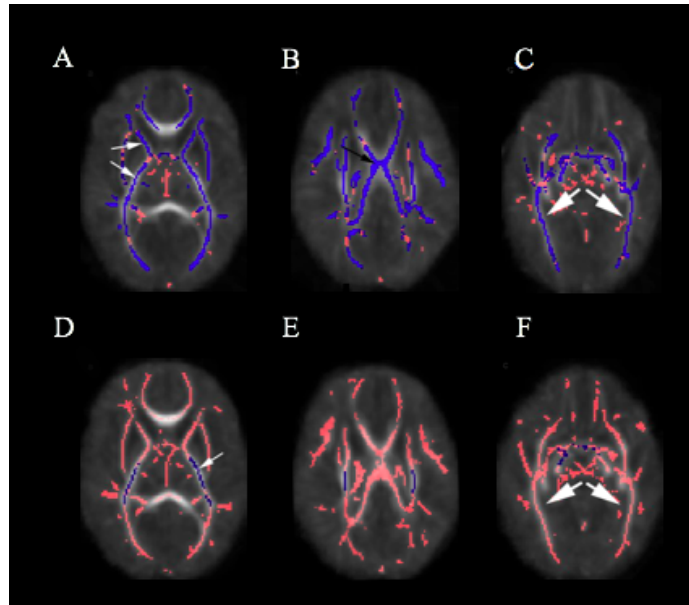
Figure 2.7.1: Tract-based spatial statistics as a biomarker of disease and therapy.

Axial images of mean FA maps of all subjects. The group mean FA skeleton is shown in pink. A-C: Areas where non-cooled infants with HIE have significantly lower FA values than healthy term neonates are shown in blue. A: internal (small white arrows) and external capsules, B: body of the corpus callosum (black arrow), C: optic radiations (large white arrows). D-F: Areas where cooled infants with HIE have significantly lower FA values than healthy term neonates are shown in blue. D: PLIC at the level of the basal ganglia and thalami (small white arrow); E: PLIC at the level of corpus callosum, F: cerebral peduncle (large white arrows indicate the optic radiations) (From Porter et al. 2010).

Chapter 3

Prediction of neurodevelopmental outcome by diffusion tensor imaging analysed using tract-based spatial statistics in infants with hypoxic-ischaemic encephalopathy treated with hypothermia

3.1 Introduction

Despite the success of hypothermic neuroprotection, additional therapies are needed that in combination with hypothermia improve neurodevelopmental outcome of infants with HIE by extending the therapeutic window or providing long-lasting additive or synergistic neuroprotection (Cilio and Ferriero 2010; Fan and van Bel 2010; Robertson et al. 2012). Intensive research is focused on identifying additional neuroprotective therapies. However, one of the limitations to progress is the large number of possible agents and the lack of consensus on which drugs to study further (Robertson et al. 2012).

An effective bench-to-bedside pipeline requires the ability to evaluate the efficacy of a treatment early using biomarkers (Baker et al. 2005; Azzopardi and Edwards 2010). Neuroimaging with advanced MRI techniques is increasingly employed in research of biomarkers in infants with HIE. MRS enables *in vivo* quantitative analysis of cerebral metabolites (Robertson and Iwata 2007; Cady et al. 2008; Azzopardi and Edwards 2010; Faulkner et al. 2011, 2012; Robertson et al. 2013a, b). Metabolite ratios, such as Lac/NAA and Lac/Cr, are the most accurate quantitative MR biomarkers of outcome in infants who suffered HIE (Shu et al. 1997; Amess et al. 1999; Robertson

et al. 1999; Kadri et al. 2003; Khong et al. 2004; Cheong et al. 2006; Shanmugalingam et al. 2006; Meyer-Witte et al. 2008; Thayyil et al. 2010). Furthermore metabolite ratios enable smaller sample sizes to detect significant differences between treatment groups than in pragmatic clinical trials. Therefore MRS can be used as a surrogate endpoint in early phase studies of additional neuroprotective therapies. However, using MRS a sample size of more than a hundred infants would still be required to detect differences between study groups (Azzopardi and Edwards 2010).

Statistically powerful whole brain voxel- and groupwise comparisons of imaging data in small groups of subjects would help more efficient early evaluation of neuroprotective therapies. Diffusion MRI has been widely used to study brain injury early following a hypoxic-ischaemic event (Wolf et al. 2001; McKinstry et al. 2002; Khong et al. 2004; Rutherford et al. 2004; Boichot et al. 2006; Ward et al. 2006; Malik et al. 2007; Winter et al. 2007; Liauw et al. 2009; Twomey et al. 2010; Artzi et al. 2011; Bednarek et al. 2012; Cheong et al. 2012; Lee et al. 2013). However these studies used manually defined ROIs, which is subjective, time consuming and prone to observer-error.

Such problems can be circumvented by TBSS, which is an objective, time-efficient, observer independent tool for cross-subject analysis of whole-brain WM instead of *a priori* chosen ROIs (Smith et al. 2006). TBSS has been used in infants who suffered HIE (Porter et al. 2010; Gao et al. 2012). TBSS analysis of DTI data offers the potential to serve as an early objective imaging biomarker after hypothermia treatment for HIE.

3.2 Aim

The aim of the study was to test the hypothesis fractional anisotropy values in the white matter, obtained in the neonatal period and assessed using tract-based spatial statistics, correlate with developmental quotient in infants with hypoxic-ischaemic encephalopathy, who underwent therapeutic hypothermia.

3.3 Methods

Ethical permission for this study was granted by the Hammersmith and Queen Charlotte's and Chelsea Hospital Research Ethics Committee. Written parental consent was obtained for each infant prior to scanning.

3.3.1 Subjects

Term infants (>36 weeks at birth) with HIE treated with hypothermia were enrolled into this study, who had a brain MRI scan with good quality DTI data in 32 noncollinear directions within 3 weeks of birth and who were assessed with the Griffiths Mental Developmental Scales (revised) (GMDS) (Huntley 1996) or have outcome data available at least at 12 months of age. Demographic data and details of perinatal history were collected from the hospital notes.

Infants who were born at less than 36 weeks, had not been treated with hypothermia within 6 hours of birth, were diagnosed with congenital or chromosomal abnormality, did not have a brain MRI scan with good quality DTI data in 32 noncollinear directions within 3 weeks of birth, or had no outcome data available at least at 12 months of age were excluded from the analysis.

3.3.2 Neurodevelopmental outcome

Outcome data were collected from hospital notes and clinic letters for each subject. Most infants attended the follow-up clinic at Queen Charlotte's and Chelsea Hospital. For the infants only seen at other hospitals, the information was obtained from their local paediatric neurodevelopmental team.

For children who were assessable with a formal neurodevelopmental test, assessments were carried out using the GMDS (Huntley 1996). The GMDS provide an overall DQ and scores for sub-scales, including locomotor, personal-social, hearing and language, eye and hand co-ordination, and performance. These sub-scales assess several distinct skill areas, such as gross motor skills including balance, co-ordination, control of movements; proficiency in daily activities, level of independence and interaction with other children; receptive and expressive language; manual dexterity, fine motor and visual monitoring skills, visuospatial skills, including speed and precision; and the ability to resolve problems, understanding basic mathematical concepts and moral issues (Huntley 1996).

The presence of cerebral palsy was defined and classified using the Surveillance of Cerebral Palsy in Europe (SCPE) (Cans et al. 2000).

The Gross Motor Function Classification System (GMFCS) was used to grade functional impairment (Gorter et al. 2009). The GMFCS describes gross motor function of children with cerebral palsy with emphasis on sitting, walking or wheeled mobility based on their usual performance at home, school and community settings.

Distinctions between levels are based on functional abilities, the need for assistive devices and quality of movements. Children classified in level I can walk without restrictions, however they tend to be limited in some of the more advanced motor skills, meanwhile children classified in level V are generally very limited in their ability to move themselves around even with the use of assisted technology. Within each level, descriptions of motor function are given for several age bands, including children less than 2 years (Palisano et al. 1997; Rosenbaum et al. 2002).

3.3.3 Magnetic resonance imaging

Infants were sedated prior to scanning with oral chloral hydrate unless sedative drugs were already administered for clinical reasons. Intensive care, including ventilation and inotropic support, was provided during the scan as required. All infants were first assessed to be clinically safe for scanning by a paediatrician. Metal check was performed before scanning as per local guidelines. Physiological parameters including heart rate, oxygen saturations and temperature were monitored throughout the scan. Hearing protection was used for each infant, compromising individually molded earplugs using silicone-based dental putty (President Putty, Coltene/Whaledent, Mahwah, NJ) placed into the external ear, and neonatal earmuffs (Natus MiniMuffs; Natus Medical Inc, San Carlos, CA). All examinations were supervised by a paediatrician experienced in MRI procedures.

MRI was performed on a 3 Tesla Philips Achieva MRI system (Best, Netherlands), with maximum gradient strength of 62 mT/m on each independent axis and slew rate of 100 mT/m/ms on each axis, using an eight-channel phased array head coil. Three dimensional magnetization prepared rapid acquisition with gradient echo (MPRAGE)

(TR: 17 ms; TE: 4.6 ms; flip angle: 13°; slice thickness: 8 mm; field of view: 210 mm; matrix: 256x256 (voxel size: 0.82x0.82x0.82)) and high-resolution T2 weighted fast spin echo images (TR: 8670 ms; TE: 160 ms; flip angle 90°; slice thickness 1 mm; field-of-view: 220 mm; matrix: 256×256 (voxel size: $0.86 \times 0.86 \times 1$)) were acquired for clinical evaluation. Single shot echo planar DTI was acquired in 32 non-collinear directions (TR: 8000 ms, TE: 49 ms, slice thickness: 2 mm, field of view: 224 mm, matrix: 128x128 (voxel size: 1.75x1.75x2 mm³), b value: 750 s/mm²). The DTI data was acquired with a sense factor of 2 and the scanning time for this sequence was 6 minutes. A perinatal radiologist reviewed the images.

3.3.4 Conventional magnetic resonance images

Conventional images were analysed visually. Images were evaluated for congenital anomalies. Abnormal appearance of the brainstem, cerebellum and the ventricles was noted if present. Presence and site of haemorrhage, sinus or venous thrombosis were documented. The pattern of injury in the WM, BGT, PLIC and cortex was classified (Okereafor et al. 2008). Each infant was given a score for the signal intensity in the PLIC (0 = normal; 1 = equivocal; 2 = abnormal), BGT (0 = normal; = mild, focal; 2 = moderate, multifocal; 3 = severe, widespread), WM (0 = normal; 1 = mild exaggerated long T1 and T2 in the periventricular WM only; 2 = moderate long T1 and T2 extending out in the subcortical WM and/or focal punctate lesions or focal area of infarction; 3 = severe widespread abnormalities including overt infarction, haemorrhage, and long T1 and T2), and cortex (0 = normal; 1 = mild involving maximum 2 sites; 2 = moderate involving 3 sites; 3 = severe involving more than 3 sites). Moderate to severe lesions in the BGT, an abnormal PLIC, or severe WM lesions were deemed to be predictive of adverse developmental outcome (Rutherford

et al. 2010). Sensitivity, specificity, PPV and NPV of conventional MRI to predict outcome were calculated.

3.3.5 Preprocessing of diffusion tensor imaging data

DTI data were analysed offline using tools implemented in FSL (www.fmrib.ox.ac.uk/fsl) (Jenkinson et al. 2004; Smith et al. 2004b). Images were brain extracted to remove all extra-cerebral tissue using the Brain Extraction Tool (BET) version 2.1 (Smith 2002). Each infant's diffusion tensor images were registered to their image acquired without diffusion weighting using affine transformation to minimise spatial distortions due to eddy currents using FMRIB's Diffusion Tool's (FDT) Eddy Current Correction tool. Diffusion tensors were calculated voxelwise, using a simple least squares fit of the tensor model to the diffusion data. From this, the tensor eigenvalues describing the diffusion strength in the primary, secondary and tertiary diffusion directions, and FA maps were calculated (Behrens et al. 2003).

Voxelwise preprocessing of the FA data was carried out using TBSS version 1.1 (Smith et al. 2006) with a protocol that has been modified to improve reliability for neonatal DTI analysis (Ball et al. 2010). The optimised protocol incorporates two additional registration steps added to the original adult protocol (Smith et al. 2006). To reduce the number of failed registrations two linear registration steps were performed (6 and 12 DOF) prior to nonlinear registration to register every subject's FA map to each other. Both the 6 DOF and the 12 DOF registration matrices were then concatenated and entered as an initial estimate for nonlinear warping. Then a registration target (best target) was identified with the lowest mean warp displacement score. Each infant's FA map was aligned to the target's space and an average FA map

was created, that is the mean FA map. The second set of registrations of the optimised protocol is a set of nonlinear registrations to align every individual FA map to the mean FA map. The aligned images were then used to create another mean FA map. By applying "thinning", a non-maximum-suppression perpendicular to the local tract structure, the mean FA skeleton was generated, which represented the centre of all tracts common to the group. This was thresholded to FA ≥ 0.15 to include the major WM pathways but exclude peripheral tracts where there was significant inter-subject variability and/or partial volume effects with grey matter. Each subject's aligned FA data were then projected onto this skeleton. Voxelwise cross-subject statistical analysis was performed with Randomise version 2.1 using univariate linear modeling as a GLM (Smith et al. 2006; Ball et al. 2010) (Figure 3.1).

Nonlinear transformation   The best target   Mean FA map   Mean FA skeleton
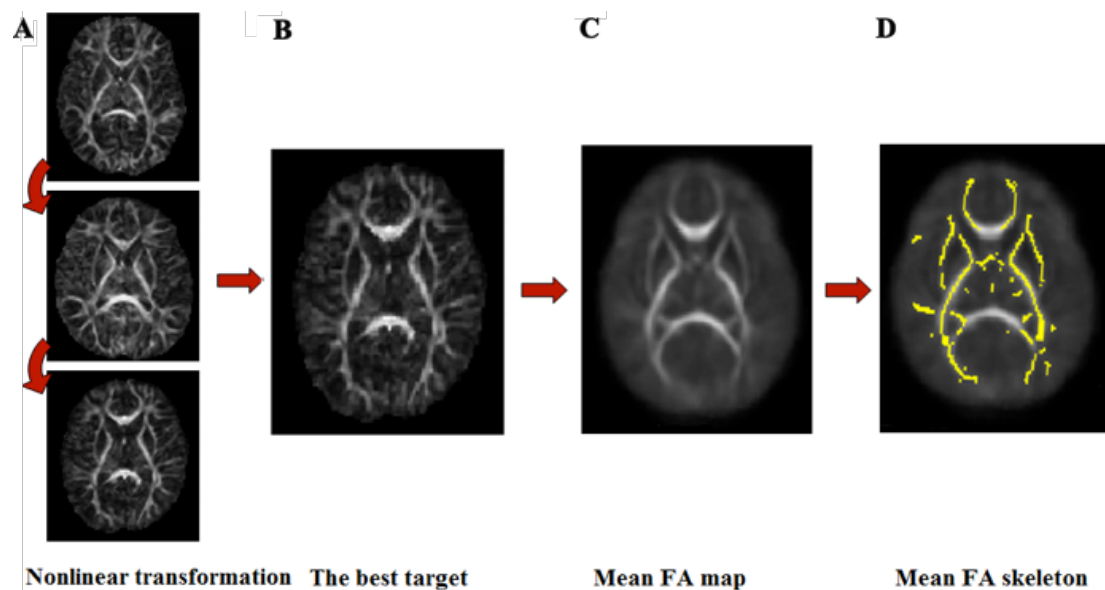
Figure 3.1: **Tract-based spatial statistics preprocessing pipleine.** *A: nonlinear alignment of individual fractional anisotropy (FA) images to each other, B: nonlinear alignment of individual FA images to the best target, C: generating the mean FA map, D: creating the mean FA skeleton for cross-subject voxelwise analysis.*

3.3.6 Analysis of diffusion tensor imaging data

TBSS was used to assess the relationship between FA obtained in the neonatal period and outcome. First, infants who died or developed such severe cerebral palsy or global developmental delay that neurodevelopmental assessment could not be performed using the GMDS were excluded before performing voxelwise cross-subject linear regression to assess the relationship between FA, corrected for PMA at scan, and DQ.

An exploratory analysis was performed to assess the correlation between the subscale scores of the GMDS and FA in the centre of the WM tracts using TBSS (Smith et al. 2006).

All infants who had outcome data available at least at 12 months were enrolled into the secondary analysis. Infants were divided into two groups: (i) infants with a favourable outcome and (ii) infants with an unfavourable outcome. Unfavourable outcome was defined as death or the presence of at least one of the following impairments: 1. DQ of 2 or more standard deviations (SDs) below the mean on GMDS (<76) (Ivens and Martin 2002); 2. GMFCS level III-V; or 3. Bilateral cortical visual impairment with no useful vision. TBSS was used to compare FA values between the two groups.

The analyses were corrected for multiple comparisons by controlling familywise error rate following threshold free cluster enhancement and $p<0.05$ was considered significant. Although FA does not pseudonormalise, it changes with increasing PMA. Therefore the results were also corrected for PMA at scan.

To demonstrate the relationship between FA and neurodevelopmental performance scores, in those regions where a significant linear correlation was observed, the FA values, adjusted for PMA at scan, in the most significant voxel was extracted and plotted against the DQ and sub-scale scores. Furthermore, for each subject FA values were also extracted from the most significant voxel in the regions where FA was significantly different between infants with a favourable and those with an unfavourable outcome.

3.4 Results

3.4.1 Subjects

Patient flow of this study is shown on Figure 3.2. The clinical characteristics of the infants are shown in Table 3.1.

A total of 121 infants with HIE received therapeutic hypothermia at Queen Charlotte's and Chelsea Hospital between 2007 and 2011. Of the 121 infants 27 did not have a brain MRI scan. Of these, outcome data was available for 12 subjects. Eleven infants died. One child assessed with the GMDS at 24 months achieved scores within normal range for age.

Of the 94 infants, who undewent a brain MRI in the neonatal period, 24 had no outcome available until 2011. Of these 24 infants 4 were not eligible to be enrolled into the study for the following reasons: n=1 less than 36 weeks at birth; n=2 abnormal chromosomes (Trisomy 21 n=1; abnormal chromosome 13 n=1); n=1 DTI data acquired in 15 noncollinear directions.

Until 2011 outcome data was available for 70 infants who underwent hypothermia for HIE and had brain MRI scan during the neonatal period.

GMDS was not performed in 31 of the 70 infants for the following reasons. Fifteen infants died. Of these 15 infants 6 were not eligible for the study for the following reasons: n= 1 less than 36 weeks at birth, n=2 DTI acquired in 15 noncollinear directions, n=1 incomplete DTI data, n=2 post-mortem MRI.

Eleven children could not be assessed with the GMDS. Of these 11 children 7 had global developmental delay and cerebral palsy with GMFCS level III-V (spastic n=2; dystonic n=3; spastic dystonic n=1; athetoid n=1). One child had right hemiplegia GMFCS level II with cognitive delay. Three children developed severe cognitive delay with microcephaly, but without significant motor problems. However, of these 11 children 9 were not eligible to be enrolled into the study for the follwoing reasons: n=7 DTI in 15 noncollinear directions, n=1 cooling started at more than 6 hours of age, n=1 treated for fibrosarcoma following the neonatal period.

Three children seen at the neonatal follow-up clinic were not assessed with the GMDS. One of them attained the maximum optimality score for neurologic examination (Haataja et al. 1999, 2001). The other 2 children were seen by a neonatal consultant but did not have a formal neurodevelopmental assessment. They were deemed by the consultant to have normal neurodevelopment based on physical examination. Two children were assessed using the Bayleys Scale of Infant Development (Bayley 1966) and achieved scores within normal range for age. However, these 5 infants were more than 21 days old at the time of the MRI and were therefore not eligible for this study.

Thirty-nine children were assessed with the GMDS at a median (range) age of 22 (6-28) months until 2011. Seven of the 39 children were excluded for the following reasons: n=1 DTI data acquired in 15 directions; n=3 more than 21 days old at the time of the MRI; n=1 less than 36 weeks at birth; n=2 follow-up at less than 12 months of age.
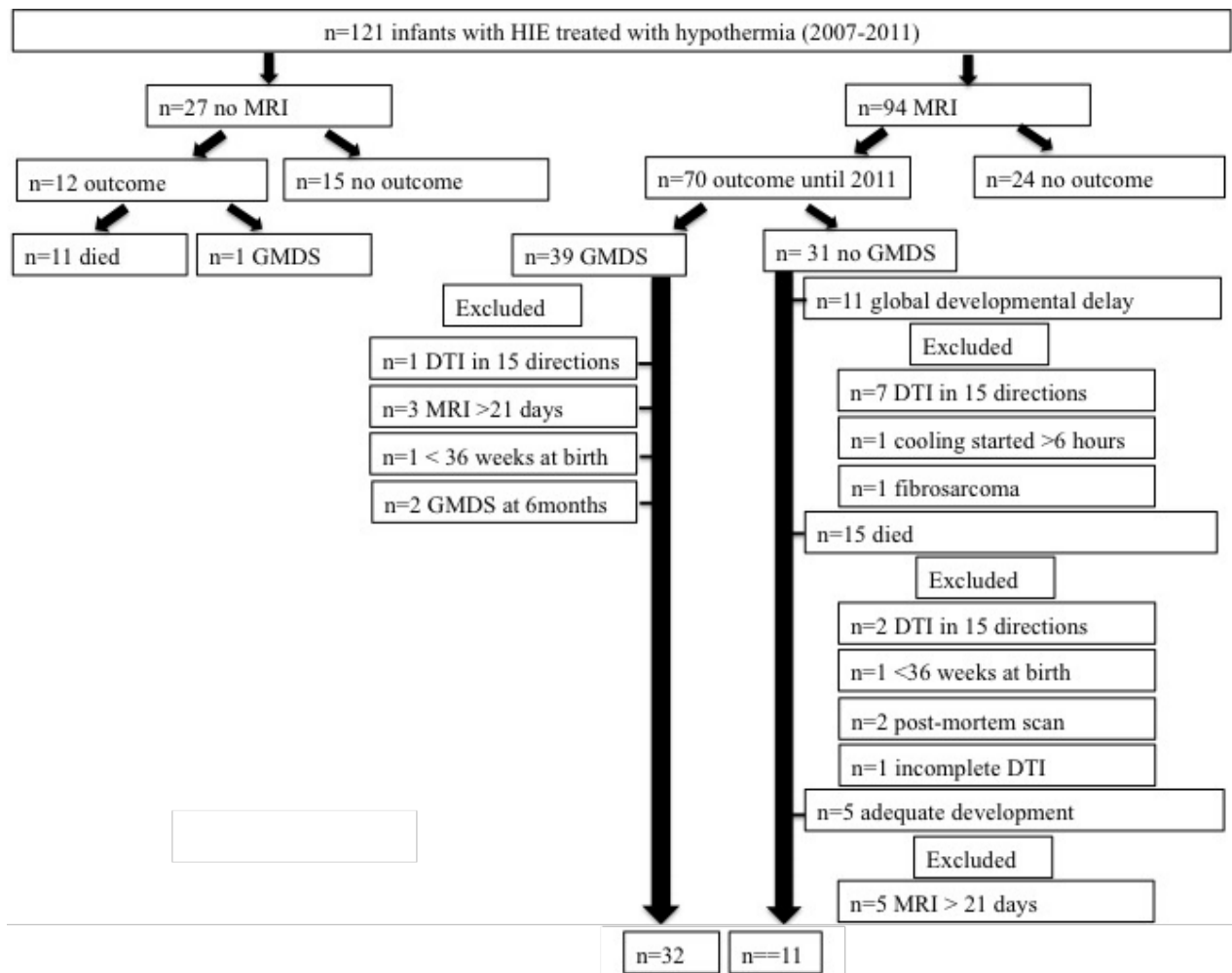
Figure 3.2: Consort diagram of patients. *HIE – hypoxic-ischaemic encephalopathy; MRI – magnetic resonance imaging; GMDS – Griffiths Mental Developmental Scales; DTI – diffusion tensor imaging.*

Clinical characteristics	Total (n=121)	Total MRI (n=94)	GMDS (n=32)	Died/cerebral palsy (n=11)
Postmenstrual age at birth [a]	39^{+4} (35^{+0}-42^{+3})	39^{+4}(35^{+0}-42^{+3})	39^{+5} (36^{+1} – 42^{+3})	39^{+5} (36^{+4} – 42^{+0})
Postmenstrual age at scan [a]	N/A	41^{+1} (36^{+4}-47^{+5})	40^{+5} (37^{+4}-43^{+4})	41^{+6} (37^{+2}-43^{+1})
Postnatal days at scan [a]	N/A	6 (3-67)	7 (3-14)	6 (3-11)
Gender male (n)	72	60	23	7
Birth weight (kg) [a]	3.28 (1.96-5.83)	3.22 (1.96-5.30)	3.22 (2.15-4.12)	3.20 (2.00 – 5.33)
Apgar score at 1 min [a]	1(0-7)	1 (0-6)	1 (0-5)	0 (0-3)
Apgar score at 5 min [a]	3 (0-9)	3 (0-9)	3 (0-8)	1 (0-4)
Apgar score at 10 min [a]	5 (0-9)	5 (0-10)	5 (0-9)	4 (0-6)
pH within 1 hour of birth [a]	6.92 (6.54-7.39)	6.96 (6.54-7.39)	6.80 (6.54-7.39)	6.71 (6.58-7.25)
Base deficit within 1 hour of birth [a]	16.64 (3.00-31.60)	15.50 (3.00-31.60)	15.39 (6.80-25.40)	22.15 (5.30-27.55)

[a]median (range)

Table 3.1: Clinical characteristics of the study infants. *Abbreviations: min – minutes; GMDS – Griffiths Mental Development Scales; N/A – not applicable*

3.4.2 Neurodevelopmental performance

For the 32 children assessed with the GMDS who were eligible to be enrolled into the study the mean±SD DQ was 91±19 and the mean±SD scores for the sub-scales were as follows: locomotor 92±23, personal-social 100±24, hearing and language 87±24, eye and hand coordination 86±18 and performance 85±17. Of these 32 children 7 were assessed between 12 and 18 months, at a median age of 12 months. Of them 4 had started to walk independently and the other 3 were walking with minimal support at the time of the assessment.

Forty-three children, including those who died or had severe neurodevelopmental delay, were eligible to be enrolled into the secondary analysis. Seventeen children had an unfavourable outcome including 9 infants who died. Six surviving children had a

DQ more than 2 SDs below the mean on GMDS, 2 of these children also developed cerebral palsy (GMFCS levels III-IV). Two other children were included with cerebral palsy (GMFCS level V). The children with cerebral palsy were assessed at a median age of 24.5 months (range: 24-28). All of them had quadriplegia (spastic n=1; dystonic n=1; dystonic-spastic n=1; athetoid n=1). One infant with cognitive delay developed a right hemiplegia (GMFCS II). None of the children had cortical visual impairment. One child required hearing aids.

3.4.3 Conventional magnetic resonance imaging findings

No congenital abnormality or thrombosis were seen on conventional MRI in any of the subjects. Four infants had mild ventriculomegaly. Extra-cerebral haemorrhage was noted in 5 subjects (posterior fossa n=2, posterior ventricle n=1, subarachnoid n=1, subdural n=1). Lesions in the BGT consistent with acute hypoxic-ischemia were detected in 27 infants; these were classified as severe in 12. The PLIC was equivocal in 5 and abnormal in 15 infants. All infants with an abnormal PLIC had either moderate (n=4) or severe (n=11) BGT lesion. WM abnormalities were present in all except 2 infants, being severe in 12 infants. Nine infants had WM abnormality only (moderate n=2, severe n=3). The cortex showed changes typical of acute hypoxic-ischaemic injury in 21 infants.

3.4.4 Correlation between conventional magnetic resonance imaging findings and outcome

The sensitivity of MRI to detect an abnormal outcome was 94% and specificity was 72%. The PPV of conventional MRI was 72% and NPV was 95% (Table 3.2). Of note, 5 out of the 7 infants with abnormal MRI and DQ less than 2SDs below the

mean had WM injury (including two infants with parasagittal infarction and one with a right sided middle cerebral artery infarction), with normal BGT. All of these infants had a DQ of less than 90 and their head circumference was less than 10th centile at the time of assessment.

Region	Pattern	n (43)	Outcome	
			Favourable	Unfavourable
Basal Ganglia and Thalami	0	16	15	1
	1	9	9	0
	2	6	3	3
	3	12	0	12
Posterior limb of the internal capsule				
	Normal	21	20	1
	Equivocal	5	3	2
	Abnormal	15	1	14
	Unable to assess	2	2	0
White matter				
	0	2	2	0
	1	4	4	0
	2	25	14	11
	3	12	5	7
Cortex				
	0	22	16	6
	1	9	6	3
	2	7	5	2
	3	5	0	5

Table 3.2: **Pattern of injury on conventional MRI and outcome.**

3.4.5 Correlation between outcome and white matter microstructure as assessed by tract-based spatial statistics

The mean FA skeleton comprised of 21357 voxels.

3.4.5.1 Correlation between white matter microstructure as assessed by tract-based spatial statistics and neurodevelopmental performance

The 9 infants who died and 2 of those who developed cerebral palsy could not be assessed using the GMDS and so were excluded from the linear regression analysis of FA values and neurodevelopmental outcome scores. In the remaining 32 infants TBSS demonstrated a significant linear correlation between DQ and FA values in 12112 voxels throughout the WM, including the centrum semiovale (CSO), corpus callosum, PLIC, external capsules, ALIC, optic radiations, frontal WM, cerebral peduncles, fornix, uncinate fascicule and cingulum.

In the exploratory analysis the number of voxels where a significant linear correlation was found between FA, corrected for PMA at scan, and sub-scale scores was 7174 for personal-social; 13243 for hearing and language; 13195 for eye-hand coordination and 8006 for performance. A significant relationship between FA and locomotor sub-scale scores was observed in the PLIC, CSO, corpus callosum, left cerebral peduncle and brainstem in 3140 voxels (Figure 3.3). These relationships remained significant when the 2 infants with cerebral palsy were removed from the analysis.

Following the whole-brain analysis, FA values, adjusted for PMA at scan, in the most significant voxel were extracted and plotted against the DQ and sub-scale scores (Figure 3.4).
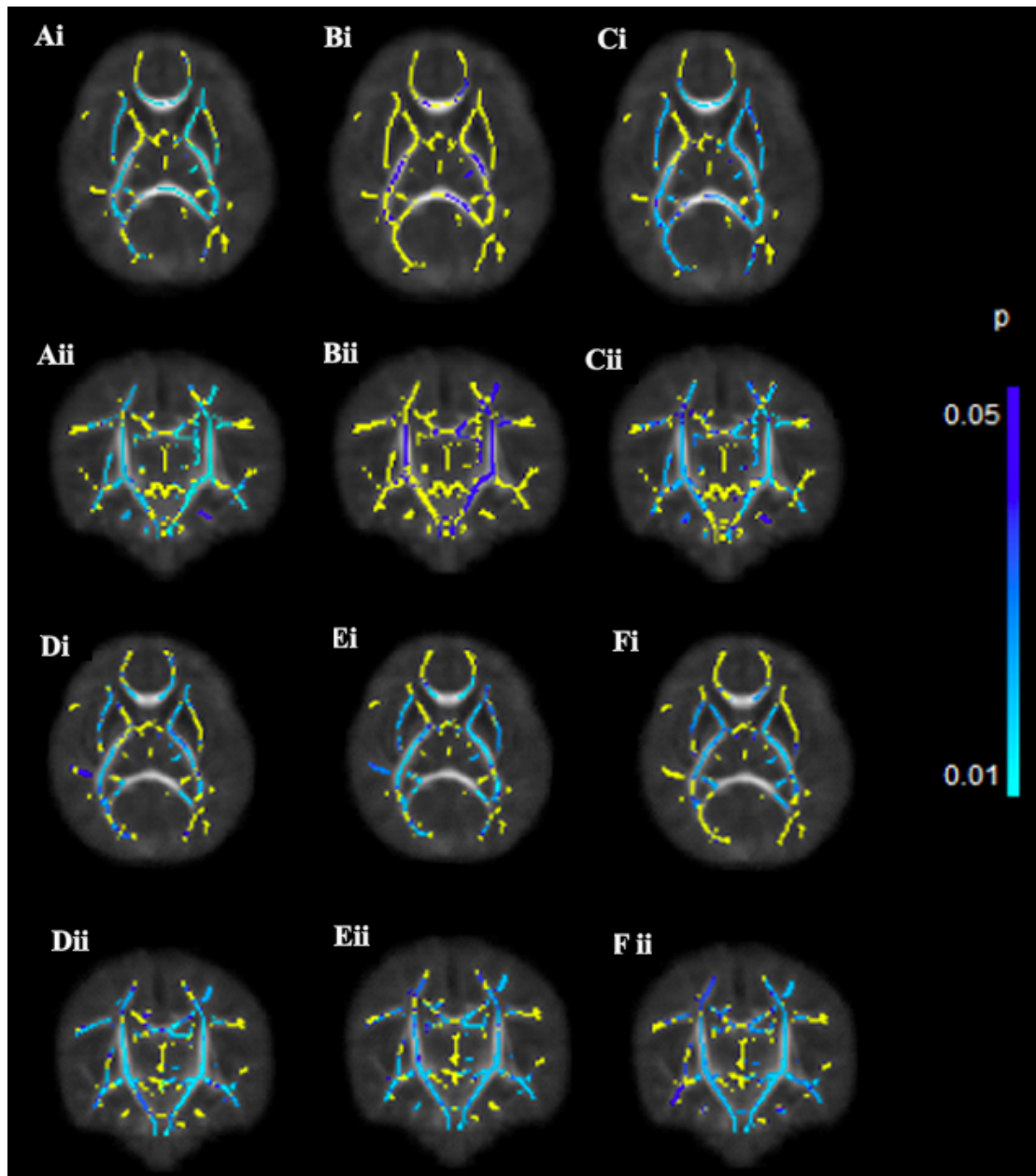
Figure 3.3: Correlation between neurodevelopmental performance scores and fractional anisotropy (FA) as assessed by tract-based spatial statistics. *Mean FA skeleton (yellow) overlaid on mean FA image. Voxels wherein FA is significantly correlated to performance scores are shown in blue. A: Developmental quotient, B: Locomotor, C: Personal-social, D: Hearing and language, E: Eye and hand co-ordination, F: Performance in the (i) axial and (ii) coronal views at the level of the posterior limb of the internal capsule and corpus callosum.*
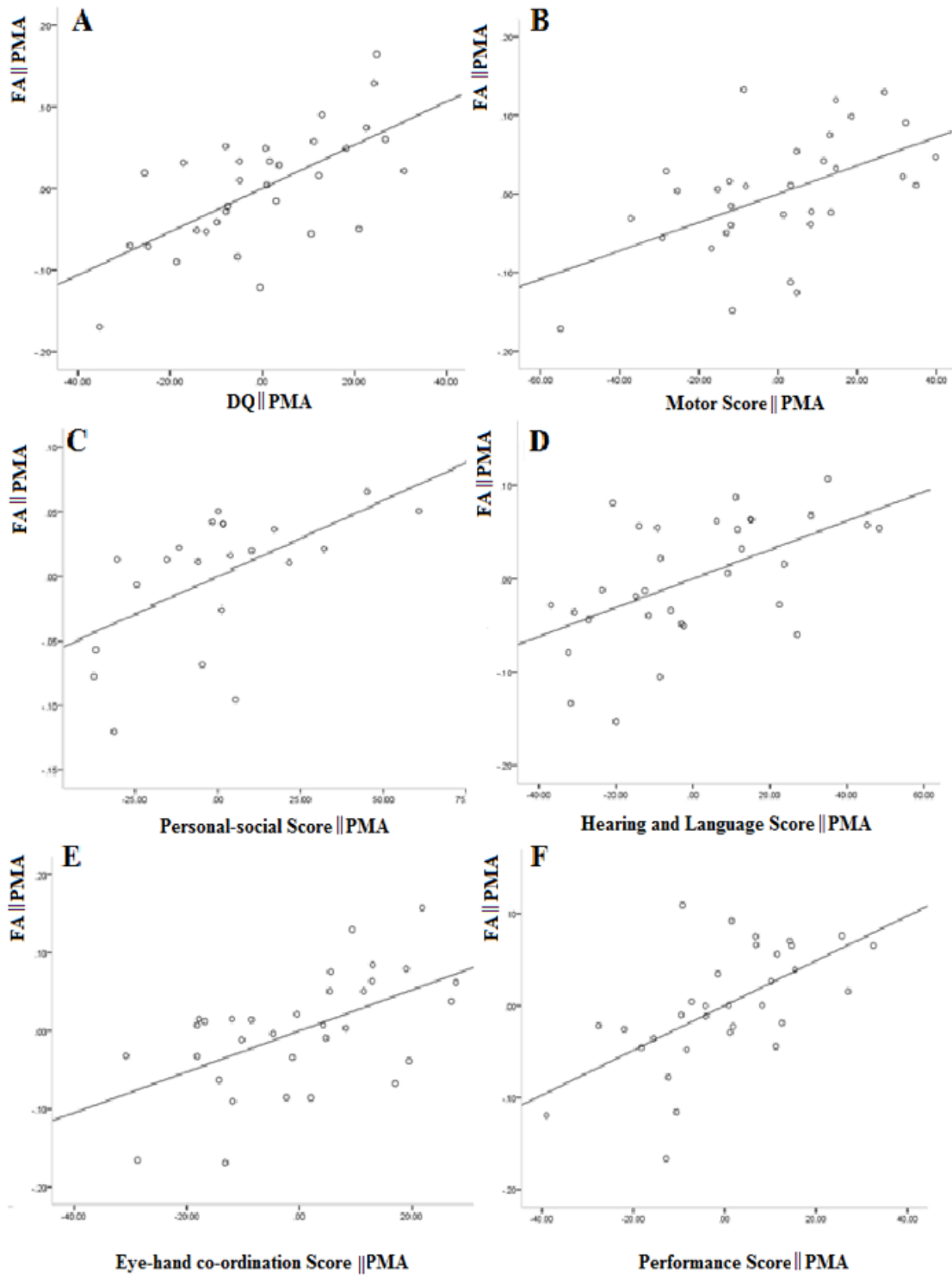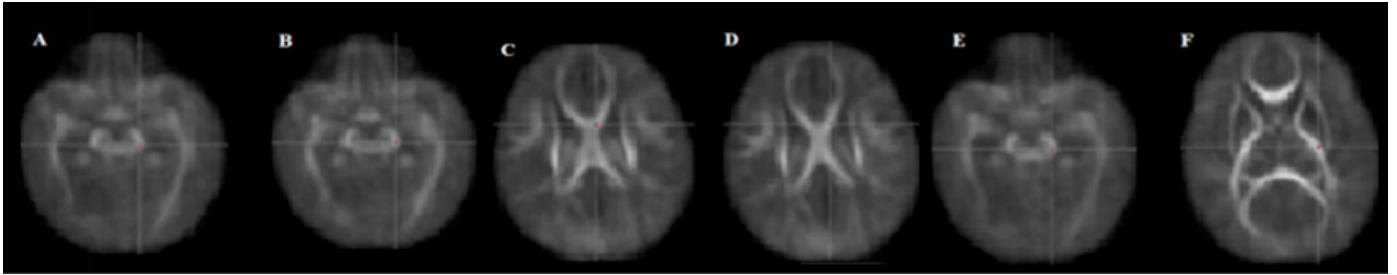
Figure 3.4: Graphs showing associations between fractional anisotropy (FA) in the most significant voxel, corrected for age at imaging, and neurodevelopmental performance scores. *The most significant voxels (red) are indicated by cross hair on the panel above. A: DQ ($R^2=0.417$), B: locomotor ($R^2=0.277$), C: personal and social ($R^2=0.326$), D: hearing and language ($R^2=0.301$), E: eye–hand coordination ($R^2=0.311$), and F: performance ($R^2=0.365$) sub-scale scores. Key: FA || PMA = residuals of FA given the model, DQ || PMA = residuals of DQ given the model; locomotor score || PMA = residuals of locomotor scores given the model; personal–social score || PMA = residuals of personal–social scores given the model; hearing and language score || PMA = residuals of hearing and language scores given the model; eye–hand coordination score || PMA = residuals of eye–hand coordination scores given the model; performance score || PMA = residuals of performance scores given the model. DQ: developmental quotient; FA: fractional anisotropy; PMA: postmenstrual age.*

3.4.5.2 Altered white matter microstructure as assessed by tract-based spatial statistics in infants with an unfavourable outcome

Following the linear regression analysis infants with a favourable (n=26) outcome were compared to those with an unfavourable (n=17) outcome, including those who died or developed cerebral palsy. Using TBSS significantly lower FA values were demonstrated in infants who had an unfavourable outcome compared to infants with a favourable outcome in several regions including the right CSO, splenium, isthmus and genu of the corpus callosum, ALIC, PLIC, external capsules, optic radiations, cerebral peduncles, fornix, cingulum and inferior longitudinal fasciculus (ILF) (Figure 3.5).
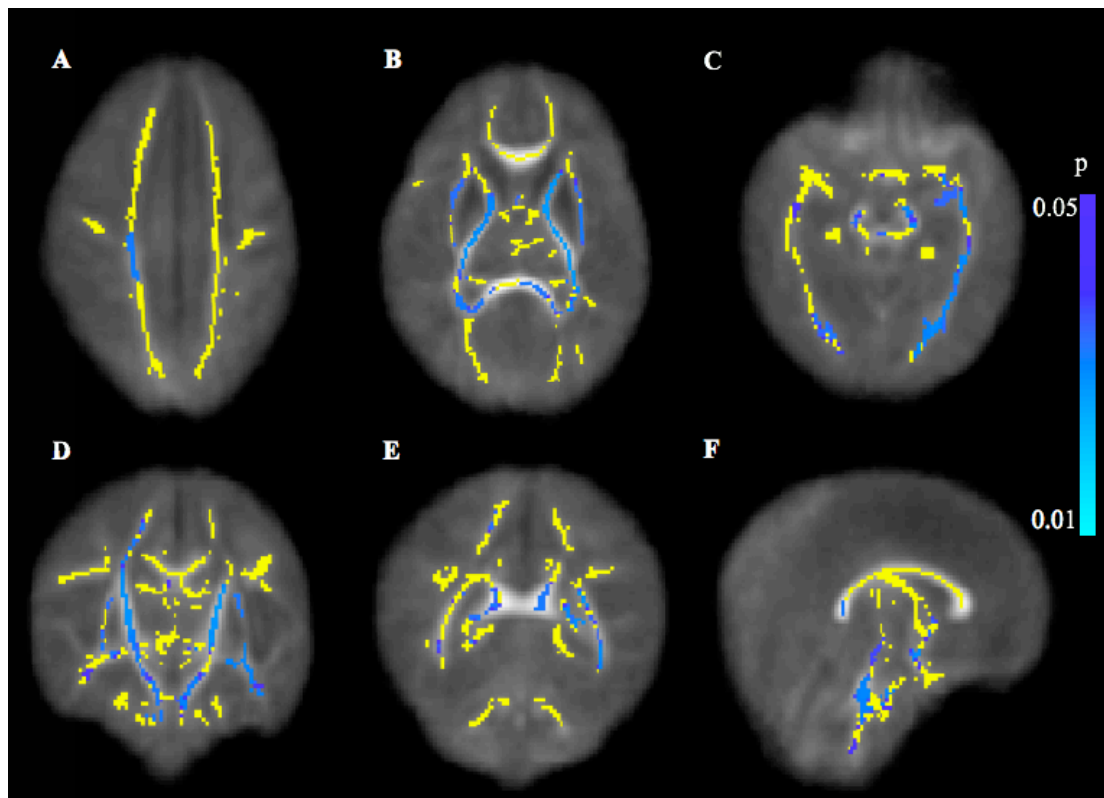
Figure 3.5: The difference in white matter structure between infants with a favourable and unfavourable outcome as assessed by tract-based spatial statistics. *Mean fractional anisotropy (FA) skeleton (yellow) is overlaid on mean FA image. Voxels where infants with unfavourable outcome had significantly lower FA values are shown in blue. Axial view (A-C) at the level of the A: centrum semiovale, B: Posterior limb of the internal capsule (PLIC), C: Cerebral peduncles. Coronal view (D-E) at the level of the D: PLIC and mid corpus callosum; E: splenium of the corpus callosum and the cerebellum. F: Midsagittal view showing the corpus callosum.*

Guided by the results of the TBSS analysis, a ROI approach was carried out to compare FA values between the two groups. FA values were extracted for each infant from the most significant voxel in regions where FA was significantly lower in the

group of infants with an unfavourable outcome. The mean FA value of each group was calculated (Figure 3.6).
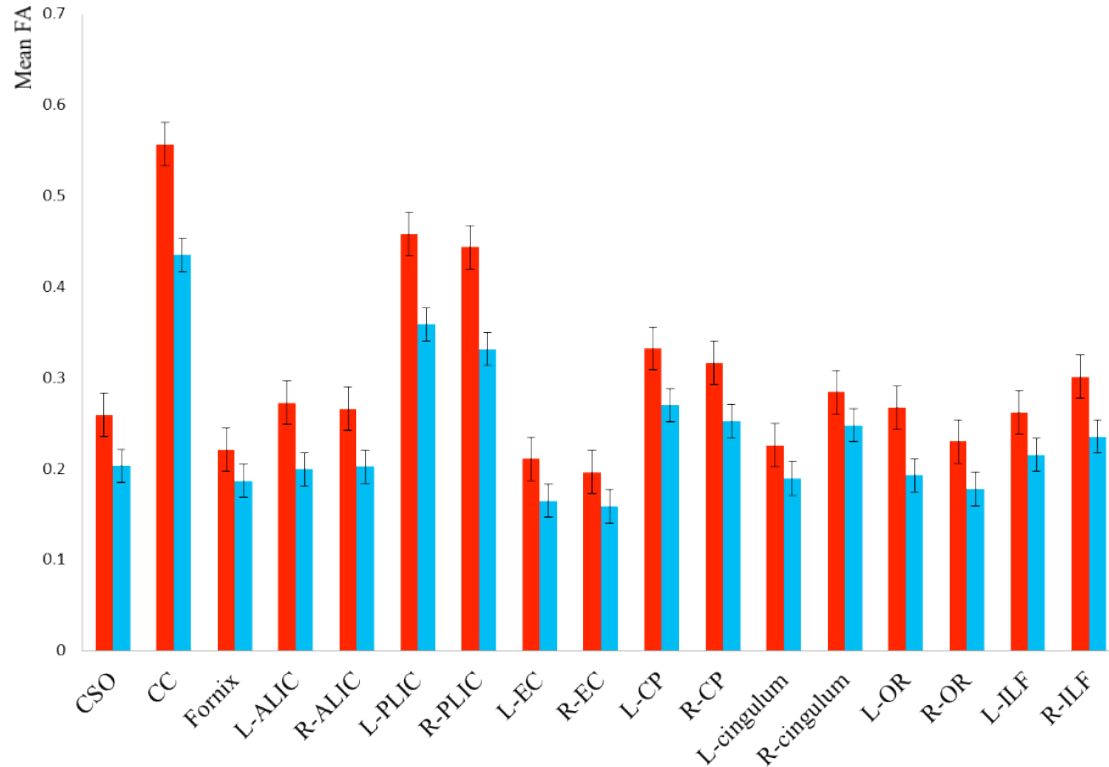
Figure 3.6: Graph showing FA values extracted from the most significant voxel in regions wherein FA was significantly lower in infants with an unfavourable outcome (blue) as compared with infants with a favourable outcome (red). *Abbreviations: FA – fractional anisotropy; L – left; R – right; CSO – centrum semiovale; CC – corpus callosum; ALIC – anterior limb of the internal capsule; PLIC – posterior limb of the internal capsule; EC – external capsule; CP – cerebral peduncle; OR – optic radiation; ILF – inferior longitudinal fasciculus.*

3.5 Discussion

In this chapter FA values in the WM obtained in the neonatal period and assessed with TBSS correlated to subsequent DQ in infants with HIE who received therapeutic hypothermia.

Neurodevelopmental outcome was evaluated using the GMDS in infants who were assessable with a formal neurodevelopmental test. The outcome of children in the present study was comparable to that reported in the cooling arm of the TOBY study (Azzopardi et al. 2009) in terms of rate of unfavourable outcome, death and hearing impairment. However, the rate of cerebral palsy, visual impairment and cognitive deficit was lower in the present study. Although defining cerebral palsy in children less than 18 months may be difficult, all the children who were seen between 12 and 18 months were either already walking independently or requiring only minimal support.

MRI provides the means to assess neuropathology non-invasively. Meanwhile visual analysis of conventional MR images is subjective, scoring systems for classification of distribution and severity of brain injury improve its accuracy. The predictive value of conventional MRI for subsequent neurological impairment is not affected by hypothermia (Rutherford et al. 2010). The predictive value of conventional MRI in the present study was comparable to that reported previously in infants who underwent therapeutic hypothermia for HIE (Rutherford et al. 2010).

Meanwhile conventional MRI is useful to assess brain injury and predict outcome in a single patient, visual analysis of conventional images is a relatively inefficient method

for preliminary evaluation of treatment effect in early phase clinical trials, as a considerable number of subjects is needed to detect a significant difference between treatment groups (Azzopardi and Edwards 2010; Rutherford et al. 2010). Furthermore, brain injury seen on conventional MRI may take several days to evolve.

DTI is a useful tool to assess brain injury early. DTI provides quantitative measures, such as ADC and FA, for objective evaluation of brain injury. Meanwhile, the utility of ADC in HIE is limited due to pseudonormalisation, which is delayed by hypothermia (Artzi et al. 2011; Bednarek et al. 2012; Cheong et al. 2012), FA values do not pseudonormalise following a hypoxic-ischaemic insult (Ward et al. 2006). FA values are lower in infants (Ward et al. 2006; Malik et al. 2007) with a history of perinatal asphyxia compared to healthy controls. Furthermore, previous studies have reported a correlation between FA and outcome following HIE (Malik et al. 2007; Brissaud et al. 2010). However these studies used manually defined ROIs, which is subjective, time consuming and potentially introduce observer-error.

Such problems can be avoided by using TBSS, which is an objective, time-efficient, observer independent tool for cross-subject analysis of whole-brain WM instead of *a priori* chosen ROIs. TBSS alleviates the alignment-related problems of the low-resolution DTI data by projecting the FA values of individual subjects onto a common FA skeleton of major WM tracts. Thus it removes problems due to partial volume effects (Smith et al. 2006). Focusing the analysis on major WM tracts as compared to the entire WM also allows TBSS to have increased statistical power and provides high confidence that FA values are taken from relevant voxels (Smith et al. 2006).

In this chapter a widespread significant linear correlation was found between FA values and outcome scores. A significant correlation was observed in the fornix, cingulum and uncinate fasciculus, structures that are associated with cognition and memory in adults (Aralasmak et al. 2006). FA values in the corpus callosum also correlated with overall DQ and certain sub-scale scores. Although the corpus callosum is not typically found to be abnormal on visual inspection of early MRI scans following HIE, a recent study found reduced callosal dimensions at 2 years of age in children who suffered moderate asphyxia which was predictive of an unfavourable outcome (Twomey et al. 2010). Furthermore a TBSS study of adolescents with a history of moderate neonatal HIE showed significantly lower FA values in the corpus callosum in association with cognitive impairment (Nagy et al. 2005).

A less widespread, but significant correlation was also found between locomotor scores and FA values in the corpus callosum and CST, similar to the results reported previously in a ROI analysis (Malik et al. 2007). The less widespread correlation might be due to several factors. The rate of motor impairment in this study was lower than that reported in previous studies. Also, the GMDS performed at less than 2 years correlated well with DQ as assessed by the Wechsler Preschool and Primary Scale of Intelligence (Wechsler 1999); however it predicted motor outcome as assessed by the Movement Assessment Battery for Children (Henderson and Sugden 1992) less accurately at school age (Barnett et al. 2004).

Furthermore, significantly lower FA values were found in several cerebral regions, such as the corpus callosum, ALIC, PLIC and frontal WM in infants with an

unfavourable outcome, including those who died or developed such severe cerebral palsy that formal neurodevelopmental assessment using GMDS could not be performed.

In summary in this study using TBSS a widespread correlation was found between WM integrity, as assessed with FA, and subsequent DQ. Furthermore with TBSS significantly lower FA values were shown in infants with HIE who developed an unfavourable outcome. These data suggest that TBSS is a qualified biomarker of outcome in infants with HIE who underwent hypothermia. However, a major disadvantage of TBSS is that it is not a feasible tool for evaluation of grey matter and peripheral WM. Therefore, in the next chapter an alternative atlas-based tissue labeling approach will be used that allows studying these cerebral regions.

Chapter 4

Mean diffusivity in cortical and deep grey matter correlates to neurodevelopmental performance in infants with hypoxic-ischaemic encephalopathy treated with hypothermia

4.1 Introduction

In Chapter 3 FA values in the WM, obtained in the neonatal period and assessed by TBSS, correlated with subsequent neurodevelopmental performance in a group of infants with HIE who underwent hypothermic neuroprotection. TBSS is a statistically powerful method for whole-brain voxelwise investigation of WM and offers the advantage of removing errors due to partial volume effects where perfect alignment of individual images is challenging (Smith et al. 2006), however it is not suitable for investigating some cerebral structures often affected in infants with HIE. Due to selective vulnerability of distinct populations of neuronal cells (Black et al. 1995), term infants demonstrate a predilection for injury to the deep grey matter following a hypoxic-ischaemic insult (Rutherford 2002; McQuillen et al. 2003; McQuillen and Ferriero, 2004; Miller et al. 2005; Martinez-Biarge et al. 2010, 2012). In this chapter, cortical and deep grey matter structures will be assessed using DTI.

In the WM, the direction of greatest diffusion correlates with the mean longitudinal direction of axons (Pierpaoli and Basser 1996; Hüppi et al. 1998; Neil et al. 1998; Peled et al. 1998), it is anisotropic and can be quantified with FA. However, at the resolution available to clinical MR systems diffusion in grey matter is relatively isotropic, FA is low hence it is not such a useful measure of injury (Shimony et al.

1999). In the cerebral grey matter apparent diffusivity is largely independent of tissue orientation, therefore MD characterizes its diffusional properties sufficiently (Pierpaoli and Basser 1996; Helenius et al. 2002; Benedetti et al. 2006). MD quantifies the overall magnitude of diffusion by providing average spatial information without indicating preferential direction. MD is affected by cellular size, shape and integrity (Pierpaoli and Basser 1996), decreases with increasing tissue barriers, such as cell membranes and myelin sheath (Basser et al. 2000), and increases in lesions with oedema, demyelination and axonal loss (Pierpaoli et al. 1993).

The isotropic model of diffusion detects structural changes in the grey matter associated with normal brain development (Toft et al. 1996; Mukherjee et al. 2002; Huppi and Dubois 2006; Bartha et al. 2007; Ball et al. 2013), healthy aging (Chiapponi et al. 2013) and different neuropathologies (Helenius et al. 2002; Benedetti et al. 2006; Neuner et al. 2011), including HIE (Wolf et al. 2001; Rutherford et al. 2004; Boichot et al. 2006; Ward et al. 2006; Malik et al. 2007; Vermeulen et al. 2008; Liauw et al. 2009; Brissaud et al. 2010; Massaro et al. 2010; Alderliesten et al. 2011; Artzi et al. 2011; Bonifacio et al. 2012; Ancora et al. 2013; Gano et al. 2013; Thakur et al. 2013). In animal models of HIE decreased MD values correlated with swollen astrocytes immediately (Li et al. 2002); and disintegrated astrocytes (Thornton et al. 1997) with reduced staining of axonal filaments within few hours after a hypoxic-ischaemic injury (Tuor et al. 1998).

Diffusion parameters of cortical and deep grey matter can be analysed by determining diffusion metrics within manually delineated ROIs. This form of analysis is suited for studies of individual patients that require quantitative assessment of diffusion

parameters in a clinically relevant time frame or assessment of a particular brain region. However, ROI analysis is prone to operator-dependent bias particularly, when brain anatomy is affected by pathology (Seo et al. 2013).

Automated segmentation methods overcome some of these limitations, when ROIs are defined by mapping the anatomical information from a brain atlas onto the individual subject's brain. Underpinning this mapping procedure are registration algorithms, which align the anatomy of the atlas with the individual subject's brain to propagate label information (Cabezas et al. 2011). Automatic segmentation of the neonatal brain is challenging due to inverted grey/WM contrast, largely unmyelinated WM around term age, high intra-class signal intensity variability and lower signal to noise ratio. However, dedicated age-specific neonatal brain atlases improve the accuracy of automated segmentation (Xue et al. 2007; Kuklisova-Murgasova et al. 2011; Serag et al. 2012).

4.2 Aim

The aim of this study was to test the hypothesis that in infants with hypoxic-ischaemic encephalopathy treated with therapeutic hypothermia mean diffusivity in cortical and deep grey matter correlates to developmental quotient.

The secondary aim was to quantify the ability of fractional anisotropy and mean diffusivity, determined within grey and white matter tissue labels, to estimate neurodevelopmental performance following hypoxic-ischaemic encephalopathy treated with hypothermia.

4.3 Methods

The Hammersmith and Queen Charlotte's and Chelsea Hospital Research Ethics Committee granted ethical permission for this study. Written parental consent was obtained for each infant prior to scanning.

4.3.1 Subjects

Term infants (>36 weeks at birth) with HIE who received hypothermic neuroprotection were enrolled into this study, who had a brain MRI scan with good quality T2 and DTI data in 32 noncollinear directions within 3 weeks of birth and who were assessed with the GMDS (Huntley 1996) at least at 12 months of age. Demographic data and details of perinatal history were collected from the hospital notes. Of note 32 subjects were also included in the TBSS study in Chapter 3.

Infants who were born at less than 36 weeks, had not been treated with hypothermia within 6 hours after birth, were diagnosed with congenital or chromosomal abnormality, did not have a brain MRI scan with good quality DTI data in 32 noncollinear directions within 3 weeks of birth, or were not assessed using the GMDS, including those who died or were severely disabled that such a test could not be performed were excluded from the analysis.

4.3.3 Neurodevelopmental assessment

Outcome data were collected from hospital notes and clinic letters for each subject. Most infants attended the follow-up clinic at Queen Charlotte's and Chelsea Hospital. For the few infants only seen at other hospitals, the information was obtained from

their local paediatric neurodevelopmental team. Subjects were assessed at least at 12 months of age using the GMDS to evaluate neurodevelopment objectively.

To determine MD/FA cutoff values to estimate outcome subjects were allocated into two groups: (i) those with a favourable and (ii) those with an unfavourable outcome. Unfavourable outcome was pre-specified as the presence of at least one of the following: 1. DQ of two or more SDs below the mean on GMDS (<76) (Ivens and Martin 2002); 2. GMFCS level III-V; or 3. Bilateral cortical visual impairment with no useful vision.

4.3.2 Magnetic resonance imaging

Infants were sedated prior to scanning using oral chloral hydrate unless sedative drugs were already administered for clinical reasons. Intensive care, including ventilation and inotropic support, was provided during the scan as required. All infants were first assessed to be clinically safe for scanning by a paediatrician. Metal check was performed before scanning as per local guidelines. Physiological parameters including heart rate, oxygen saturations and temperature were monitored throughout the scan. Hearing protection was used for each infant, compromising individually moulded earplugs using silicone-based dental putty (President Putty, Coltene/Whaledent, Mahwah, NJ) placed into the external ear, and neonatal earmuffs (Natus MiniMuffs; Natus Medical Inc, San Carlos, CA). All examinations were supervised by a paediatrician experienced in MRI procedures.

MRI was performed on a 3 Tesla Philips Achieva MRI system (Best, Netherlands), with maximum gradient strength of 62 mT/m on each independent axis and slew rate

of 100 mT/m/ms on each axis, using an eight-channel phased array head coil. Three dimensions MPRAGE (TR: 17 ms; TE: 4.6 ms; flip angle: 13°; slice thickness: 8 mm; field of view: 210 mm; matrix: 256x256 (voxel size: 0.82x0.82x0.82)) and high-resolution T2 weighted fast spin echo images (TR: 8670 ms; TE: 160 ms; flip angle 90°; slice thickness 1 mm; field-of-view: 220 mm; matrix: 256×256 (voxel size: $0.86 \times 0.86 \times 1$)) were acquired for clinical evaluation and registration purposes. Single shot echo planar DTI was acquired in 32 noncollinear directions (TR: 8000 ms, TE: 49 ms, slice thickness: 2 mm, field of view: 224 mm, matrix: 128x128, voxel size: 1.75x1.75x2 mm³, b value: 750 s/mm²). The DTI data was acquired with a sense factor of 2 and the scanning time for this sequence was 6 minutes. A perinatal radiologist reviewed the images.

4.3.4 Overview of image analysis pipeline

Each step of the image analysis pipeline (Figure 4.1) will be discussed in details in the next paragraphs. Atlas-based (Serag et al. 2012) automatic segmentation of the T2 weighted images was performed based on tissue type (Makropoulos et al. 2012). Of the segmented T2 weighted image 3 tissue labels (cortex, thalami, WM) were generated in each infant's native T2 space. Tissue labels were propagated to diffusion space through multiple registration steps. MD and FA values were then determined within each tissue label for each infant. Statistical analysis included linear regression to test the correlation between DQ and FA/MD in grey matter. Then the ability of FA and MD, determined within tissue labels, to estimate unfavourable outcome was quantified by calculating the area under the receiver operating characteristic (ROC) curve (AUC).

Segmentation of T$_2$ weighted images
⬇
Generation of tissue labels in T$_2$ space
⬇
Propagation of tissue labels to diffusion space
⬇
Calculation of MD and FA values within each tissue label
⬇
Statistical analysis
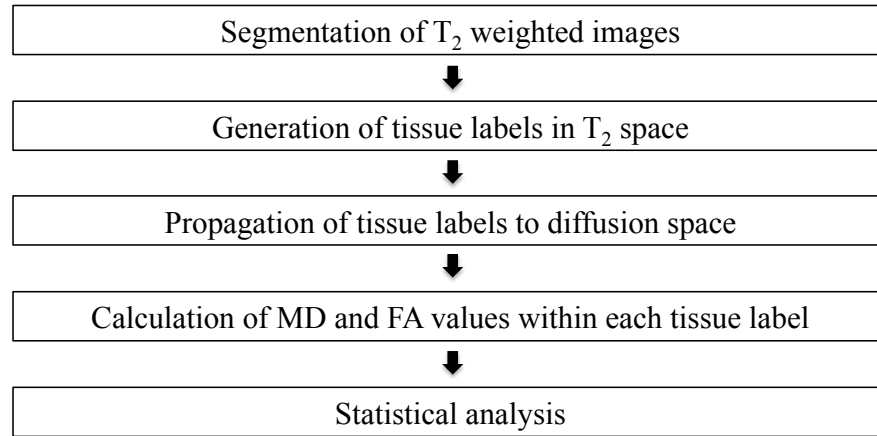
Figure 4.1: Overview of image analysis pipeline. *Abbreviations: FA – fractional anisotropy, MD – mean diffusivity*

4.3.5 Preprocessing of diffusion tensor imaging data

DTI data was analysed offline using tools implemented in FSL as previously described (www.fmrib.ox.ac.uk/fsl) (Jenkinson et al. 2004; Smith et al. 2004). Images were brain extracted to remove all extra-cerebral tissue using BET version 2.1 (Smith 2002). Each infant's diffusion tensor images were registered to their image acquired without diffusion weighting using affine transformation to minimise spatial distortions due to eddy currents using FSL FDT's Eddy Current Correction tool (Jenkinson et al. 2004; Smith et al. 2004). Diffusion tensors were calculated voxelwise, using a simple least squares fit of the tensor model to the diffusion data. From this, the tensor eigenvalues describing the diffusion strength in the primary, secondary and tertiary diffusion directions, and FA and MD maps were calculated (Behrens et al. 2003).

4.3.6 Preprocessing of T2 weighted data

Conventional MR data was preprocessed and analysed using tools implemented in FSL (www.fmrib.ox.ac.uk/fsl) (Jenkinson et al. 2004; Smith et al. 2004) and IRTK (Rueckert et al. 1999; Studholme et al. 1999; Schnabel et al. 2001).

T2 weighted images were skull stripped with FSL's BET version 2.1 (Smith 2002). As tissue segmentation approaches rely on assumptions regarding the shape of the underlying distribution of signal intensities of various tissue types the raw T2 weighted datasets were intensity normalised and corrected for bias field inhomogeneity (van Leemput et al. 2001; Dugas-Phocion et al. 2004; Xue et al. 2007).

4.3.7 Atlas-based automatic brain segmentation

A spatiotemporal non-rigid neonatal atlas was used to propagate age-specific probabilistic tissue priors to each infant's T2 space (Serag et al. 2012). A corresponding atlas template according to age was aligned to each subject's T2 weighted image using rigid, affine and nonlinear transformations with IRTK (Rueckert et al. 1999; Studholme et al. 1999; Schnabel et al. 2001). Tissue labels were then propagated to the subject's native T2 space with the inverse nonlinear transformation of the template to T2 registration (Makropoulos et al. 2012). Of the segmented T2 weighted image, 3 tissue labels, including the cortex, thalami and WM, were generated in each infant's native T2 space. Tissue labels for each individual were visually checked and manually corrected where necessary.

4.3.8 Propagation of tissue labels to diffusion space

Tissue labels were spatially transformed to the diffusion space through multiple registration steps. The diffusion space image acquired without diffusion weighting (B0) of each individual was aligned to the corresponding T2 weighted structural image through rigid, linear and nonlinear transformations with IRTK (Rueckert et al. 1999; Studholme et al. 1999; Schnabel et al. 2001). The inverse nonlinear transformation matrix was used to propagate tissue labels from T2 to diffusion space. Tissue labels overlaid on the B0 image were visually checked and manually corrected where necessary (Figure 4.2).
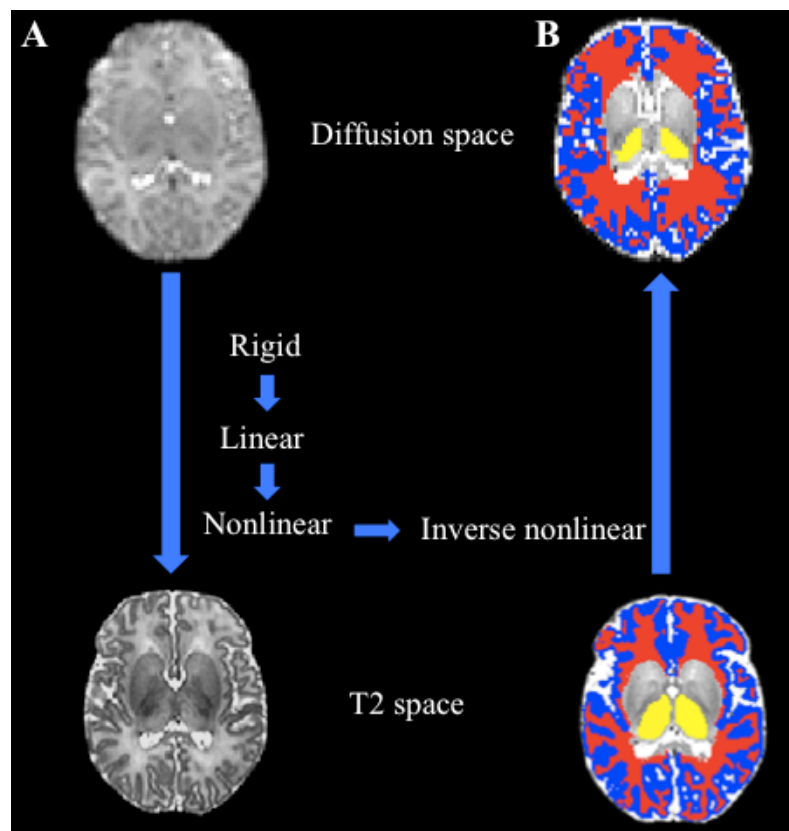
Figure 4.2: Propagation of tissue labels from T2 to diffusion space. A: *Diffusion to T2 transformation through rigid, linear and nonlinear steps. B: Propagation of T2-space tissue labels by applying the inverse nonlinear diffusion to T2 transformation matrix.*

4.3.9 Correlation between diffusion measures and neurodevelopmental performance scores

FA and MD values were determined for each subject within each tissue label.

Linear regression was performed to assess the correlation between DQ and FA and MD. For each infant within each tissue label FA and MD values were plotted against DQ using SPSS (IBM SPSS version 22). As MD changes with increasing PMA and also pseudonormalises following a hypoxic-ischaemic insult, MD values were adjusted for both PMA and days of birth at scan. Although, FA does not pseudonormalise, it changes with increasing PMA. For consistency FA values were also corrected for PMA and days of birth at scan.

Hypothesis testing was corrected for multiple comparisons considering 3 tissue labels and $p<0.016$ was considered significant.

An exploratory analysis was performed to assess the correlation between the subscale scores of the GMDS and FA and MD determined within each tissue label. The results of the exploratory analysis were corrected for multiple comparisons considering 3 tissue labels and 6 developmental outcome scores and $p<0.003$ was considered significant.

4.3.10 Receiver operating characteristic analysis

Following the linear regression infants were divided into two groups, those with a favourable and an unfavourable outcome to perform ROC analysis with SPSS (IBM SPSS version 22). Area under the ROC curve was used to quantify the ability of FA and MD, obtained within grey and WM tissue labels, to estimate unfavourable outcome. MD and FA cutoff values to estimate unfavourable outcome were determined.

4.4 Results

4.4.1 Subjects

Patient flow of this study is shown on Figure 4.3. The clinical characteristics of the infants are shown in Table 4.1.

A total of 121 infants with HIE received therapeutic hypothermia at Queen Charlotte's and Chelsea Hospital between 2007 and 2011. Of the 121 infants 27 did not have a brain MRI scan. Of these, outcome data was available for 12 subjects. Eleven infants died. One child assessed with the GMDS at 24 months achieved scores within normal range for age.

Of the 94 infants, who undewent a brain MRI in the neonatal period, 11 had no outcome available. Of these 11 infants 4 were not eligible to be enrolled into the study for the following reasons: n=1 less than 36 weeks at birth; n=2 abnormal chromosomes (Trisomy 21 n=1; abnormal chromosome 13 n=1); n=1 DTI data acquired in 15 noncollinear directions.

Until 2013 outcome data was available for 83 infants who underwent hypothermia for HIE and a brain MRI scan during the neonatal period.

GMDS was not performed in 31 of the 83 infants for the following reasons. Fifteen infants died. Of these 15 infants 6 were not eligible for the study for the following reasons: n= 1 less than 36 weeks at birth, n=2 DTI acquired in 15 noncollinear directions, n=1 incomplete DTI data, n=2 post-mortem MRI.

Eleven children developed severe disability and could not be assessed with the GMDS. Of these 11 children 7 had global developmental delay and cerebral palsy with GMFCS level III-V (spastic n=2; dystonic n=3; spastic dystonic n=1; athetoid n=1). One child had right hemiplegia GMFCS level II with cognitive delay. Three children developed severe cognitive delay with microcephaly, but without significant motor problems. However, of these 11 children 9 were not eligible to be enrolled into the study for the follwoing reasons: n=7 DTI in 15 noncollinear directions, n=1 cooling started at more than 6 hours of age, n=1 treated for fibrosarcoma following the neonatal period.

Three children seen at the neonatal follow-up clinic were not assessed with the GMDS. One of them attained the maximum optimality score for neurologic examination (Haataja et al. 1999, 2001). A further 2 children were seen by a neonatal consultant but did not have a formal neurodevelopmental assessment. They were deemed by the consultant to have normal neurodevelopment based on physical examination. Two children were assessed using the Bayleys Scale of Infant Development (Bayley 1966) and achieved scores within normal range for age. However, these 5 infants were more than 21 days old at the time of the MRI and therefore were not eligible for this study.

Fifty-two children were assessed with the GMDS at a median (range) age of 22.7 (6-35.5) months until 2013. Seven of the 52 children were excluded for the following reasons: n=1 DTI data acquired in 15 directions; n=3 more than 21 days old at the time the MRI; n=1 less than 36 weeks at birth; n=2 follow-up at less than 12 months

of age. A further 5 children were excluded for whom at least 2 of the subscales of the GMDS could not be scored.

Excluded subjects had significantly lower Apgar scores at 5 minutes. There was no significant difference in any other clinical characteristics.
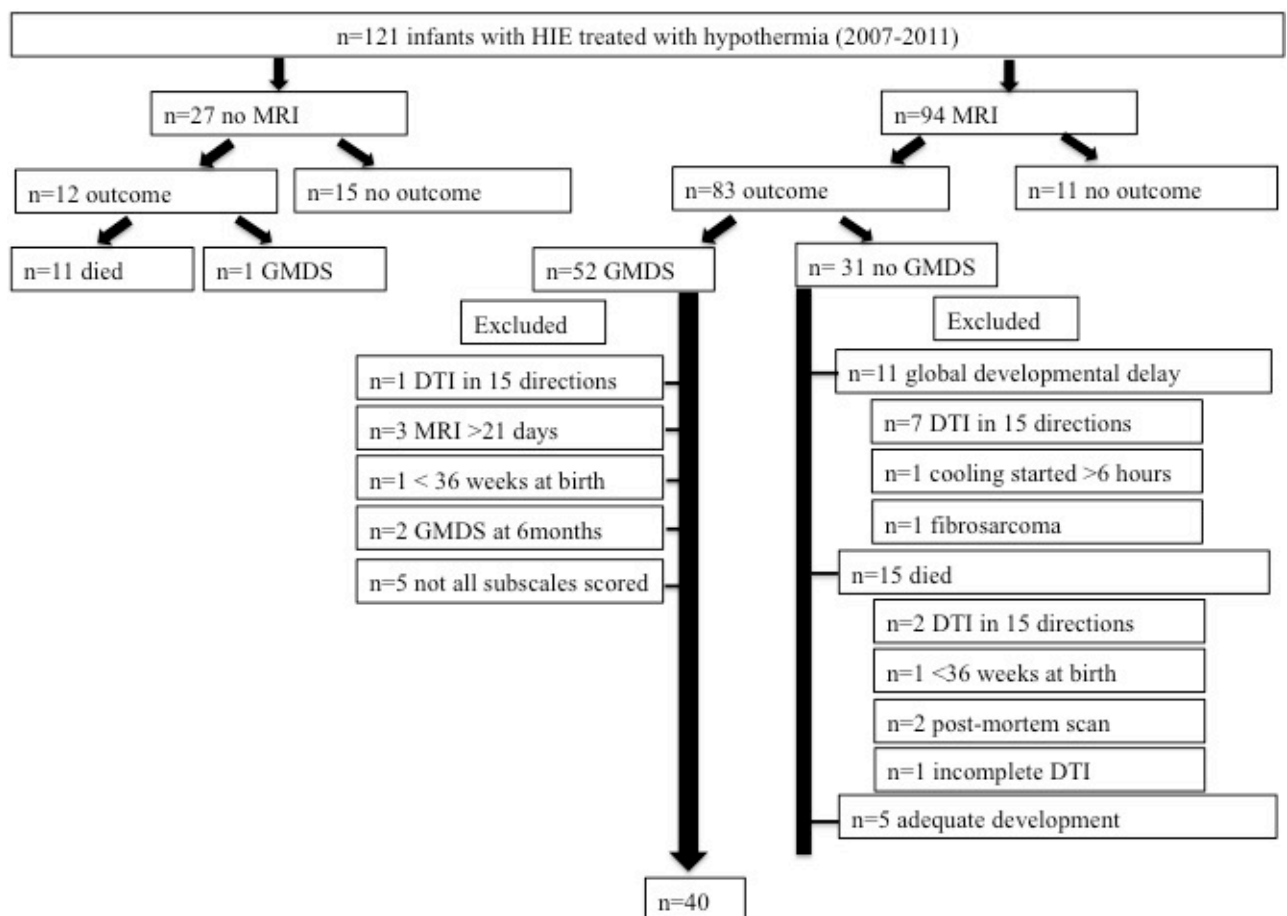
Figure 4.3: Consort diagram of patients. *Abbraviations: HIE – hypoxic-ischaemic encephalopathy; MRI – magnetic resonance imaging; GMDS – Griffiths Mental Developmental Scales; DTI – diffusion tensor imaging*

Clinical characteristics	Total (n=121)	Total MRI (n=94)	GMDS (n=40)	Excluded (n=81)
Postmenstrual age at birth [a]	39^{+4} (35^{+0}-42^{+3})	39^{+4}(35^{+0}-42^{+3})	39^{+5} (36^{+4} – 42^{+3})	39^{+4} (35^{+0} – 41^{+2})
Postmenstrual age at scan [a]	N/A	41^{+1} (36^{+4}-47^{+5})	40^{+5} (37^{+4}-43^{+4})	41^{+2} (36^{+4}-47^{+5})
Postnatal days at scan [a]	N/A	6 (3-67)	7 (3 – 20)	6 (3-67)
Gender male (n)	72	60	29	43
Birth weight (kg) [a]	3.28 (1.96-5.83)	3.22 (1.96-5.30)	3.22 (2.15-4.12)	3.30 (1.96 – 5.83)
Apgar score at 1 min [a]	1(0-7)	1 (0-6)	2 (0-5)	1 (0-7)
Apgar score at 5 min [a]	3 (0-9)	3 (0-9)	4 (0-8)	3 (0-9)
Apgar score at 10 min [a]	5 (0-9)	5 (0-10)	5 (0-9)	4 (0-9)
pH within 1 hour of birth [a]	6.92 (6.54-7.39)	6.96 (6.54-7.39)	6.97 (6.54-7.39)	6.90 (6.58-7.30)
Base deficit within 1 hour of birth [a]	16.64 (3-31.6)	15.50 (3.00-31.60)	15.39 (6.80-25.40)	17.43 (5.30-31.60)

[a] median (range)

Table 4.1: Clinical characteristics of the study infants.

4.4.2 Neurodevelopmental performance

Of the 40 children assessed using the GMDS 7 developed an unfavourable outcome. One of these subjects had significant language delay, 2 had hearing impairment, one of them had hearing aid. One child had astigmatism, left squint with long-sightedness. The mean±SD DQ was 91±20 and the mean±SD quotients for the sub-scales were as follows: locomotor 93±23, personal-social 100±25, hearing and language 85±26, eye and hand coordination 89±21; and performance 89±18.

4.4.3 Correlation between diffusion measures and neurodevelopmental performance

Following correction for multiple comparisons, PMA and days of birth at scan a significant correlation was found between DQ and MD determined within thalamic and cortical tissue labels (p=0.0002 and p=0.005 respectively). However, there was no correlation between DQ and FA in the thalami and cortex.

In an exploratory analysis significant linear correlation was found between MD in the thalami and locomotor (p=0.0005), personal-social (p=0.0002), eye-hand coordination (p=0.0002) and performance (p=0.002) scores after correction for multiple comparisons, PMA and days of birth at scan. However, FA in the thalami did not correlate to any of the subscale scores. Following correction for multiple comparisons no correlation was found between MD/FA in the cortex and any of the subscale scores of the GMDS.

FA values within WM tissue labels significantly correlated to DQ (p=0.0002) after correction for multiple comparisons, PMA and days of birth at scan. In an exploratory analysis a significant linear correlation was found between FA values in the WM and locomotor (p=0.0029), personal-social (p=0.0002), hearing and language (p=0.0001) and eye-hand coordination scores (p=0.0020). However, no correlation was found between MD in the WM and DQ or any other subscale scores (Table 4.2; Figure 4.4).

		Thalami		Cortex		White matter	
		p	R^2	p	R^2	p	R^2
DQ	FA	0.0162	0.079	0.0876	0.025	**0.0002**	0.224
	MD	**0.0002**	0.223	**0.0050**	0.057	0.0415	0.081
A	FA	0.0114	0.101	0.1352	0.017	**0.0029**	0.137
	MD	**0.0005**	0.203	0.0940	0.004	0.1344	0.030
B	FA	0.09495	0.018	0.1757	0.006	**0.0002**	0.231
	MD	**0.0002**	0.195	0.0061	0.041	0.0050	0.163
C	FA	0.0350	0.057	0.0580	0.043	**0.0001**	0.262
	MD	0.0058	0.099	0.0030	0.101	0.0150	0.121
D	FA	0.0264	0.063	0.0757	0.031	**0.0020**	0.146
	MD	**0.0002**	0.206	0.0084	0.050	0.090	0.048
E	FA	0.0174	0.080	0.2127	0.042	0.020	0.065
	MD	**0.0016**	0.145	0.0135	0.006	0.4742	-

Table 4.2: Correlation between diffusion measures and subscale scores within each region of interest. *P values are displayed without correction for multiple comparisons. A – locomotor, B – personal-social, C – hearing and language, D – eye-hand coordination, DQ – developmental quotient, E – performance score, FA – fractional anisotropy, MD – mean diffusivity*

4.4.4 Receiver operating characteristic analysis

A significant area under the ROC curve was demonstrated for MD in grey matter and FA in WM to estimate unfavourable outcome. FA within WM tissue labels showed the largest AUC (Figure 4.4, Table 4.3).
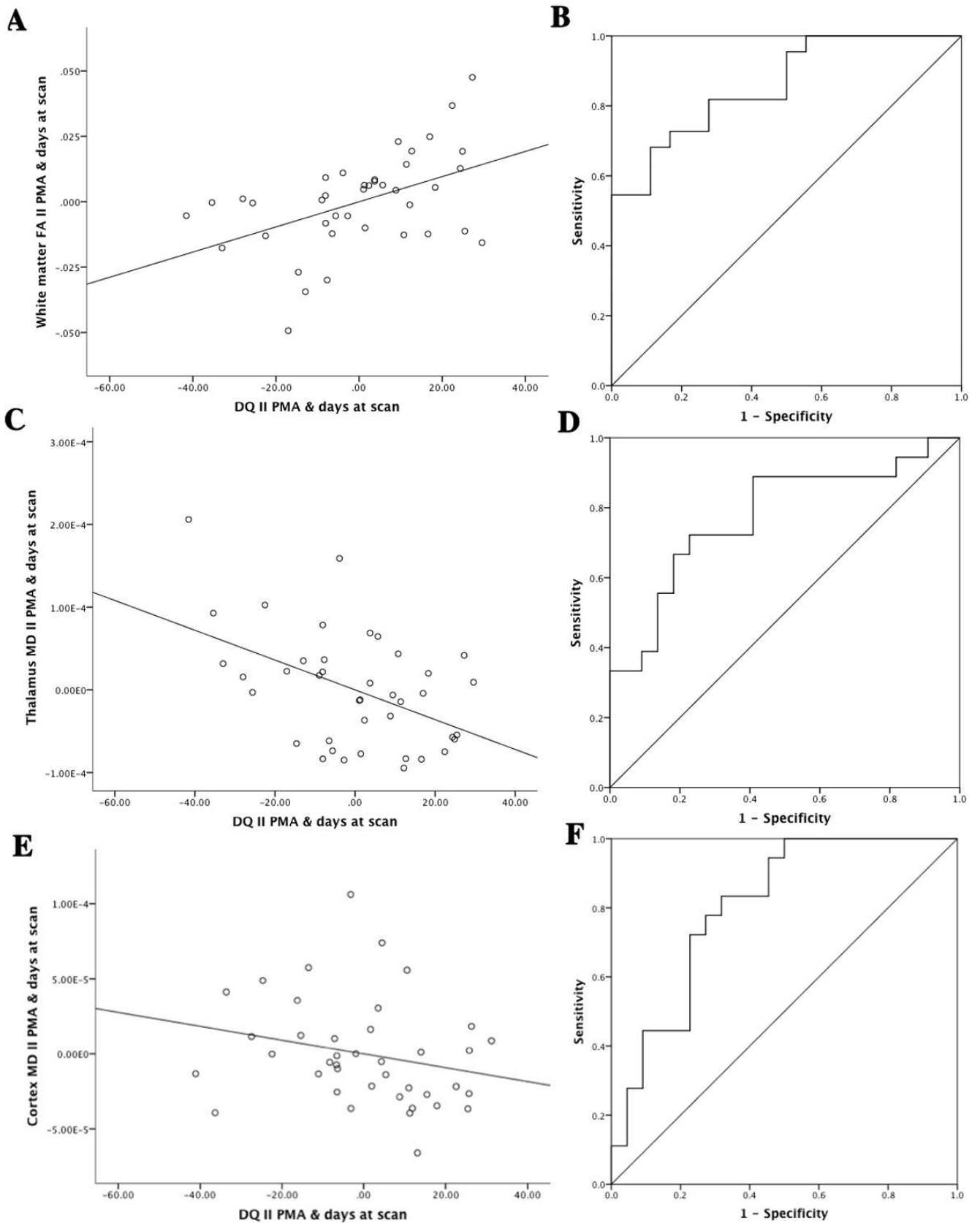
Figure 4.4: Graphs showing correlation between diffusion measures and developmental quotient. *Following correction for multiple comparisons significant linear correlation was found between A: fractional anisotropy (FA) in the white matter and developmental quotient (DQ) ($R^2=0.224$), B: area under the curve (AUC)=0.859; C: mean diffusivity (MD) in the thalami and DQ ($R^2=0.223$), D: AUC=0.775; E: MD in the cortex and DQ ($R^2=0.057$), F: AUC=0.803 Key: White matter FA || PMA & days at scan = residuals of white matter FA given the model; DQ || PMA & days at scan = residuals of DQ given the model; Thalamus MD || PMA & days at scan = residuals of thalamus MD given the model; Cortex MD || PMA & days at scan = residuals of cortex MD given the model. PMA – postmenstrual age.*

	AUC	SE	Significance	95% CI
White matter FA	0.859	0.057	0.000	0.747-0.970
Thalami MD	0.775	0.077	0.003	0.625-0.926
Cortex MD	0.803	0.069	0.001	0.667-0.939

Table 4.3: Results of the receiver operating characteristic analysis. *Abbreviations: AUC – area under the curve, CI – confidence interval, FA – fractional anisotropy, MD – mean diffusivity, SE – standard error.*

Sensitivity, specificity, PPV and NPV for FA and MD cutoff values to estimate unfavourable outcome are shown in Table 4.4.

White matter FA	Sensitivity	95% CI	Specificity	95% CI	PPV	NPV
0.155	72	0.52-0.87	78	0.55-0.91	88	70
0.157	73	0.52-0.87	83	0.61-0.94	84	71
0.161	68	0.47-0.84	89	0.67-0.97	88	70
Thalami MD						
1029.7	59	0.39-0.77	89	0.67-0.97	87	64
1071.8	77	0.57-0.9	72	0.49-0.88	77	72
1074.5	82	0.62-0.93	61	0.39-0.80	72	73
Cortex MD						
1193.5	63	0.43-0.80	83	0.61-0.94	82	65
1197.2	73	0.52-0.87	78	0.55-0.91	80	70
1202.1	77	0.57-0.9	72	0.49-0.88	77	72

Table 4.4: Sensitivity, specificity, positive predictive value (PPV) and negative predictive value (NPV) for different white matter fractional anisotropy (FA), thalami and cortex mean diffusivity (MD) $[10^{-3}mm^2/sec]$ **cutoff values.** CI – confidence intervals.

4.5. Discussion

Due to selective vulnerability (McQuillen et al 2003; McQuillen and Ferriero 2004) neuronal cells in the deep grey matter are highly susceptible to excitotoxicty (Vexler and Ferriero 2001), probably as a consequence of high concentration of EAA receptors in term infants (Black et al. 1995).

In this chapter the grey matter was assessed using DTI. Diffusion MRI has been applied to study brain injury in term neonates following a hypoxic-ischaemic event using both an ROI approach (Wolf et al. 2001; Boichot et al. 2006; Vermeulen et al. 2008; Liauw et al. 2009; Twomey et al. 2010; Alderliesten et al. 2011; Ancora et al. 2013) and TBSS (Porter et al. 2010; Gao et al. 2012; Lally et al. 2014). However, there have been relatively few studies investigating the correlation between diffusion measures and neurodevelopmental performance scores following HIE (Malik et al. 2007; Hunt et al. 2004).

In this chapter correlation between diffusion measures, including FA and MD in grey matter and early neurodevelopmental performance as assessed with the GMDS (Huntley 1996) was tested. Each scale of the GMDS was devised to measure one developmental aspect as completely as possible (Griffiths 1970). However, each subscale shows a moderately high correlation with the DQ suggesting a common factor of general developmental abilities or a latent variable within each subscale (Luiz et al. 1999). Therefore in the present study hypothesis testing was limited to assess the correlation between DQ and FA and MD. The analysis of correlation between subscale scores and diffusion measures was exploratory.

A significant correlation was demonstrated between MD in the grey matter and DQ at 2 years of age as assessed with the GMDS (Huntley 1996). However, no correlation was found between FA in grey matter structures and DQ. This is consistent with previous observations that showed MD to be a more suitable parameter for evaluation of microstructural damage to the grey matter, where there is less cyto-architectural directionality at the resolution of DTI acquisition (Alexander et al. 2007). Decreased MD following a hypoxic-ischaemic insult is due to a failure of the sodium/potassium ATPase pump that leads to sodium, calcium, and water influx from the extracellular space to the intracellular compartment (Sotak 2002). Such changes observed on diffusion MRI of infants with HIE corresponded to intracellular cytotoxic oedema, neuronal degeneration, necrosis, apoptosis, and gliosis on histopathology (Roelants-Van Rijn et al. 2001).

However, the utility of MD is limited due to pseudonormalisation (Wolf et al. 2001; McKinstry et al. 2002; Hunt et al. 2004; Rutherford et al. 2004; Boichot et al. 2006; Winter et al. 2007; Liauw et al. 2009), hence postnatal age at scanning must be taken into account. Furthermore, hypothermia delays pseudonormalisation, which takes place at approximately 12 days in infants who underwent cooling (Bednarek et al. 2012) in contrast to 8 to 10 days in infants who did not receive hypothermia (Wolf et al. 2001; McKinstry et al. 2002; Hunt et al. 2004; Rutherford et al. 2004; Boichot et al. 2006; Winter et al. 2007; Liauw et al. 2009). Although three patients in the present study were scanned at more than 12 days, statistical analyses of MD values were corrected for not only PMA but also postnatal age in days at the time of the scan.

Although FA changes with increasing PMA (Wimberger et al 1995; Huppi et al 1998; Neil et al 1998; Klingberg et al 1999; Hermoye et al 2006), it does not pseudonormalise following a hypoxic-ischaemic insult (Ward et al. 2006; Malik et al. 2007). In previous ROI studies FA was predictive of outcome following HIE (Malik et al. 2007; Ancora et al. 2013) and in Chapter 3 FA, analysed with TBSS, correlated to neurodevelopmental performance scores in infants who underwent hypothermia. However, TBSS is not suitable for evaluating grey matter. To quantify the predictive value of diffusion measures obtained in grey and WM, in this chapter the WM was assessed using the tissue label segmentation approach. FA obtained within WM tissue labels showed a larger AUC to estimate unfavourable outcome, than MD in grey matter structures. This is in line with a recent study where of the diffusion measures FA in fronto-parietal WM was the most accurate predictor of outcome (Ancora et al. 2013).

Although normal values for diffusion parameters obtained in healthy neonates have been published (Huppi et al. 1998; Tanner et al. 2000; Forbes et al. 2002; Mukherjee et al. 2002; Miller et al. 2003; Rutherford et al. 2004; Bartha et al. 2007) and cutoff values have been determined to predict prognosis in a single subject with HIE (Rutherford et al. 2004; Ward et al. 2006; Winter et al. 2007; Ancora et a. 2013), direct comparison of studies is challenging, especially in case of rotationally variant diffusion measures that depend on the scanner and the scanning parameters (Nomura et al 1994; Takeda et al 1997).

ROIs were manually drawn in most of the previous studies (Wolf et al. 2001; Boichot et al. 2006; Ward et al. 2006; Vermulen et al. 2008; Liauw et al. 2009; Twomey et al.

2010; Alderliesten et al. 2011). However, in a recent study objective placement of ROIs was achieved by co-registering individual B0 images to create a study-specific template. ROIs were then generated in the study-specific template space and subsequently projected back to each subject's diffusion space (Ancora et al. 2013).

In the present study a fully automated segmentation method was applied that has been specified for the neonatal brain (Kuklisova-Murgasova et al. 2011; Makropoulos et al. 2012; Serag et al. 2012). Tissue labels have been propagated from an age-specific probabilistic neonatal atlas to each subject's native T2 and then to diffusion space. However, due to propagation of tissue labels from high to low resolution partial volume effects, especially at boundaries of CSF and cortex, and cortex and WM, may significantly influence the accuracy of diffusion measurements (Falconer et al. 1997; Zacharopoulos et al. 1998; Hirsch et al. 1999; Shimony et al. 1999). Furthermore, distribution of diffusion parameters is non-uniform within brain structures; hence the measured values within tissue labels might have been averaged out.

TBSS overcomes some of these limitations. By constraining the analysis to the centre of the WM tracts it avoids errors due to partial volume effects and the disadvantage of averaged out measurements (Smith et al. 2006). The results of an ROI and voxelwise study might be different even within the same population due to intra- and inter-observer differences in placement and size of ROIs, or the smoothing step introduced in the voxelwise methods (Schmithorst et a. 2002). However, in this thesis a significant linear correlation was found between DQ and FA values in the WM obtained both within tissue labels and in the centre of the tracts.

The potential bias introduced by excluding more than half of the subjects is an important limitation to this study. Excluded infants had a significantly lower Apgar score at 5 minutes. However, the Apgar score is a measure of the infant's condition at birth that incorporates subjective components. Furthermore, the Apgar score at 5 minutes correlates poorly with future neurologic outcome in term infants (Casey et al. 2001; Moster et al. 2001).

Twenty percent of the subjects did not have a brain MRI. Notably, the rate of death was more than twice in this group of infants than amongst those who underwent imaging in the neonatal period. Although MRI is safe, the procedure might be burdening to critically ill neonates if not performed under optimal circumstances. The indication and timing of the scan must be planned carefully, considering the clinical condition of the infant, and safety during sedation, transport and scanning (van Wezel-Meijler et al. 2009).

Furthermore as opposed to the survivors who were imaged at a median age of 7 days, infants who died after undergoing MRI were imaged at a median age of 5 days. Most of these infants died following redirection of care in the neonatal period and meanwhile early imaging may have reinforced the clinicians' perception about the probable outcome, these infants demonstrated a more acute pattern of injury involving the whole brain.

Children with cerebral palsy were deemed to have too severe developmental impairment to be assessed with the GMDS (Huntley 1996) and were excluded from the primary analysis. The use of standard measures of intelligence for assessing

children with cerebral palsy poses challenges (Goldkamp 1984; Scheiman 1984; Gangliardi et al. 2013), as the link between limitations in motor domain and neurophysiological skills is not straightforward (Nordmark et al. 2001; Pirila et al. 2004). However, intelligence quotient of survivors with severe cerebral palsy following HIE was estimated to be as low as 48 at 8 years of age (Robertson et al. 1989).

Since the TBSS study (Chapter 3) has been completed outcome data using the GMDS (Huntley 1996) became available for a further 13 children. However, 5 subjects were excluded from the present analysis, because not all subscales of the GMDS could be scored at 24 months of age. This might have been due to short attention spells, which was documented in their clinic letter. Survivors of HIE, even in the absence of cerebral palsy, might be at increased risk of later behavioural, memory and cognitive problems (Lindstorm et al. 2009; van Kooij et al. 2010), hence long-term follow-up of such children is crucial (de Vries and Jongmans 2010).

In summary, diffusion MRI is a suitable method to assess tissue injury following HIE both in the grey and WM. MD in grey matter and FA in WM correlate to subsequent neurodevelopmental performance scores. This data suggest that both FA and MD might be used as a biomarker of outcome in infants with HIE treated who received therapeutic hypothermia. However, DTI does not provide information on functional consequences of a hypoxic-ischaemic insult, therefore in the next chapter resting state fMRI will be used to study changes in functional connectivity in infants with HIE.

Chapter 5

Altered functional connectivity in infants with hypoxic-ischaemic encephalopathy

5.1 Introduction

In previous chapters, DTI was used to characterize the impact of a hypoxic-ischaemic insult on cerebral white and grey matter and to relate these findings to subsequent outcome using voxelwise and tissue segmentation approaches in infants who underwent hypothermia for HIE. However, the predictive power of diffusion MRI techniques is somewhat limited owing to the complex relationship between cerebral structure and function. Functional MRI is ideally suited to study functional consequences of perinatal brain injury (Seigher and Huppi 2010).

Task-driven fMRI was applied in infants with brain injury (Born et al. 2000; Sie et al. 2001; Seigher and Huppi 2010). In these studies, absence of activation and abnormal functional laterality were considered to be markers of altered brain function. However, in healthy infants both positive and negative BOLD responses to stimulation have been detected (Yamada et al. 1997; 2000; Born et al. 1998; 2000; 2002; Martin et al. 1999; Souweidane et al. 1999; Morita et al. 2000; Altman et al. 2001; Anderson et al. 2001; Dehaene-Lambertz et al. 2002; Konishi et al. 2002; Muramoto et al. 2002; Erberich et al. 2003; 2006; Marcar et al. 2004; Arichi et al. 2010, 2012), therefore altered BOLD signal, as a marker of abnormal brain function, should be interpreted with caution. Furthermore, lack of subject cooperation limits

task-driven fMRI studies in infants. Collecting data during rest is therefore ideally suited for neonates with or without brain injury.

Resting state fMRI measures neural activity indirectly by assessing spontaneous, coherent, low frequency fluctuations in BOLD signal within widely distributed brain regions that together constitute RSNs (Beckmann et al. 2005; Fox et al. 2005; Smith et al. 2009). Spontaneous brain activity consumes the vast majority of cerebral energy resources therefore provides a rich source of disease-related signal changes and also makes studying multiple cortical systems at the same time possible (Fox et al. 2010). Moreover, results of previous resting state fMRI studies in healthy term (Fransson et al. 2009) and preterm infants (Doria et al. 2010; Smyser et al. 2010) provide a reference for comparison. Longitudinal studies suggest that the degree of correlation between the BOLD signal timeseries in distinct brain regions in preterm infants up to 4 years of age is similar to that of healthy term born neonates (Lee et al. 2013). An area of considerable interest is to understand the effects of neonatal brain injury. A single study in preterm infants with moderate-severe WM injury demonstrated disruptions to both long and short-range functional connectivity, with the ipsilesional hemisphere being the most affected (Smyser et al. 2013).

Structural and metabolic changes of the brain related to HIE have been studied extensively, however to date there have been no studies assessing the effect of a hypoxic-ischaemic insult on functional connectivity in neonates.

5.2 Aim

The aim of this study was to assess functional resting state networks in infants with hypoxic-ischaemic encephalopathy who underwent hypothermia and in healthy control neonates to test the hypothesis that functional connectivity is altered following hypoxic-ischaemic encephalopathy treated with hypothermia.

5.3 Methods

The Hammersmith and Queen Charlotte's and Chelsea Hospital Research Ethics Committee granted ethical permission for this study. Written parental consent was obtained for each infant before scanning.

5.3.1 Subjects

Two groups of infants were enrolled, infants with HIE who received therapeutic cooling and healthy term neonates. Infants were born at or after 36 weeks gestation and underwent brain MRI with good quality of resting state fMRI data within 5 weeks of birth.

Infants in the HIE group received therapeutic hypothermia at Queen Charlotte's and Chelsea Hospital, without additional neuroprotective therapies.

Infants enrolled as healthy term controls were born in good condition following an unremarkable pregnancy, did not require resuscitation and had an uneventful neonatal period up to the time of the scan. Only infants with no cerebral abnormalities detected on visual analysis of brain MRI were enrolled as healthy controls.

To avoid bias, resting state data of a separate group of healthy infants was used to define reference networks for dual regression. Demographic data of all infants was collected from hospital notes.

5.3.2 Magnetic resonance imaging

Subjects were sedated prior to the scan using oral chloral hydrate, unless the infant was already on medication with sedative effect for clinical reasons. Subjects in the HIE group underwent brain MRI following rewarming for clinical reasons. Term control infants underwent brain MRI as part of other research studies.

 MPRAGE, T2 and DTI sequences were acquired as described in Chapter 3.3.3. Functional resting state data were obtained with the following parameters: TR 1500 ms, TE 45 ms, in-plane resolution of 2.5 mm^2, slice thickness of 3.25 mm, 22 slices, and 256 total volumes. Acquisition of the functional resting state sequence lasted for 6.5 minutes. A perinatal radiologist reviewed the images of all subjects.

5.3.3 Preprocessing and analysis of diffusion tensor imaging data

Cerebral structural differences between infants with HIE and healthy controls were assessed with TBSS. DTI data was preprocessed using FSL's FDT (Behrens et al. 2003). Voxelwise preprocessing of the FA data was carried out with TBSS version 1.1 (Smith et al. 2006) using a protocol that has been modified to improve reliability for neonatal DTI analysis (Ball et al. 2010). Voxelwise cross-subject statistical analysis was performed with Randomise version 2.1 to compare FA values of infants with HIE to those of healthy controls (Smith et al. 2006). The results were corrected for multiple comparisons by controlling for familywise error rate following threshold

free cluster enhancement and p<0.05 was considered significant. The results were also corrected for age at birth and age at scan.

5.3.4 Overview of resting state functional magnetic resonance imaging data analysis pipeline

Each step of the image analysis pipeline will be discussed in details in the next paragraphs. Each resting state fMRI dataset was preprocessed. Resting state functional connectivity was compared between the study groups using a hypothesis-free data-driven approach, dual regression and a hypothesis-driven method, SBCA. In a secondary analysis functional connectivity scores were calculated within the HIE group and correlated with subsequent neurodevelopmental outcome (Figure 5.1).
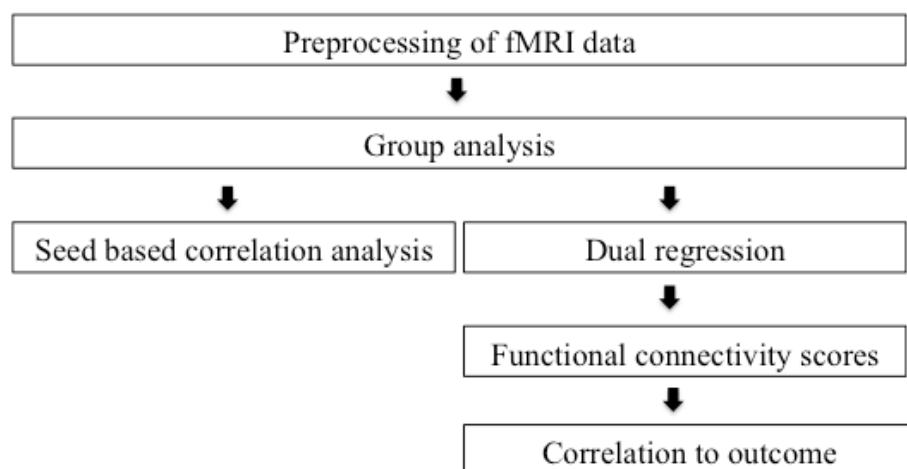
Figure 5.1: Overview of fMRI data analysis pipeline.

5.3.5 Preprocessing of resting state functional magnetic resonance imaging data

Resting state data of each subject was visually inspected to assess quality. Datasets with significant intra- or extra-cerebral haemorrhage, scanner or major motion artefacts were excluded.

Resting state data was preprocessed and analysed off-line using tools implemented in FSL (www.fmrib.ox.ac.uk/fsl) (Smith et al. 2004b). Preprocessing steps were carried out using Multivariate Exploratory Linear Optimised Decomposition into Independent Components (MELODIC) version 3.0. Preprocessing steps included correction for subject movement by applying rigid transformations (6 DOF) of all BOLD contrast image volumes with Motion Correction using FLIRT (MCFLIRT) (Jenkinson and Smith 2001; Jenkinson et al. 2002). The middle image volume timeseries was defined as a reference and all the other volumes were registered onto this reference with affine registration using FLIRT (Woolrich et al. 2001). Datasets with an estimated absolute motion greater than 2.5 mm as assessed by MCFLIRT were discarded. All voxels containing non-brain tissue were excluded, using BET version 2.1 (Smith 2002). Slice-timing correction was applied to remove temporal drifts from the data. All volumes of the datasets were spatially smoothed using a Gaussian isotropic filter with a FWHM of 5 mm. A high pass filter was applied with a cut-off of 200 seconds to remove noise that is unlikely to be part of the signal. Each individual dataset was registered to a T2 weighted neonatal template using FLIRT (Woolrich et al. 2001). The preprocessed filtered functional datasets were used for further analysis.

Nuisance signals were removed from the data by multiple regression before functional connectivity analyses were performed. The preprocessed resting state data of each subject was regressed on CSF signal and 6 motion parameters. The average timeseries of the CSF signal was generated using a mask compromising 3 ROIs manually drawn in the third and lateral ventricles (Fox et al. 2005). Six motion parameters (around X,

Y and Z axes and rotational parameters around 3 axes) were calculated in the motion correction step using MCFLIRT (Jenkinson et al. 2002).

5.3.6 Group analysis of resting state functional magnetic resonance imaging data

Spontaneous fluctuation of the BOLD signal was compared between infants with HIE treated with hypothermia and healthy term control neonates using a hypothesis-free ICA-based (Beckmann and Smith 2004) approach in combination with dual regression (Beckmann et al. 2009; Filippini et al. 2009), and a hypothesis-driven method, SBCA (Biswal et al. 1995).

5.3.6.1 Dual regression

Dual regression involved an initial group ICA decomposition of resting state data of a separate group of healthy term infants (n=8) to define a set of group-average spatial maps, as reference networks.

The set of spatial maps was used to generate subject-specific versions of the spatial maps, and associated timeseries, using dual regression (Beckmann et al. 2009; Filippini et al. 2009). First, for each subject, the group-average spatial maps were regressed (as spatial regressors in a multiple regression) into the subject's 4-dimension dataset. This resulted in a set of subject-specific timeseries, one per group-average spatial map. Next, these timeseries were regressed (as temporal regressors in a multiple regression) into the same 4-dimension dataset, resulting in a set of subject-specific spatial maps, one per group-level spatial map. The resulting spatial maps for each subject were tested for voxelwise between-subject differences using nonparametric permutation testing with Randomise version 2.1 (Figure 5.2). The

results were corrected for multiple comparisons by controlling for familywise error rate following threshold free cluster enhancement and p<0.05 was considered significant. The results were also corrected for PMA and age in days at scan.
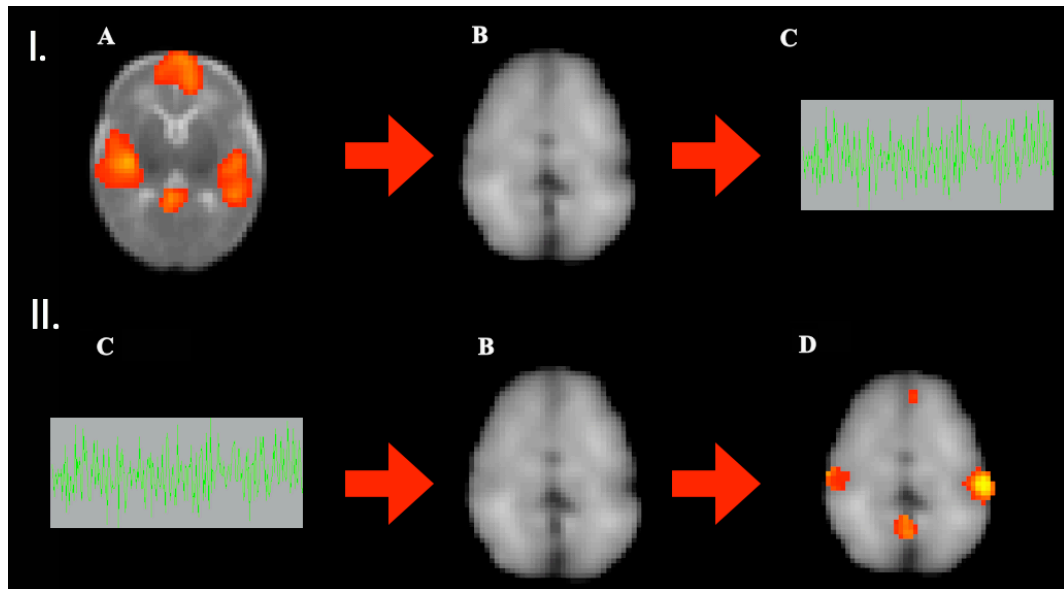
Figure 5.2: Dual regression pipeline. *I. First, for each subject, the group-average spatial map (A) was regressed into the subject's four-dimension dataset (B) resulting in a subject-specific timeseries (C). II. Then, the subject-specific timeseries (C) was regressed into the same four-dimension dataset (B), resulting in a subject-specific spatial map (D). The spatial maps for each subject were tested for voxelwise between-subject differences.*

5.3.6.2 Seed-based correlation analysis

SBCA is based on the assumption that in resting state data low frequency temporal fluctuations of the BOLD signal are correlated between functionally connected regions (Biswal et al. 1995). Based on a priori assumptions about the spatial localisation of RSNs, seed masks were generated on an age-specific neonatal template (Doria et al. 2010). Seed masks were placed in the left auditory, somatomotor and

visual cortices to assess the auditory, somatomotor and visual networks. The MPFC was considered as part of the DMN (Figure 5.3). Statistical maps were then generated by calculating the correlation of each voxel's timeseries in the resting state data with the timeseries of voxels in the seed mask to find temporally consistent RSNs (Beckmann et al. 2005).
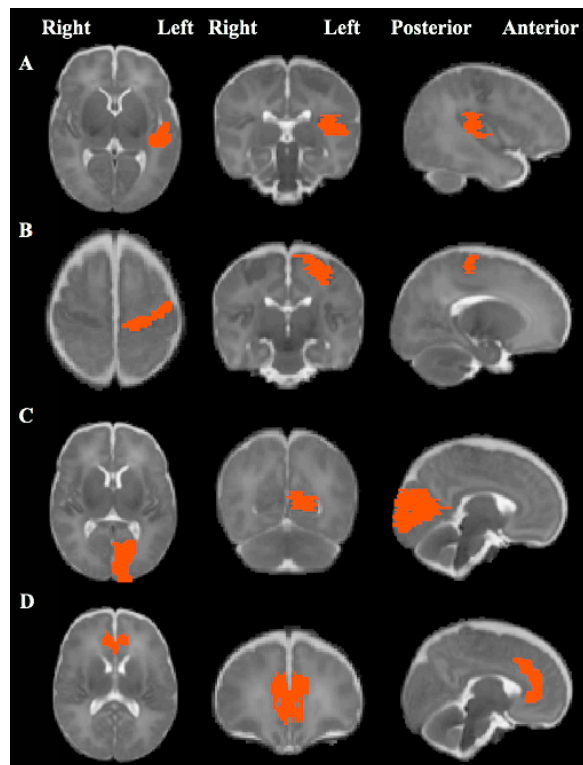
Figure 5.3: Seed regions for seed-based correlation analysis. *Seed masks (red) are overlaid on a term infant template in the transverse (first column), coronal (second column) and sagittal (third column) views. A: Auditory, B: Somatomotor, C: Visual, D: Medio-prefrontal cortex seed mask.*

Seed masks were propagated from the template to the individual resting state fMRI space for each subject through multiple registration steps. The neonatal T2 weighted template was aligned to each subject's preprocessed filtered resting state dataset using

212

linear registration as implemented in FLIRT (Jenkinson and Smith 2001; Jenkinson et al. 2002). Each seed mask was then registered onto the individual preprocessed resting state dataset using the inverse of the above affine transformation matrix. Using FSL tools (Smith et al. 2004b), the first eigen timeseries from the seed regions was extracted. Partial correlation coefficients from the seed regions were then calculated for all other voxels in the brain. This resulted in one image per subject, reflecting the correlation between the seed mask and each voxel of the brain. The correlation coefficients were Fisher's R to Z transformed (Vincent et al. 2007; Shehzad et al. 2009). Then each individual Z map was spatially transformed to the neonatal template to perform group analysis.

The individual Z transformed template-space statistical maps were merged. Randomise version 2.1 was used for voxelwise comparison of the study groups. The results were corrected for multiple comparisons by controlling for familywise error rate following threshold free cluster enhancement and $p < 0.05$ was considered significant. The results were also corrected for PMA and age in days at scan.

An explanatory variable was used to control for possible differences in brain volumes (Figure 5.4). Individual T2 weighted images were brain extracted using BET version 2.1 and bias-field corrected using FMRIB's Automated Segmentation Tool (FAST) (Zhang et al. 2001). Preprocessed T2 weighted images were aligned to the neonatal T2 weighted template through multiple registration steps, including rigid, linear and nonlinear, using tools implemented in IRTK (Denoton et al. 1999; Rueckert et al. 1999; Schnabel et al. 2001). Final alignment was achieved with nonlinear transformation that was represented by a FFD matrix (Schnabel et al. 2007). Maps of

Jacobian determinants were generated for a given transformation, specified by the FFD matrix. The Jacobian determinants were used as an index of volume difference. The Jacobian determinants represent regions of expansion (>1), contraction (<1) and volume preservation ($=1$). The individual T2 weighted images were divided by the Jacobian maps using FSL (Smith et al. 2004). The divided individual images were merged and used as an explanatory variable in the GLM.
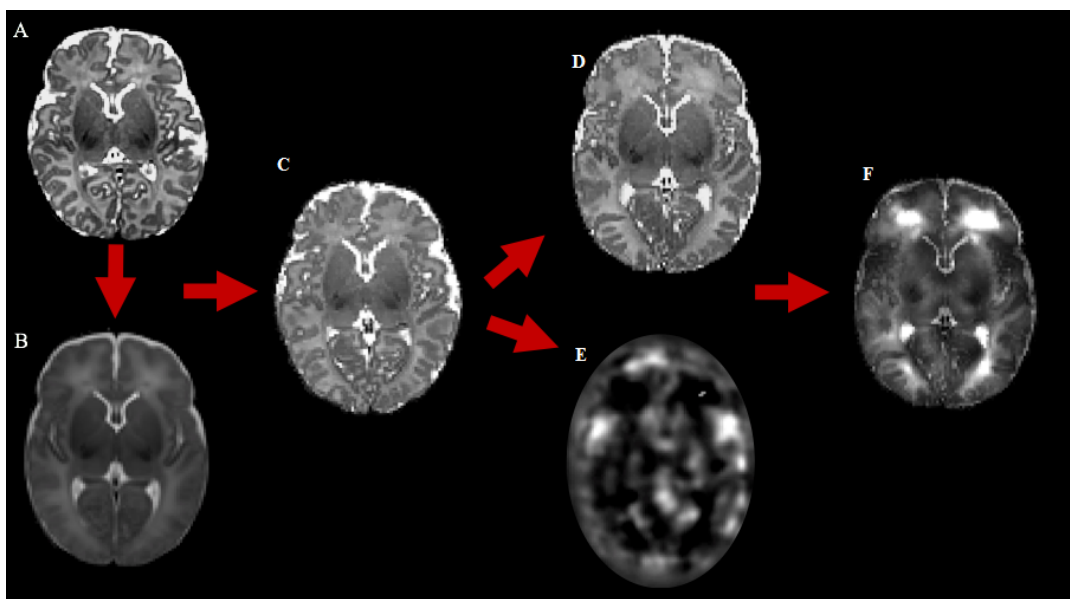
Figure 5.4: Pipeline for generating input for the explanatory variable to control for differences in brain volumes. *Individual preprocessed T2 weighted images (A) were aligned to a term infant template (B) with linear registration (C). Then the linear registration matrix was used to further refine the alignment by nonlinear transformation resulting in a transformed image (D) and Jacobian determinants (E). Finally the nonlinearly transformed template-space image (D) was divided by the Jacobian determinants (E). The output (F) of this pipeline for each infant was merged and used in the general linear model to control for the differences in brain volumes.*

To investigate the effect of sedation, infants with HIE who were sedated using other medication than chloral hydrate were excluded and voxelwise comparison of the study groups was repeated using Randomise version 2.1.

5.3.7 Outcome of infants with hypoxic-ischaemic encephalopathy

Information on neurodevelopmental outcome of infants who suffered HIE was collected from hospital notes and clinic letters. Infants with HIE were allocated into two groups, those with a favourable and those with an unfavourable outcome. Unfavourable outcome was defined as death or the presence of at least one of the following impairments: 1. DQ with 2 or more SDs below the mean; 2. GMFCS level III-V; or 3. Bilateral cortical visual impairment with no useful vision.

5.3.8 Correlation between functional connectivity scores and outcome

Subsequent to dual regression functional connectivity measures indexing the strength of connectivity between a given ROI and the rest of the RSN was extracted as follows. ROIs were defined using the peaks of functional connectivity local maxima from each component of dual regression that were the centre of a 5 mm diameter spherical mask. Functional connectivity scores were subsequently extracted from the ROIs for each individual. The measures derived from this analysis are considered as an index of strength of functional connectivity from each ROI to the rest of the network (Sharp et al. 2011; Bonnelle et al. 2012). Functional connectivity scores were tested for normality. Mean connectivity scores of infants with a favourable outcome were compared to those with an unfavourable outcome within each ROI using independent t- or nonparametric tests as appropriate. Statistical analysis was carried out using SPSS (IBM SPSS version 22).

5.4 Results

5.4.1 Subjects

A total of 121 subjects with HIE received therapeutic hypothermia at Queen Charlotte's Hospital between 2007 and 2011. Of the 121 infants 27 did not have a brain MRI scan. Resting state data was acquired in 31 infants. Of these 16 infants were excluded due to intra-cerebral haemorrhage (n=3), large extra-cerebral haemorrhage (n=1), and motion artefact (n=12).

Resting state data was acquired in 84 healthy term infants. Sixty-one datasets were excluded for the following reasons: Nyquist ghosting (n=16), motion artefact (n=38), abnormal MRI finding (n=1), and no sedation (n=6). Fifteen consecutive good quality resting state datasets were included in the healthy control group. The data of the remaining 8 healthy infants was used to define group-average reference networks for dual regression.

Clinical characteristics of the subjects enrolled into the study are shown in Table 5.1. No statistical difference was found between the study groups for gestational age (p=0.65), birth weight (p=0.67) or head circumference at birth (p=0.68). Infants in the HIE group had significantly higher base deficit (p=0.002), significantly lower cord pH (p=0.003), and Apgar scores at 5 and 10 minutes (p=0.001).

		HIE (n=15)	Healthy control (n=15)	Healthy subjects to define reference networks (n=8)
Age at [a]	birth	40^{+2} (36^{+0} - 41^{+4})	40^{+2} (36^{+1} - 41^{+6})	39^{+3} (36^{+0} - 41^{+6})
	scan	41^{+2} (36^{+3} - 45^{+0})	42^{+2} (39^{+6} - 45^{+3})	43^{+0} (37^{+3} – 44^{+0})
Gender (male) (n)		6	7	4
Birth weight (kg) [a]		3.2 (2.2-4.6)	3.5 (2.6-4.0)	3.2 (2.0-4.1)
pH [a]		6.9 (6.8-7.3)	7.24 (7.12-7.29)	7.24 (7.01-7.34)
Base deficit [a]		14.2 (10.4-22.4)	2.4 (1.6-5.1)	7.4 (3-11.4)
Apgar[a]	5 min	4 (1-9)	10 (10)	10 (9-10)
	10 min	5 (2-9)	10 (10)	10 (10)

[a] Median (range)

Table 5.1: Clinical characteristics of the study infants.

5.4.2 Magnetic resonance imaging

All infants underwent brain MR imaging within 5 weeks of birth. Median age at scan was 41^{+2} weeks (6 days) in the HIE and 42^{+2} weeks (14 days) in the control group. There was a significant difference in age at scan between the study groups (p=0.02).

Chloral hydrate was used for sedation before scanning, except for 5 infants in the HIE group who were already on medication with a sedative effect (oral Phenobarbital n=2, intravenous Morphine n=2, intravenous Midazolam n=1).

Seven infants in the HIE group required respiratory support during the scan (conventional ventilation n=4; nasal oxygen n=3). There was no statistical difference in the carbon dioxide level as measured by capillary blood gas around the time of the scan between infants who required respiratory support and those who were self-

ventilating in air during the scan (p=0.062). However, 3 subjects, including 1 on nasal oxygen had no capillary blood gas done on the day of the scan.

5.4.3 Conventional magnetic resonance imaging

No congenital abnormality or thrombosis was demonstrated on conventional MRI in any of the infants. In the HIE group the WM was abnormal in all subjects. In 4 neonates there were no other changes. Lesions in the BGT consistent with an acute hypoxic-ischaemic insult were detected in 10 infants. The PLIC was abnormal in 6 and equivocal in 2 neonates. The cortex was abnormal in 4 subjects.

In the control group the conventional MRI findings were appropriate for age in all infants. However, one infant had mild ventricular asymmetry.

5.4.4 Structural changes of white matter in infants with hypoxic-ischaemic encephalopathy as assessed by tract-based spatial statistics

The WM skeleton consisted of 23286 voxels. Significantly lower FA values were demonstrated in infants with HIE treated with hypothermia compared to healthy controls in cerebral regions including the splenium of the corpus callosum, bilateral optic radiations, cingulum and ILF, left CSO and external capsule, right PLIC and cerebral peduncle (Figure 5.5).
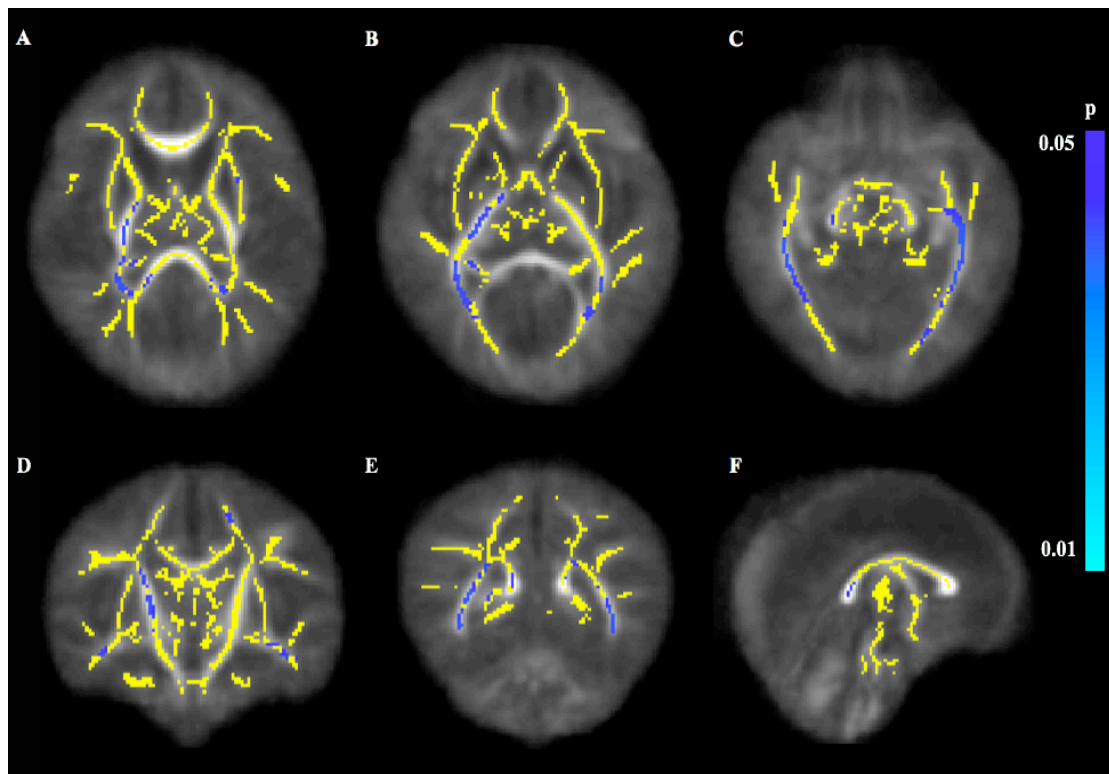
Figure 5.5: The difference in white matter structure between infants with hypoxic-ischaemic encephalopathy (HIE) and healthy term controls as assessed by tract-based spatial statistics. *Mean fractional anisotropy (FA) skeleton (yellow) overlaid on the mean FA image in transverse (A-C), coronal (D-E) and sagittal (F) views. Voxels where infants with HIE had significantly lower FA values are shown in blue. A: right posterior limb of the internal capsule (PLIC), left external capsule, splenium of the corpus callosum, B: right PLIC, bilateral optic radiations, C: right cerebral peduncle, bilateral optic radiations, D: left corona radiata, right PLIC, bilateral inferior longitudinal fasciculi, E: bilateral optic radiations, F: splenium of the corpus callosum.*

5.4.5 Group analysis of resting state functional magnetic resonance imaging data

5.4.5.1 Dual regression

Reference networks were identified in a separate group of 8 healthy term infants using ICA temporal concatenation. Four ICs, representing the default mode, auditory, somatomotor and visual networks were used as reference networks (Figure 5.6).
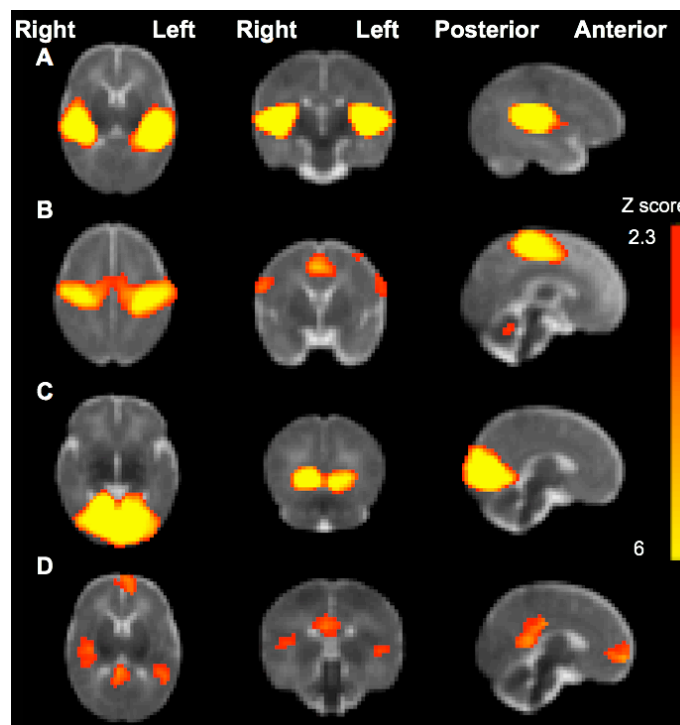
Figure 5.6: Reference networks for dual regression. *Networks are displayed as Z maps, overlaid on a T2 weighted term neonatal template in the transverse (first column), coronal (second column) and sagittal (third column) views. A: Auditory, B: Somatomotor, C: Visual, D: Default mode network.*

In the control group RSNs were spatially similar to the reference networks. RSNs showed bilateral inter- and intra-hemispheric connections on a group level. For the DMN, activation was detected in the MPFC and bilaterally in the temporo-parietal

cortices. For the auditory, somatomotor and visual networks bilateral distribution was identified in the primary and secondary auditory, primary and supplementary motor and primary and extrastriate visual cortices respectively (Figure 5.7).
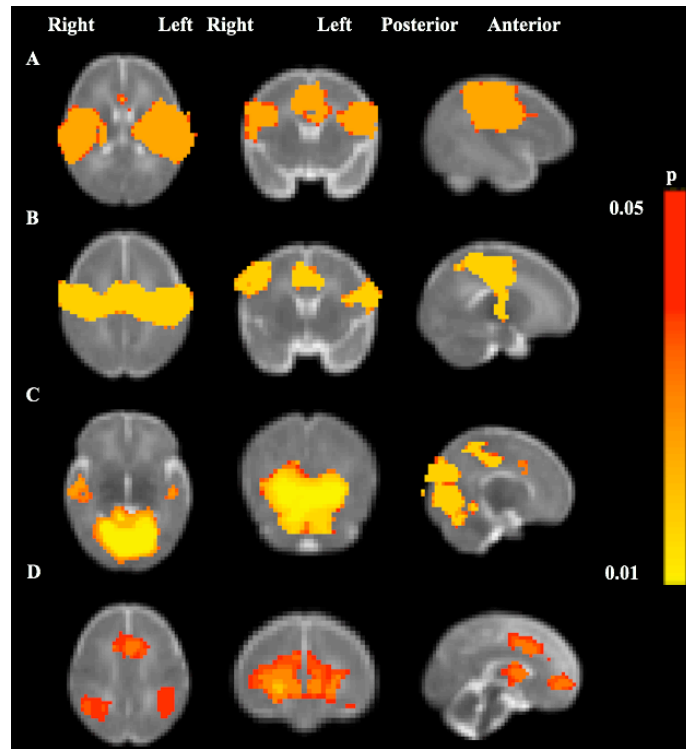
Figure 5.7: Resting state networks in the control infants as identified by dual regression. *Group mean maps are overlaid on a term T2 weighted template in the transverse (first column), coronal (second column) and sagittal (third column) views. A: Auditory, B: Somatomotor, C: Visual, D: Default mode network.*

In the group of infants who suffered HIE networks were more likely to be unilateral with no long-range intra-hemispheric connections (Figure 5.8).
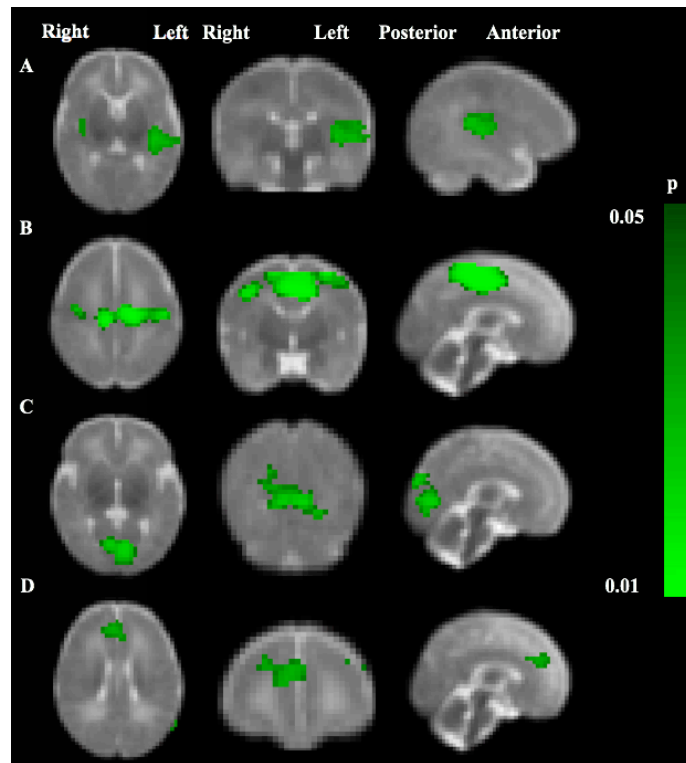
Figure 5.8: Resting state networks in the infants with hypoxic-ischaemic encephalopathy as identified by dual regression. *Group mean maps are overlaid on a term T2 weighted template in the transverse (first column), coronal (second column) and sagittal (third column) views. A: Auditory, B: Somatomotor, C: Visual, D: Default mode network.*

Significantly lower (p<0.05) functional connectivity was found in infants with HIE compared to healthy controls using dual regression (Figure 5.9).
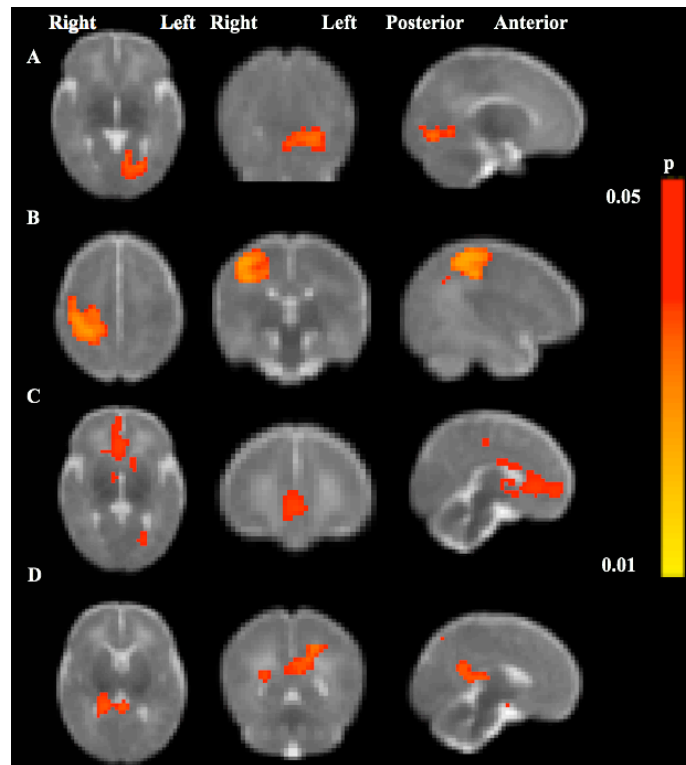
Figure 5.9: Statistical difference maps generated by dual regression. *Difference maps are overlaid on a T2 weighted template in the transverse (first column), coronal (second column) and sagittal (third column) views. A: Auditory, B: Somatomotor, C: Visual, D: Default mode network.*

5.4.5.2 Seed-based correlation analysis

In the control group the full range of RSNs was identified on a group level using SBCA. Networks showed bilateral inter- and intra-hemispheric connections. A left sided seed mask in the primary auditory cortex was used to test the auditory network. Symmetrical bilateral activation was found in the primary and secondary auditory cortices, as well as in the anterior cingulate and supramarginal gyri and the thalami. When investigating the sensorimotor network with a seed mask in the left somatomotor cortex, bilateral activation was identified in the pre- and post-central gyri, as well as in the supplementary motor area and premotor cortex. A seed mask in

the left primary visual cortex was used to test the visual network, and bilateral activation was located in the primary visual cortex extending into the extrastriate visual areas. With a seed mask in the MPFC, as part of the DMN, functional connectivity was identified in the MPFC and in the parietal cortices bilaterally, but not in the PCC (Figure 5.10).
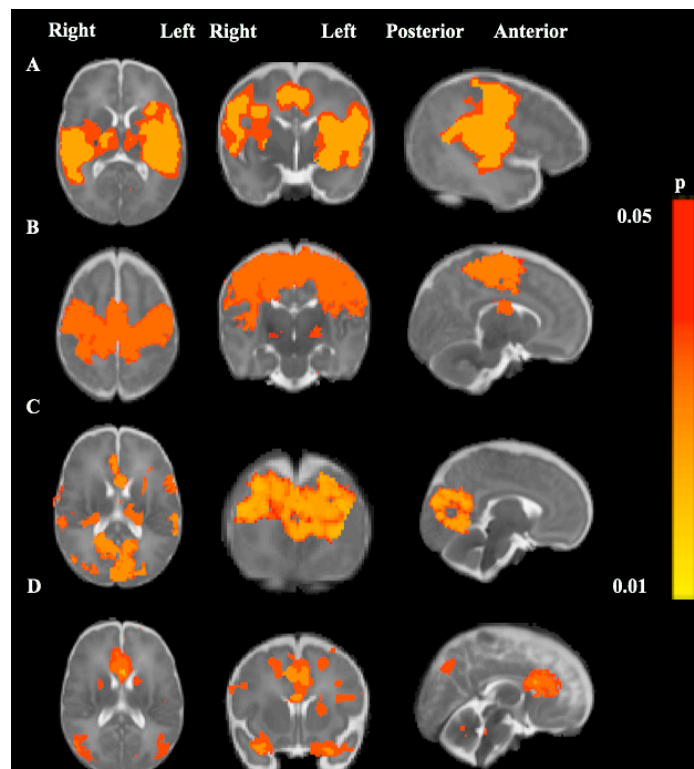
Figure 5.10: Resting state networks in the control infants as identified by seed-based correlation analysis. *Seed masks in A, B and C were placed in the left hemisphere. Group mean maps are overlaid on a term infant template in the transverse (first column), coronal (second column) and sagittal (third column) views. A: Auditory, B: Somatomotor, C: Visual, D: Default mode network.*

In the group of infants who suffered perinatal asphyxia treated with hypothermia, RSNs were more localised, with less extensive inter-hemispheric and no long-range

intra-hemispheric correlation on a group level. In the auditory network bilateral activation was found, however it was localised around the primary auditory cortex, being more extensive ipsi-lateral to the seed mask. The somatomotor network was localised in the primary motor and the somatosensory area, with less activation on the contra-lateral side of the seed mask. Activation of the visual cortex was unilateral in the primary visual cortex with no inter- or long-range intra-hemispheric connections. The DMN was localised in the prefrontal cortex, around the location of the seed mask (Figure 5.11).
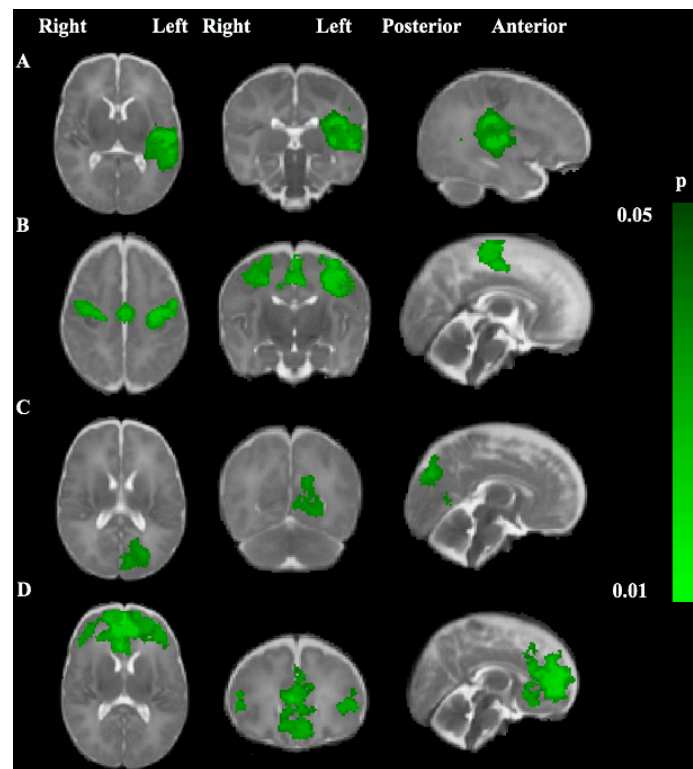
Figure 5.11: Resting state networks in the infants with hypoxic-ischaemic encephalopathy as identified by seed-based correlation analysis. *Seed masks in A, B and C were placed in the left hemisphere. Group mean maps are overlaid on a term infant template in the transverse (first column), coronal (second column) and sagittal (third column) views. A: Auditory, B: Somatomotor, C: Visual, D: Default mode network.*

A significant difference was found in functional connectivity between the two groups within each network after correcting for age at birth, age at scan and controlling for brain volume (Figure 5.12). The difference between the two groups remained significant when infants who were sedated with agents other than oral chloral hydrate were excluded from the analysis.
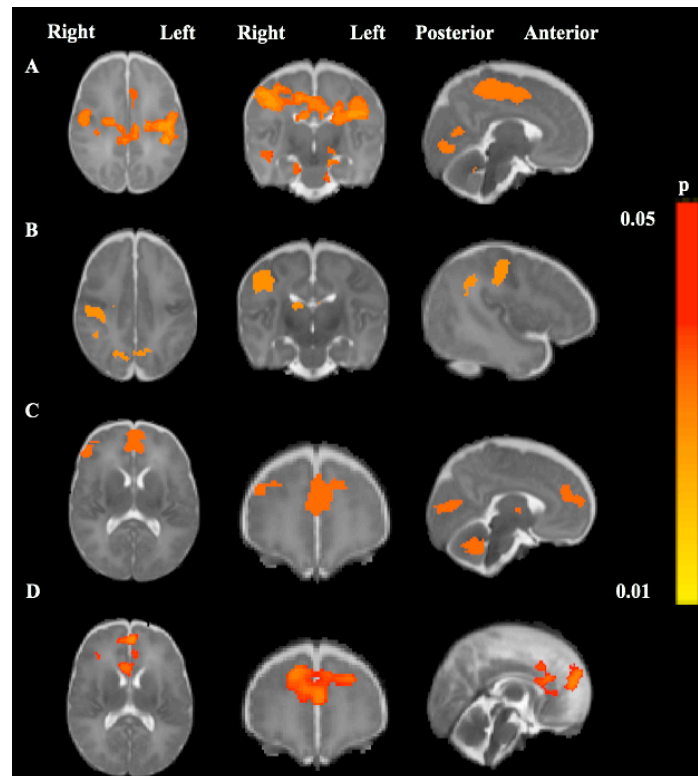
Figure 5.12: Statistical difference maps, generated by seed-based correlation analysis. *Difference maps are overlaid on a T2 weighted template in the transverse (first column), coronal (second column) and sagittal (third column) views. A: Auditory, B: Somatomotor, C: Visual, D: Default mode network.*

5.4.6 Neurodevelopmental outcome in infants with hypoxic-ischaemic encephalopathy

In the HIE group, infants were assessed at a median (range) age of 24 (12-24.5) months. Three infants died in the neonatal. Another 4 infants developed an unfavourable outcome. Three of these had cerebral palsy (athetoid n=1 and spastic quadriplegia n=2) with GMFCS levels III-V. One infant, assessed using the GMDS, achieved scores more than 2 SDs below the mean.

Eight infants had a favourable outcome. Six of them were assessed using a formal neurodevelopmental test. One child was tested using the Bayley Scales of Infant Development (Bayley 1966) and 5 with the GMDS (Huntley 1996). Two children seen by a neonatal consultant were thought to develop appropriately, however no formal neurodevelopmental test was performed.

5.4.7 Correlation between functional connectivity scores and outcome

Infants with unfavourable outcome had lower functional connectivity scores within each network compared to those with a favourable outcome (Figure 5.13). However, following correction for multiple comparisons the difference was significant in the auditory and motor networks only.
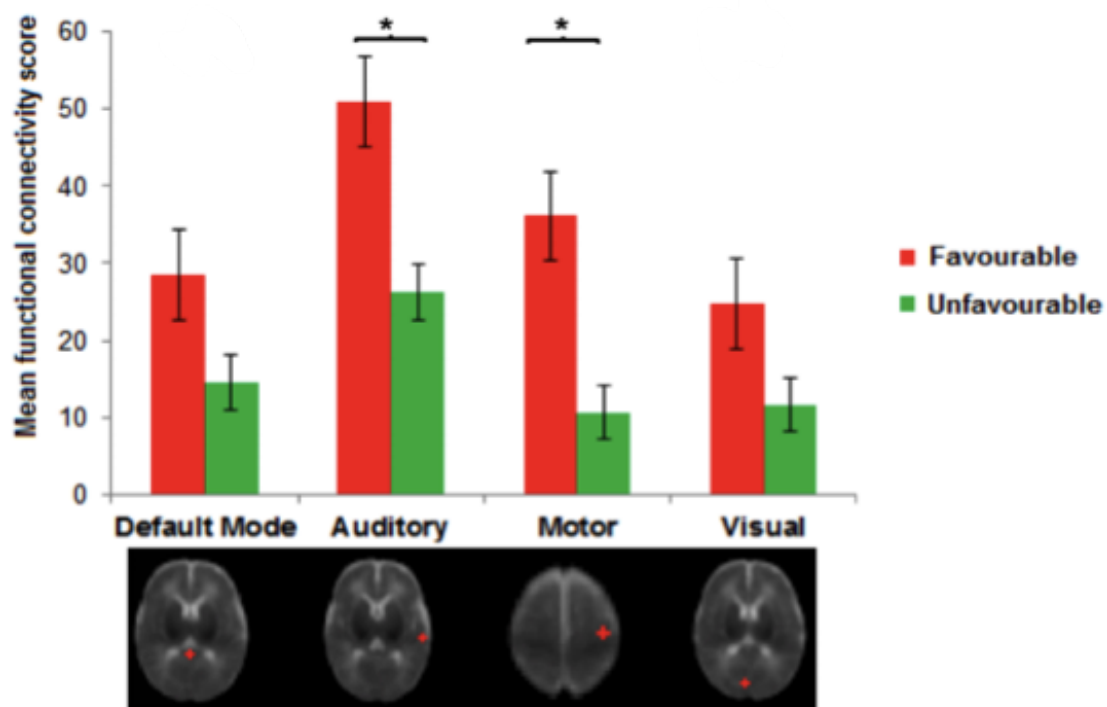
Figure 5.13: **Mean functional connectivity scores of infants with a favourable (red) and with an unfavourable (green) outcome.** *Infants with a favourable outcome had higher mean functional connectivity scores within each networks compared to those with unfavourable outcome. X axis: default mode, auditory*, somatomotor*, visual networks. Y axis: mean functional connectivity scores. Regions of interest are shown in the panel as red crosses.*

5.5 Discussion

This chapter explores the impact of a hypoxic-ischaemic brain injury on functional connectivity in the neonatal period. Consistent with previous studies, RSNs were identified in the control group with a distribution similar to that characteristically seen in adults (Fransson et al. 2009; Doria et al. 2010). Although RSNs were present in infants who suffered HIE, inter- and intra-hemispheric functional connectivity was diminished. In addition to this diminished functional connectivity, evidence for structural disruption of the WM was observed in infants with HIE as assessed with TBSS.

Brain structure changes rapidly during foetal and early postnatal life. Synaptic connections are remodelled in response to endogenous and sensory-driven inputs leading to early organisation of cortical circuits (Tau and Peterson 2010). The results of the present study suggest that a hypoxic-ischaemic insult during this critical period of brain development alters RSNs. This finding is consistent with experimental (Honey and Sporns 2008; Wang et al. 2010) and human studies (Sharp et al. 2011) that demonstrated changes in larger scale inter-regional interactions following brain injury (De Vico et al. 2009; Tsirka et al. 2011).

Furthermore, within the HIE group infants who developed an unfavourable outcome had lower functional connectivity scores compared to those with a favourable outcome. Therefore the observed changes in functional connectivity may have long-term significance. This is in line with previous studies in adults where changes in functional connectivity associated with brain injury correlated to cognitive function (Andrews-Hanna et al. 2007; Damoiseaux et al. 2008; Greicius et al. 2009; Bonnelle

et al. 2012). Additionally, a correlation has been observed between cognitive ability and efficacy of organisation of RSNs (Song et al. 2008; van den Heuvel et al. 2009) as well as integrity of WM tracts (Chiang et al. 2009; Li et al. 2009), establishing a link between functional and structural connectivity (Vincent et al. 2006; Hagmann et al. 2008; Skudlarski et al. 2008; Honey et al. 2009).

This is the first study to assess the impact of HIE on functional connectivity, and while these results suggest that fMRI may have a role in assessing neonatal brain injury, there are several limitations. Although there was no significant difference in gestational age at birth of the two groups, healthy control infants were significantly older at the time of the scan and therefore were exposed to a different ex utero environment for a longer time. Analyses were controlled for age at scan, however it may introduce bias because experience, along with maturation, leads to strengthening of functional connectivity (Dosenbach et al. 2007; Fair et al. 2007). However, such strengthening is likely to be a gradual process, which may manifest over several years (Fair et al. 2008; 2010), therefore its impact in the neonatal period may be negligible.

Head movement during MRI frequently occurs in neonates and may result in spurious correlation patterns (Power et al. 2011). There are several ways of minimising subject motion (Green et al. 1994; Fitzsimmons et al. 1997), adjusting for it either during image acquisition (Thesen et al. 2000; Mathiak and Posse 2001; Welch et al. 2002; Speck et al. 2006) or through post-acquisition preprocessing steps (Woods et al. 1992; Hajnal et al. 1995; Friston et al. 1996; Biswal and Hyde, 1997; Ciulla and Deek, 2002; Tremblay et al. 2005). While effects of small movements can be corrected with such measures, datasets with severe movement are frequently discarded. In the

present study a considerable proportion of the datasets in each group was excluded due to motion artefact. Although discarding datasets with motion may introduce bias as greater head motion may correlate with an abnormal neurological state in adults (Wylie et al. 2014), no significant difference was found between included and excluded subjects within each group in terms of clinical characteristics.

Sedation is frequently used in neonates to minimise subject motion during scanning. Although in the present study most subjects were sedated with chloral hydrate, a few infants who suffered HIE were on other sedative medications. The exploratory analysis revealed that the significant difference in functional connectivity between controls and infants with HIE persisted following exclusion of those subjects who were sedated using drugs other than chloral hydrate. These findings are consistent with electrophysiological studies showing that the amplitude and character of neural responses are not affected by induced sedation (Sisson and Siegel 1989; Avlonitou et al. 2011). In a neonatal resting state fMRI study sedation with chloral hydrate did not affect the identification or topology of resting state networks (Doria et al. 2010). Furthermore, CBF is unchanged by low-dose chloral hydrate sedation as measured by phase contrast angiography (Arichi et al. 2012; Valera et al. 2012).

Application of fMRI to evaluate functional consequences of brain injury requires preservation of neurovascular coupling as neurovascular coupling and cerebral autoregulation control CBF. Previous studies suggested that neurovascular coupling between spontaneous neural activity and haemodynamic fluctuations is inversely related to the baseline CBF (Dirnagl et al. 1993; Hudetz et al. 1995; Obrig et al. 2000; Cohen et al. 2002; Mulderink et al. 2002; Liau et al. 2008). In general, vasodilation

reduces, while vasoconstriction increases the amplitude of spontaneous fluctuations (Kemna and Posse 2001; Cohen et al. 2002).

In neonatal animal models physiological regional differences in autoregulation and CBF are apparent due to regional differences in metabolic activity (Ashwal et al. 1980; Cavazzuti and Duffy 1982; Pasternak and Groothuis. 1985; Lyons et al. 1987; Gleason et al. 1989; Nehlig et al. 1989; Szymonowicz et al. 1990). Baseline CBF is higher and more stable in the brainstem, BGT and cortex, while WM has limited adaptive capacity (Young et al. 1982; Szymonowicz et al. 1990). Following a hypoxic-ischaemic event, once autoregulation fails, CBF becomes pressure-passive (Lou et al. 1979) leading to an increase in CBF minutes after the insult, lasting up to several hours (Cope and Delpy 1988), followed by a decline toward the baseline (Vanucci et al. 1997). A delayed increase in CBF occurs 12-24 hours after the injury (Pryds et al. 1990) that may persist for several days (Archer et al. 1986; Ramaekers et al. 1990). CBF then returns to normal by around 130 hours even following a severe hypoxic-ischaemic episode (Archer et al. 1986; van Bel et al. 1987; Ment et al. 1988; Ramaekers et al. 1990). Although CBF was not measured in the present study, the median postnatal age at scan of infants who suffered HIE was 6 days, by which time changes in CBF are expected to have returned to baseline (Archer et al. 1986; van Bel et al. 1987; Ramaekers et al. 1990). Therefore it is unlikely that changes in CBF during the acute phase of a hypoxic-ischaemic insult influenced the results of the present study.

Carbon dioxide is a potent vasodilator that modulates neurovascular coupling (Symon et al. 1973; Cavazzuti and Duffy, 1982; Vanucci et al. 1997). The hypercapnia model

was used in both animal (Symon et al. 1975; Ueki et al. 1988; Kim and Ugurbil, 1997; Davis et al. 1998; Hoge et al. 1999; Corfield et al. 2001; Duong et al. 2001) and human studies (Andrade et al. 2006; Leoni et al. 2008) to investigate preservation of neurovascular coupling. Hypercapnia decreased functional connectivity in the motor cortex (Biswal et al. 1997), however in animal studies mild levels of hypercapnia did not affect spontaneous neural activity (Jones et al. 2005; Sicard and Duong 2005; Zappe et al. 2008). Although, carbon dioxide challenge was applied in neonates (Sankaran et al. 1981; 1984; Toft et al. 1995), ethical considerations limit its utility.

About half of the infants in the HIE group required respiratory support during the scan. Although capillary carbon dioxide level was within normal range for all subjects, an exploratory analysis showed a trend towards lower levels in infants who required respiratory support. However, the present study was not designed to incorporate this variable in the analysis and capillary blood gas analysis was performed for clinical indications. As such the timing of this test varied considerably between subjects.

The results of this chapter suggest that functional connectivity is diminished in infants who suffered HIE and received therapeutic hypothermia as compared to healthy term infants. Furthermore, reduced functional connectivity is associated with unfavourable outcome. However, there are several limitations to resting state fMRI analysis in neonates, especially in those with brain injury, hence further studies are needed to assess its utility as an imaging biomarker.

Chapter 6

Limitations

There are several limitations to this thesis. Stringent eligibility criteria were used to select a patient population that is representative of the real population of infants who suffered HIE and received hypothermia. However a substantial proportion of the infants were excluded. About 20% of the infants who received therapeutic hypothermia during the study period did not have a brain MRI scan and therefore was not eligible for this study. The rate of death was higher in this group than amongst those who underwent MRI in the neonatal period. Although MRI is a safe technique, the procedure might be hazardous in unstable neonates and requires careful preparation considering safety of the infant as the ultimate priority (Merchant et al. 2009; van Wezel-Meijler et al. 2009).

About 10% of the patients who had a brain MRI scan during the neonatal period were excluded from the analysis due to lack of follow-up. However, there is growing evidence that childhood survivors of HIE are at increased risk of cognitive, behavioural and memory problems even in absence of cerebral palsy (De Vries and Jongmans 2010; Van Handel et al. 2012). Therefore all children with a history of neonatal HIE should be enrolled into a follow-up program (Robertson and Perlman 2006).

About one-third of the children were excluded because their outcome data were not comparable to the rest of the cohort. Hypothermia is usually provided in tertiary

neonatal units. However follow-up is often carried out in local hospitals. Therefore it might be difficult to ensure that the same neurodevelopmental test is used for all children.

Objective assessment of neurodevelopment in children with cerebral palsy and/or cognitive delay is a further challenge (Goldkamp 1984; Scheiman 1984; Gagliardi et al. 2013). The link between limitations in motor domain and neurophysiological skills is not always straightforward (Nordmark et al. 2001; Pirila et al. 2004), and intelligence quotient of survivors with severe cerebral palsy following HIE is often only estimated (Robertson et al. 1989).

It would have been novel to include the same cohort of infants in all three studies. As DTI data were acquired for clinical purposes more infants were eligible to be enrolled into the DTI studies (Chapters 3 and 4). Furthermore, more children is included in the tissue label segmentation study in Chapter 4, than in the TBSS study in Chapter 3 as outcome data with the GMDS became available for more infants. However, post-hoc analysis with the 32 infants included in the TBSS study yielded the same results.

Resting state fMRI data were acquired in only 25% of the infants who underwent hypothermia during the study period, because this sequence was obtained merely for research purposes. Furthermore, resting state fMRI sequence is sensitive to motion and a considerable proportion of the datasets was discarded due to motion artefact. Discarding datasets with motion may introduce bias as greater head motion correlates with an abnormal neurological state in adults (Wylie et al. 2014). However, in this

study clinical characteristics of infants who were excluded due to motion artefact did not differ significantly of those who were included.

A further limitation of the resting state study is that the application of fMRI to evaluate functional consequences of brain injury requires preservation of neurovascular coupling. Application of the hypercapnia challenge offers the potential to investigate neurovascular coupling (Ueki et al. 1988; Kim and Ugurbil, 1997; Davis et al. 1998; Hoge et al. 1999; Corfield et al. 2001; Duong et al. 2001; Andrade et al. 2006; Leoni et al. 2008). However, ethical considerations limit its utility in neonates. Neurovascular coupling and cerebral autoregulation control CBF. Although CBF becomes pressure-passive once autoregulation fails following a hypoxic-ischaemic event (Lou et al. 1979), it returns to baseline by around 130 hours after the insult (van Bel et al. 1987; Ment et al. 1988; Ramaekers et al. 1990). The median age at scan of infants who suffered HIE was 6 days, therefore it is unlikely that changes in CBF during the acute phase of a hypoxic-ischaemic insult influenced the results. However, it would have been of value to estimate CBF in these patients.

There are several limitations inherent to the post-acquisition analysis methods applied in this thesis. Although TBSS has been used in animal models of neurological conditions (Ruest et al. 2011; Sierra et al. 2011; Manninen et al. 2013), unlike MRS it has not been used in experimental studies of HIE. The major limitation of TBSS is that it only allows studying the centre of the WM tracts, therefore it is not a feasible tool for assessment of the grey matter, which is frequently injured following a perinatal hypoxic-ischaemic event due to selective vulnerability of neuronal cells in term infants (Black et al. 1995; McQuillen et al. 2003; McQuillen and Ferriero 2004).

The atlas-based tissue labelling segmentation method applied in Chapter 4 overcomes this limitation and permits evaluation of cortical and deep grey matter. However, this technique involves label propagation from a high-resolution structural to a low-resolution diffusion tensor image. Therefore partial volume effects, especially at boundaries of CSF and cortex, and cortex and WM, may influence the accuracy of diffusion measurements (Falconer et al. 1997; Zacharopoulos et al. 1998; Hirsch et al. 1999; Shimony et al. 1999). Furthermore, distribution of diffusion parameters is non-uniform within brain structures; hence these parameters determined within tissue labels might be averaged out.

Post-acquisition analysis methods applied in this thesis rely on precise spatial correspondence of images between and/or within subjects. Registration-related issues are mainly due to difficulties in registration of the rapidly developing neonatal brain and to aligning images with pathology-related deformations. However, modified image processing pipelines adapted to the neonatal brain have been applied (Ball et al. 2010; Makropoulos et al. 2012).

Chapter 7

Conclusions

Prior to implementation of hypothermic neuroprotection about 25% of children with moderate and more than half of those with severe HIE died or developed major disability (Shankaran et al. 1991; Marlow et al. 2005; de Vries and Jongman 2010). However, meta-analyses of the large randomized controlled clinical trials show compelling evidence that moderate hypothermia reduces neuronal injury and improves neurodevelopmental outcome of infants with HIE (Edwards et al. 2010; Jacobs et al. 2013). Although therapeutic cooling results in an increased rate of survival with intact neurological function, hypothermic neuroprotection is only partial as nearly half of the subjects still have an unfavourable outcome (Edwards et al. 2010; Jacobs et al. 2013). Therefore there is an urgent need for identifying treatments that augment the beneficial effects of hypothermia.

The complex mechanism of hypoxic-ischaemic brain injury offers the potential for intervening at different levels in the cascade to achieve a more prominent reduction of neuronal injury and enhance cell growth, differentiation, and integration into neural networks (Gonzales and Ferriero 2009). As injury evolves over extensive periods of time through different phases, treatments initiated before, during or after hypothermia may improve neuroprotection by extending the therapeutic window or providing long-lasting additive or synergistic effect (Cillio and Ferriero 2010; Fan and Van Bel 2010; Robertson et al. 2012). Currently intensive bench-based and early phase clinical research is focused on developing additional neuroprotective therapies.

However, the large number of possible interventions and the lack of consensus on which has the potential to succeed limit progression. Qualified biomarkers are required to test these promising therapies efficiently so only those with a high chance of success progress into pragmatic trials (Azzopardi and Edwards 2010).

Neuroimaging studies are increasingly employed in the development of biomarkers (Ment et al. 2009; Azzopardi and Edwards 2010; Thayyil et al. 2010). Currently used MR techniques, including MRS, diffusion and conventional MRI assess anatomy and pathology non-invasively and are utilized in directing medical care. Cerebral metabolite ratios measured by MRS and visual evaluation of conventional MR images predict early neurodevelopmental functioning accurately following HIE in a single patient (Martinez-Biarge et al. 2010; 2011; 2012; Degraeuwe et al. 2013). Furthermore, these methods have been proved to be biomarkers of brain injury and are surrogate endpoints in studies of neuroprotective therapies (Rutherford et al. 2010; Thayyil et al. 2010). Using these techniques a smaller number of subjects are required to detect significant differences between treatment groups than in pragmatic clinical trials. However the number is still considerable. Therefore these are relatively inefficient methods for rapid preliminary evaluation of potential therapies in early phase clinical studies (Azzopardi and Edwards 2010).

Statistically powerful whole brain voxelwise cross-subject comparison of imaging data supports effective evaluation of potential neuroprotective interventions. The motivation of this thesis was to assess advanced MRI techniques, including DTI and resting state fMRI, as imaging biomarkers of neurodevelopmental performance in infants with HIE who underwent therapeutic hypothermia.

Although TBSS is not a feasible tool to detect cerebral changes or predict outcome in a single patient, its major advantage is the potential for objective cross-subject analysis of diffusion MRI data in small groups of patients (Smith et al. 2006). Therefore it offers the potential to test efficacy of neuroprotective treatments in early phase clinical trials (Porter et al. 2010). In Chapter 3 FA values in the WM, obtained in the neonatal period and assessed by TBSS, correlated with subsequent neurodevelopmental performance scores suggesting that TBSS is a qualified imaging biomarker of outcome in these infants. However, this technique only allows assessment of the centre of the WM tracts, therefore it is not suitable to study grey matter, which is often damaged following an acute hypoxic-ischaemic event.

To address this limitation, in Chapter 4 I used a neonatal atlas-based automated tissue labeling approach to segment central and cortical grey and whole brain WM. MD in grey matter structures, obtained in the neonatal period correlated to subsequent neurodevelopmental performance scores. Of note, although the central grey matter is the primary site of injury on conventional MRI following HIE; FA within WM tissue labels also correlated to neurodevelopmental performance scores. It is not clear from this quantitative analysis whether WM involvement is primary or secondary to grey matter injury. However, in the context of imaging biomarkers, these data suggest that WM FA assessed either by voxelwise or tissue labeling methods, is a reliable approach in this population to estimate neurodevelopmental performance. FA in WM and MD in grey matter may be used as an imaging biomarker of outcome following HIE treated with hypothermia.

However, diffusion MRI does not provide information on functional consequences of brain injury and so, in Chapter 5, I assessed the feasibility of resting state fMRI (Biswal et al. 1995; Beckmann et al. 2005) to evaluate the impact of a hypoxic-ischaemic brain injury on the BOLD signal, which is considered to be an indirect marker of neural activity. This study suggested that cerebral structural changes following HIE accompany diminished functional connectivity. Furthermore reduced functional connectivity was associated with subsequent unfavourable outcome. However, it is not known whether functional connectivity is altered primarily following a hypoxic-ischaemic insult or secondary to structural changes. Furthermore limitations in resting state fMRI analysis in infants with brain injury warrant further studies to assess its feasibility as an imaging biomarker.

In summary, the results of this thesis suggest that although functional connectivity was diminished in infants with HIE, resting state fMRI needs further study to assess its utility as an imaging biomarker following a hypoxic-ischaemic brain injury. However, FA in WM and MD in grey matter correlate to early neurodevelopmental performance scores in infants who suffered HIE and received therapeutic hypothermia and may be applied as imaging biomarkers of outcome in this population.

MRS, conventional and diffusion MRI have an important role in preliminary evaluation of candidate neuroprotective therapies. However given the complexity of brain injury cascade and the variety of putative neuroprotective treatments a single biomarker is unlikely to succeed therefore an integrated use of a combination of biomarkers is essential.

Chapter 8

Future directions

8.1 Improving early imaging biomarkers of neonatal brain injury

Assessing the effect of combined neuroprotective therapies will be challenging. Relatively large sample sizes will probably be required to discern the incremental benefits of an additional therapy compared with control groups already treated with a neuroprotective agent. Moreover, it is entirely possible that the benefits of any treatment may be modest, but still clinically important. Incorporating surrogate endpoints as primary outcome measures in designs of future neonatal neuroprotection studies will aid rapid assessment of efficacy of treatments and adaptation of study design strategies, which will reduce sample size requirements and deliver more cost-effective clinical trials (Silverstein and Barks 2013).

8.2 Limitations to diffusion tensor imaging

Although DTI is exquisitely sensitive to neonatal brain injury and provides objective measures that correlate with subsequent outcome, DTI indices lack specificity (Farquharson et al. 2013). The diffusion tensor model has been constructed on the assumption that each imaging voxel contains a single diffusing process that follows Gaussian distribution. However the relatively large voxel size in diffusion imaging in comparison to the underlying microstructure means that a single voxel may contain a mixture of CSF, grey and WM. Therefore the diffusion signal is comprised of different diffusion profiles. Even within WM, a voxel may contain a variety of fibre populations with different orientations (Tuch et al. 2002). Furthermore, different

structural changes may give rise to the same alterations of DTI parameters (Tournier et al. 2011). For instance the degree of anisotropy is influenced by a number of factors, such as axonal count and diameter, inter-axon spacing, coherence of axon orientations, membrane permeability and myelination. Therefore a reduction in anisotropy may be caused by a reduction in neurite density, an increase in neurite dispersion, as well as an increase in radial or a decrease in axial diffusivity due to disruption of cell membranes (Beaulieu 2009). DTI alone cannot distinguish between these possible changes and is therefore non-specific.

8.3 Beyond the diffusion tensor model

The diffusion profile within a voxel can be measured more accurately by acquiring data with increased angular resolution, such as high angular resolution diffusion imaging (HARDI) (Stanisz et al. 1997; Behrens et al. 2003; Assaf and Basser 2005; Barazany et al. 2009; Alexander et al. 2010; Zhang et al. 2012).

Acquiring HARDI data with multiple b-values allows neurite orientation dispersion and density imaging (NODDI), enabling the diffusion profile of multiple compartments in a single voxel to be modeled within a clinically feasible acquisition time (Zhang et al. 2012). The NODDI tissue model classifies the environment into three categories: intracellular, extracellular and CSF compartments and provides quantitative indices of neurite morphology, such as neurite density and fibre orientation dispersion that are comparable to independent measures derived from histology. Neurite density correlated with both optical myelin staining and estimations of neurite density using electron microscopy (Jespersen et al. 2010), meanwhile orientation dispersion of cortical neuronal processes showed agreement to that

quantified using a quantitative Golgi analysis (Jespersen et al. 2012). Parameters determined from NODDI disentangle changes, which contribute to alterations in DTI measures and thus provide information about specific alterations in microstructure in the living human brain. Such direct markers of microstructural complexity of grey and WM can be analyzed using established post-processing methods described in this thesis. TBSS is feasible for voxelwise, cross-subject analysis of novel indices of cerebral microstructure within the centre of the WM tracts. Meanwhile grey and whole WM can be assessed using an atlas-based tissue labeling segmentation approach.

Furthermore HARDI data analyzed using constrained spherical deconvolution (CSD) allows the resolution of multiple fibre orientations in each imaging voxel, and so overcomes the limitations of DTI to estimate crossing fibres. This approach enables detailed tractography analysis of complex WM fasciculi (Tournier et al. 2007; 2011).

8.4 Potential applications of advanced diffusion magnetic resonance imaging techniques in neonatal brain injury

To date, pilot studies have shown that acquiring HARDI data is feasible in the neonatal brain (Counsell et al. 2014; Kunz et al. 2014). Pilot data demonstrated abnormalities in neurite density in moderate-severe HIE (Lally et al. 2014). Furthermore, CSD based tractography using high b value HARDI data performed better in mapping complex WM tracts in the neonatal brain than DTI approaches (Mondi et al. 2014).

8.5 Neonatal neuroprotection

Neuroprotective therapies are currently being developed in experimental studies and tested in early phase clinical trials to reduce the burden of brain injury not only following HIE, but in other neonatal conditions, including prematurity and congenital heart disease.

Additional therapies, such as Xenon (Lobo et al. 2013; Azzopardi et al. 2013), topiramate (Filippi et al. 2012), erythropoietin (Elmahdy et al. 2010; McPherson and Juul 2010; Wu et al. 2012) and magnesium sulphate (Hossain et al. 2013; Nguyen et al. 2013), are being studied in clinical trials to improve outcome of infants with HIE. Furthermore, clinical studies of erythropoietin (Fauchere et al. 2008; Zhang et al. 2014), melatonin (Gitto et al. 2013; Merchant et al. 2013; Biran et al. 2014) and magnesium sulphate (Bain et al. 2012; Bickford et al. 2013) are taking place with the aim of reducing neurocognitive deficits in children who were born preterm. The field of neuroprotection in infants with congenital heart disease is less advanced, however trials of maternal administration of free radical scavengers, anti-inflammatory and anticytokine agents, and postnatal administration of erythropoietin (Andropoulos et al. 2013) are underway.

By combining CSD and NODDI, it might be possible to assess complex architecture of WM fibre bundles and explore neurite morphology *in vivo* in both grey and WM in the neonatal brain. Such novel direct measures of tissue microstructure in combination with existing MR techniques may improve the accuracy of early imaging biomarkers for assessing neonatal brain injury, plasticity and the effectiveness of putative combined neuroprotective treatments in the neonatal population.

References

Aaslid R, Lindegaard KF, Sorteberg W, Nornes H. Cerebral autoregulation dynamics in humans. Stroke. 1989; 20: 45–52.

Aden U, Dahlberg V, Fredholm BB, Lai LJ, Chen Z, Bjelke B. MRI evaluation and functional assessment of brain injury after hypoxic ischemia in neonatal mice. Stroke 2002;33:1405–1410.

Ahmann PA, Dykes FD, Lazzara A, Holt PJ, Giddens DP, Carrigan TA. Relationship between pressure passivity and subependymal intraventricular hemorrhage as assessed by pulsed Doppler ultrasound. Pediatrics 1983;72:665–669.

Akisu M, Huseyinov A, Yalaz M, Cetin H, Kultursay N. Selective head cooling with hypothermia suppresses the generation of platelet-activating factor in cerebrospinal fluid of newborn infants with perinatal asphyxia. Prostaglandins Leukot Essent Fatty Acids. 2003;69(1):45-50.

Albensi BC, Schweizer MP, Rarick TM, Filloux F. Magnetic resonance imaging of hypoxic-ischemic brain injury in the neonatal rat. Invest. Radiol. 1998:33,377–385.

Alderliesten T, de Vries LS, Benders MJ, Koopman C, Groenendaal F. MR imaging and outcome of term neonates with perinatal asphyxia: value of diffusion-weighted MR imaging and ¹H MR spectroscopy. Radiology. 2011;261(1):235-42.

Alexander AL, Lee JE, Lazar M, Field AS. Diffusion tensor imaging of the brain. Neurotherapeutics. 2007;4(3):316-29.

Alexander DC, Hubbard PL, Hall MG, Moore EA, Ptito M, Parker GJ, Dyrby TB. Orientationally invariant indices of axon diameter and density from diffusion MRI. Neuroimage. 2010;1;52(4):1374-89.

Alfarra H, Alfarra, Sadiq M. Review article: Neural tube defects between folate metabolism and genetics. Indian Journal of Human Genetics, 2011;17(3):126-131.

Aljabar P, Bhatia KK, Murgasova M, Hajnal JV, Boardman JP, Srinivasan L, Rutherford MA, Dyet LE, Edwards AD, Rueckert D. Assessment of brain growth in early childhood using deformation-based morphometry. Neuroimage. 2008; 1;39(1):348-58.

Allegaert K, Daniels H, Naulers G, Tibboel, D, Devlieger, H. Pharmacodynamics of chloral hydrate in former preterm infants. Eur J Pediatr. 2005;164:403–407.
Allsopp T. Life and death in the nervous system. Trends Neurosci. 1993;16(1):1-3

Altman N.R., B. Bernal. Brain activation in sedated children: auditory and visual functional MR imaging. Radiology 2001;221:56–63.

Altun A, Ugur-Altun B. Melatonin: therapeutic and clinical utilization. Int J Clin Pract 2007;61:835-45.

Aly H, Abd-Rabboh L, El-Dib M, Nawwar F, Hassan H, Aaref M, Abdelrahman S, Elsayed A. Ascorbic acid combined with ibuprofen in hypoxic ischemic encephalopathy: a randomized controlled trial. J Perinatol 2009;29:438-43

Amess PN, Penrice J, Cady EB, Lorek A, Wylezinska M, Cooper CE, D'Souza P, Tyszczuk L, Thoresen M, Edwards AD, Wyatt JS, Reynolds EO. Mild hypothermia after severe transient hypoxia-ischemia reduces the delayed rise in cerebral lactate in the newborn piglet. Pediatr Res. 1997;41(6):803-8.

Amess PN, Penrice J, Wylezinska M, Lorek A, Townsend I, Wyatt IS, Amiel-Tison C, Cady EB. Early brain proton magnetic resonance spectroscopy and neonatal neurology related to neurodevelopmental outcome at 1 year in term infants after presumed hypoxic-ischemic brain injury. Dev Med Child Neurol 1999;41(7):436-445

Amiel-Tison C, Ellison P. Birth asphyxia in the fullterm newborn: early assessment and outcome. Dev Med Child Neurol. 1986 Oct;28(5):671-82. Review

Anand A, Li Y, Wang Y, Wu J, Gao S, Bukhari L, Mathews VP, Kalnin A, Lowe MJ. Antidepressant effect on connectivity of the mood-regulating circuit: an fMRI study. Neuropsychopharmacology 2005;30, 1334–1344.

Ancora G, Testa C, Grandi S, Tonon C, Sbravati F, Savini S, Manners DN, Gramegna LL, Tani G, Malucelli E, Corvaglia LT, Faldella G, Lodi R. Prognostic value of brain proton MR spectroscopy and diffusion tensor imaging in newborns with hypoxic-ischemic encephalopathy treated by brain cooling. Neuroradiology. 2013;55(8):1017-25.

Anderson AW, Marois R, Colson ER, Peterson BS, Duncan CC, Ehrenkranz RA, Schneider KC, Gore JC, Ment LR.Neonatal auditory activation detected by functional magnetic resonance imaging Magn Reson Imaging, 2001;19:1–5

Anderson JM, Belton NR. Water and electrolyte abnormalities in the human brain after severe intrapartum asphyxia. J Neurol Neurosurg Psychiatry. 1974 May;37(5):514-20.

Andrade KC, Pontes-Neto OM, Leite JP, Santos AC, Baffa O, de Araujo DB. Quantitative aspects of brain perfusion dynamic induced by BOLD fMRI. Arq Neuropsiquiatr. 2006;64:895– 898.

Andrews-Hanna JR, Snyder AZ, Vincent JL, Lustig C, Head D, Raichle ME, Buckner RL. Disruption of large-scale brain systems in advanced aging. Neuron. 2007 Dec 6;56(5):924-35.

Andropoulos DB, Brady K, Easley RB, Dickerson HA, Voigt RG, Shekerdemian LS, Meador MR, Eisenman CA, Hunter JV, Turcich M, Rivera C, McKenzie ED, Heinle JS, Fraser CD Jr. Erythropoietin neuroprotection in neonatal cardiac surgery: a phase I/II safety and efficacy trial. J Thorac Cardiovasc Surg. 2013;146(1):124-31

Anjari M, Srinivasan L, Allsop JM, Hajnal JV, Rutherford MA, Edwards AD, Counsell SJ. Diffusion tensor imaging with tract-based spatial statistics reveals local white matter abnormalities in preterm infants. Neuroimage. 2007;15;35(3):1021-7.

Anjari M, Counsell SJ, Srinivasan L, Allsop JM, Hajnal JV, Rutherford MA, Edwards AD. The association of lung disease with cerebral white matter abnormalities in preterm infants. Pediatrics. 2009;124(1):268-76.

Anthony MY, Evans DH, Levene MI. A study of cyclical variations in cerebral blood flow velocity. Arch Dis Child 1991;66:12–16

Anthony MY, Evans DH, Levene MI. Neonatal cerebral blood flow velocity responses to changes in posture. Arch Dis Child 1998;69:304–308

Anthony MY. Cerebral Autoregulation in Sick Infants. Pediatric Research 2000;48:3–5

Antier D, Franconi F, Sannajust F. Idazoxan does not prevent but worsens focal hypoxic-ischemic brain damage in neonatal Wistar rats. J. Neurosci. Res. 1999;58: 690–696.

Anton ES, Marchionni MA, Lee KF, Rakic P. Role of GGF/neuregulin signaling in interactions between migrating neurons and radial glia in the developing cerebral cortex. Development. 1997;124(18):3501-10.

Anton G. Uber die Betheiligung der basalen Gehringanglien bei Bewegungsstorungen und insbesondere bei der Chorea; nut Demonstrationem von Gehirnschaitten. Wiener Klinische Wochenschrift 6:859-861.

Aralasmak A, Ulmer JL, Kocak M, Salvan CV, Hillis AE, Yousem DM. Association, commissural, and projection pathways and their functional deficit reported in literature. J Comput Assist Tomogr 2006;30(5):695-715 Review

Archer LN, Levene MI, Evans DH. Cerebral artery Doppler ultrasonography for prediction of outcome after perinatal asphyxia. Lancet 1986; 2: 1116–18

Arichi T, Fagiolo G, Varela M, Melendez-Calderon A, Allievi A, Merchant N, Tusor N, Counsell SJ, Burdet E, Beckmann CF, Edwards AD. Development of BOLD signal hemodynamic responses in the human brain. Neuroimage. 2012;1; 63(2): 663–673

Arroyo EJ, Scherer SS. On the molecular architecture of myelinatedfibers. Histochem Cell Biol. 2000;113(1):1-18. Review.

Artzi M, Sira LB, Bassan H, Gross-Tsur V, Berger I, Marom R, Leitner Y, Bental Y, Shiff Y, Geva R, Weinstein M, Bashat DB. Brain diffusivity in infants with hypoxic-ischemic encephalopathy following whole body hypothermia: preliminary results. J Child Neurol. 2011;26(10):1230-6.

Ashwal S, Majcher JS, Vain N, Longo LD. Patterns of fetal lamb regional cerebral blood flow during and after prolonged hypoxia. Pediatr Res. 1980;14(10):1104-10.

Assaf M, Jagannathan K, Calhoun VD, Miller L, Stevens MC, Sahl R, O'Boyle JG, Schultz RT, Pearlson GD. Abnormal functional connectivity of default mode sub-networks in autism spectrum disorder patients. Neuroimage 2010 53(1):247-56.

Assaf Y, Basser PJ. Composite hindered and restricted model of diffusion (CHARMED) MR imaging of the human brain. Neuroimage. 2005;1;27(1):48-58.

Atkinson AJ, Colburn WA, Victor G. DeGruttola. Biomarkers and surrogate endpoints: preferred definitions and conceptual framework. Clin Pharmacol Ther 2001;69:89-95.

Attwell D, Iadecola C. The neural basis of functional brain imaging signals. Trends in neurosciences 2002;25, 621-625.

Avlonitou E, Balatsouras DG, Margaritis E. Use of chloral hydrate as a sedative for auditory brainstem response testing in a pediatric population. Int. J. Pediatr. Otorhinolaryngol. 2011;75(6):760–763

Azzopardi D, Wyatt JS, Cady EB, Delpy DT, Baudin J, Stewart AL, Hope PL, Hamilton PA, Reynolds EO. Prognosis of newborn infants with hypoxic-ischemic brain injury assessed by phosphorus magnetic resonance spectroscopy. Pediatr Res 1989;25:445-51.

Azzopardi D, Strohm B, Edwards AD, Halliday H, Juszczak E, Levene M, Thoresen M, Whitelaw A, Brocklehurst P; Steering Group and TOBY Cooling Register participants. Treatment of asphyxiated newborns with moderate hypothermia in routine clinical practice: how cooling is managed in the UK outside a clinical trial. Arch Dis Child Fetal Neonatal Ed. 2009;94(4):F260-4.

Azzopardi D, Strohm B, Edwards AD, Dyet L, Halliday HL, Juszczak E, Kapellou O, Levene M, Marlow N, Porter E, Thoresen M, Whitelaw A, Brockehurst P, TOBY Study Group. Moderate hypothermia to treat perinatal asphyxial encephalopathy; N Engl J Med; 2010;18;362(11):1056

Azzopardi D, Edwards AD. Magnetic resonance biomarkers of neuroprotective effects in infants with hypoxic ischemic encephalopathy. Semin Fetal Neonatal Med. 2010;15(5):261-9

Azzopardi D, Robertson NJ, Kapetanakis A, Griffiths J, Rennie JM, Mathieson SR, Edwards AD. Anticonvulsant effect of xenon on neonatal asphyxial seizures. Arch Dis Child Fetal Neonatal Ed. 2013;98(5):F437-9.

Back SA, Volpe JJ. Cellular and molecular pathogenesis of periventricular white matter injury. Ment Retard Dev Disabil Res Rev 1997;3:180-189

Back SA, Luo NL, Borenstein NS, Levine JM, Volpe JJ, Kinney HC. Late oligodendrocyte progenitors coincide with the developmental window of vulnerability for human perinatal white matter injury. J Neurosci. 2001;15;21(4):1302-12.

Back SA, Luo NL, Borenstein NS, Volpe JJ, Kinney HC. Arrested oligodendrocyte lineage progression during human cerebral white matter development: dissociation between the timing of progenitor differentiation and myelinogenesis. J Neuropathol Exp Neurol. 2002;61(2):197-211.

Back SA. Perinatal white matter injury: the changing spectrum of pathology and emerging insights into pathogenetic mechanisms. Mental Ret Dev Dis 2006;12:129-40.

Badawi N, Dixon G, Felix JF, Keogh JM, Petterson B, Stanley FJ, Kurinczuk JJ. Autism following a history of newborn encephalopathy: more than a coincidence? Dev Med Child Neurol 2006;48:85–89.

Badawi N, Kurinczuk JJ, Keogh JM, Alessandri LM, O'Sullivan F, Burton PR, Pemberton PJ, Stanley FJ. Intrapartum risk factors for newborn encephalopathy: the Western Australian case-control study. BMJ. 1998;317(7172):1549.

Bain E, Middleton P, Crowther CA. Different magnesium sulphate regimens for neuroprotection of the fetus for women at risk of preterm birth. Cochrane Database Syst Rev. 2012;15(2):CD009302.

Bajcsy R, Kovačič S. Multiresolution elastic matching. Comput Vis Graph Image Process 1989;46:1-21.

Baker M. In biomarkers we trust? Nature Biotechnol 2005 23(3):297-304

Ball G, Counsell SJ, Anjari M, Merchant N, Arichi T, Doria V, Rutherford MA, Edwards AD, Rueckert D, Boardman JP. An optimised tract-based spatial statistics protocol for neonates: applications to prematurity and chronic lung disease. Neuroimage 2010;15;53(1):94-102.

Ball G, Boardman JP, Rueckert D, Aljabar P, Arichi T, Merchant N, Gousias IS, Edwards AD, Counsell SJ. The effect of preterm birth on thalamic and cortical development. Cereb Cortex 2012;22:1016-10124

Bao XL, Yu RJ, Li ZS. 20 Item neonatal behavioural neurological assessment used in predicting prognosis of asphyxiated newborn. Chin Med J 1993;106: 21 1-5

Barazany D, Basser PJ, Assaf Y. In vivo measurement of axon diameter distribution in the corpus callosum of rat brain. Brain. 2009;132(Pt 5):1210-20.

Barkovich AJ. MR and CT evaluation of profound neonatal and infantile asphyxia. Am J Neuroradiol 13, 1992;959–972.

Barkovich AJ, Baranski K, Vigneron D, Partridge JC, Hallam DK, Hajnal BL, Ferriero DM. Proton MR spectroscopy for the evaluation of brain injury in asphyxiated, term neonates. AJNR Am J Neuroradiol. 1999;20(8):1399-405.

Barkovich AJ, Miller SP, Bartha A, Newton N, Hamrick SE, Mukherjee P, Glenn OA, Xu D, Partridge JC, Ferriero DM, Vigneron DB. MR imaging, MR spectroscopy, and diffusion tensor imaging of sequential studies in neonates with encephalopathy. Am. J. Neuroradiol 2006;27:533–547

Barnett AL, Mercuri E, Rutherford M, Haataja L, Frisone MF, Henderson S, Cowan F, Dubowitz L. Neurological and perceptual-motor outcome at 5–6 years of age in children with neonatal encephalopathy: relationship with neonatal brain MRI. Neuropediatrics 2002;33:242–248.

Barnett AL, Guzzetta A, Mercuri E, Henderson SE, Haataja L, Cowan F, Dubowitz L. Can the Griffiths scales predict neuromotor and perceptual-motor impairment in term infants with neonatal encephalopathy? Arch Dis Child 2004;89:637–643

Barrick TR, Charlton RA, Clark CA, Markus HS. White matter structural decline in normal ageing: a prospective longitudinal study using tract-based spatial statistics. Neuroimage. 2010;51(2):565-77.

Bartels A, Zeki S. Brain dynamics during natural viewing conditions—a new guide for mapping connectivity in vivo. Neuroimage 2005;24:339–349

Bartha AI, Yap KR, Miller SP, Jeremy RJ, Nishimoto M, Vigneron DB, Barkovich AJ, Ferriero DM. The normal neonatal brain: MR imaging, diffusion tensor imaging, and 3D MR spectroscopy in healthy term neonates. AJNR 2007;28(6):1015-21.

Basser PJ, Pajevic S, Pierpaoli C, Duda J, Aldroubi A. In vivo fiber tractography using DT-MRI data. Magn Reson Med. 2000;44(4):625-32.

Bassi L, Ricci D, Volzone A, Allsop JM, Srinivasan L, Pai A, Ribes C, Ramenghi LA, Mercuri E, Mosca F, Edwards AD, Cowan FM, Rutherford MA, Counsell SJ. Probabilistic diffusion tractography of the optic radiations and visual function in preterm infants at term equivalent age. Brain 2008;131(Pt 2):573-82.

Bassi L, Chew A, Merchant N, Ball G, Boardman J, Allsop JM, Doria V, Arichi T, Mosca F, Edwards AD, Cowan FM, Rutherford MA, Counsell SJ. Diffusion tensor imaging in preterm infants with punctate white matter lesions. Pediatr Res 2012;69:561-566.

Bastin ME, Armitage PA. On the use of water phantom images to calibrate and correct eddy current induced artefacts in MR diffusion tensor imaging. Magn Reson Imaging 2000;18:681–687.

Bayley N. Bayley Scales of Infant and Toddler Development®, Third Edition (Bayley-III®) Screening Test. Child Development. 1966;37(1):39-50

Beaulieu C, Allen PS. Determinants of anisotropic water diffusion in nerves. Magn Reson Med. 1994a;31(4):394-400.

Beaulieu C, Allen PS. Water diffusion in the giant axon of the squid: implications for diffusion-weighted MRI of the nervous system. Magn Reson Med. 1994b;32(5):579-83.

Beaulieu C, Allen PS. An in vitro evaluation of the effects of local magnetic-susceptibility-induced gradients on anisotropic water diffusion in nerve. MagnReson Med. 1996;36(1):39-44.

Beaulieu C, Fenrich FR, Allen PS. Multicomponent water proton transverse relaxation and T2-discriminated water diffusion in myelinated and nonmyelinated nerve. Magn Reson Imaging. 1998;16(10):1201-10.

Beaulieu C. The basis of anisotropic water diffusion in the central nervous system: a technical review. NMR Biomed. 2002;15(7-8):435-55. Review.

Beaulieu C. The biological basis of diffusion anisotropy. In **Johansen- Berg H**, Behrens T.E.J. Diffusion MRI: From Quantitative Measurement to In vivo Neuroanatomy. Elsevier Inc. 2009 1st edition.

Beckmann CF, Smith SM. Probabilistic independent component analysis for functional magnetic resonance imaging. IEEE Trans Med Imaging 2004;23:137–152.

Beckmann CF, DeLuca M, Devlin JT, Smith SM. Investigations into resting-state connectivity using independent component analysis. Philos Trans R Soc Lond B Biol Sci. 2005;29;360(1457):1001-13.

Beckmann C, Mackay C, Filippini N, Smith S. Group comparison of resting-state fmri data using multi-subject ica and dual regression. 15th Annual Meeting of Organization for Human Brain Mapping; 2009. poster 441 SU-AM.

Bednarek N, Mathur A, Inder T, Wilkinson J, Neil J, Shimony J. Impact of therapeutic hypothermia on MRI diffusion changes in neonatal encephalopathy. Neurology. 2012;1;78(18):1420-7.

Behrens T.E., Woolrich M.W., Jenkinson M., Johansen-Berg H., Nunes R.G., Clare S., Matthews P.M., Brady J.M., Smith S.M.. Characterization and propagation of uncertainty in diffusion-weighted MR imaging. Magn. Reson. Med. 2003;50:1077–1088.

Beilharz EJ, Williams CE, Dragunow M, Sirimanne ES, Gluckman PD. Mechanisms of delayed cell death following hypoxic-ischemic injury in the immature rat: evidence for apoptosis during selective neuronal loss. Brain Res Mol Brain Res. 1995;29(1):1-14.

Bell BA, Symon L, Branston NM. Cerebral blood flow and time thresholds for the formation of ischemic cerebral oedema, and effect of reperfusion in baboons. J Neurosurg 1985;62:31–41

Benedetti B, Charil A, Rovaris M, Judica E, Valsasina P, Sormani MP, Filippi M. Influence of aging on brain gray and white matter changes assessed by conventional, MT, and DT MRI. Neurology. 2006;28;66(4):535-9.

Bennet L, Roelfsema V, Pathipati P, Quaedackers J, Gunn AJ. Relationship between evolving epileptiform activity and delayed loss of mitochondrial activity after asphyxia measured by near-infrared spectroscopy in preterm fetal sheep. J Physiol 2006;572:141-54.

Bennet L, JA, Gluckman PD, Gunn AJ. Pathophysiology of asphyxia. In: Levene M, Chervenack FA, editors. Fetal and neonatal neurology and neurosurgery. 4th ed. Philadelphia: Churchill Livingstone/Elsevier; 2009:470-90.

Bennet L, Booth L, Gunn AJ. Potential biomarkers for hypoxic-ischemic encephalopathy. Semin Fetal Neonatal Med. 2010;15(5):253-60.

Bentivoglio M, Tassi L, Pech E, Costa C, Fabene PF, Spreafico R.Cortical development and focal cortical dysplasia.Epileptic Disord. 2003;5Suppl 2:S27-34.

Bentourkia, M., Michel, C., Ferriere, G., Bol, A., Coppens, A., Sibomana, M., Bausart, R., Labar, D., DeVolder, A. G. Evolution of brain glucose metabolism with age in epileptic infants, children and adolescents. Brain Dev. 1998. 20: 524–529.

Berger H. Uber des Elektrenkephalogramm des Menschen. Archiv fur Psychiatrie und Nervenkrankheiten 1929;87:527–580.

Bergeron L, Yuan J. Sealing one's fate: control of cell death in neurons. Curr Opin Neurobiol. 1998;8(1):55-63. Review.

Bickford CD, Magee LA, Mitton C, Kruse M, Synnes AR, Sawchuck D, Basso M, Senikas VM, von Dadelszen P; MAG-CP Working Group. Magnesium sulphate for fetal neuroprotection: a cost-effectiveness analysis. BMC Health Serv Res. 2013;19(13):527

Bielas S, Higginbotham H, Koizumi H, Tanaka T, Gleeson JG. Cortical neuronal migration mutants suggest separate but intersecting pathways. Annu Rev Cell Dev Biol. 2004;20:593-618. Review.

Biran V, Phan Duy A, Decobert F, Bednarek N, Alberti C, Baud O. Is melatonin ready to be used in preterm infants as a neuroprotectant? Dev Med Child Neurol. 2014 Feb 27. [Epub ahead of print]

Bishop G. Cyclic changes in excitability of the optic pathway of the rabbit. Am J Physio 1933;103:213–224.

Biswal B, Yetkin FZ, Haughton VM, Hyde JS. Functional connectivity in the motor cortex of resting human brain using echo-planar MRI. Magn Reson Med 1995;34:537–541.

Biswal BB, Hyde JS. Contour-based registration technique to differentiate between task-activated and head motion-induced signal variations in fMRI. Magn Reson Med 1997; 38:470–476.

Biswal B, Hudetz AG, Yetkin FZ, Haughton VM, Hyde JS. Hypercapnia reversibly suppresses low frequency fluctuations in the human motor cortex during rest using echo-planar MRI. J Cereb Blood Flow Metab 1997;17(3):301–8.

Black SM, Bedolli MA, Martinez S, Bristow JD, Ferriero DM, Soifer SJ. Expression of neuronal nitric oxide synthase corresponds to regions of selective vulnerability to hypoxia-ischaemia in the developing rat brain. Neurobiol Dis 1995;2:145-55.

Blaschke AJ, Staley K, Chun J. Widespread programmed cell death in proliferative and postmitotic regions of the fetal cerebral cortex. Development 1996;122:1165–1174

Bloch F, Hansen WW, Packard M. Nuclear induction. Phys Rev 1946;69:127.

Bluhm RL, Miller J, Lanius RA, Osuch EA, Boksman K, Neufeld R, Theberge J, Schaefer B, Williamson P. Spontaneous low-frequency fluctuations in the BOLD signal in schizophrenic patients: anomalies in the default network. Schizophr. Bull. 2007;33, 1004–1012.

Bodammer N, Kaufmann J, Kanowski M, Tempelmann C. Eddy current correction in diffusion-weighted imaging using pairs of images acquired with opposite diffusion gradient polarity. Magn Reson Med 2004;51:188 –193.

Boichot C, Walker PM, Durand C, Grimaldi M, Chapuis S, Gouyon JB, Brunotte F. Term neonate prognoses after perinatal asphyxia: contributions of MR imaging, MR spectroscopy, relaxation times, and apparent diffusion coefficients. Radiology 2006;239**,** 839–848.

Bolanos J, Almeida A, Stewart V, Peuchen S, Land J, Clark J, Heales SJ. Nitric oxide-mediated mitochondrial damage in the brain: mechanisms and implications for neurodegenerative diseases. J Neurochem 1997;68:2227-40.

Bonavita S, Gallo A, Sacco R, Corte MD, Bisecco A, Docimo R, Lavorgna L, Corbo D, Costanzo AD, Tortora F, Cirillo M, Esposito F, Tedeschi G. Distributed changes in defaultmode resting-state connectivity in multiple sclerosis. Mult Scler 2011;17:411–422.

Bonifacio SL, Saporta A, Glass HC, Lee P, Glidden DV, Ferriero DM, Barkovich AJ, Xu D. Therapeutic hypothermia for neonatal encephalopathy results in improved microstructure and metabolism in the deep gray nuclei. AJNR Am J Neuroradiol. 2012;33(11):2050-5.

Bonnelle V, Leech R, Kinnunen KM, Ham TE, Beckmann CF, De Boissezon X, Greenwood RJ, Sharp DJ. Default mode network connectivity predicts sustained attention deficits after traumatic brain injury. J Neurosci. 2011;21;31(38):13442-51.

Bonnelle V, Ham TE, Leech R, Kinnunen KM, Mehta MA, Greenwood RJ, Sharp DJ. Salience network integrity predicts default mode network function after traumatic brain injury. Proc Natl Acad Sci U S A. 2012;20;109(12):4690-5.

Bookstein FL. Thin-plate splines and the atlas problem for biomedical images. In Information Processing in Medical Imaging: Proc. 12th International Conference (IPMI'91), pages 326–342, 1991.

Born P, Rostrup E, Leth H, Peitersen B, Lou HC. Change of visually induced cortical activation patterns during development. Lancet. 1996;24;347(9000):543.

Born AP, Leth H, Miranda MJ, Rostrup E, Stensgaard A, Peitersen B, Larsson HBW, Lou HC. Visual activation in infants and young children studied by functional magnetic resonance imaging. Pediatric Res. 1998;44: 578–583.

Born AP, Miranda MJ, Rostrup E, Toft PB, Peitersen P, Larsson HB, Lou HC. Functional magnetic resonance imaging of the normal and abnormal visual system in early life. Neuropediatrics, 2000;31:24–32.

Born AP, Rostrup E, Miranda MJ, Larsson HB, Lou HC. Visual cortex reactivity in sedated children examined with perfusion MRI (FAIR). Magn Reson Imaging, 2002;20:199–205.

Boveroux P, Vanhaudenhuyse A, Bruno MA, Noirhomme Q, Lauwick S, Luxen A, Degueldre C, Plenevaux A, Schnakers C, Phillips C, Brichant JF, Bonhomme V,

Maquet P, Greicius MD, Laureys S, Boly M. Breakdown of within- and between-network resting state functional magnetic resonance imaging connectivity during propofol-induced loss of consciousness. Anesthesiology. 2010;113(5):1038-5.

Bredt DS, Snyder SH. Nitric oxide mediates glutamate-linked enhancement of cGMP levels in the cerebellum. Proc Natl Acad Sci USA 1989;86:9030-3.

Bressler J. Klinische und pathologisch-anamoische Beitrae zur Mikrogyrie. Archiv fur Psychiatrie 31:566-573.

Brissaud O, Amirault M, Villega F, Periot O, Chateil JF, Allard M Efficiency of fractional anisotropy and apparent diffusion coefficient on diffusion tensor imaging in prognosis of neonates with hypoxic-ishaemic encephalopathy: a methodologic prospective pilot study. AJNR 2010;31:282-87.

Brody BA, Kinney HC, Kloman AS, Gilles FH. Sequence of central nervous system myelination in human infancy. I. An autopsy study of myelination. J NeuropatholExp Neurol. 1987;46(3):283-301.

Bunge RP.Glial cells and the central myelin sheath. Physiol Rev. 1968;48(1):197-251. Review.

Burdjalov VF, Baumgart S, Spitzer AR. Cerebral function monitoring: a new scoring system for the evaluation of brain maturation in neonates. Pediatrics. 2003;112:855–861.

Burns C, Boardman J, Rutherford M, Cowan FM. Patterns of cerebral injury and neurodevelopmental outcome following symptomatic neonatal hypoglycemia. Pediatrics, 2008;122:65–74

Burzynska AZ, Preuschhof C, Bäckman L, Nyberg L, Li SC, Lindenberger U, Heekeren HR. Age-related differences in white matter microstructure: region-specific patterns of diffusivity. NeuroImage. 2010 Feb 1;49(3):2104-12.

Busto R, Globus MY, Dietrich WD, Martinez E, Valdés I, Ginsberg MD. Effect of mild hypothermia on ischemia-induced release of neurotransmitters and free fatty acids in rat brain. Stroke. 1989;20(7):904-10.

Buxton RB. Introduction into functional magnetic resonance imaging. 2nd edition 2009. Cambridge. p7.

Bystron I, Molnár Z, Otellin V, Blakemore C. Tangential networks of precocious neurons and early axonal outgrowth in the embryonic human forebrain. J Neurosci. 2005;16;25(11):2781-92.

Cabezas M, Oliver A, Lladó X, Freixenet J, Caudra MB. A review of atlas-based segmentation formagnetic resonance brain images. Comput Methods Prog Biomed. 2011; 104:158-177

Cady EB, Iwata O, Bainbridge A, Wyatt JS, Robertson NJ. Phosphorus magnetic resonance spectroscopy 2 h after perinatal cerebral hypoxia-ischemia prognosticates outcome in the newborn piglet. J Neurochem. 2008;107(4):1027-35.

Calhoun VD, Adali T, Pearlson GD, Pekar JJ. A method for making group inferences from functional MRI data using independent component analysis. Hum. Brain Mapp. 2001;14, 140–151.

Cans C. Surveillance of Cerebral Palsy in Europe: a collaboration of cerebral palsy surveys and registers. Dev Med Child Neurol 2000;42:816–824.

Carroll M, Beek O. Protection against hippocampal CA1 cell loss by post-ischaemic hypothermia is dependent on delay of initiation and duration. Metab Brain Dis 1992;7:45-50.

Carter AR, Shulman GL, Corbetta M. Why use a connectivity-based approach to study stroke and recovery of function? Neuroimage. 2012;1;62(4):2271-80. Review.

Casey BM, McIntire DD, Leveno KJ. The continuing value of the Apgar score for the

assessment of the newborn infants. N Engl J Med. 2001;344:467–471

Castillo J, Rama R, Dávalos A. Nitric oxide-related brain damage in acute ischemic stroke. Stroke. 2000;31(4):852-7.

Cavazzuti M, Duffy TE. Regulation of local cerebral blood flow in normal and hypoxic newborn dogs. Ann Neurol. 1982;11(3):247-57.

Caviness VS, Takahashi T, Nowakowski RS. Neocortical malformation as consequence of nonadaptive regulation of neuronogenetic sequence. Ment Retard Dev Disabil Res Rev. 2000;6(1):22-33. Review.

Caviness VS, Goto T, Tarui T, Takahashi T, Bhide PG, Nowakowski RS. Cell output, cell cycle duration and neuronal specification: a model of integrated mechanisms of the neocortical proliferative process. Cereb Cortex. 2003;13(6):592-8.

Chau V, Poskitt KJ, Miller SP. Advanced neuroimaging techniques for the term newborn with encephalopathy. Pediatr Neurol. 2009;40(3):181–188

Chen J, Tu Y, Moon C, Matarazzo V, Palmer A, Ronnett G. The localization of neuronal nitric oxide synthase may influence its role in neuronal precursor proliferation and synaptic maintenance. Dev Biol 2004;269:165-82.

Cheong JL, Cady EB, Penrice J, Wyatt JS, Cox IJ, Robertson NJ. Proton MR spectroscopy in neonates with perinatal cerebral hypoxiceischemic injury: metabolite peak-area ratios, relaxation times, and absolute concentrations. Am J Neuroradiol 2006;27:1546-54.

Cheong JL, Coleman L, Hunt RW, Lee KJ, Doyle LW, Inder TE, Jacobs SE; Infant Cooling Evaluation Collaboration. Prognostic utility of magnetic resonance imaging in neonatal hypoxic-ischemic encephalopathy: substudy of a randomized trial. Arch Pediatr Adolesc Med. 2012;1;166(7):634-4

Chiang MC, Barysheva M, Shattuck DW, Lee AD, Madsen SK, Avedissian C,

Klunder AD, Toga AW, McMahon KL, de Zubicaray GI, Wright MJ, Srivastava A, Balov N, Thompson PM. Genetics of brain fiber architecture and intellectual performance. J Neurosci. 2009;18;29(7):2212-24.

Chiapponi C, Piras F, Piras F, Fagioli S, Caltagirone C, Spalletta G. Cortical Grey Matter and Subcortical White Matter Brain Microstructural Changes in Schizophrenia Are Localised and Age Independent: A Case-Control Diffusion Tensor Imaging Study. PLoS ONE 2013;8(10):e75115

Chiron, C., Raynaud, C., Maziere, B., Zilbovicius, M., Laflamme, L., Masure, M. C., Dulac, O., Bourguigon, M., Syrota, A. Changes in regional cerebral blood flow during brain maturation in children and adolescents. J. Nucl. Med. 1992. 33: 696–703

Christensen GE, Rabbitt RD, Miller MI. Deformable templates using large deformation kinematics. IEEE Trans Image Process 1996;5:1435-1447.

Christensen GE, Johnson HJ. Invertibility and transitivity analysis for nonrigid image registration. J Electron Imaging 2003;12:106–17.

Chugani, H. T., Phelps, M. E., Mazziotta, J. C. Positron emission tomography study of human brain functional development. Ann. Neurol. 1987;22: 487–497.

Church JA, Fair DA, Dosenbach NU, et al. Control networks in paediatric Tourette syndrome show immature and anomalous patterns of functional connectivity. Brain 2009;132:225–38.

Cilio MR, Ferriero DM. Synergistic neuroprotective therapies with hypothermia. Semin Fetal Neonatal Med. 2010;15(5):293-8.

Ciulla C, Deek FP. Performance assessment of an algorithm for the alignment of fMRI time series. Brain Topogr 2002; 14:313–332

Clarke DD, Sokoloff L. Circulation and energy metabolism of the brain. In: Agranoff BW, Siegel GJ. Basic neurochemistry. Molecular, cellular and medical aspects. Philadelphia. Lippincott-Raven 1999 Ed 6 pp 637–670.

Cohen ER, Ugurbil K, Kim SG. Effect of basal conditions on the magnitude and dynamics of the blood oxygenation level-dependent fMRI response. J Cereb Blood Flow Metab 2002;22(9):1042–53.

Cole DM, Smith SM, Beckmann CF. Advances and pitfalls in the analysis and interpretation of resting-state FMRI data. Front Syst Neurosci. 2010;6;4:8.

Collins DL, Evans AC. Animal: validation and applications of nonlinear registration-based segmentation. Int J Pattern Recogn Artificial Intelligence 1997;11:1271–94.

Cooper CE, Cope M, Springett R, Amess PN, Penrice J, Tyszczuk L, Punwani S, Ordidge R, Wyatt J, Delpy DT. Use of mitochondrial inhibitors to demonstrate that cytochrome oxidase near-infrared spectroscopy can measure mitochondrial dysfunction noninvasively in the brain. J Cereb Blood Flow Metab 1999;19:27-38.

Cope M, Delpy DT. A system for the long-term measurement of cerebral blood and tissue oxygenation in newborn infants by near infra-red transillumination. Med Biol Eng Comput 1988;26:289–94

Copp AJ, Greene ND, Murdoch JN. Dishevelled: linking convergent extension with neural tube closure. Trends Neurosci. 2003;26(9):453-5.

Corbo ET, Bartnik-Olson BL, Machado S, Merritt TA, Peverini R, Wycliffe N, Ashwal S. The effect of whole-body cooling on brain metabolism following perinatal hypoxic-ischemic injury. Pediatr Res. 2012;71(1):85-9.

Corfield DR, Murphy K, Josephs O, Adams L, Turner R. Does hypercapnia-induced cerebral vasodilation modulate the hemodynamic response to neural activation? Neuroimage. 2001;13(6 Pt 1):1207-11.

Coskun A, Lequin M, Segal M, Vigneron DB, Ferriero DM, Barkovich AJ. Quantitative analysis of MR images in asphyxiated neonates: correlation with neurodevelopmental outcome. AJNR Am J Neuroradiol. 2001;22(2):400–405

Counsell SJ, Dyet LE, Larkman DJ, Nunes RG, Boardman JP, Allsop JM, Fitzpatrick J, Srinivasan L, Cowan FM, Hajnal JV, Rutherford MA, Edwards AD. Thalamo-cortical connectivity in children born preterm mapped using probabilistic magnetic resonance tractography. Neuroimage. 2007;1;34(3):896-904.

Counsell SJ, Edwards AD, Chew AT, Anjari M, Dyet LE, Srinivasan L, Boardman JP, Allsop JM, Hajnal JV, Rutherford MA, Cowan FM. Specific relations between neurodevelopmental abilities and white matter microstructure in children born preterm. Brain. 2008;131(Pt 12):3201-8.

Counsell SJ, Zhang H, Hughes E, Steele H, Tusor N, Ball G, Makrploulos A, Allsop JM, Nongena P, Wurie J, Alexander D, Hajnal JV, Edwards AD. In vivo assement of neurite density in the preterm brain using diffusion magnetic resonance imaging. ISMRM abstract. 2014

Covey M, Murphy M, Hobbs C, Smith R, Oorschot D. Effect of the mitochondrial antioxidant, Mito Vitamin E, on hypoxic-ischemic striatal injury in neonatal rats: a dose-response and stereological study. Exp Neurol 2006;199:513-9.

Cowan WM, Fawcett JW, O'Leary DD, Stanfield BB. Regressive events in neurogenesis. Science. 1984;21;225(4668):1258-65.

Cowan FM. Magnetic resonsnce imaging of the normal infant brain: term to 2 years. In Rutherford M. MRI of the neonatal brain. 2002 Saunders.

Cowan F, Rutherford M, Groenendaal F, Eken P, Mercuri E, Bydder GM, Meiners LC, Dubowitz LM, de Vries LS. Origin and timing of brain lesions in term infants with neonatal encephalopathy. Lancet. 2003;1;361(9359):736-42

Crum WR, Hartkens T, Hill DLG. Non-rigid image registration: theory and practice. The British Journal of Radiology 2004;77:S140–S153.

Cullen S, Gross E. The anaesthetic properties of xenon in animals and human beings; with additional observations on krypton. Science 1951;113:580-2.

Dai D, Wang J, Hua J, He H. Classification of ADHD children through multimodal magnetic resonance imaging. Front Syst Neurosci. 2012;6:63.

Damaraju E, Phillips JR, Lowe JR, Ohls R, Calhoun VD, Caprihan A. Resting-state functional connectivity differences in premature children. Front Syst Neurosci. 2010;17;4. pii: 23.

Dammann O, O'Shea TM. Cytokines and perinatal brain damage. Clin Perinatol 2008 35(4):643–663.

Damoiseaux JS, Beckmann CF, Arigita EJ, Barkhof F, Scheltens P, Stam CJ, Smith SM, Rombouts SA. Reduced resting-state brain activity in the "default network" in normal aging. Cereb Cortex 2008;18:1856–1864.

Davis MH, Khotanzad A, Flamig DP, Harms SE. A physics-based coordinate transformation for 3-D image matching. IEEE Transactions on Medical Imaging, 1997;16(3):317–328.

Davis TL, Kwong KK, Weisskoff RM, Rosen BR. Calibrated functional MRI: mapping the dynamics of oxidative metabolism. Proc Natl Acad Sci U S A. 1998;17;95(4):1834-9.

de Haan M, Wyatt JS, Roth S, Vargha-Khadem F, Gadian D, Mishkin . Brain and cognitive-behavioural development after asphyxia at term birth. Dev Sci 2006;9(4):350–358.

De Vico Fallani F, Astolfi L, Cincotti F, Mattia D, la Rocca D, Abiloni F, Vegso B, Kozmann G, Nagy Z. Evaluation of the brain network organization from EEG signals:

a preliminary evidence in stroke patient. The Anatomical Record 2009;292: 2023–2031.

De Vries LS, Toet MC. Amplitude integrated electroencephalography in the full-term newborn. Clin Perinatol. 2006;33:619-632. a

De Vries LS, Verboon-Maciolek MA, Cowan FM, Groenendaal F. The role of cranial ultrasound and magnetic resonance imaging in the diagnosis of infections of the central nervous system. Early Hum Dev 2006;82:819-825. b

De Vries LS, Cowan FM. Evolving understanding of hypoxic-ischemic encephalopathy in the term infant. Semin Pediatr Neurol 2009;16:216–225.

De Vries LS, Jongmans MJ. Long-term outcome after neonatal hypoxic-ischaemic encephalopathy. Arch Dis Child Fetal Neonatal Ed. 2010;95(3):F220-4.

Debbané M, Lazouret M, Lagioia A, Schneider M, Van De Ville D, Eliez S. Resting-state networks in adolescents with 22q11.2 deletion syndrome: associations with prodromal symptoms and executive functions. Schizophr Res. 2012;139(1-3):33-9.

DeBoy CA, Zhang J, Dike S, Shats I, Jones M, Reich DS, Mori S, Nguyen T, Rothstein B, Miller RH, Griffin JT, Kerr DA, Calabresi PA. High resolution diffusion tensor imaging of axonal damage in focal inflammatory and demyelinating lesions in rat spinal cord. Brain. 2007;130(Pt 8):2199-210.

Degraeuwe PL, Jaspers GJ, Robertson NJ, Kessels AG. Magnetic resonance spectroscopy as a prognostic marker in neonatal hypoxic-ischemic encephalopathy: a study protocol for an individual patient data meta-analysis. Syst Rev. 2013;25;2:96.

Dehaene-Lambertz G., S. Dehaene, L. Hertz-Pannier. Functional neuroimaging of speech perception in infants. Science 2002;298:2013–2015.

Deipolyi AR, Mukherjee P, Gill K, Henry RG, Partridge SC, Veeraraghavan S, Jin H, Lu Y, Miller SP, Ferriero DM, Vigneron DB, Barkovich AJ. Comparing

microstructural and macrostructural development of the cerebral cortex in premature newborns: diffusion tensor imaging versus cortical gyration. Neuroimage 2005;27:579–586.

DeLong GR. Autism, amnesia, hippocampus, and learning. Neurosci Biobehav Rev 1992;16:63–70.

Demers E, McPherson R, Juul S. Erythropoietin protects dopaminergic neurons and improves neurobehavioral outcomes in juvenile rats after neonatal hypoxia-ischemia. Pediatr Res 2005;58:297-301.

Derbyshire JA, Wright GA, Henkelman RM, Hinks RS. Dynamic scan-plane tracking using MR position monitoring. J Magn Reson Imaging 1998;8:924–932.

Detrait ER, George TM, Etchevers HC, Gilbert JR, Vekemans M, Speer MC. Human neural tube defects: developmental biology, epidemiology, and genetics. Neurotoxicol Teratol. 2005;27(3):515-24. Review.

Diebler MF, Farkas-Bargeton E, Wehrlé R. Developemtnal changes of enzymes associated with energy metabolism and the synthesis of some neurotransmitters in discrete areas of human neocortex. Journal of Neurochemistry 1979;32:429–435.

Digicaylioglu M, Lipton S. Erythropoietin-mediated neuroprotection involves cross-talk between Jak2 and NF-kappaB signalling cascades. Nature 2001;412:641-7.

Dijkhuizen RM, van der Marel K, Otte WM, Hoff EI, van der Zijden JP, van der Toorn A, van Meer MP. Functional MRI and Diffusion Tensor Imaging of Brain Reorganization After Experimental Stroke. Transl Stroke Res. 2012;3(1):36-43.

Dilenge ME, Majnemer A, Shevell MI. Long-term developmental outcome of asphyxiated term neonates. J Child Neurol 2001;16:781–792.

Dingley JTJ, Porter H, Thoresen M. Xenon provides short-term neuroprotection in neonatal rats when administered after hypoxia-ischemia. Stroke 2006;37:501–6.

Dingley J, Tooley J, Liu X, Scull-Brown E, Elstad M, Chakkarapani E, Sabir H, Thoresen M. Xenon Ventilation During Therapeutic Hypothermia in Neonatal Encephalopathy: A Feasibility Study. Pediatrics. 2014 Apr 28. [Epub ahead of print]

Dinse A, Föhr KJ, Georgieff M, Beyer C, Bulling A, Weigt HU. Xenon reduces glutamate-, AMPA-, and kainate-induced membrane currents in cortical neurones. Br J Anaesth. 2005;94(4):479-85.

Dirnagl U, Lindauer UA, Villringer. Role of nitric oxide in the coupling of cerebral blood flow to neuronal activation in rats. Neuroscience Letters 1993;149:43–46.

Dixon G, Badawi N, Kurinczuk J, Keogh JM, Silburn SR, Zubrick SR, Stanley FJ. Early developmental outcomes after newborn encephalopathy. Pediatrics 2002. 10926–33.33.

Dobbing J, Sands J. Quantitative growth and development of human brain. Arch Dis Child. 1973;48(10):757-67.

Dodd J, Jessell TM. Axon guidance and the patterning of neuronal projections in vertebrates. Sience. 1988;4;242(4879):692-9. Review.

Doria V, Beckmann CF, Arichi T, Merchant N, Groppo M, Turkheimer FE, Counsell SJ, Murgasova M, Aljabar P, Nunes RG, Larkman DJ, Rees D, Edwards AD. Emergence of resting state networks in the preterm human brain. PNAS 2010;16;107(46):20015-20020.

Dosenbach NU, Fair DA, Miezin FM, Cohen AL, Wenger KK, Dosenbach RA, Fox MD, Snyder AZ, Vincent JL, Raichle ME, Schlaggar BL, Petersen SE. Distinct brain networks for adaptive and stable task control in humans. Proc Natl Acad Sci U S A. 2007;26;104(26):11073-8.

Dugas-Phocion G, Gonzalez MA, Lebrun C, Chanalet S, Bensa, C, Malandain G, Ayache N. Hierarchical segmentation of multiple sclerosis lesions in multi-sequence

MRI. In: ISBI04, 2004;1:157–160

Duong TQ, Iadecola C, Kim SG. Effect of hyperoxia, hypercapnia, and hypoxia on cerebral interstitial oxygen tension and cerebral blood flow. Magn Reson Med. 2001;45(1):61-70.

Edwards AD, Yue X, Squier MV, Thoresen M, Cady EB, Penrice J, Cooper CE, Wyatt JS, Reynolds EO, Mehmet H. Specific inhibition of apoptosis after cerebral hypoxia-ischaemia by moderate post-insult hypothermia. Biochem Biophys Res Commun. 1995;26;217(3):1193-9.

Edwards AD, Yue X, Cox P, Hope PL, Azzopardi DV, Squier MV, Mehmet H. Apoptosis in the brains of infants suffering intrauterine cerebral injury. Pediatr Res. 1997;42(5):684-9.

Edwards AD, Brocklehurst P, Gunn AJ, Halliday HL, Juszczak E, Levene M, Strohm B, Thoresen M, Whitelaw A, Azzopardi D. Neurological outcomes at 18 months of age after moderate hypothermia for perinatal hypoxic-ischemic encephalopathy: synthesis and meta-analysis of trial data; BMJ 2010;9;340-c363.

Eken P, Jansen GH, Groenendaal F, Rademaker KJ, de Vries LS. Intracranial lesions in the fullterm infant with hypoxic–ischaemic encephalopathy: ultrasound and autopsy correlation. Neuropediatrics 1994;25, 301–307.

Eken P, Toet MC, Groenendaal F, de Vries LS. Predictive value of early neuroimaging, pulsed Doppler and neurophysiology in full term infants with hypoxic-ischaemic encephalopathy. Arch Dis Child Fetal Neonatal Ed 1995; 73: F75–80.

El-Ayouty M, Abdel-Hady H, El-Mogy S, Zaghlol H, El-Beltagy M, Aly H. Relationship between electroencephalography and magnetic resonance imaging findings after hypoxic-ischemic encephalopathy at term. Am J Perinatol. 2007;24(8):467-73.

Ellenberg JH, Nelson KB. The association of cerebral palsy with birth asphyxia: a

definitional quagmire. Dev Med Child Neurol. 2013;55(3):210-6

Ellis M, Manandhar D. Progress in perinatal asphyxia. Semin Neonatal 1991;4:183-191.

Elmahdy H, El-Mashad AR, El-Bahrawy H, El-Gohary T, El-Barbary A, Aly H. Human recombinant erythropoietin in asphyxia neonatorum: pilot trial. Pediatrics. 2010;125(5):e1135-42.

Elsen PA, Pol E-JD, Viergever MA. Medical image matching – a review with classification. IEEE Eng Med Biol Mag. 1993;12(1):26–39

Erberich SG, Friedlich P, Seri I, Nelson MD Jr., Bluml S. Functional MRI in neonates using neonatal head coil and MR compatible incubator Neuroimage, 2003;(20)683–692

Erberich SG, Panigrahy A, Friedlich P, Seri I, Nelson MD, Gilles F. Somatosensory lateralization in the newborn brain. Neuroimage. 2006;1;29(1):155-61.

Ethell IM, Pasquale EB. Molecular mechanisms of dendritic spine development and remodeling. Prog Neurobiol. 2005;75(3):161-205.

Evans JW, Todd RM, Taylor MJ, Strother SC. Group specific optimization of fMRI processing steps for child and adult data. Neuroimage 2010;50:479–490.

Ever L, Gaiano N. Radial 'glial' progenitors: neurogenesis and signaling. Curr Opin Neurobiol. 2005;15(1):29-33. Review.

Evrard P, Gressens P, Volpe JJ. New concepts to understand the neurological consequences of subcortical lesions in the premature brain. Biol Neonate. 1992;61(1):1-3.

Fabian RH, Perez-Polo J, Kent TA. Perivascular nitric oxide and superoxide in neonatal cerebral hypoxia-ischemia. Am J Physiol Heart Circ Physiol 2010;295:h1809-14.

Fair DA, Dosenbach NU, Church JA, Cohen AL, Brahmbhatt S, Miezin FM, Barch DM, Raichle ME, Petersen SE, Schlaggar BL. Development of distinct control networks through segregation and integration. Proc Natl Acad Sci USA 2007;104:13507–13512.

Fair DA, Cohen AL, Dosenbach NU, Church JA, Miezin FM, Barch DM, Raichle ME, Petersen SE, Schlaggar BL. The maturing architecture of the brain's default network. Proc Natl Acad Sci USA 2008;105:4028–4032.

Fair DA, Posner J, Nagel BJ, et al. Atypical default network connectivity in youth with attention-deficit/hyperactivity disorder. Biol Psychiatry 2010;68:1084 –91.

Falconer JC, Narayana PA. Cerebrospinal fluid-suppressed high-resolution diffusion imaging of human brain. Magn Reson Med. 1997;37(1):119-23.

Fan X, van Bel F. Pharmacological neuroprotection after perinatal asphyxia. J Matern Fetal Neonatal Med. 2010;23 Suppl 3:17-9.

Faraci FM, Sobey CG. Role of potassium channels in regulation of cerebral vascular tone. J Cereb Blood Flow Metab. 1998;18(10):1047-63. Review.

Farquharson S, Tournier JD, Calamante F, Fabinyi G, Schneider-Kolsky M, Jackson GD, Connelly A. White matter fiber tractography: why we need to move beyond DTI. J Neurosurg. 2013;118(6):1367-77.

Fauchere J, Dame C, Vonthein R, Koller B, Arri S, Wolf M, bucher H. An approach to using recombinant erythropoietin for neuroprotection in very preterm infants. Pediatrics 2008;122:375-82.

Faulkner S, Bainbridge A, Kato T, Chandrasekaran M, Kapetanakis AB, Hristova M, Liu M, Evans S, De Vita E, Kelen D, Sanders RD, Edwards AD, Maze M, Cady EB, Raivich G, Robertson NJ. Xenon augmented hypothermia reduces early lactate/N-acetylaspartate and cell death in perinatal asphyxia. Ann Neurol. 2011;70(1):133-50.

Faulkner SD, Downie NA, Mercer CJ, Kerr SA, Sanders RD, Robertson NJ. A xenon recirculating ventilator for the newborn piglet: developing clinical applications of xenon for neonates. Eur J Anaesthesiol. 2012;29(12):577-85.

Fellman V, Raivio KO. Reperfusion injury as the mechanism of brain damage after perinatal asphyxia. Pediatr Res. 1997;41(5):599-606.

Fenton A, Evans DH, Levene MI. On-line cerebral blood flow velocity and blood pressure measurements in neonates: a new method. Arch Dis Child 1990;65:11–14

Ferrer I, Soriano E, del Rio JA, Alcántara S, Auladell C. Cell death and removal in the cerebral cortex during development. Prog Neurobiol. 1992;39(1):1-43. Review.

Ferriero DM. Neonatal brain injury. N Engl J Med 2004; 351:1985.

Fiala JC, Spacek J, Harris KM. Review: Dendritic spine pathology: Cause or consequence of neurological disorders. Brain Research Reviews. 2002;39:29–54.

Filippi L, Fiorini P, Daniotti M, Catarzi S, Savelli S, Fonda C, Bartalena L, Boldrini A, Giampietri M, Scaramuzzo R, Papoff P, Del Balzo F, Spalice A, la Marca G, Malvagia S, Della Bona ML, Donzelli G, Tinelli F, Cioni G, Pisano T, Falchi M, Guerrini R. Safety and efficacy of topiramate in neonates with hypoxic ischemic encephalopathy treated with hypothermia (NeoNATI). BMC Pediatr. 2012;5(12):144

Filippini N, MacIntosh BJ, Hough MG, Goodwin GM, Frisoni GB, Smith SM, Matthews PM, Beckmann CF, Mackay CE. Distinct patterns of brain activity in young carriers of the APOEepsilon4 allele. Proc. Natl. Acad. Sci.U.S.A. 2009;106, 7209–7214.

Finer NN, Robertson CM, Richards RT, Pinnel LE, Peters KL. Hypoxic-ischemic encephalopathy in term neonates: Perinatal factors and outcome. J Pediatr 1981;98:112-117.

Fitzsimmons JR, Scott JD, Peterson DM, Wolverton BL, Webster CS, Lang PJ. Integrated RF coil with stabilization for fMRI human cortex. Magn Reson Med 1997;38:15–18.

Flint AC, Liu X, Kriegstein AR. Nonsynaptic glycine receptor activation during early neocortical development. Neuron. 1998;20(1):43-53.

Forbes HS. Cerebral circulation; observation and measurement of pial vessels. Arch Neurol Psychiatry 1928;19:751–761

Forbes KP, Pipe JG, Bird R. Neonatal Hypoxic-ischemic Encephalopathy: Detection with Diffusion-weighted MR Imaging. AJNR Am J Neuroradiol 2000;21:1490–1496.

Forbes KP, Pipe JG, Bird CR. Changes in brain water diffusion during the 1st year of life. Radiology. 2002;222(2):405-9.

Fox MD, Snyder AZ, Vincent JL, Corbetta M, Van Essen DC, Raichle METhe human brain is intrinsically organized into dynamic, anticorrelated functional networks. Proc Natl Acad Sci USA . 2005;102:9673–9678.

Fox MD, Raichle ME. Spontaneous fluctuations in brain activity observed with functional magnetic resonance imaging. Nat Rev Neurosci. 2007;8:700–711.

Fox MD, Zhang D, Snyder AZ, Raichle ME. The global signal and observed anticorrelated resting state brain networks. J Neurophysiol 2009;101:3270–3283.

Fox MD, Greicius M. Clinical applications of resting state functional connectivity. Front Syst Neurosci 2010;4:19.

Frankenburg WK, Dodds JB. The Denver Developmental Screening Test. Pediatrics. 1967;71(2) 181-191.

Franks NP, Dickinson R, de Sousa SL, Hall AC, Lieb WR. How does xenon produce anaesthesia? Nature. 1998;26;396(6709):324.

Fransson P. Spontaneous low-frequency BOLD signal fluctuations: an fMRI investigation of the resting-state default mode of brain function hypothesis. Hum Brain Mapp 2005;26:15–29.

Fransson P, Skiöld B, Horsch S, Nordell A, Blennow M, Lagercrantz H, Aden U. Resting-state networks in the infant brain. Proc Natl Acad Sci USA 2007;104:15531-15536.

Fransson P, Skiöld B, Engström M, Hallberg B, Mosskin M, Aden U, Lagercrantz H, Blennow M. Spontaneous brain activity in the newborn brain during natural sleep--an fMRI study in infants born at full term. Pediatr Res. 2009;66(3):301-5.

Fransson P, Aden U, Blennow M, Lagercrantz H. The functional architecture of the infant brain as revealed by resting-state fMRI. Cereb Cortex. 2011;21(1):145-54.

Friston KJ, Williams S, Howard R, Frackowiak RS, Turner R. Movement-related effects in fMRI time-series. Magn Reson Med 1996;35:346–355.

Fukunaga M, Horovitz SG, van Gelderen P, de Zwart JA, Jansma JM, Ikonomidou VN, Chu R, Deckers RH, Leopold DA, Duyn JH. Large-amplitude, spatially correlated fluctuations in BOLD fMRI signals during extended rest and early sleep stages. Magn Reson Imaging 2006;24:979–992.

Gadian DG, Aicardi J, Watkins KE. et al Developmental amnesia associated with early hypoxic-ischaemic injury. Brain 2000;123499–507.

Gagliardi C, Tavano A, Turconi AC, Borgatti R. Sequence memory skills in Spastic Bilateral Cerebral Palsy are age independent as in normally developing children.

Disabil Rehabil. 2013;35(6):506-12.

Gaillard WD, Grandin CB, Xu B. Developmental aspects of pediatric fMRI: considerations for image acquisition, analysis, and interpretation. Neuroimage. 2001 Feb;13(2):239-49. Review.

Gallagher TA, Nemeth AJ, Hacein-Bey L. An introduction to the Fourier transform: relationship to MRI. AJR Am J Roentgenol. 2008;190(5):1396-405.

Gano D, Chau V, Poskitt KJ, Hill A, Roland E, Brant R, Chalmers M, Miller SP. Evolution of pattern of injury and quantitative MRI on days 1 and 3 in term newborns with hypoxic-ischemic encephalopathy. Pediatr Res. 2013;74(1):82-7.

Gao J, Li X, Hou X, Ding A, Chan KC, Sun Q, Wu EX, Yang J. Tract-based spatial statistics (TBSS): application to detecting white matter tract variation in mild hypoxic-ischemic neonates. Conf Proc IEEE Eng Med Biol Soc. 2012;2012:432-5.

Gao W, Zhu H, Giovanello KS, Smith JK, Shen D, Gilmore JH, Lin W. Evidence on the emergence of the brain's default network from 2-week-old to 2-year-old healthy pediatric subjects. Proc Natl Acad Sci U S A. 2009;21;106(16):6790-5.

Gao W, Gilmore JH, Giovanello KS, Smith JK, Shen D, Zhu H, Lin W. Temporal and spatial evolution of brain network topology during the first two years of life. PLoS One. 2011;6(9):e25278.

Garavito RM, Mulichak AM. The structure of mammalian cyclooxygenases. Annu Rev Biophys Biomol Struct. 2003;32:183-206. Review.

Garby L, Sjolin S, Vuille JC. Studies on erythrokinetics in infancy. Acta Pediatr. 1962;51: 245–254.

Gavrilescu M, Stuart GW, Rossell S, Henshall K, McKay C, Sergejew AA, Copolov D, Egan GF. Functional connectivity estimation in fMRI data: influence of preprocessing and time course selection. Hum Brain Mapp 2008;29:1040–1052.

George S, Gunn AJ, Westgate JA, et al. Fetal heart rate variability and brainstem injury after asphyxia in preterm fetal sheep. Am J Physiol Regul Integr Comp Physiol 2004;287:R925-33.

Gilles FH. Myelination in the neonatal brain. Hum Pathol. 1976;7(3):244-8.

Gilles FH, Leviton A, Doolin EC. The developing human brain: growth and epidemiologic neuropathology. Wright-PSG Inc Boston 1983.

Gitto E, Marseglia L, Manti S, D'Angelo G, Barberi I, Salpietro C, Reiter RJ. Protective role of melatonin in neonatal diseases. Oxid Med Cell Longev. 2013;2013:980374.

Gizewska M, Hnatyszyn G, Sagan L, Cyry1owski L, Zekanowski C, Modrzejewska M, Nestorowicz B, Kubalska J, Walczak M. Maternal tetrahydrobiopterin deficiency: the course of two pregnancies and follow-up of two children in a mother with 6-pyruvoyl-tetrahydropterin synthase deficiency. J Inherit Metab Dis 2009; Suppl 1:S83-9.

Gjedde A, Marrett S. Glycolysis in neurons, not astrocytes, delays oxidative metabolism of human visual cortex during sustained checkerboard stimulation in vivo. J Cereb Blood Flow Metab. 2001 ;21(12):1384-9.

Gleason CA, Short BL, Jones MD Jr. Cerebral blood flow and metabolism during and after prolonged hypocapnia in newborn lambs. J Pediatr. 1989;115(2):309-14.

Globus MY, Alonso O, Dietrich WD, Busto R, Ginsberg MD. Glutamate release and free radical production following brain injury: effects of posttraumatic hypothermia. J Neurochem. 1995;65(4):1704-1.

Gluckman PD, Wyatt JS, Azzopardi D, Ballard R, Edwards AD, Ferriero DM, Polin RA, Robertson CM, Thoresen M, Whitelaw A, Gunn AJ. Selective head cooling with

mild systemic hypothermia after neonatal encephalopathy: multicentre randomised trial. Lancet 2005;365:663–70.

Golden JA, Chernoff GF Multiple sites of anterior neural tube closure in humans: evidence from anterior neural tube defects (anencephaly). Pediatrics. 1995;95(4):506-10.

Goldkamp O. Treatment effectiveness in cerebral palsy. Arch Phys Med Rehabil. 1984;65(5):232-4.

Golubnitschaja O, Yeghiazaryan K, Cebioglu M, Morelli M, Herrera-Marschitz M. Birth asphyxia as the major complication in newborns: moving towards improved individual outcomes by prediction, targeted prevention and tailored medical care EPMA Journal 2011; 2:197–210.

Gonzalez FF, Miller SP. Does perinatal asphyxia impair cognitive function without cerebral palsy? Arch Dis Child Fetal Neonatal Ed 2006;91(6):F454-9.

Gonzalez FF, Abel R, Almli CR, Mu D, Wendland M, Ferriero DM. Erythropoietin sustains cognitive function and brain volume after neonatal stroke. Dev Neurosci 2009;31:403-11.

Gonzalez FM, Ferriero DM. Neuroprotection in the Newborn Infant. Clin Perinatol. 2009;36(4): 859–880.

Gonzalez FF, Fang A, Ferriero DM. Is erythropoietin the answer? Pediatr Res. 2011;69(1):2-3.

Good CD, Scahill RI, Fox NC, Ashburner J, Friston KJ, Chan D, Crum WR, Rossor MN, Frackowiak RS. Automatic differentiation of anatomical patterns in the human brain: Validation with studies of degenerative dementias. Neuroimage 2002;17:29-46.

Goodman CS, Shatz CJ. Developmental mechanisms that generate precise patterns of neuronal connectivity. Cell. 1993;72 Suppl:77-98. Review.

Gorter JW, Ketelaar M, Rosenbaum P, Helders PJ, Palisano R. Use of the GMFCS in infants with CP: the need for reclassification at age 2 years or older. Dev Med Child Neurol 2009;51:46-52.

Gould SJ, Howard S. An immunohistological study of macrophages in the human fetal brain. Neuropathol Appl Neurobiol. 1991;17(5):383-90.

Govaert P, Zingman A, Jung YH, Dudink J, Swarte R, Zecic A, Meersschaut V, van Engelen S, Lequin M. Network injury to pulvinar with neonatal arterial ischemic stroke. Neuroimage 2008;39:1850-7.

Green MV, Seidel J, Stein SD, Tedder TE, Kempner KM, Kertzman C, Zeffiro TA. Head movement in normal subjects during simulated PET brain imaging with and without head restraint. J Nucl Med 1994;35:1538–1546.

Greicius MD, Krasnow B, Reiss AL, Menon V. Functional connectivity in the resting brain: a network analysis of the default mode hypothesis. Proc Natl Acad Sci U S A. 2003;7;100(1):253-8

Greicius MD, Flores BH, Menon V, Glover GH, Solvason HB, Kenna H, Reiss AL, Schatzberg, AF. Resting-state functional connectivity in major depression: abnormally increased contributions from subgenual cingulate cortex and thalamus. Biol. Psychiatry 2007;62, 429–437.

Greicius MD, Kiviniemi V, Tervonen O, Vainionpaa V, Alahuhta S, Reiss AL, Menon V. Persistent default-mode network connectivity during light sedation. Hum Brain Mapp 2008;29:839–847.

Greicius M. Resting-state functional connectivity in neuropsychiatric disorders. Curr Opin Neurol. 2008;21(4):424-30.

Greisen G. Intravenous 133xe clearance in preterm neonates with respiratory distress. Internal validation of cbf infinity as a measure of global cerebral blood flow. Scand J Clin Lab Invest 1988;48:673-8.

Griffiths R. The abilities of babies. London: University of London Press. 1954

Groenendaal F, Roelants-Van Rijn AM, van der GJ, Toet MC, de Vries LS. Glutamate in cerebral tissue of asphyxiated neonates during the first week of life demonstrated in vivo using proton magnetic resonance spectroscopy. Biol Neonate 2001;79:254-7.

Gross JB (Chair), American Society of Anesthesiologists Task Force on Sedation and Analgesia by Non-anesthesiologists, et al. Practice guidelines for sedation and analgesia by nonanesthesiologists. Anesthesiology 2002;96:1004–1017.

Grow J, Barks JD. Pathogenesis of hypoxic-ischemic cerebral injury in the term infant: current concepts.Clin Perinatol. 2002;29(4):585-602.

Gruss M, Bushell TJ, Bright DP, Lieb WR, Mathie A, Franks NP.Two-pore-domain K+ channels are a novel target for the anesthetic gases xenon, nitrous oxide, and cyclopropane. Mol Pharmacol. 2004;65(2):443-52.

Guan J, Gunn AJ, Sirimanne ES, Tuffin J, Gunning MI, Clark R, Gluckman PD. The window of opportunity for neuronal rescue with insulin-like growth factor-1 after hypoxia-ischemia in rats is critically modulated by cerebral temperature during recovery. J Cereb Blood Flow Metab 2000;20:513–519

Gulani V, Iwamoto GA, Lauterbur PC. Apparent water diffusion measurements in electrically stimulated neural tissue. MagnReson Med. 1999;41(2):241-6.

Gunn AJ, Gunn TR, de Haan HH, Williams CE, Gluckman PD. Dramatic neuronal rescue with prolonged selective head cooling after ischemia in fetal lambs. J Clin Invest. 1997;15;99(2):248-56.

Gunn AJ, Gunn T, Gunning M, Williams C, Gluckman P. Neuroprotection with prolonged head cooling started before postischemic seizures in fetal sheep. Pediatrics 1998;102:1098-106.

Gunn AJ, Thoresen M. Hypothermic neuroprotection. NeuroRx. 2006;3(2):154-69. Review.

Gunn AJ, Gluckman PD. Head cooling for neonatal encephalopathy: the state of the art. Clin Obstet Gynecol 2007;50:636–51.

Gunn AJ, Bennet L. Timing of injury in the fetus and neonate. Curr Opin Obstet Gynecol 2008;20:175-81.

Haataja L, Mercuri E, Regev R, Cowan F, Rutherford M, Dubowitz V, Dubowitz L.. Optimality score for the neurological examination of the infant at 12 and 18 months of age. J Pediatr 1999;135:153–161.

Haataja L, Mercuri E, Guzzetta A, Rutherford M, Counsell SJ, Frisone M, Cioni G, Cowan F. Neurologic examination in infants with hypoxic-ischemic encephalopathy at age 9 to 14 months: use of optimality scores and correlation with magnetic resonance imaging findings. J Pediatr 2001;138:332-7.

Hagberg B, Hagberg G. The changing panorama of cerebral palsy – bilateral spastic forms in particular. Acta Paediatr 1996;416:48–52.

Hagberg H, Peebles D, Mallard C. Models of white matter injury: Comparison of infectious, hypoxic-ischemic, and excitotoxic insults. Ment Retard Dev Disabil Res Rev 2002;8:30–38

Hagmann P, Jonasson L, Maeder P, Thiran JP, Wedeen VJ, Meuli R. Understanding diffusion MR imaging techniques: from scalar diffusion-weighted imaging todiffusion tensor imaging and beyondRadiographics. 2006;26 Suppl 1:S205-23. Review.

Hagmann P, Cammoun L, Gigandet X, Meuli R, Honey CJ, Wedeen VJ, Sporns O. Mapping the structural core of human cerebral cortex. PLoS Biol. 2008;1;6(7):e159.

Hajnal JV, Saeed N, Soar EJ, Oatridge A, Young IR, Bydder GM. A registration and interpolation procedure for subvoxel matching of serially acquired MR images. J Comput Assist Tomogr 1995;19:289–296.

Hajnal JV, Hill D, Hawkes DJ, editors. Medical image registration. 2001. New York: CRC Press.

Hamel E. Cholinergic modulation of the cortical microvascular bed. Progress in brain research 2004;145, 171-178.

Hamilton PA, Hope PL, Cady EB, Delpy DT, Wyatt JS, Reynolds EO. Impaired energy metabolism in brains of newborn infants with increased cerebral echodensities. Lancet 1986;1:1242-6.

Hanrahan JD, Sargentoni J, Azzopardi D, Manji K, Cowan FM, Rutherford MA, Cox IJ, Bell JD, Bryant DJ, Edwards AD. Cerebral metabolism within 18 hours of birth asphyxia: a proton magnetic resonance spectroscopy study. Pediatr Res 1996;39:584-90.

Hanrahan JD, Cox IJ, Edwards AD, Cowan FM, Sargentoni J, Bell JD, Bryant DJ, Rutherford MA, Azzopardi D. Persistent increases in cerebral lactate concentration after birth asphyxia. Pediatr Res 1998;44:304-11.

Hansen SS. Feed-and-sleep: a non-invasive and safe alternative to general anaesthesia when imaging very young children. Radiographer 2009;56:5–8.

Hardeland R. Antioxidative protection by melatonin: multiplicity of mechanisms from radical detoxification to radical avoidance. Endocrine 2005;27:119-30.

Harder DR, Alkayed NJ, Lange AR, Gebremedhin D, Roman RJ. Functional hyperemia in the brain: hypothesis for astrocyte-derived vasodilator metabolites. Stroke; a journal of cerebral circulation 1998;29, 229-234.

Harsan LA, Poulet P, Guignard B, Parizel N, Skoff RP, Ghandour MS. Astrocytic hypertrophy in dysmyelination influences the diffusion anisotropy of white matter. J Neurosci Res. 2007;85(5):935-44.

Haselgrove JC, Moore JR. Correction for distortion of echo-planar images used to calculate the apparent diffusion coefficient. MagnReson Med 1996;36:960 –964.

Hatten ME. Central nervous system neuronal migration. Annu Rev Neurosci. 1999;22:511-39. Review.

Hawkes DJ. Registration methodology: introduction. In: Hajnal JV, Hill D, Hawkes DJ, editors. Medical image registration. 2001. New York: CRC Press.

Haynes RL, Borenstein NS, Desilva TM, Folkerth RD, Liu LG, Volpe JJ, Kinney HC. Axonal development in the cerebral white matter of the human fetus and infant. J Comp Neurol. 2005;4;484(2):156-67.

He BJ, Snyder AZ, Vincent JL, Epstein A, Shulman GL, Corbetta M. Breakdown of functional connectivity in frontoparietal networks underlies behavioral deficits in spatial neglect. Neuron 2007;53, 905–918.

Heard K. Acetylcysteine for acetaminophen poisoning. N Engl J Med 2008;359:285-92.

Heep A, Scheef L, Jankowski J, Born M, Zimmermann N, Sival D, Bos A, Gieseke J, Bartmann P, Schild H, Boecker H. Functional magnetic resonance imaging of the sensorimotor system in preterm infants. Pediatrics. 2009;123(1):294-300.

Helenius J, Soinne L, Perkiö J, Salonen O, Kangasmäki A, Kaste M, Carano RA, Aronen HJ, Tatlisumak T. Diffusion-weighted MR imaging in normal human brains

in various age groups. AJNR Am J Neuroradiol. 2002;23(2):194-9.

Heller C, Constantinou JC, VandenBerg K, Benitz W, Fleisher BE. Sedation administered to very low birth weight premature infants. J Perinatol. 1997;17(2):107-12.

Hellstrom-Westas L, Rosen I. Continuous brain-function monitoring: state of the art in clinical practice.Semin Fetal Neonatal Med. 2006;11:503-511.

Henderson SE, Sugden DA. Movement assessment battery for children. Kent: The Psychological Corporation, 1992.

Hermoye L, Saint-Martin C, Cosnard G, Lee SK, Kim J, Nassogne MC, Menten R, Clapuyt P, Donohue PK, Hua K, Wakana S, Jiang H, van Zijl PC, Mori S. Pediatric diffusion tensor imaging: normal database and observation of the white matter maturation in early childhood. Neuroimage. 2006;15;29(2):493-504.

Higgins RD, Raju TN, Perlman J, Azzopardi DV, Blackmon LR, Clark RH, Edwards AD, Ferriero DM, Gluckman PD, Gunn AJ, Jacobs SE, Eicher DJ, Jobe AH,Laptook AR, LeBlanc MH, Palmer C, Shankaran S, Soll RF, Stark AR, Thoresen M, Wyatt J. Hypothermia and perinatal asphyxia: executive summary of the National Institute of Child Health and Human Development workshop. J Pediatr 2006,148(2):170–175.

Hill DL, Batchelor PG, Holden M, Hawkes DJ. Medical image registration. Phys Med Biol 2001;46:1-45.

Hirsch JG, Bock M, Essig M, Schad LR. Comparison of diffusion anisotropy measurements in combination with the flair-technique. Magn Reson Imaging. 1999;17(5):705-16.

Hoge RD, Atkinson J, Gill B, Crelier GR, Marrett S, Pike GB. Investigation of BOLD signal dependence on cerebral blood flow and oxygen consumption: the deoxyhemoglobin dilution model. Magn Reson Med. 1999;42(5):849-63.

Honey CJ, Sporns O. Dynamical consequences of lesions in cortical networks. Hum Brain Mapp. 2008; 29(7):802–809.

Honey CJ, Sporns O, Cammoun L, Gigandet X, Thiran JP, Meuli R, Hagmann P. Predicting human resting-state functional connectivity from structural connectivity. Proc Natl Acad Sci U S A. 2009;10;106(6):2035-40.

Hope PL, Costello AM, Cady EB, Delpy DT, Tofts PS, Chu A, Hamilton PA, Reynolds EO, Wilkie DR. Cerebral energy metabolism studied with phosphorus NMR spectroscopy in normal and birth-asphyxiated infants. Lancet 1984;2(8399):366-70.

Horovitz SG, Fukunaga M, de Zwart JA, van Gelderen P, Fulton SC, Balkin TJ, Duyn JH. Low frequency BOLD fluctuations during resting wakefulness and light sleep: a simultaneous EEG-fMRI study. Hum Brain Mapp. 2008;29(6):671-82.

Horsfield MA. Mapping eddy current induced fileds for the correction of diffusion-weighted echo planar images. Magn Reson Imaging1999;17:1335–1345.

Hossain MM, Mannan MA, Yeasmin F, Shaha CK, Rahman MH, Shahidullah M. Short-term outcome of magnesium sulfate infusion in perinatal asphyxia. Mymensingh Med J. 2013;22(4):727-35

Howseman AM, Bowtell RW. Functional magnetic resonance imaging: imaging techniques and contrast mechanisms. Philos Trans R Soc Lond B Biol Sci. 1999;354:1179–1194.

Huang BY, Castillo M. Hypoxic-ischemic brain injury: Imaging findings from birth to adulthood. Radiographics. 2008;28(2)417-440.

Huang J, Agus D, Winfree C, Kiss S, Mack W, McTaggart R, Choudhri TF, Kim LJ, Mocco J, Pinsky DJ, Fox WD, Israel RJ, Boyd TA, Golde DW, Connolly ES. Dehydroascorbic acid, a blood-brain barrier transportable form of vitamin C, mediates

potent cerebroprotection in experimental stroke. Proc Natl Acad Sci U S A 2001;98:11720-4.

Hudetz AG, Smith JJ, Lee JG, Bosnjak ZJ, Kampine JP. Modification of cerebral laser-Doppler flow oscillations by halothane, PCO2, and nitric oxide synthase blockade. Am J Physiol 1995;269(1 Pt 2):H114–20

Hughes EJ, Bond J, Svrckova P, Makropoulos A, Ball G, Sharp DJ, Edwards AD, Hajnal JV, Counsell SJ. Regional changes in thalamic shape and volume with increasing age. Neuroimage. 2012;15;63(3):1134-42.

Hui Xue H, Srinivasan L, Jiang S, Rutherford M, Edwards AD, Rueckert D, Hajnal JV. Automatic segmentation and reconstruction of the cortex from neonatal MRI. Neuroimage 2007;15;38(3):461-77.

Hunt RW, Neil JJ, Coleman LT, Kean MJ, Inder TE. Apparent diffusion coefficient in the posterior limb of the internal capsule predicts outcome after perinatal asphyxia. Pediatrics 2004;114:999-1003.

Hunter JV, Wilde EA, Tong KA, Holshouser BA. Emerging imaging tools for use with traumatic brain injury research. J Neurotrauma. 2012 Mar 1;29(4):654-71.

Huntley M. The Griffiths Mental Development Scales: from birth to 2 years. Association for research in infant and child development (ARICD). 1996

Hüppi P, Maier S, Peled S, Zientara G, Barnes, Jolesz FA, Volpe JJ. Microstructural development of human newborns cerebral white matter assessed in vivo by diffusion tensor MRI. Pediatr Res, 1998;44:584–590

Hüppi PS, Dubois J. Diffusion tensor imaging of brain development. Semin Fetal Neonatal Med. 2006;11(6):489-97

Husson I, Mesplès B, Bac P, Vamecq J, Evrard P, Gressens P. Melatoninergic neuroprotection of the murine periventricular white matter against neonatal excitotoxic challenge. Ann Neurol. 2002;51(1):82-92.

Huttenlocher PR, de Courten C, Garey LJ, Van der Loos H. Synaptogenesis in human visual cortex--evidence for synapse elimination during normal development. Neurosci Lett. 1982;13;33(3):247-52.

Hutton LC, Abbass M, Dickinson H, Ireland Z, Walker DW. Neuroprotective properties of melatonin in a model of birth asphyxia in the spiny mouse (Acomys cahirin cahirinus). Dev Neurosci 2009;31:437-51.

Hyndman BW, Kitney RI, Sayers B. Spontaneous rhythms in physiological controls systems. Nature 1971;233:339–341

Hyvarinen A, Karhunen J, Oja E. Independent Component Analysis. 2001 John Wiley & Sons Inc.

Iadecola, C. Neurovascular regulation in the normal brain and in Alzheimer's disease. Nature reviews 2004;5, 347-360.

Ikeda T, Murata Y, Quilligan EJ, Choi BH, Parer JT, Doi S, Park SD. Physiologic and histologic changes in near-term fetal lambs exposed to asphyxia by partial umbilical cord occlusion. Am J Obstet Gynecol 1998;178:24–32

Ioroi T, Peeters-Scholte C, Post I, Leusink C, Gronendaal F, van Bel F. Changes in cerebral haemodynamics, regional oxygen saturation and amplitude-integrated continuous EEG during hypoxia-ischaemia and reperfusion in newborn piglets. Exp Brain Res. 2002;144(2):172-7.

Iwata O, Iwata S, Thorton JS, Vita E, Bainbridge A, Herbert L, Scaravilli F, Peebles D, Wyatt JS, Cady EB, Robertson NJ. `Therapeutic time window` duration decreases with increasing severity of cerebral hypoxia-ischemia under normothermia and delayed hypothermia in newborn piglets. Brain Res. 2007;1154:173-180.

Jackson T, Xu A, Vita J, Keaney JJ. Ascorbate prevents the interaction of superoxide and nitric oxide only at very high physiological concentrations. Circ Res 1998;83:916-22.

Jacobs B, Driscoll L, Schall M. Life-span dendritic and spine changes in areas 10 and 18 of human cortex: A quantitative golgi study. Journal of comparative neurology. 1997;386:661–680.

Jacobs M, Schall M, Prather M, Kapler E, Driscoll L, Baca S, Jacobs J, Ford K, Wainwright M, Treml M. Regional dendritic and spine variation in human cerebral cortex: a quantitative golgi study. Cerebral Cortex. 2001; 11:558–571.

Jacobs SE, Hunt R, Tarnow-Mordi W, Inder T, Davis P. Cooling for newborns with hypoxic ischaemic encephalopathy. Cochrane Database Syst Rev. 2007;17;(4):CD003311. Review.

Jacobs SE, Berg M, Hunt R, Tarnow-Mordi WO, Inder TE, Davis PG. Cooling for newborns with hypoxic ischaemic encephalopathy. Cochrane Database Syst Rev. 2013;31;1:CD003311.

Jan J, O'Donnell M. Use of melatonin in the treatment of paediatric sleep disorders. J Pineal Res 1996;21:193-9. 44.

Jatana M, Singh I, Singh A, Jenkins D. Combination of systemic hypothermia and N-acetylcysteine attenuates hypoxic-ischemic brain injury in neonatal rats. Pediatr Res 2006;59:684-9.

Jenkinson M. Registration, atlases and cortical flattening in Functional MRI an introduction to methods. ed. M.P. Jezzard P, Smith SM 2001, New York, USA: Oxford University Press.

Jenkinson M, Smith SM. A global optimisation method for robust affine registration of brain images. Medical Image Analysis, 2001;5(2):143-156.

Jenkinson M, Bannister PR, Brady JM, Smith SM. Improved optimisation for the robust and accurate linear registration and motion correction of brain images. NeuroImage, 2002;17(2):825-841.

Jenkinson M, Beckmann CF, Behrens TE, Woolrich MW, Smith SM. FSL. Neuroimage. 2012;15;62(2):782-9.

Jensen EC, Bennet L, Hunter CJ, Power GG, Gunn AJ. Post-hypoxic hypoperfusion is associated with suppression of cerebral metabolism and increased tissue oxygenation in near-term fetal sheep. J Physiol 2006;572:131-9.

Jespersen SN, Bjarkam CR, Nyengaard JR, Chakravarty MM, Hansen B, Vosegaard T, Østergaard L, Yablonskiy D, Nielsen NC, Vestergaard-Poulsen P. Neurite density from magnetic resonance diffusion measurements at ultrahigh field: comparison with light microscopy and electron microscopy. Neuroimage. 2010; 1;49(1):205-16.

Jespersen SN, Leigland LA, Cornea A, Kroenke CD. Determination of axonal and dendritic orientation distributions within the developing cerebral cortex by diffusion tensor imaging. IEEE Trans Med Imaging. 2012;31(1):16-32.

Jezzard P, Barnett AS, Pierpaoli C. Characterization of and correction for eddy current artifacts in echo planar diffusion imaging. Magn Reson Med 1998;39:801-812.

Jezzard P, Clare S. Sources of distortion in functional MRI data. Hum Brain Mapp. 1999;8:80–85.

Ji H, Stanton B, Igarashi J, Li H, Martasek P, Roman L, et al. Minimal pharmacophoric elements and fragment hopping, an approach directed at molecular diversity and isozyme selectivity. Design of selective neuronal nitric oxide synthase inhibitors. J Am Chem Soc 2008;130:3900-14.

Ji H, Tan S, Igarashi J, Li H, Derrick M, Martasek P, Silverman EB. Selective neuronal nitric oxide synthase inhibitors and the prevention of cerebral palsy. Ann Neurol 2009;65:209-17 a

Ji H, Li H, Martasek P, Roman L, Poulos T, Silverman R. Discovery of highly potent and selective inhibitors of neuronal nitric oxide synthase by fragment hopping. J Med Chem 2009;52:779-97 b

Jiang T, He Y, Zang Y, Weng X. Modulation of functional connectivity during the resting state and the motor task. Hum Brain Mapp 2004;22:63–71

Joel SE, Caffo BS, van Zijl P, Pekar J. On the Relationship Between Seed-Based and ICA-Based Measures of Functional Connectivity. Magn Reson Med 2011;66(3)644-57.

Johansen- Berg H, Behrens T.E.J. Diffusion MRI: From Quantitative Measurement to In vivo Neuroanatomy. Elsevier Inc. 2009 1st edition.

Johnson HJ, Christensen GE. 2002. Consistent landmark and intensity-based image registration. IEEE Trans Med Imaging 21:450-461.

Johnston MV. Neurotransmitters and vulnerability of the developing brain. Brain Dev. 1995 Sep-Oct;17(5):301-6. Review.

Jones DK. Gaussian modeling of the diffusion signal. Chapter in Johansen- Berg H, Behrens T.E.J. Diffusion MRI: From Quantitative Measurement to In vivo Neuroanatomy. Elsevier Inc. 2009 1st edition.

Jones DK, Cercignani M. Twenty-five pitfalls in the analysis of diffusion MRI data. NMR Biomed. 2010 Aug;23(7):803-20.

Jones M, Berwick J, Hewson-Stoate N, Gias C, Mayhew J. The effect of hypercapnia on the neural and hemodynamic responses to somatosensory stimulation. Neuroimage 2005;27(3):609–23.

Jones TB, Bandettini PA, Kenworthy L, et al. Sources of group differences in functional connectivity: an investigation applied to autism spectrum disorder. Neuroimage 2010;49:401–14.

Jorch G, Jorch N. Failure of autoregulation of cerebral blood flow in neonates studied by pulsed Doppler ultrasound of the internal carotid artery. Eur J Pediatr 1987;146:468–472.

Joshi SH, Cabeen RP, Joshi AA, Woods RP, Narr KL, Toga AW. 2010. Diffeomorphic sulcal shape analysis for cortical surface registration. Proc IEEE Comput Soc Conf Comput Vis Pattern Recognit 13-18:475-482.

Juul S, Anderson D, Li Y, Christensen R. Erythropoietin and erythropoietin receptor in the developing human central nervous system. Pediatr Res 1998;43:40-9.

Juul SE, McPherson, RJ, MR, Bauer LA, Ledbetter KJ, Gleason CA, Mayock DE. A phase I/II trial of high-dose erythropoietin in extremely low birth weight infants: pharmacokinetics and safety. Pediatrics 2008;122:383-91.

Kaandorp J, van Bel F, Veen S, Derks J, Groenendaal F, Rijken M, Roze E, Venema MM, Rademaker CM, Bos AF, Benders MJ. Long-term neuroprotective effects of allopurinol after moderate perinatal asphyxia. Follow-up of two randomised controlled trials. Arch Dis Child. 2012;97(3):F162-6.

Kaandorp JJ, Benders MJ, Rademaker CM, Torrance HL, Oudijk MA, de Haan TR, Bloemenkamp KW, Rijken M, van Pampus MG, Bos AF, Porath MM, Oetomo SB, Willekes C, Gavilanes AW, Wouters MG, van Elburg RM, Huisjes AJ, Bakker SC, van Meir CA, von Lindern J, Boon J, de Boer IP, Rijnders RJ, Jacobs CJ, Uiterwaal CS, Mol BW, Visser GH, van Bel F, Derks JB. Antenatal allopurinol for reduction of birth asphyxia induced brain damage (ALLO-Trial); a randomized double blind placebo controlled multicenter study. BMC Pregnancy Childbirth 2010;10:8.

Kaandorp JJ, Derks JB, Oudijk MA, Torrance HL, Harmsen MG, Nikkels PG, van

Bel F, Visser GH, Giussani DA. Antenatal allopurinol reduces hippocampal brain damage after acute birth asphyxia in late gestation fetal sheep. Reprod Sci. 2014;21(2):251-9.

Kadri M, Shu S, Holshouser B, et al. Proton magnetic resonance spectroscopy improves outcome prediction in perinatal CNS insults. J Perinatol. 2003;23(3):181–185.

Kannikeswaran N, Mahajan PV, Sethuraman U, Groebe A, Chen X. Sedation medication received and adverse events related to sedation for brain MRI in children with and without developmental disabilities. Paediatr Anaesth 2009;19:250–6.

Kapellou O, Counsell SJ, Kennea N, Dyet L, Saeed N, Stark J, Maalouf E, Duggan P, Ajayi-Obe M, Hajnal J, Allsop JM, Boardman J, Rutherford MA, Cowan F,Edwards AD. Abnormal cortical development after premature birth shown by altered allometric scaling of brain growth. PLoS Med. 2006;3(8):e265.

Karbasforoushan H, Woodward ND. Resting-State Networks In Schizophrenia. Curr Top Med Chem. 2012;(21)2404-14.

Kaur C, Sivakumar V, Ling E. Melatonin protects periventricular white matter from damage due to hypoxia. J Pineal Res 2010;48:185-93.

Kay BP, Difrancesco MW, Privitera MD, Gotman J, Holland SK, Szaflarski JP. Reduced default mode network connectivity in treatment-resistant idiopathic generalized epilepsy. Epilepsia. 2013;54(3):461-70.

Kelen D, Robertson NJ.Experimental treatments for hypoxic ischaemic encephalopathy. Early Hum Dev. 2010;86(6):369-77.

Kellert BA, McPherson RJ, Juul SE. A comparison of high-dose recombinant erythropoietin treatment regimens in brain-injured neonatal rats. Pediatr Res 2007;61:451-5.

Kemna LJ, Posse S. Effect of respiratory CO_2 changes on the temporal dynamics of the hemodynamic response in functional MR imaging. Neuroimage 2001;14(3):642–9.

Kennedy D.P., Redcay E., Courchesne E. Failing to deactivate: resting functional abnormalities in autism. Proc. Natl Acad. Sci. USA, 2006:103;8275–8280.

Kennedy DP, Courchesne E. Functional abnormalities of the default network during self- and other-reflection in autism. Soc. Cogn. Affect. Neurosci., 2008:3; 177–190 a.

Kennedy DP, Courchesne E. The intrinsic functional organization of the brain is altered in autism. Neuroimage, 2008:39;1877–1885 b.

Khong PL, Tse C, Wong IY, et al. Diffusion weighted imaging and proton magnetic resonance spectroscopy in perinatal hypoxicischemic encephalopathy: association with neuromotor outcome at 18 months of age. J Child Neurol. 2004;19(11):872– 881

Kilic E, Kilic U, Soliz J, Bassetti CL, Gassmann M, Hermann DM Brain-derived erythropoietin protects from focal cerebral ischemia by dual activation of ERK-1/-2 and Akt pathways. FASEB J. 2005;19(14):2026-8.

Kim SG, Ugurbil K. Functional magnetic resonance imaging of the human brain. J Neurosci Methods. 1997;27;74(2):229-43. Review.

Kinnala A, Rikalainen H, Lapinleimu H. Cerebral magnetic resonance imaging and ultrasonography findings after neonatal hypoglycemia. Pediatrics 1999;103, 724–729.

Kinney HC, Armstron DD. Perinatal neuropathology. In Graham DI, Lantos PL (eds): Greenfield's neuropathology, ed 6. London: Arnold, 2002.

Kinney HC, Brody BA, Kloman AS, Gilles FH. Sequence of central nervous system myelination in human infancy. II. Patterns of myelination in autopsied infants. J NeuropatholExp Neurol. 1988;47(3):217-34.

Kirton A, Shroff M, Visvanathan T, deVeber G. Quantified corticospinal tract diffusion restriction predicts neonatal stroke outcome. Stroke 2007;38:974–980

Kiviniemi VJ, Haanpää H, Kantola JH, Jauhiainen J, Vainionpää V, Alahuhta S, Tervonen O. Midazolam sedation increases fluctuation and synchrony of the resting brain BOLD signal. Magn Reson Imaging. 2005;23(4):531-7.

Kiviniemi V, Starck T, Remes J, Long X, Nikkinen J, Haapea M, Veijola J, Moilanen I, Isohanni M, Zang YF, Tervonen O. Functional segmentation of the brain cortex using high model order group PICA. Hum. Brain Mapp. 2009;30,3865–3886.

Klatzo I. Brain oedema following brain ischemia and the influence of therapy. Br Anaesthesia 1985;57:18-22.

Klingberg T, Vaidya CJ, Gabrieli JD, Moseley ME, Hedehus M. Myelination and organization of the frontal white matter in children: a diffusion tensor MRI study. Neuroreport. 1999;9;10(13):2817-21.

Ko KR, Ngai AC, Winn HR. Role of adenosine in regulation of regional cerebral blood flow in sensory cortex. Am J Physiol. 1990;259(6 Pt 2):H1703-8.

Komuro H, Rakic P. Distinct modes of neuronal migration in different domains of developing cerebellar cortex. J Neurosci. 1998;15;18(4):1478-90.

Konishi Y, Taga G, Yamada H, Hirasawa K. Functional brain imaging using fMRI and optical topography in infancy. Sleep Med 2002;3:S41–S43.

Kostovic I, Judas M, Rados M, Hrabac P. Laminar organization of the human fetal cerebrum revealed by histochemical markers and magnetic resonance imaging. Cereb Cortex 2002;12:536–544.

Kostović I, Jovanov-Milosević N. The development of cerebral connections during the first 20-45 weeks' gestation. Semin Fetal Neonatal Med. 2006;11(6):415-22.

Kriegstein AR, Noctor SC. Patterns of neuronal migration in the embryonic cortex. Trends Neurosci. 2004;27(7):392-9. Review.

Kuklisova-Murgasova M, Aljabar P, Srinivasan L, Counsell SJ, Doria V, Serag A, Gousias IS, Boardman JP, Rutherfor MA, Edwards AD, Hajnal JV, Rueckert D. A dynamic 4D probabilistic atlas of the developing brain. Neuroimage, 2011;54(4):2750-63.

Kunz N, Zhang H, Vasung L, O'Brien KR, Assaf Y, Lazeyras F, Alexander DC, Hüppi PS. Assessing white matter microstructure of the newborn with multi-shell diffusion MRI and biophysical compartment models. Neuroimage. 2014;28;96C:288-299.

Kuschinsky W, Wahl M, Bosse O, Thurau K. Perivascular potassium and pH as determinants of local pial arterial diameter in cats. A microapplication study. Circ Res. 1972;31(2):240-7.

L'Abee C, de Vries LS, van der GJ, Groenendaal F. Early diffusion-weighted MRI and 1H-magnetic resonance spectroscopy in asphyxiated full-term neonates. Biol Neonate 2005;88:306-12.

Lally PJ, Price DL, Pauliah SS, Bainbridge A, Kurien J, Sivasamy N, Cowan FM, Balraj G, Ayer M, Satheesan K, Ceebi S, Wade A, Swamy R, Padinjattel S, Hutchon B, Vijayakumar M, Nair M, Padinharath K, Zhang H, Cady EB, Shankaran S, Thayyil S. Neonatal encephalopathic cerebral injury in South India assessed by perinatal magnetic resonance biomarkers and early childhood neurodevelopmental outcome. PLoS One. 2014;5;9(2):e87874.

Lally PJ, Zhang H, Pauliah SS, Price DL, Bainbridge A, Cady EB, Shankaran S, Thayyil S. Neurite density index correlates with childhood neurological outcome after neonatal encephalopathy. Neonatal Society Spring Meeting 2014

Lane GA, Nahrwold ML, Tait AR, Taylor-Busch M, Cohen PJ, Beaudoin AR. Anesthetics as teratogens: nitrous oxide is fetotoxic, xenon is not. Science 1980;210:899-901.

Lante F, Meunier J, Guiramand J, De Jesus Ferreira M, Cambonie G, Aimar R, et al. Late N-acetylcysteine treatment prevents the deficits induced in the offspring of dams exposed to an immune stress during gestation. Hippocampus 2008;18:602-9.

Lante F, Meunier J, Guiramand J, Maurice T, Cavalier M, de Jesus Ferreira M, Aimar R, Cohen-Solal C, Vignes M, Barbanel G. Neurodevelopmental damage after prenatal infection: role of oxidative stress in the fetal brain. Free Radic Biol Med 2007;42: 1231-45.

Laptook AR, Shankaran S, Ambalavanan N, Carlo WA, McDonald SA, Higgins RD, Das A. Hypothermia Subcommittee of the NICHD Neonatal Research Network. Outcome of term infants using apgar scores at 10 minutes following hypoxiceischemic encephalopathy. Pediatrics 2009;124:1619e26.

Larroche J-C. Developemntal pathology of the neonate. 1977. Amsterdam: Excerpta Medica.

Larroche J-C. Perinatal brain damage. In: Adams JH, Corsellis JAN, Duchen LW (editors). Greenfield's neuropathology. 1984. Arnold. London.

Larson-Prior LJ, Zempel JM, Nolan TS, Prior FW, Snyder AZ, Raichle ME. 2009. Cortical network functional connectivity in the descent to sleep. Proc Natl Acad Sci USA 106:4489–4494.

Lasky JL, Wu H. Notch signaling, brain development, and human disease. Pediatr Res. 2005;57(5 Pt 2):104R-109R. Review.

Lassen NA. Cerebral blood flow and oxygen consumption in man. Physiological Review Am J Physiol 39:183–233.

Laurienti PJ. Deactivations, global signal, and the default mode of brain function. J Cogn Neurosci. 2004;16(9):1481-3.

Lauritzen, M. Reading vascular changes in brain imaging: is dendritic calcium the key? Nature reviews 2005;6, 77-85.

Lawn J, Cousens S, Zupan J; Lancet Neonatal Survival Steering Team. 4 million neonatal deaths: when? Where? Why? Lancet. 2005 Mar 5-11;365(9462):891-900.

Le Bihan D, Turner D, MacFall JR. Temperature mapping with MR imaging of molecular diffusion: application to hyperthermia. Radiology 1989;171:853– 857.

Le Strange E, Saeed N, Cowan FM, Edwards AD, Rutherford MA. MR imaging quantification of cerebellar growth following hypoxic-ischemic injury to the neonatal brain. AJNR Am J Neuroradiol. 2004;25:463–468

Lee EC, Kwatra NS, Vezina G, Khademian ZP. White matter integrity on fractional anisotropy maps in encephalopathic neonates post hypothermiatherapy with normal-appearing MR imaging. Pediatr Radiol. 2013;43(6):709-15.

Lee W, Morgan BR, Shroff MM, Sled JG, Taylor MJ. The development of regional functional connectivity in preterm infants into early childhood. Neuroradiology. 2013;55 Suppl 2:105-11

Leech RW, Alvord EC. Anoxic–ischemic encephalopathy in the human neonatal period. The significance of brain stem involvement. Arch Neurol 1977;34, 109–113.

Leech RW, Shuman RM. Holoprosencephaly and related midline cerebral anomalies: a review. J Child Neurol. 1986;1(1):3-18. Review.

Lehmann TM, Gonner C, Spitzer K. Survey: Interpolation methods in medical image processing. IEEE Trans Med Imaging 1999;18:1049-1075.

Leijser LM, Cowan FM: "State-of-the-art" neonatal cranial ultrasound. Ultrasound 2007;15:6-17.

Leijser LM, de Vries LS, Rutherford MA, Manzur AY, Groenendaal F, de Koning TJ, van der Heide-Jalving M, Cowan FM. Cranial ultrasound in metabolic disorders presenting in the neonatal period: Characteristic features and comparison with MR imaging. AJNR Am J Neuroradiol 2007;28:1223-1231. a

Leijser LM, Vein AA, Liauw L, Strauss T, Veen S, Wezel-Meijler Gv. Source Prediction of short-term neurological outcome in full-term neonates with hypoxic-ischaemic encephalopathy based on combined use of electroencephalogram and neuro-imaging. Neuropediatrics. 2007;38(5):219-27. b

Lemire RJ, Loeser JD, Leech RW, Alvoed EC. Normal and abnormal development of the human nervous system. Medical Dept., Harper & Row, 1975.

Leoni RF, Mazzeto-Betti KC, Andrade KC, de Araujo DB. Quantitative evaluation of hemodynamic response after hypercapnia among different brain territories by fMRI. Neuroimage. 2008;41:1192–1198.

Lepomäki V, Matomäki J, Lapinleimu H, Lehtonen L, Haataja L, Komu M, Parkkola R; PIPARI Study Group. Effect of antenatal growth on brain white matter maturation in preterm infants at term using tract-based spatial statistics. Pediatr Radiol. 2013 Jan;43(1):80-5.

Levene MI, Chervenak FA, Whittle M. Fetal and eonatal neurology and neurosurgery. 2002 3rd edition. Churchill Livingstone; Elsevier Science Ltd.

Levene MI. The asphyxiated newborn infant. In Levene MI, Chervenak FA, Whittle M. Fetal and eonatal neurology and neurosurgery. 2002 3rd edition. Churchill Livingstone; Elsevier Science Ltd.

Lewis CM, Baldassarre A, Committeri G, Romani GL, Corbetta M. Learning sculpts the spontaneous activity of the resting human brain. Proc Natl Acad Sci USA 2009;106:17558–17563.

Li AM, Chau V, Poskitt KJ, Sargent MA, Lupton BA, Roland E, Miller SP. White Matter Injury in Term Newborns with Neonatal Encephalopathy. Pediatr. Res. 2009;65:85–89

Li J, Iadecola C. Nitric oxide and adenosine mediate vasodilation during functional activation in cerebellar cortex. Neuropharmacology. 1994;33(11):1453-61.

Li W, Huang Y, Li Y, Chen X. Brain network evolution after stroke based on computational experiments. PLoS One. 2013;20;8(12):e82845.

Li X, Lu ZL, Tjan BS, Dosher BA, Chu W. Blood oxygenation level-dependent contrast response functions identify mechanisms of covert attention in early visual areas. Proc Natl Acad Sci USA 2008;105:6202–6207.

Liao R, McKeown MJ, Krolik JL. Isolation and minimization of head motion-induced signal variations in fMRI data using independent component analysis. Magn Reson Med. 2006;55(6):1396-413.

Liau J, Perthen J, Liu TT. The Relation between BOLD amplitude and Baseline Cerebral Blood Flow Depends on the Analysis Scale. Proceedings of the 16th ISMRM; Toronto. 2008a. p. 854

Liauw L, van Wezel-Meijler G, Veen S, van Buchem MA, van der Grond J Do apparent diffusion coefficient measurements predict outcome in children with neonatal hypoxic-ischemic encephalopathy? AJNR 2009;30:264-270.

Lin WC, Zhu Q, Gao W, et al: Functional connectivity MR imaging reveals cortical functional connectivity in the developing brain. AJNR Am J Neuroradiol 2008 29:1883-1889.

Lindström K, Hallberg B, Blennow M, Wolff K, Ferneli E, Westgren M. Moderate neonatal encephalopathy: pre- and perinatal risk factors and long-term outcome. Acta Obstet Gynecol Scand 2008;87:503–9.

Lindström K, Lagerroos P, Gillberg C, Fernell E. Teenage outcome after being born at term with moderate neonatal encephalopathy. Pediatr Neurol. 2006;35(4):268-74.

Lipper EG, Voorhies TM, Ross G, Vannucci RC, Auld PAM. Early predictors of one-year outcome for infants asphyxiated at birth. Dev Med Child Neurol 1986; 28: 303-9.

Litman RS, Soin K, Salam A. Chloral Hydrate Sedation in Term and Preterm Infants: An Analysis of Efficacy and Complications. Anesth Analg. 2010; 110:3739-746.

Liu H, Buckner RL, Talukdar T, Tanaka N, Madsen JR, Stufflebeam SM. Task-free presurgical mapping using functional magnetic resonance imaging intrinsic activity. J. Neurosurg. 2009;111, 746–754.

Liu WC, Flax JF, Guise KG, et al: Functional connectivity of the sensorimotor area in naturally sleeping infants. Brain Res 2008;1223:42-49.

Lobo N, Yang B, Rizvi M, Ma D. Hypothermia and xenon: novel noble guardians in hypoxic-ischemic encephalopathy? J Neurosci Res. 2013;91(4):473-8.

Loeliger M, Watson CS, Reynolds JD, Penning DH, Harding R, Bocking AD, Rees SM. Extracellular glutamate levels and neuropathology in cerebral white matter following repeated umbilical cord occlusion in the near term fetal sheep. Neuroscience 2003; 116:705–714

Lopez AD, Mathers CD. Measuring the global burden of disease and epidemiological transitions: 2002-2030. Ann Trop Med Parasitol. 2006;100(5-6):481-99. Review.

Lorek A, Takei Y, Cady EB, Wyatt JS, Penrice J, Edwards AD, Peebles D, Wylezinska M, Owen-Reece H, Kirkbrie V. Delayed (secondary) cerebral energy

failure after acute hypoxia-ischemia in the newborn piglet: continuous 48 hours studies by phosphorus resonance spectroscopy. Pediatr Res. 1994;36: 699-706.

Lou HC, Lassen NA, Fnis-Hansen B. Impaired autoregulation of cerebral blood flow in distressed newborn infants. J Pediatr 1979;94:118121

Lou HC. Etiology and pathogenesis of attention-deficit hyperactivity disorder (ADHD): significance of prematurity and perinatal hypoxic-haemodynamic encephalopathy. Acta Paediatr 1996;85:1266–1271.

Low JA, Lindsay BG, Derrick EJ. Threshold of metabolic acidosis associated with newborn complications. Am J Obstet Gynecol 1997;177:1391-4.

Lowe MJ, Phillips MD, Lurito JT, Mattson D, Dzemidzic M, Mathews VP. Multiple sclerosis: low-frequency temporal blood oxygen level-dependent fluctuations indicate reduced functional connectivity initial results. Radiol 2002;224:184–192.

Lu W, Chen ML, Olivera GH, Ruchala KJ, Mackie TR. Fast free-form deformable registration via calculus of variations. Phys Med Biol. 2004;21;49(14):3067-87.

Luchetti F, Canonico B, Betti M, Arcangeletti M, Pilolli F, Piroddi M, Canesi L, Papa S, Galli F. Melatonin signaling and cell protection function. FASAB J 2010;24:3603-24.

Luiz DM, Foxcroft CD, Stewart R. The construct validity of the Griffiths Scales of Mental Development. Child Care Health Dev. 2001;27(1):73-83.

Lyons DT, Vasta F, Vannucci RC. Autoradiographic determination of regional cerebral blood flow in the immature rat. Pediatr Res. 1987;21(5):471-6.

Ma D, Hossain M, Chow A, Arshad M, Battson RM, Sanders RD, Mehmet H, Edwards AD, Franks NP, Maze M. Xenon and hypothermia combine to provide neuroprotection from neonatal asphyxia. Ann Neurol. 2005;58(2):182-93.

Ma D, Williamson P, Januszewski A, Nogaro MC, Hossain M, Ong LP, Shu Y, Franks NP, Maze M. Xenon mitigates isoflurane-induced neuronal apoptosis in the developing rodent brain. Anesthesiology. 2007;106(4):746-53.

Macey, P. M., Macey, K. E., Kumar, R., Harper, R. M. A method for removal of global effects from fMRI time series. Neuroimage 22, 2004;360–366.

MacLennan A. A template for defining a causal relation between acute intrapartum events and cerebral palsy: international consensus statement. BMJ. 1999;16;319(7216):1054-9. Review.

Madsen JT, Jansen P, Hesslinger C, Meyer M, Zimmer J, GramsbergenJB. Tetrahydrobiopterin precursor sepiapterin provides protection against neurotoxicity of 1-methyl-4-phenylpyridinium in nigral slice cultures. J Neurochem 2003;85:214-23.

Maintz JB, Viergever M. A survey of medical image registration. Med Image Anal. 1998;2(1):1-36.

Makropoulos A, Ledig C, Aljabar P, Sear A, Hajnal J, Edwards AD, Counsell SJ, Rueckert D. Automatic tissue and structural segmentation of neonatal brain MRI using expectation-maximization, MICCAI Grand Challenge on Neonatal Brain Segmentation 2012

Malik GK, Trivedi R, Gupta RK, Hasan KM, Hasan M, Gupta A, Pandey CM, Narayana PA. Serial quantitative diffusion tensor MRI of the term neonates with hypoxic-ischemic encephalopathy (HIE). Neuropediatrics 2006;37(6):337-43.

Maneru C, Junque C, Botet F, Tallad M, Guardia J. Neuropsychological long-term sequelae of perinatal asphyxia. Brain Inj 2001;151029–1039.

Maneru C, Serra-Grabulosa JM, Junque C, Salgado-Pineda P, Bargallo N, Olondo M, Botet-Mussons F, Tallada M, Mercader JM. Residual hippocampal atrophy in asphyxiated term neonates. J Neuroimaging 2003;13(1):68–74.

Manninen O, Koskenkorva P, Lehtimäki KK, Hyppönen J, Könönen M, Laitinen T, Kalimo H, Kopra O, Kälviäinen R, Gröhn O, Lehesjoki AE, Vanninen R. White matter degeneration with Unverricht-Lundborg progressive myoclonus epilepsy: a translational diffusion-tensor imaging study in patients and cystatin B-deficient mice. Radiology 2013;269(1):232-9.

Manning SM, Jennings R, Madsen JR. Pathophysiology, prevention, and potential treatment of neural tube defects. Ment Retard Dev Disabil Res Rev. 2000;6(1):6-14. Review.

Mansfield P. Multi-planar image formation using NMR spin echoes. J Phys C: Solid State Phys 1977;10:L55.

Marcar V.L., A.E. Strassle, T. Loenneker, U. Schwarz, E. Martin. The influence of cortical maturation on the BOLD response: an fMRI study of visual cortex in children. Pediatr Res, 56 (2004), pp. 967–974.

Marchetti I, Koster EH, Sonuga-Barke EJ, De Raedt R. The default mode network and recurrent depression: a neurobiological model of cognitive risk factors. Neuropsychol Rev. 2012 Sep;22(3):229-51.

Margulies DS, Böttger J, Long X, Lv Y, Kelly C, Schäfer A, Goldhahn D, Abbushi A, Milham MP, Lohmann G, Villringer A. Resting developments: a review of fMRI post-processing methodologies for spontaneous brain activity. Magma. 2010;23(5-6):289-307.

Marina-Pallida M. Cajal-Retzius cells in the development of the neocortex. Trends Neurosci 1998;21:64-71.

Marina-Pallida M. Ontogenesis of the pyramidal cell of the mammalian neocortex and developmental cytoarchitectonics: a unifying theory. J Comp Neur 1992; 321:233-240.

Marlow N, Rose AS, Rands CE, Draper ES. Neuropsychological and educational problems at school age associated with neonatal encephalopathy. Arch Dis Child Fetal Neonatal Ed. 2005;90(5):F380-7.

Marlow N, Wolke D, Bracewell MA, Samara M, Group ES. Neurologic and developmental disability at six years of age after extremely preterm birth. N Engl J Med. 2005;352(1):9 –19.

Martin E, Buchli R, Ritter S, Schmid R, Largo RH, Boltshauser E, Fanconi S, Duc G, Rumpel H. Diagnostic and prognostic value of cerebral 31P magnetic resonance spectroscopy in neonateswith perinatal asphyxia. Pediatr Res. 1996;40(5):749-58.

Martin JL, Ma D, Hossain M, Xu J, Sanders RD, Franks NP, Maze M. Asynchronous administration of xenon and hypothermia significantly reduces brain infarction in the neonatal rat. Br J Anaesth 2007;98(2):236-40.

Martin, E, Joeri P, Loenneker T, Ekatodramis D, Vitacco D, Hennig J, Marcar VL. Visual processing in infants and children studied using functional MRI. Pediatr. Res. 1999;46: 135–140.

Martinez-Biarge M, Diez J, Kapellou O, Allsop J, Rutherford MA, Cowan FM. Predicting motor outcome and death in infants with central grey matter damage associated with hypoxic-ischemic encephalopathy. Neonatal Society Autumn Meeting 2009.

Martinez-Biarge M, Diez-Sebastian J, Rutherford MA, Cowan FM. Outcomes after central grey matter injury in term perinatal hypoxic-ischaemic encephalopathy. Early Hum Dev. 2010;86(11):675-82.

Martinez-Biarge M, Diez-Sebastian J, Kapellou O, Gindner D, Allsop JM, Rutherford MA, Cowan FM. Predicting motor outcome and death in term hypoxic-ischemic encephalopathy. Neurology. 2011;14;76(24):2055-61.

Martinez-Biarge M, Bregant T, Wusthoff CJ, Chew AT, Diez-Sebastian J, Rutherford MA, Cowan FM. White Matter and Cortical Injury in Hypoxic-Ischemic Encephalopathy: Antecedent Factors and 2-Year Outcome. J Pediatr. 2012;161:799-807.

Martuzzi R, Ramani R, Qiu M, Rajeevan N, Constable RT. Functional connectivity and alterations in baseline brain state in humans. Neuroimage. 2010;1;49(1):823-34.

Mata M, Fink DJ, Gainer H, Smith CB, Davidsen L, Savaki H, Schwartz WJ, Sokoloff L. Activity-dependent energy metabolism in rat posterior pituitary primarily reflects sodium pump activity. J Neurochem. 1980;34(1):213-5.

Mathiak K, Posse S. Evaluation of motion and realignment for functional magnetic resonance imaging in real time. Magn Reson Med. 2001;45(1):167-71.

Mathur AM, Neil JJ, McKinstry RC, Inder TE. Transport, monitoring, and successful brain MR imaging in unsedated neonates. Pediatr Radiol 2008;38:260–264.

Matsushita H, Johnston M, Lange M, Wilson M. Protective effect of erythropoietin in neonatal hypoxic ischemia in mice. Neuroreport 2003;14:1757-61.

McKinstry RC, Miller JH, Snyder AZ, Mathur A, Schefft GI, Almli CR, Shimony JS, Shiran SI, Neil JJ. A prospective, longitudinal diffusion tensor imaging study of brain injury in newborns. Neurol, 2002;59(6):824-33.

McManus MF, Golden JA. Neuronal migration in developmental disorders. J Child Neurol. 2005;20(4):280-6. Review.

McPherson RJ, Juul SE. Erythropoietin for infants with hypoxic-ischemic encephalopathy. Curr Opin Pediatr. 2010;22(2):139-45

McQuillen PS, Sheldon RA, Shatz CJ, Ferriero DM. Selective vulnerability of subplate neurons after early neonatal hypoxia-ischemia. J Neurosci 2003;23:3308-15.

McQuillen PS, Ferriero DM. Selective vulnerability in the developing central nervous system. Pediatr. Neurol. 2004;30:227–235

McRobbie W, Elizabeth A. Moore, Martin J. Graves, Martin R. Prince. MRI from picture to proton. Cambridge University Press 2010.

Meek JH, Elwell CE, McCormick DC, Edwards AD, Townsend JP, Stewart AL, Wyatt JS. Abnormal cerebral haemodynamics in perinatally asphyxiated neonates related to outcome. Arch Dis Child Fetal Neonatal Ed 1999; 81: F110–5.

Meng S, Qiao M, Foniok T, Tuor UI. White matter damage precedes that in gray matter despite similar magnetic resonance imaging changes following cerebral hypoxia-ischemia in neonatal rats. Exp Brain Res. 2005;166: 56–60.

Meng S, Qiao M, Scobie K, Tomanek B, Tuor UI. Evolution of magnetic resonance imaging changes associated with cerebral hypoxia-ischemia and a relatively selective white matter injury in neonatal rats. Pediatr Res. 2006;59:554–559.

Ment LR, Stewart WB, Gore JC, Duncan CC. Beagle puppy model of perinatal asphyxia: alterations in cerebral blood flow and metabolism. Pediatr Neurol. 1988;4(2):98-104.

Ment LR, Hirtz D, Hüppi PS. Imaging biomarkers of outcome in the developing preterm brain. Lancet Neurol. 2009;8(11):1042-55.

Merchant N, Groves A, Larkman DJ, Counsell SJ, Thomson MA, Doria V, Groppo M, Arichi T, Foreman S, Herlihy DJ, Hajnal JV, Srinivasan L, Foran A, Rutherford M, Edwards AD, Boardman JP. A patient care system for early 3.0 Tesla magnetic resonance imaging of very low birth weight infants. Early Hum Dev. 2009;85(12):779-83.

Merchant NM, Azzopardi DV, Hawwa AF, McElnay JC, Middleton B, Arendt J, Arichi T, Gressens P, Edwards AD. Pharmacokinetics of Melatonin in Preterm Infants. Br J Clin Pharmacol. 2013 76(5):725-33

Mercuri E, Ricci D, Cowan F, Lessing D, Frisone MF, Haajta L, Counsell SJ, Dubowitz LM, Rutherford MA. Head growth in infants with hypoxic-ischemic encephalopathy: correlation with neonatal magnetic resonance imaging. Pediatrics 2000;106:235-243.

Mercuri E, Rutherford M, Barnett A, Foglia C, Haataja L, Counsell S, Cowan F, Dubowitz L. MRI lesions and infants with neonatal encephalopathy. Is the Apgar score predictive? Neuropediatrics. 2002;33(3):150-6.

Meyer C. R., Boes J. L., Kim B., Bland P. H. Zasadny K. R., Kison P. V., Koral K., Frey K. A., Wahl R. L. Demonstration of accuracy and clinical versatility of mutual information for automatic multimodality image fusion using affine and thin-plate spline warped geometric deformations. Medical Image Analysis, 1997 1(3):195–207.

Meyer-Witte S, Brissaud O, Brun M, Lamireau D, Bordessoules M, Chateil JF. Prognostic value of MR in term neonates with neonatal hypoxic-ischemic encephalopathy: MRI score and spectroscopy: about 26 cases. Arch Pediatr. 2008;15(1):9 –23

Mi S, Hu B, Hahm K, Luo Y, KamHui ES, Yuan Q, Wong WM, Wang L, Su H, Chu TH, Guo J, Zhang W, So KF, Pepinsky B, Shao Z, Graff C, Garber E, Jung V, Wu EX, Wu W. LINGO-1 antagonist promotes spinal cord remyelination and axonal integrity in MOG-induced experimental autoimmune encephalomyelitis. Nat Med. 2007;13(10):1228-33.

Miller JH, McKinstry RC, Philip JV, Mukherjee P, Neil JJ. Diffusion-tensor MR imaging of normal brain maturation: a guide to structural development and myelination. Am. J. Roentgenol. 2003;180, 851–859.

Miller SL, Yan EB, Castillo-Mel_endez M, Jenkin G, Walker DW. Melatonin provides neuroprotection in the late-gestation fetal sheep brain in response to umbilical cord occlusion. Dev Neurosci 2005;27:200-10.

Miller SP, Ramaswamy V, Michelson D, Barkovich AJ, Holshouser B, Wycliffe N, Glidden DV, Deming D, Partridge JC, Wu YW, MD, Ashwal S, Ferriero DM. Patterns of brain injury in term neonatal encephalopathy. J Pediatrics 2005;146(4):453–460

Milligan DWA. Failure of autoregulation and intraventricular haemorrhage in preterm infants. Lancet 1980;1:896–898.

Mistraletti G, Sabbatini G, Taverna M, Figini MA, Umbrello M, Magni P, Ruscica M, Dozio E, Esposti R, DeMartini G, Fraschini F, Rezzani R, Reiter RJ, Iapichino G.Pharmacokinetics of orally administered melatonin in critically ill patients. J Pineal Res 2010;48:142-7.

Mo Z, Moore AR, Filipovic R, Ogawa Y, Kazuhiro I, Antic SD, Zecevic N.. Human cortical neurons originate from radial glia and neuron-restricted progenitors. J Neurosci 2007;11;27(15):4132-45.

Mohammadi B, Kollewe K, Samii A, Krampfl K, Dengler R, Mu¨nte TF. Changes of resting state brain networks in amyotrophic lateral sclerosis. Exp Neurol 2009;217:147–153.

Mojsilović J, Zecević N. Early development of the human thalamus: Golgi and Nissl study. Early Hum Dev. 1991;27(1-2):119-44.

Mondi V, Tournier JD, Salvan P, Lingam I, Barnett M, Rosch R, Tusor N, Wurie J, Nongena P, Allsop J, Edwards AD, Hajnal JV, Counsell SJ. Constrained Spherical Deconvolution Based Tractography In The Neonatal Brain. PAS abstract 752776, 2014.

Monk CS, Peltier SJ, Wiggins L., Weng SJ, Carrasco M, Risi S, Lord C. Abnormalities of intrinsic functional connectivity in autism spectrum disorders. Neuroimage, 2009;47:764–772.

Monsoro-Burq AH, Bontoux M, Vincent C, Le Douarin NM. The developmental relationships of the neural tube and the notochord: short and long term effects of the notochord on the dorsal spinal cord. Mech Dev. 1995;53(2):157-70.

Morishita E, Masuda S, Nagao M, Yasuda Y, Sasaki R. Erythropoietin receptor is expressed in rat hippocampal and cerebral cortical neurons, and erythropoietin prevents in vitro glutamate-induced neuronal death. Neuroscience 1997;76:105-16.

Morita T, Kochiyama T, Yamada H, Konishi Y, Yonekura Y, Matsumura Sadato N. Difference in the metabolic response to photic stimulation of the lateral geniculate nucleus and the primary visual cortex of infants: a fMRI study. Neurosci Res 2000;38:63–70.

Morriss MC, Zimmerman RA, Bilaniuk LT, Hunter JV, Haselgrove JC. Changes in brain water diffusion during childhood. Neuroradiology 1999;41, 929–934.

Moseley ME, Mintorovitch J, Cohen Y, Asgari HS, Derugin N, Norman D, Kucharczyk J.Early detection of ischemic injury: comparison of spectroscopy, diffusion-, T2-, and magnetic susceptibility-weighted MRI in cats. Acta Neurochir Suppl 1990;51:207-9.

Moster D, Lie RT, Irgens LM, Bjerkedal T, Markestad T. The association of Apgar score with subsequent death and cerebral palsy: a population-based study in term infants. J Pediatr. 2001;138:798–803

Moster D, Lie RT, Markestad T. Joint association of Apgar scores and early neonatal symptoms with minor disabilities at school age. Arch Dis Child Fetal Neonatal Ed 2002;86:F16–F21.

Muenke M, Cohen MM. Genetic approaches to understanding brain development: holoprosencephaly as a model. Ment Retard Dev Disabil Res Rev. 2000;6(1):15-21. Review.

Mukherjee P, Miller JH, Shimony JS, Philip JV, Nehra D, Snyder AZ, Conturo TE, Neil JJ, McKinstry RC. Diffusion-tensor MR imaging of gray and white matter development during normal human brain maturation. AJNR 2002;23:1445–1456.

Mulderink TA, Gitelman DR, Mesulam MM, Parrish TB. On the use of caffeine as a contrast booster for BOLD fMRI studies. Neuroimage 2002;15:37–44.

Mulkey SB, Yap VL, Swearingen CJ, Riggins MS, Kaiser JR, Schaefer GB. Quantitative cranial magnetic resonance imaging in neonatal hypoxic-ischemic encephalopathy. Pediatr Neurol. 2012;47(2):101-8.

Murakami Y, Yamashita Y, Matsuishi T. Cranial MRI of neurologically impaired children suffering from neonatal hypoglycaemia. Pediatr Radiol 1999;29, 23–27.

Muramoto S., H. Yamada, N. Sadato, H. Kimura, Y. Konishi, K. Kimura *et al.* Age dependent change in metabolic response to photic stimulation of the primary visual cortex in infants: functional magnetic resonance imaging study. J Comput Assist Tomogr, 2002;26:894–901.

Murray DM , Lowe E, O'Rourke D, Azzopardi D, Hellstrom-Westas L, Boylan GB. A Comparison of Continuous Multi Channel EEG with Aeeg for the Prediction of Outcome at 24 Months in Hypoxic-Ischaemic Encephalopathy. Pediatric Research 2010;68, 54–55.

Murray DM, Boylan GB, Ryan CA, Connolly S. Early EEG findings in hypoxic-ischemic encephalopathy predict outcomes at 2 years. Pediatrics 2009;124:459-67.

Murray DM, O'Riordan MN, Horgan R, et al. Fetal heart rate patterns in neonatal hypoxic-ischemic encephalopathy: relationship with early cerebral activity and neurodevelopmental outcome. Am J Perinatol 2009;26:605-12.

Nadarajah B, Brunstrom JE, Grutzendler J, Wong RO, Pearlman AL. Two modes of radial migration in early development of the cerebral cortex. Nat Neurosci. 2001;4(2):143-50.

Nagdyman N, Komen W, Ko HK, Muller C, Obladen M. Early biochemical indicators of hypoxiceischemic encephalopathy after birth asphyxia. Pediatr Res 2001;49:502e6.

Nagy Z, Lindström K, Westerberg H, Skare S, Andersson J, Haliberg B, Lilja A, Flodmark O, Lagercrantz H, Klingberg T, Fernell E. Diffusion tensor imaging on teenagers, born at term with moderate hypoxic-ischemic encephalopathy. Pediatr Res 2005;58:936–40.

Nair G, Tanahashi Y, Low HP, Billings-Gagliardi S, Schwartz WJ, Duong TQ. Myelination and long diffusion times alter diffusion-tensor-imaging contrast in myelin-deficientshiverer mice. Neuroimage. 2005;15;28(1):165-74.

Nakashima K, Todd MM. Effects of hypothermia on the rate of excitatory amino acid release after ischemic depolarization. Stroke. 1996;27(5):913-8.

Nanni L, Croen LA, Lammer EJ, Muenke M. Holoprosencephaly: molecular study of a California population. Am J Med Genet. 2000;14;90(4):315-9.

Narayanan V. Apoptosis in development and disease of the nervous system: 1. Naturally occurring cell death in the developing nervous system. Pediatr Neurol. 1997;16(1):9-13. Review.

Nehlig A, Pereira de Vasconcelos A, Boyet S. Postnatal changes in local cerebral blood flow measured by the quantitative autoradiographic [14C]iodoantipyrine technique in freely moving rats. J Cereb Blood Flow Metab. 1989;9(5):579-88.

Neil J, Shiran S, McKinstry R, Schefft G, Snyder A, Almli C, Akbudak E, Aronovitz JA, Miller SP, Lee BC, Conturo TE. Normal brain in human newborns: apparent diffusion coefficient and diffusion anisotropy measured by using diffusion tensor MR imaging Radiology, 1998;209:57–66

Neil JJ and Inder TE. Detection of wallerian degeneration in a newborn by diffusion

magnetic resonance imaging (MRI). J. Child. Neurol. 2006;21:115–118

Nelson KB, Bingham P, Edwards EM, Horbar JD, Kenny MJ, Inder T, Pfister RH, Raju T, Soll RF. Antecendents of neonatal encephalopathy in the Vermont Oxford Network Encephalopathy Registry. Paediatrics. 2012;130(5):878-86.

Nelson KB, Ellenberg JH. Antecedents of cerebral palsy. Multivariate analysis of risk.N Engl J Med. 1986;10;315(2):81-6.

Nelson KB, Leviton A. How much of neonatal encephalopathy is due to birth asphyxia? Am J Dis Child 1991;145(11):1325-31.

Neuner I, Kupriyanova Y, Stöcker T, Huang R, Posnansky O, Schneider F, Shah NJ. Microstructure assessment of grey matter nuclei in adult tourette patients by diffusion tensor imaging. Neurosci Lett. 2011;3;487(1):22-6.

Nguyen L, Borgs L, Vandenbosch R, Mangin JM, Beukelaers P, Moonen G, Gallo V, Malgrange B, Belachew S. The Yin and Yang of cell cycle progression and differentiation in the oligodendroglial lineage. Ment Retard Dev Disabil Res Rev. 2006;12(2):85-96. Review.

Nguyen TM, Crowther CA, Wilkinson D, Bain E. Magnesium sulphate for women at term for neuroprotection of the fetus. Cochrane Database Syst Rev. 2013;28(2):CD009395.

Nguyen TS, Winn HR, Janigro D. ATP-sensitive potassium channels may participate in the coupling of neuronal activity and cerebrovascular tone. Am J Physiol Heart Circ Physiol. 2000;278(3):H878-8.

Noctor SC, Martínez-Cerdeño V, Kriegstein AR. Contribution of intermediate progenitor cells to cortical histogenesis. Arch Neurol. 2007;64(5):639-42. Review.

Nomura Y, Sakuma H, Takeda K, Tagami T, Okuda Y, Nakagawa T. Diffusional anisotropy of the human brain assessed with diffusion-weighted MR: relation with normal brain development and aging. Am J Neuroradiol 1994;15, 231–238.

Nordmark E, Hägglund G, Lagergren J. Cerebral palsy in southern Sweden II. Gross motor function and disabilities. Acta Paediatr. 2001;90(11):1277-82.

Northington FJ, Ferriero DM, Flock DL, Martin LJ. Delayed neurodegeneration in neonatal rat thalamus after hypoxia-ischemia is apoptosis. J Neurosci 2001;21:1931-8.

O'Brien F, Iwata O, Thornton J, De Vita E, Sellwood M, Iwata S., Delayed whole-body cooling to 33 or 35 degrees c and the development of impaired energy generation consequential to transient cerebral hypoxia-ischemia in the newborn piglet, Pediatrics 2006;117:1549–1559.

Oatridge A, Cowan F, Schwieso J et al. Age related changes in the apparent diffusion coefficient of white and grey matter in the normal infant brain. SMRM Abst. 1995, p. 1282.

Obrig H, Neufang M, Wenzel R, Kohl M, Steinbrink J, Einhaupl K, Villringer A. Spontaneous low frequency oscillations of cerebral hemodynamics and metabolism in human adults. Neuroimage 2000;12(6):623–39.

Ogawa S, Lee TM, Kay AR, Tank DW. Brain magnetic resonance imaging with contrast dependent on blood oxygenation. Proc Natl Acad Sci U S A. 1990;87(24):9868-72.

Ohshiro T, Weliky M. Subplate neurons foster inhibition. Neuron. 2006 Sep 7;51(5):524-6.

Okatani Y, Okamoto K, Hayashi K, Wakatsuki A, Tamura S, Sagara Y. Maternal-fetal transfer of melatonin in pregnant women near term. J Pineal Res 1998;25:129-34.

Okereafor A, Allsop J, Counsell SJ, Fitzpatrick J, Azzopardi D, Rutherford MA, Cowan FM. Patterns of brain injury in neonates exposed to perinatal sentinel events. Pediatrics. 2008;121(5):906-14.

Okumura A, Hayakawa F, Kato T, Kuno K, Watanabe K. MRI findings in patients with spastic cerebral palsy. I: Correlation with gestational age at birth. Dev Med Child Neurol 1997;39:363–368

Oliveira FP, Tavares JM. Medical image registration: a review. Comput Methods Biomech Biomed Engin 2012 1-21.

Ono J, Harada K, Mano T, Sakurai K, Okada S. Differentiation of dys- and demyelination using diffusional anisotropy. Pediatr Neurol. 1997;16(1):63-6.

Oppenheim RW. Cell death during development of the nervous system. Annu Rev Neurosci. 1991;14:453-501. Review.

Ordidge RJ, Mansfield P, Coupland RE. 1981. Rapid biomedical imaging by NMR. Br J Radiol 54:850-855.

Osredkar D, Thoresen M, Maes E, Flatebø T, Elstad M, Sabir H. Hypothermia is not neuroprotective after infection-sensitized neonatal hypoxic-ischemic brain injury. Resuscitation. 2014;85(4):567-72

Pacher P, Beckman JS, Liaudet L. Nitric oxide and peroxynitrite in health and disease. Physiol Rev. 2007;87(1):315-424.

Paintlia MK, Paintlia AS, Barbosa E, Singh I, Singh AK. N-acetylcysteine prevents endotoxin-induced degeneration of oligodendrocyte progenitors and hypomyelination in developing rat brain. J Neurosci Res 2004;78:347-61.

Palisano R, Rosenbaum P, Walter S, Russell D, Wood E, Galuppi B. Development and reliability of a system to classify gross motor function in children with cerebral palsy. Developmental Medicine & Child Neurology, 1997;39, 214-223.

Palmer C, Towfighi J, Roberts RL, Heitjan DF. Allopurinol administered after inducing hypoxia-ischemia reduces brain injury in 7-dayold rats. Pediatr Res 1993;33:405-11.

Panigrahy A, Bluml S. Advances in magnetic resonance neuroimaging techniques in the evaluation of neonatal encephalopathy. Top Magn Reson Imaging 2007;18(1):3–29.

Pannek K, Guzzetta A, Colditz PB, Rose SE. Diffusion MRI of the neonate brain: acquisition, processing and analysis techniques. Pediatr Radiol. 2012;42(10):1169-82.

Pantoni L, Garcia JH, Gutierrez JA. Cerebral white matter is highly vulnerable to ischemia. Stroke 1996;27:1641–1646

Pape K, Wigglesworth JS. Haemorrhage, ischemia and the perinatal brain. 1979. London: Spastics International.

Papile LA, Rudolph AM, Heymann MA. Autoregulation of cerebral blood flow in the preterm fetal lamb. Pediatr Res. 1985;19(2):159-61.

Parikh N, Katsetos C, Ashraf Q, Haider S, Legido A, Delivoria-Papadopoulos M, Mishra OP. Hypoxia-induced caspase-3 activation and DNA fragmentation in cortical neurons of newborn piglets: role of nitric oxide. Neurochem Res 2003;28:1351-7.

Partridge SC, Mukherjee P, Henry RG, Miller SP, Berman JI, Jin H, Lu Y, Glenn OA, Ferriero DM, Barkovich AJ, Vigneron DB. Diffusion tensor imaging: serial quantitation of white matter tract maturity in premature newborns. Neuroimage 2004;22:1302–1314.

Partridge SC, Mukherjee P, Berman JI, Henry RG, Miller SP, Lu Y, Glenn OA, Ferriero DM, Barkovich AJ, Vigneron DB. Tractography-based quantitation of diffusion tensor imaging parameters in white matter tracts of preterm newborns.J MagnReson Imaging.2005;22(4):467-74.

Pasternak JF, Groothuis DR. Autoregulation of cerebral blood flow in the newborn beagle puppy. Biol Neonate. 1985;48(2):100-9.

Pasternak JF, Predey TA, Mikhael MA. Neonatal asphyxia: vulnerability of basal ganglia, thalamus and brainstem. Pediatr Neurol 1991;**7**, 147–149.

Pawela CP, Biswal BB, Hudetz AG, Schulte ML, Li R, Jones SR, Cho YR, Matloub HS, Hyde JS. A protocol for use of medetomidine anesthesia in rats for extended studies using task-induced BOLD contrast and resting-state functional connectivity. Neuroimage. 2009;15;46(4):1137-4.

Pearlman AL, Faust PL, Hatten ME, Brunstrom JE. New directions for neuronal migration. Curr Opin Neurobiol. 1998;8(1):45-54. Review.

Peebles DM, Edwards AD, Wyatt JS, Bishop AP, Cope M, Delpy DT, Reynolds EO. Changes in human fetal cerebral hemoglobin concentration and oxygenation during labor measured by nearinfrared spectroscopy. Am J Obstet Gynecol 1992;166:1369-73.

Peeters-Scholte C, van den Tweel E, Groenendaal F, van Bel F. Redox state of near infrared spectroscopy-measured cytochrome aa(3) correlates with delayed cerebral energy failure following perinatal hypoxia-ischaemia in the newborn pig. Exp Brain Res. 2004;156(1):20-6.

Pei Z, Pang SF, Cheung RT. Pretreatment with melatonin reduces volume of cerebral infarction in a rat middle cerebral artery occlusion stroke model. J Pineal Res 2002;32:168–72.

Pei Z, Pang S, Cheung R. Administration of melatonin after onset of ischemia reduces the volume of cerebral infarction in a rat middle cerebral artery occlusion stroke model. Stroke 2003;34:770–5.

Peled S, Gudbjartsson H, Westin CF, Kikinis R, Jolesz FA. Magnetic resonance imaging shows orientation and asymmetry of white matter fiber tracts. Brain Res. 1998;5;780(1):27-33.

Pellerin, L., and Magistretti, P.J. Neuroenergetics: calling upon astrocytes to satisfy hungry neurons. Neuroscientist 2004;10, 53-62.

Peltier SJ, Kerssens C, Hamann SB, Sebel PS, Byas-Smith M, Hu X. Functional connectivity changes with concentration of sevoflurane anesthesia. Neuroreport. 2005;28;16(3):285-8.

Pennock J M, Patient preparation, safety and hazards in imaging infants and children, In: M. Rutherford, Editor, MRI of the neonatal brain, W.B. Saunders, London 2002;3–15.

Penrice J, Cady EB, Lorek A, Wylezinska M, Amess PN, Aldridge RF, Stewart A, Wyatt JS, Reynolds EO. Proton magnetic resonance spectroscopy of the brain in normal preterm and term infants, and early changes after perinatal hypoxiaeischemia. Pediatr Res 1996;40:6-14.

Perlman J. Intervention strategies for neonatal hypoxic-ischemic cerebral injury. Clin Ther 2006;28:1353-65.

Perlman JM, Goodman S, Kreusser KL, Volpe JJ. Reduction in IVH by elimination of fluctuating cerebral blood flow velocity in preterm infants with respiratory distress syndrome. N Engl J Med 1985;312:1353–1357

Perlman JM, McMenamin JB, Volpe JJ. Fluctuating CBFV in RDS. Relation to the development of intraventricular hemorrhage. N Engl J Med 1983;309:204–209

Perlman JM. Brain injury in the term infant. Semin Perinatol. 2004;28(6):415-24.

Peterson BS, Potenza MN, Wang Z, et al. An FMRI study of the effects of psychostimulants on default-mode processing during stroop task performance in youths with ADHD. Am J Psychiatry 2009, 166(11):1286–1294.

Petersson KH, Pinar H, Stopa EG, Faris RA, Sadowska GB, Hanumara RC, Stonestreet BS. White matter injury after cerebral ischemia in ovine fetuses. Pediatr Res 2000; 51:768–776

Pezzani C, Radvanyi-Bouvet MF, Relier JP, Monod N. Neonatal electroencephalography during the first twenty-four hours of life in full-term newborn infants. Neuropediatrics 1986;17:11-8.

Pfister RH, Bingham P, Edwards EM, Horbar JD, Kenny MJ, Inder T, Nelson KB, Raju T, Soll RF. The Vermont Oxford Neonatal Encephalopathy Registry: rationale, methods, and initial results. BMC Pediatr. 2012;22;12:84.

Pierpaoli C, Righini A, Linfante I, Tao-Cheng JH, Alger JR, Di Chiro G. Histopathologic correlates of abnormal water diffusion in cerebral ischemia: diffusion-weighted MR imaging and light and electron microscopic study. Radiology. 1993;189(2):439-48.

Pierpaoli C, Basser PJ. Toward a quantitative assessment of diffusion anisotropy. Magn. Reson. Med. 1996;36:893–906; (erratum 37:972;1997).

Pierpaoli C, Jezzard P, Basser PJ, Barnett A, Di Chiro Gl. Diffusion tensor imaging of the human brain. Radiology 1996;201, 637–648.

Pierrat V.H.N., Liska A., Thomas D., Subtil D., Truffert P. Groupe d'Etudes en Epidemiologie Perinatale. Prevalence, causes, and outcome at 2 years of age of newborn encephalopathy: population based study. Arch Dis Child Fetal Neonatal Ed, 2005;90:F257–261.

Pirila S, van der Meere J, Korhonen P, Ruusu-Niemi P, Kyntaja M, Nieminen P, Korpela R. A retrospective neurocognitive study in children with spastic diplegia. Dev Neuropsychol. 2004;26(3):679-90.

Pluim JP, Fitzpatrick JM. Image registration. IEEE Trans Med Imaging. 2003;22(11):1341-3.

Poncelet, B. P., Wedeen, V. J., Weisskoff, R. M., and Cohen, M. S. Brain parenchyma motion: Measurement with cine echoplanar MR imaging. 1992. Radiology 185: 645–651.

Porter BE, Tennekoon G. Myelin and disorders that affect the formation and maintenance of this sheath. Ment Retard Dev Disabil Res Rev. 2000;6(1):47-58. Review.

Porter EJ, Counsell SJ, Edwards AD, Allsop J, Azzopardi D. Tract-based spatial statistics of magnetic resonance images to assess disease and treatment effects in perinatal asphyxial encephalopathy. Pediatr Res 2010;68:205–9.

Power JD, Barnes KA, Snyder AZ, Schlaggar BL, Peterson SE. Spurious but systematic correlations in functional connectivity networks arise from subject motion. Neuroimage 2012; 59(3): 2142-54.

Prentice RL. Surrogate endpoints in clinical trials: definition and operational criteria. Stat Med. 1989;8(4):431-40.

Probyn M, Cock M, Duncan J, Tolcos M, Hale N, Shields A, Rees SM, Harding R. The anti-inflammatory agent N-acetyl cysteine exacerbates endotoxininduced hypoxemia and hypotension and induces polycythemia in the ovine fetus. Neonatology 2010;98:118-27

Pryds O, Griesen G, Lou H, Hansen B. Heterogeneity of cerebral vasoreactivity in preterm infants supported by mechanical ventilation. J Pediatr 1989;115:638–645.

Pryds O, Greisen G, Lou H, Friis-Hansen B. Vasoparalysis associated with brain damage in asphyxiated term infants. J Pediatr 1990;117: 119–25.

Pryds O, Andersen GE, Hansen B. Cerebral blood flow reactivity in spontaneously breathing preterm infants shortly after birth. Acta Paediatr Scand 1990;79:391–396

Pryds O, Edwards AD. Cerebral blood flow in the newborn infant. Arch Dis Child Fetal Neonatal Ed. 1996; 74(1): F63–F69.

Purcell EM, Torrey HC, Pound RV. Resonance absorption by nuclear magnetic moments in a solid. Phys Rev 1946;69:37-38.

Qiao M, Latta P, Meng S, Tomanek B, Tuor UI. Development of acute edema following cerebral hypoxia-ischemia in neonatal compared with juvenile rats using magnetic resonance imaging. Pediatr Res. 2004;55:101–106.

Qiao M, Meng S, Scobie K, Foniok T, Tuor UI. Magnetic resonance imaging of differential gray versus white matter injury following a mild or moderate hypoxic-ischemic insult in neonatal rats. Neurosci Lett. 2004;368:332–336.

Qing M, Nimmesgern A, Heinrich PC, Schumacher K, Vazquez-Jimenez JF, Hess J, von Bernuth G, Seghaye MC. Intrahepatic synthesis of tumor necrosis factor-alpha related to cardiac surgery is inhibited by interleukin-10 via the Janus kinase (Jak)/signal transducers and activator of transcription (STAT) pathway. Crit Care Med. 2003;31(12):2769-75.

Rabacchi S, Bailly Y, Delhaye-Bouchaud N, Mariani J. Involvement of the N-methyl D-aspartate (NMDA) receptor in synapse elimination during cerebellar development. Science. 1992;26;256(5065):1823-5.

Radanovic M, Azambuja M, Mansur LL, Porto CS, Scaff M. Thalamus and language: interface with attention, memory and executive funciotn. Arq Neuropsiquiatr. 2003;61(1):34-42.

Rademakers RP, van der Knaap MS, Verbeeten B Jr, Barth PG, Valk J. Central cortico-subcortical involvement: a distinct pattern of brain damage caused by perinatal and postnatal asphyxia in term infants. J Comput Assist Tomogr 1995;19:256–263.

Raichle ME, MacLeod AM, Snyder AZ, Powers WJ, Gusnard DA, Shulman GL. A default mode of brain function. Proc Natl Acad Sci USA 2001;98:676–82.

Raichle ME. Neuroscience. The brain's dark energy. Science. 2006;24;314(5803):1249-50.

Raichle ME. A brief history of human brain mapping. Trends Neurosci 2009.32:118–126.

Raichle ME. A paradigm shift in functional brain imaging. J Neurosci. 2009;14;29(41):12729-34.

Raichle ME. The restless brain. Brain Connect. 2011;1(1):3-12. Review.

Rakic P. Timing of major ontogenetic events in the visual cortex of the rhesus monkey. UCLA Forum Med Sci. 1975;(18):3-40. Review.

Rakic P. Defects of neuronal migration and the pathogenesis of cortical malformations. Prog Brain Res. 1988;73:15-37. Review.

Rakic P. A small step for the cell, a giant leap for mankind: a hypothesis of neocortical expansion during evolution. Trends Neurosci. 1995;18(9):383-8.

Rakic P, Zecevic N. Programmed cell death in the developing human telencephalon. Eur J Neurosci 2000;12:2721-2734.

Rakic P. Less is more: progenitor death and cortical size. Nat Neurosci. 2005;8(8):981-2.

Ramaekers VT, Casaer P, Daniels H, Marchal G. Upper limits of brain blood flow

autoregulation in stable infants of various conceptional age. Early Hum Dev 1990;24:249–258.

Ransom B. R,Kettenham H. (ed.) 1995. Neuroglia. Oxford University Press.

Rennie JM. Roberton's textbook of neonatology. London: Churchill Livingstone, 2005: 1128.

Reppert S, Chez R, Anderson A, Klein D. Maternal-fetal transfer of melatonin in the non-human primate. Pediatr Res 1979;13:788-91.

Rezaie P, Male D. Mesoglia & microglia--a historical review of the concept of mononuclear phagocytes within the central nervous system. J Hist Neurosci. 2002;11(4):325-74.

Rezaie P, Dean A, Male D, Ulfig N. Microglia in the cerebral wall of the human telencephalon at second trimester. Cereb Cortex. 2005;15(7):938-49.

Riggs B, Bronstein A, Kulig K, Archer P, Rumack B. Acute acetaminophen overdose during pregnancy. Obstet Gynaecol 1989;74:247-53.

Rio C, Rieff HI, Qi P, Khurana TS, Corfas G. Neuregulin and erbB receptors play a critical role in neuronal migration. Neuron. 1997 Jul;19(1):39-50. Erratum in: Neuron 1997;19(6):1349.

Robertson CM, Finer NN. Term infants with hypoxic- ischemic encephalopathy: outcome at 3.5 years. Dev Med Child Neurol 1985;27:473–484.

Robertson CM, Finer NN. Educational readiness of survivors of neonatal encephalopathy associated with birth asphyxia at term. J Dev Behav Pediatr 1988;9:298–306.

Robertson CM, Finer NN, Grace MG. School performance of survivors of neonatal encephalopathy associated with birth asphyxia at term. J Pediatr 1989. 114753–760.

Robertson CM, Perlman M. Follow-up of the term infant after hypoxic-ischemic encephalopathy. Paediatr Child Health. 2006;11(5):278-82.

Robertson NJ, Cox IJ, Cowan FM, Counsell SJ, Azzopardi D, Edwards AD. Cerebral intracellular lactic alkalosis persisting months after neonatal encephalopathy measured by magnetic resonance spectroscopy. Pediatr Res 1999;46:287-96.

Robertson NJ, Lewis RH, Cowan FM, et al. Early increases in brain myo-inositol measured by proton magnetic resonance spectroscopy in term infants with neonatal encephalopathy. Pediatr Res 2001;50:692-700.

Robertson NJ, Cowan FM, Cox IJ, Edwards AD. Brain alkaline intracellular pH after neonatal encephalopathy. Ann Neurol 2002;52:732-42.

Robertson NJ, Iwata O. Bench to bedside strategies for optimizing neuroprotection following perinatal hypoxiaeischaemia in high and low resource settings. Early Hum Dev 2007;83:801-11.

Robertson NJ, Tan S, Groenendaal F, van Bel F, Juul SE, Bennet L, Derrick M, Back SA, Valdez RC, Northington F, Gunn AJ, Mallard C. J. Which neuroprotective agents are ready for bench to bedside translation in the newborn infant? Pediatr. 2012;160(4):544-552.

Robertson NJ, Faulkner S, Fleiss B, Bainbridge A, Andorka C, Price D, Powell E, Lecky-Thompson L, Thei L, Chandrasekaran M, Hristova M, Cady EB, Gressens P, Golay X, Raivich G. Melatonin augments hypothermic neuroprotection in a perinatal asphyxia model. Brain. 2013;136(Pt 1):90-105. A

Robertson NJ, Kato T, Bainbridge A, Chandrasekaran M, Iwata O, Kapetanakis A, Faulkner S, Cheong J, Iwata S, Hristova M, Cady E, Raivich G. Methyl-isobutyl amiloride reduces brain Lac/NAA, cell death and microglial activation in a perinatal asphyxia model. J Neurochem. 2013;124(5):645-57. B

Rocca MA, Valsasina P, Absinta M, Riccitelli G, Rodegher ME, Misci P, Rossi P, Falini A, Comi G, Filippi M. Defaultmode network dysfunction and cognitive impairment in progressive MS. Neurol 2010;74:1252–1259.

Roelants-van Rijn AM, Nikkels PG, Groenendaal F, van Der Grond J, Barth PG, Snoeck I, Beek FJ, de Vries LS. Neonatal diffusion-weighted MR imaging: relation with histopathology or follow-up MR examination. Neuropediatrics. 2001;32(6):286-94.

Roessler E, Muenke M. How a Hedgehog might see holoprosencephaly. Hum Mol Genet. 2003;1;12 Spec No 1:R15-25. Review.

Rohlfing T, Maurer CR Jr, Dean D, Maciunas RJ. Effect of changing patient position from supine to prone on the accuracy of a Brown-Roberts-Wells stereotactic head frame system. Neurosurgery. 2003;52(3):610-8.

Rohlfing T, Sullivan EV, Pfefferbaum A. Deformation-based brain morphometry to track the course of alcoholism: Differences between intra-subject and inter-subject analysis. Psychiatry Res 2006;146:157-170.

Rohr K, Stiehl HS, Sprengel R, Buzug TM, Weese J, Kuhn MH. 2001. Landmark-based elastic registration using approximating thin-plate splines. IEEE Trans Med Imaging 20:526-534.

Roland EH, Hill A, Norman MG et al. () Selective brainstem injury in an asphyxiated newborn. Ann Neurol, 1988;23:89–92.

Rose SE, Hatzigeorgiou X, Strudwick MW, Durbridge G, Davies PS, Colditz PB. Altered white matter diffusion anisotropy in normal and preterm infants at term-equivalent age. Magn Reson Med 2008;60:761–767.

Rosenbaum P, Walter S, Hanna S, Palisano R, Russell D, Raina P, Wood E, Bartlett D, Galuppi B. Prognosis for gross motor function in cerebral palsy: Creation of motor

development curves. Journal of the American Medical Association, 2002;288 (11), 1357-1363.

Rosenknantz T, Diana D, Munson J. Regulation of cerebral blood flow velocity in non-asphyxiated, very low birth weight infants with hyaline membrane disease. J Perinatol 1988;8:303–308

Roth SC, Edwards AD, Cady EB, et al. Relation between cerebral oxidative metabolism following birth asphyxia, and neurodevelopmental outcome and brain growth at one year. Dev Med Child Neurol 1992;34:285-95.

Roth SC, Baudin J, Cady E, Johal K, Townsend JP, Wyatt JS. Relation of decreed cerebral oxidative metabolism with neurodevelopmental outcome and head circumference at 4 years. Dev Med Child Neur. 1997;39(11):718-25.

Rueckert D, Sonoda LI, Hayes C, Hill DL, Leach MO, Hawkes DJ. Nonrigid registration using free-form deformations: Application to breast MR images. IEEE Trans Med Imaging 1999;18:712-721.

Ruest T, Holmes WM, Barrie JA, Griffiths IR, Anderson TJ, Dewar D, Edgar JM. High-resolution diffusion tensor imaging of fixed brain in a mouse model of Pelizaeus Merzbacher disease: comparison with quantitative measures of white matter pathology. NMR Biomed 2011;24(10):1369-79.

Rutherford M, Cowan F, Manzur AY, Dubowitz LM, Pennock JM, Hajnal JV, Young IR, Bydder GM. MR imaging of anisotropically restricted diffusion in the brain of neonates and infants. J Comput Assist Tomogr 1991;15, 188–198.

Rutherford MA, Pennock JM, Dubowitz LM. Cranial ultrasound and magnetic resonance imaging in hypoxic-ischaemic encephalopathy: A comparison with outcome. Dev Med Child Neurol 1994;36:813-825.

Rutherford MA, Pennock JM, Schwieso JE, Cowan FM, Dubowitz LM. Hypoxic ischaemic encephalopathy: early magnetic resonance imaging findings and their evolution. Neuropediatrics. 1995;26(4):183-91.

Rutherford M. MRI of the neonatal brain. 2002.W.B. Saunders. London

Rutherford M. The asphyxiated term infant in M. Rutherford, Editor, MRI of the neonatal brain. 2002. W.B. Saunders, London

Rutherford M, Counsell S, Allsop J, Boardman J, Kapellou O, Larkman D, Hajnal J, Edwards D, Cowan F. Diffusion-weighted magnetic resonance imaging in term perinatal brain injury: a comparison with site of lesion and time from birth. Pediatrics. 2004;114(4):1004-14.

Rutherford MA, Azzopardi D, Whitelaw A, Cowan F, Renowden S, Edwards AD, Thoresen M. Mild hypothermia and the distribution of cerebral lesions in neonates with hypoxic-ischemic encephalopathy. Pediatrics. 2005;116(4):1001-6

Rutherford M, Ramenghi LA, Edwards AD, Brocklehurst P, Halliday H, Levene M, Strohm B, Thoresen M, Whitelaw A, Azzopardi D. Assessment of brain tissue injury after moderate hypothermia in neonates with hypoxic-ischaemic encephalopathy: a nested substudy of a randomised controlled trial. Lancet Neurol. 2010;9(1):39-45.

Rybakowski C, Mohar B, Wohlers S, Leichtweiss H, Schroder H. The transport of vitamin C in the isolated human near-term placenta. Eur J Obstet Gynecol Reprod Biol 1995;62:107-14.

Sadowsky D, Yellon S, Mitchell M, Nathanielsz P. Lack of effect of melatonin on myometrial electromyographic activity in the pregnant sheep at 138-142 days gestation (term = 147 days gestation). Endocronology 1991;128:1812-8.

Samuelsen GB, Larsen KB, Bogdanovic N, Laursen H, Graem N, Larsen JF, Pakkenberg B. The changing number of cells in the human fetal forebrain and its subdivisions: a stereological analysis. Cereb Cortex. 2003;13(2):115-22.

Sankaran K, Peters K, Finer N. Estimated cerebral blood flow in term infants with hypoxic-ischemic encephalopathy. Pediatr Res. 1981;15(11):1415-8.

Sankaran K. Hypoxic-ischemic encephalopathy: cerebrovascular carbon dioxide reactivity in neonates. Am J Perinatol. 1984;1(2):114-7.

Sarnat HB, Sarnat MS. Neonatal encephalopathy following fetal distress: A clinical and electroencephalographic study. Arch Neurol 1976;33:696–705

Sarnat HB. CNS malformations: gene locations of known human mutations. Eur J Paediatr Neurol. 2005;9(6):427-31.

Saunders DE, Thompson C, Gunny R, Jones R, Cox T, Chong WK. Magnetic resonance imaging protocols for paediatric neuroradiology. Pediatr Radiol 2007;37:789–797.

Savman K, Blennow M, Gustafson K, Tarkowski E, Hagberg H. Cytokine response in cerebrospinal fluid after birth asphyxia. Pediatr Res 1998 43(6):746–751.

Schaper M, Gergely S, Lykkesfeldt J, Zbaren J, Leib S, Tauber M, Christen S. Cerebral vasculature is the major target of oxidative protein alterations in bacterial meningitis. J Neuropathol Exp Neurol 2002;61:605-13.

Schapiro MB, Holland SK, Schmithorst VJ, Wilke M, Weber Byars A, Strawsburg R. Functional magnetic resonance imaging (fMRI) brain activation increases with age in children performing a finger tapping task. Ann Neurol. 2002;52:S135

Scheiman MM. Optometric findings in children with cerebral palsy. Am J Optom Physiol Opt. 1984;61(5):321-3.

Schmithorst VJ, Wilke M, Dardzinski BJ, Holland SK. Correlation of white matter diffusivity and anisotropy with age during childhood and adolescence: a cross-sectional diffusion-tensor MR imaging study. Radiology. 2002;222(1):212-8.

Schnabel J.A., Rueckert D., Quist M., Blackall J. M., Castellano Smith A. D., Hartkens T., Penney G. P., Hall W. A., Liu H., Truwit C. L., Gerritsen F. A., Hill D. L. G., Hawkes D. J. A generic framework for non-rigid registration based on non-uniform multi-level free-form deformations. In Fourth Int. Conf. on Medical Image Computing and Computer-Assisted Intervention (MICCAI '01) 2001 pages 573-581, Utrecht, NL

Schulzke SM, Rao S, Patole SK. A systematic review of cooling for neuroprotection in neonates with hypoxic ischemic encephalopathy - are we there yet? BMC Pediatr. 2007;5;7:30.

Scott RJ, Hegyi L. Cell death in perinatal hypoxic-ischaemic brain injury. Neuropathol Appl Neurobiol. 1997;23(4):307-14.

Seeley WW, Crawford RK, Zhou J, Miller BL, Greicius MD. Neurodegenerative diseases target large-scale human brain networks. Neuron 2009;62:42–52

Seghier ML, Hüppi PS. The role of functional magnetic resonance imaging in the study of brain development, injury, and recovery in the newborn. Semin Perinatol. 2010;34(1):79-86. Review.

Seller MJ. Sex, neural tube defects, and multisite closure of the human neural tube. Am J Med Genet. 1995;25;58(4):332-6.

Seo Y, Shinar H, Morita Y, Navon G. Anisotropic and restricted diffusion of water in the sciatic nerve: A (2)H double-quantum-filtered NMR study. MagnReson Med. 1999;42(3):461-6.

Seo Y, Wang ZJ, Ball G, Rollins NK. Diffusion tensor imaging metrics in neonates-a comparison of manual region-of-interest analysis vs. tract-based spatial statistics.

Pediatr Radiol. 2013;43(1):69-79.

Serag A, Aljabar P, Ball G, Counsell SJ, Boardman JP, Rutherford MA, Edwards AD, Hajnal JV, Rueckert D. Construction of a consistent high-definition spatio-temporal atlas of the developing brain using adaptive kernel regression. Neuroimage 2012;59:2255–2265

Shalak LF, Laptook AR, Velaphi SC, Perlman JM. Amplitude-integrated electroencephalography coupled with an early neurologic examination enhances prediction of term infants at risk for persistent encephalopathy. Pediatrics 2003;111:351-7.

Shankaran S, Woldt E, Koepke T, Bedard MP, Nandyal R. Acute neonatal morbidity and long-term central nervous system sequelae of perinatal asphyxia in term infants. Early Hum Dev 1991;25:135–148.

Shankaran S, Laptook AR, Ehrenkranz RA, Tyson JE, McDonald SA, Donovan EF, Fanaroff AA, Poole WK, Wright LL, Higgins RD, Finer NN, Carlo WA, Duara S, Oh W, Cotten CM, Stevenson DK, Stoll BJ, Lemons JA, Guillet R, Jobe AH; National Institute of Child Health and Human Development Neonatal Research Network. Whole-body hypothermia for neonates with hypoxic-ischemic encephalopathy. N Engl J Med. 2005;13;353(15):1574-84.

Shanmugalingam S, Thornton JS, Iwata O, Bainbridge A, O'Brien FE, Priest AN, Ordidge RJ, Cady EB, Wyatt JS, Robertson NJ. Comparative prognostic utilities of early quantitative magnetic resonance imaging spi-spin realxometry and proton magnetic resonance spectroscopy in neonatal encephalopathy. Pediatrics 2006;118(4)1467-77.

Sharp DJ, Beckmann CF, Greenwood R, Kinnunen KM, Bonnelle V, De Boissezon X, Powell JH, Counsell SJ, Patel MC, Leech R. Default mode network functional and structural connectivity after traumatic brain injury. Brain. 2011;134(Pt 8):2233-47.

Shehzad Z, Kelly AM, Reiss PT, Gee DG, Gotimer K, Uddin LQ, Lee SH, Margulies DS, Roy AK, Biswal BB, Petkova E, Castellanos FX, Milham MP. The Resting Brain: Unconstrained yet Reliable. Cereb Cortex. 2009;19(10):2209-29.

Sheline YI, Raichle ME. Resting State Functional Connectivity in Preclinical Alzheimer's Disease. Biol Psychiatry. 2013;1;74(5):340-7.

Shimony JS, McKinstry RC, Akbudak E, Aronovitz JA, Snyder AZ, Lori NF, Cull TS, Conturo TE. Quantitative diffusion-tensor anisotropy brain MR imaging: normative human data and anatomic analysis. Radiology. 1999;212(3):770-84.

Shimony JS, Zhang D, Johnston JM, Fox MD, Roy A, Leuthardt EC. Resting-state spontaneous fluctuations in brain activity: a new paradigm for presurgical planning using fMRI. Acad. Radiol. 2009;16, 578–583.

Shu SK, Ashwal S, Holshouser BA, Nystrom G, Hinshaw DB Jr. Prognostic value of 1HMRS in perinatal CNS insults. Pediatr Neurol. 1997;17(4):309 –318

Sicard KM, Duong TQ. Effects of hypoxia, hyperoxia, and hypercapnia on baseline and stimulus-evoked BOLD, CBF, and CMRO2 in spontaneously breathing animals. Neuroimage 2005;25(3):850–8.

Sie LTL, Rombouts SA, Valk IJ, Hart AA, Scheltens P, van der Knaap MS. Functional MRI of visual cortex in sedated 18 month-old infants with or without periventricular leukomalacia. Dev Med Child Neurol, 2001;43:486–490.

Sierra A, Laitinen T, Lehtimäki K, Rieppo L, Pitkänen A, Gröhn O. Diffusion tensor MRI with tract-based spatial statistics and histology reveals undiscovered lesioned areas in kainate model of epilepsy in rat. Brain Struct Funct. 2011;216(2):123-35.

Silverstein F, Barks J. Combining hypothermia with other therapies for neonatal neuroprotection. In: Edwards D, Azzopardi D, Gunn A. Neonatal neural rescue. Cambridge University Press. 2013

Sirimanne ES, Blumberg RM, Bossano D, Gunning M, Edwards AD, Gluckman PD, Williams CE. The effect of prolonged modification of cerebral temperature on outcome after hypoxic-ischemic brain injury in the infant rat. Pediatr Res. 1996;39(4 Pt 1):591-7.

Sisson DF, Siegel J. Chloral hydrate anesthesia: EEG power spectrum analysis and effects on VEPs in the rat. Neurotoxicol. Teratol. 1989;11(1):51–56.

Skudlarski P, Jagannathan K, Calhoun VD, Hampson M, Skudlarska BA, Pearlson G. Measuring brain connectivity: diffusion tensor imaging validates resting state temporal correlations. Neuroimage. 2008;15;43(3):554-61

Smith SL, Hall ED. Mild pre- and posttraumatic hypothermia attenuates blood-brain barrier damage following controlled cortical impact injury in the rat. J Neurotrauma. 1996;13(1):1-9.

Smith SM. Fast robust automated brain extraction. Human Brain Mapping. 2002;17(3):143-155.

Smith SM. Overview of fMRI analysis. British J of Rad. 2004;77,S167-1755.a

Smith SM, Jenkinson M, Woolrich MW, Beckmann CF, Behrens TE, Johansen-Berg H, Bannister PR, De Luca M, Drobnjak I, Flitney DE, Niazy RK, Saunders J, Vickers J, Zhang Y, De Stefano N, Brady JM, Matthews PM. Advances in functional and structural MR image analysis and implementation as FSL. Neuroimage. 2004;23 Suppl 1:S208-19. Review.b

Smith SM, Jenkinson M, Johansenberg H, Rueckert D, Nichols TE, Mackay CE. Tract-Based Spatial Statistics: voxelwise analysis of multi-subject diffusion data; Neuroimage 2006;31:1487-505.

Smith SM, Fox PT, Miller KL, Glahn DC, Fox PM, Mackay PE, Filippini N, Watkins KE, Toro R, Laird AR, Beckmann CF. Correspondence of the brain's

functional architecture during activation and rest. Proc Natl Acad Sci USA 2009;106:13040-13045.

Smits M, Visch-Brink EG, van de Sandt-Koenderman ME, van der Lugt A. Advanced magnetic resonance neuroimaging of language function recovery after aphasic stroke: a technical review. Arch Phys Med Rehabil. 2012;93(1 Suppl):S4-14. Review.

Smyser CD, Inder TE, Shimony JS, Hill JE, Degnan AJ, Snyder AZ, Neil JJ. Longitudinal analysis of neural network development in preterm infants. Cereb Cortex. 2010;20(12):2852-62.

Smyser CD, Snyder AZ, Shimony JS, Blazey TM, Inder TE, Neil JJ. Effects of white matter injury on resting state fMRI measures in prematurely born infants. PLoS One. 2013;9;8(7):e68098.

Sokoloff L, Mangold R, Wechsler RL, Kenney C, Kety SS. The effect of mental arithmetic on cerebral circulation and metabolism. J Clin Invest 1955;34:1101–1108.

Sokoloff L, Reivich M, Kennedy C, Des Rosiers MH, Patlak CS, Pettigrew KD, Sakurada O, Shinohara M. The [14C]deoxyglucose method for the measurement of local cerebral glucose utilization: theory, procedure, and normal values in the conscious and anesthetized albino rat. J Neurochem. 1977;28(5):897-916.

Sokoloff L. Localization of functional activity in the central nervous system by measurement of glucose utilization with radioactive deoxyglucose. J Cereb Blood Flow Metab. 1981;1(1):7-36. Review.

Sokoloff L. Energetics of functional activation in neural tissues. Neurochem Res. 1999;24(2):321-9. Review.

Sokoloff L. The physiological and biochemical bases of functional brain imaging. Cogn Neurodyn. 2008;2(1):1-5.

Song M, Zhou Y, Li J, Liu Y, Tian L, Yu C, Jiang T. Brain spontaneous functional connectivity and intelligence. Neuroimage. 2008;1;41(3):1168-76.

Song SK, Sun SW, Ramsbottom MJ, Chang C, Russell J, Cross AH. Dysmyelination revealed through MRI as increased radial (but unchanged axial) diffusion of water. Neuroimage. 2002;17(3):1429-36.

Sotak CH. The role of diffusion tensor imaging in the evaluation of ischemic brain injury: a review. NMR Biomed. 2002;15:561–569.

Spandou E, Papadopoulou Z, Soubasi V, Karkavelas G, Simeonidou C, Pazaiti A, Guiba-Tziampiri O. Erythropoietin prevents long-term sensorimotor deficits and brain injury following neonatal hypoxia-ischemia in rats. Brain Res 2005;1045:22-30.

Speck O, Hennig J, Zaitsev M. Prospective real-time sliceby- slice motion correction for fMRI in freely moving subjects. MAGMA 2006;19:55–61.

Stamatakis EA, Adapa RM, Absalom AR, Menon DK. Changes in resting neural connectivity during propofol sedation. PLoS One. 2010;2;5(12):e14224

Stanisz GJ, Szafer A, Wright GA, Henkelman RM. An analytical model of restricted diffusion in bovine optic nerve. Magn Reson Med. 1997;37(1):103-11.

Strohm B, Hobson A, Brocklehurst P, Edwards AD, Azzopardi D; UK TOBY Cooling Register. Subcutaneous fat necrosis after moderate therapeutic hypothermia in neonates. Pediatrics. 2011;128(2):e450-2.

Studholme C, Hill DLG, Hawkes DJ. An Overlap Invariant Entropy Measure of 3D Medical Image Alignment. Pattern Recognition 1999;32(1):71-86.

Subsol G, Roberts N, Doran M, Thirion JP, Whitehouse GH. Automatic analysis of cerebral atrophy. Magn Reson Imaging 1997;15:917-927.

Sun FT, Miller LM, Rao AA, D'Esposito M. Functional connectivity of cortical networks involved in bimanual motor sequence learning. Cereb Cortex 2007;17:1227–1234.

Symon L, Held K, Dorsch NWC. A study of regional autoregulation in the cerebral circulation to increase perfusion pressure in normocapnia and hypercapnia. Stroke 1973;4:139–147

Symon L, Crockard HA, Dorsch NW, Branston NM, Juhasz J. Local cerebral blood flow in vascular reactivity in chronic stable stroke in baboons. Stroke 1975;6:482–492

Szymonowicz W, Walker AM, Yu VY, Stewart ML, Cannata J, Cussen L. Regional cerebral blood flow after hemorrhagic hypotension in the preterm, near-term, and newborn lamb. Pediatr Res. 1990;28(4):361-6.

Tagin MA, Woolcott CG, Vincer MJ, Whyte RK, Stinson DA Hypothermia for Neonatal Hypoxic Ischemic Encephalopathy: An Updated Systematic Review and Meta-analysis. Arch Pediatr Adolesc Med. 2012;1;166(6):558-66.

Takahashi M, Hackney DB, Zhang G, Wehrli SL, Wright AC, O'Brien WT, Uematsu H, Wehrli FW, Selzer ME. Magnetic resonance microimaging of intraaxonal water diffusion in live excised lamprey spinal cord.ProcNatlAcadSci U S A. 2002;10;99(25):16192-6.

Takashima S, Mito T, Becker LE. Dendritic development of motor neurons in the cervical anterior horn and hypoglossal nucleus of normal infants and victims of sudden infant death syndrome. Neuropediatrics. 1990;21(1):24-6.

Takeda K, Nomura Y, Sakuma H, Takami T, Okuda Y, Nakagawa T. MR assessment of normal brain development in neonates and infants: comparative study of T1- and diffusion-weighted images. J Comput Assist Tomogr 1997;21, 1–7.

Takeichi M. Cadherins: key molecules for selective cell-cell adhesion. IARC Sci Publ. 1988;(92):76-9.

Tanner SF, Ramenghi LA, Ridgway Berry JP, Saysell E, Martinez MA, Arthur RJ, Smith MA, Levene MI. Quantitative comparison of intrabrain diffusion in adults and preterm and term neonates and infants. Am. J. Roentgenol. 2000;174**,** 1643–1649.

Tau GZ, Peterson BS. Normal development of brain circuits. Neuropsychopharmacology. 2010;35(1):147-68.

Tedeschi G, Trojsi F, Tessitore A, Corbo D, Sagnelli A, Paccone A, D'Ambrosio A, Piccirillo G, Cirillo M, Cirillo S, Monsurro` MR, Esposito F. Interaction between aging and neurodegeneration in amyotropic lateral sclerosis. Neurobiol Aging. 2012;33(5):886-98.

Tekgul H, Bourgeois BFD, Gauvreau K, Bergin AM. Electroencephalography in neonatal seizures: comparison of a reduced montage and full 10/20 montage. Pediatr Neurol. 2005;32:155–161.

Thakur NH, Spencer AJ, Kilbride HW, Lowe LH. Findings and patterns on MRI and MR spectroscopy in neonates after therapeutic hypothermia for hypoxic ischemic encephalopathy treatment. South Med J. 2013;106(6):350-5.

Thayyil S, Chandrasekaran M, Taylor A, et al. Cerebral magnetic resonance biomarkers in neonatal encephalopathy: a meta-analysis. Pediatrics 2010;125:382-95.

Thesen S, Heid O, Mueller E, Schad LR. Prospective acquisition correction for head motion with image-based tracking for real-time fMRI. Magn Reson Med. 2000;44(3):457-65.

Thompson CM, Puterman AS, Linley LL, Hann FM, van der Elst CW, Molteno CD, Malan AF. The value of a scoring system for hypoxic ischaemic encephalopathy in predicting neurodevelopmental outcome. Acta Paediatr 1997; 86: 757-61

Thompson DK, Inder TE, Faggian N, Johnston L, Warfield SK, Anderson PJ, Doyle LW, Egan GF. Characterization of the corpus callosum in very preterm and full-term infants utilizing MRI. Neuroimage 2011;55:479–490

Thompson PM, Toga AW. A surface-based technique for warping three-dimensional images of the brain. IEEE Trans Med Imaging 1996;15:402-417.

Thoresen M, Penrice J, Lorek A, Cady EB, Wylezinska M, Kirkbride V, Cooper CE, Brown GC, Edwards AD, Wyatt JS, et al. Mild hypothermia after severe transient hypoxia-ischemia ameliorates delayed cerebral energy failure in the newborn piglet. Pediatr Res. 1995;37(5):667-70.

Thoresen M, Bågenholm R, Løberg EM, Apricena F, Kjellmer I. Posthypoxic cooling of neonatal rats provides protection against brain injury. Arch Dis Child Fetal Neonatal Ed. 1996;74(1):F3-9

Thoresen M, Wyatt J. Keeping a cool head, post-hypoxic hypothermia--an old idea revisited. Acta Paediatr. 1997;86(10):1029-33. Review.

Thoresen M, Hellström-Westas L, Liu X, de Vries LS. Effect of hypothermia on amplitude-integrated electroencephalogram in infants with asphyxia. Pediatrics. 2010;126(1):e131-9

Thornberg E, Thiringer K. Normal patterns of cerebral function monitor traces in term and preterm neonates. Acta Paediatr Scand. 1990;79:20 –25.

Thornton JS, Ordidge RJ, Penrice J, Cady EB, Amess PN, Punwani S, Clemence M, Wyatt JS. Anisotropic water diffusion in white and gray matter of the neonatal piglet brain before and after transient hypoxia-ischaemia. Magn Reson Imaging. 1997;15(4):433-40.

Tichauer KM, Elliott JT, Hadway JA, Lee TY, St Lawrence K. Cerebral metabolic rate of oxygen and amplitude-integrated electroencephalography during early reperfusion after hypoxia-ischemia in piglets. J Appl Physiol 2009;106:1506-12.

Toet M, Lemmers PMA, van Schelven LJ, Van Bel F. Cerebral oxygenation and electrical activity after birth asphyxia: their relation to outcome. Pediatrics 2006;117:333–9.

Toft PB, Leth H, Lou HC, Pryds O, Peitersen B, Henriksen O. Local vascular CO_2 reactivity in the infant brain assessed by functional MRI. Pediatr Radiol. 1995;25(6):420-4.

Toft PB, Leth H, Peitersen B, Lou HC, Thomsen C. The apparent diffusion coefficient of water in gray and white matter of the infant brain.J Comput Assist Tomogr. 1996;20(6):1006-11.

Torrance HL, Benders MJ, Derks JB, Rademaker CM, Bos AF, Van Den Berg P, Longini M, Buonocore G, Venegas M, Baquero H, Visser GH, Van Bel F. Maternal allopurinol during fetal hypoxia lowers cord blood levels of the brain injury marker S-100B. Pediatrics 2009;124:350-7.

Tournier JD, Calamante F, Connelly A. Robust determination of the fibre orientation distribution in diffusion MRI: non-negativity constrained super-resolved spherical deconvolution. Neuroimage. 2007;1;35(4):1459-72.

Tournier JD, Mori S, Leemans A. Diffusion tensor imaging and beyond. Magn Reson Med. 2011;65(6):1532-56

Traill Z, Squier M, Anslow P. Brain imaging in neonatal hypoglycaemia. Arch Dis Child Fetal Neonatal Ed 1998;79, F145–147.

Tremblay M, Tam F, Graham SJ. Retrospective coregistration of functional magnetic resonance imaging data using external monitoring. Magn Reson Med 2005;53:141–149.

Tsirka V, Simos PG, Vakis A, Kanatsouli K, Vourkas M, Erimaki S, Pachou E, Micheloyannis S. Mild traumatic brain injury: Graph-model characterization of brain

networks for episodic memory. International Journal of Psychophysiology 2011;79: 89–96.

Tuch DS, Reese TG, Wiegell MR, Makris N, Belliveau JW, Wedeen VJ. High angular resolution diffusion imaging reveals intravoxel white matter fiber heterogeneity. Magn Reson Med. 2002;48(4):577-82.

Tuor UI, Kozlowski P, Del Bigio MR, Ramjiawan B, Su S, Malisza K, Saunders JK. Diffusion- and T2-weighted increases in magnetic resonance images of immature brain during hypoxia-ischemia: transient reversal posthypoxia. Exp Neurol. 1998;150(2):321-8

Twomey E, Twomey A, Ryan S, Murphy J, Donoghue VB MR imaging of term infants with hypoxic-ischaemic encephalopathy as a predictor of neurodevelopmental outcome and late MRI appearances. Pediatr Radiol 2010;40(9):1526-35

Tyszka JM, Readhead C, Bearer EL, Pautler RG, Jacobs RE. Statistical diffusion tensor histology reveals regional dysmyelination effects in the shiverer mouse mutant.Neuroimage. 2006;15;29(4):1058-65.

Uddin, L. Q., Supekar, K., and Menon, V. Typical and atypical development of functional human brain networks: insights from resting-state FMRI. Front. Syst. Neurosci. 2010;4:21.

Ueki M, Linn F, Hossmann KA. Functional activation of cerebral blood flow and metabolism before and after global ischemia of rat brain. J Cereb Blood Flow Metab. 1988;8(4):486-94.

Uludag, K., Dubowitz, D.J., Yoder, E.J., Restom, K., Liu, T.T., and Buxton, R.B. Coupling of cerebral blood flow and oxygen consumption during physiological activation and deactivation measured with fMRI. NeuroImage 2004;23, 148-155.

Van Bel F, van de Bor M, Stijnen T, Baan J, Ruys JH. Cerebral blood flow velocity pattern in healthy and asphyxiated newborns: a controlled study. Eur J Pediatr.

1987;146(5):461-7

Van Bel F, Lemmers P, Naulaers G. Monitoring neonatal regional cerebral oxygen saturation in clinical practice: value and pitfalls. Neonatology 2008;94:237-44.

Van Bogaert P., David, P., Gillain, C. A., Wikler, D., Damhaut, P., Scalais, E., Nuttin, C., Wetzburger, C., Szliwowski, H. B., Metens, T., Goldman, S. Perisylvian dysgenesis. Clinical, EEG, MRI and glucose metabolism features in 10 patients. Brain 1998;121:2229–2238.

Van den Heuvel MP, Mandl RC, Kahn RS, Hulshoff Pol HE. Functionally linked resting-state networks reflect the underlying structural connectivity architecture of the human brain. Hum Brain Mapp. 2009;30(10):3127-41.

Van Den Heuvel MP, Hulshoff Pol HE. Exploring the brain network: a review on resting state functional magnetic resonance imaging functional connectivity. Eur Neuropshychopharmacol 2010;20(8):519-34.

Van der Knaap MS and Valk J. Myelination as an expression of the functional maturity of the brain. Dev Med Child Neurol 1991;33, 849–857.

Van Handel, Swaab H, de Vries L, Jongmans M. Long-term cognitive and behavioral consequences of neonatal encephalopathy following perinatal asphyxia: a review. Eur J Pediatr 2007;166:645–654.

Van Handel M, Swaab H, de Vries LS, Jongmans MJ. Behavioral outcome in children with a history of neonatal encephalopathy following perinatal asphyxia. J Pediatr Psychol. 2010;35(3):286-95.

Van Handel M, de Sonneville L, de Vries LS, Jongmans MJ, Swaab H. Specific memory impairment following neonatal encephalopathy in term-born children. Dev Neuropsychol. 2012;37(1):30-50.

Van Kooij BJ, van Handel M, Nievelstein RA, Groenendaal F, Jongmans MJ, de

Vries LS. Serial MRI and neurodevelopmental outcome in 9- to 10-year-old children with neonatal encephalopathy. J Pediatr. 2010;157(2):221-227.e2

Van Kooij BJ, de Vries LS, Ball G, van Haastert IC, Benders MJ, Groenendaal F, Counsell SJ. Neonatal tract-based spatial statistics findings and outcome in preterm infants. AJNR Am J Neuroradiol. 2012;33(1):188-94.

van Leemput K, Maes F, Vandermeulen D, Colchester ACF, Suetens P. Automated segmentation of multiple sclerosis lesions by model outlier detection. IEEE Transactions on Medical Imaging 2001;20(8):677–688

Van Rooij LGM, Toet MC, Osredkar D, van Huffelen AC, Groenendaal F, de Vries LS. Recovery of amplitude integrated electroencephalographic background patterns within 24 hours of perinatal asphyxia.Arch. Dis. Child. Fetal Neonatal Ed. 2005;90:F245-F251.

Van Schie PE, Becher JG, Dallmeijer AJ, Barkhof F, Van Weissenbruch MM, Vermeulen RJ. Motor testing at 1 year improves the prediction of motor and mental outcome at 2 years after perinatal hypoxic-ischaemic encephalopathy. Dev Med Child Neurol. 2010;52(1):54-9.

Vannucci RC, Perlman JM. Interventions for perinatal hypoxic-ischemic encephalopathy. Pediatrics. 1997;100(6):1004-14. Review.

Varela M, Groves AM, Arichi T, Hajnal JV. Mean cerebral blood flow measurements using phase contrast MRI in the first year of life. NMR Biomed. 2012;25(9):1063-72.

Vasquez-Vivar J, Whitsett J, Derrick M, Ji X, Yu L, Tan S. Tetrahydrobiopterin in the prevention of hypertonia in hypoxic fetal brain. Ann Neurol 2009;66:323-31.

Vemuri P, Jones DT, Jack CR Jr. Resting state functional MRI in Alzheimer's Disease. Alzheimers Res Ther. 2012;10;4(1):2.

Verma UL, Archbald F, Tejani N, Handwerker SM. Cerebral function monitor in the neonate. I. Normal patterns. Dev Med Child Neurol. 1984;26:154 –161.

Vermeulen RJ, van Schie PE, Hendrikx L, Barkhof F, van Weissenbruch M, Knol DL, Pouwels PJ. Diffusion-weighted and conventional MR imaging in neonatal hypoxic ischemia: two-year follow-up study. Radiology 2008;249(2):631-9

Vexler ZS, Ferriero DM. Molecular and biochemical mechanisms of perinatal brain injury. Semin Neonatol 2001;6:99-108.

Vincent JL, Snyder AZ, Fox MD, Shannon BJ, Andrews JR, Raichle ME, Buckner RL. Coherent spontaneous activity identifies a hippocampal-parietal memory network. J Neurophysiol. 2006;96(6):3517-31

Vincent JL, Patel GH, Fox MD, Snyder AZ, Baker JT, Van Essen DC, Zempel JM, Snyder LH, Corbetta M, Raichle ME. Intrinsic functional architecture in the anaesthetized monkey brain. Nature 2007;447:83–86.

Viniker DA, Maynard DE, Scott DF. Cerebral function monitor studies in neonates. Clin Electroenceph. 1984;15:185–192.

Vitte P, Harthe C, Lestage P, Claustrat B, Bobillier P. Plasma, cerebrospinal fluid, and brain distribution of 14C-melatonin in rat: a biochemical and autoradiographic study. J Pineal Res 1988;5:437-53.

Viviani B, Bartesaghi S, Corsini E, Villa P, Ghezzi P, Garau A, Galli CL, Marinovich M. Erythropoietin protects primary hippocampal neurons increasing the expression of brain-derived neurotrophic factor. J Neurochem 2005;93:412-21.

Volpe JJ. Subplate neurons--missing link in brain injury of the premature infant? Pediatrics. 1996;97(1):112-3.

Volpe JJ. Neurology of the newborn. 5th edition. Philadelphia: Saunders/Elsevier; 2008.

Walsh CA. Genetics of neuronal migration in the cerebral coretx. Ment Retard Dev Disabil Res Rev. 2000;6(1):34-40. Review.

Wang L, Chopp M, Gregg S, Zhang R, Teng H, Jiang A, Feng Y, Zhang ZG. Neural progenitor cells treated with EPO induce angiogenesis through the production of VEGF. J Cereb Blood Flow Metab 2008;28:1361-8.

Wang L, Yu C, Chen H, Qin W, He Y, Fan F, Zhang Y, Wang M, Li K, Zang Y, Woodward TS, Zhu C. Dynamic functional reorganization of the motor execution network after stroke. Brain. 2010;133(Pt 4):1224-38.

Wang X, Svedin P, Nie C, Lapatto R, Zhu C, Gustavsson M, Sandberg M, Karlsson JO, Romero R, Hagberg H, Mallard C. N-acetylcysteine reduces lipopolysaccharide-sensitized hypoxic-ischemic brain injury. Ann Neurol 2007;61:263-71.

Ward P, Counsell S, Allsop J, Cowan F, Shen Y, Edwards AD, Rutherford M. Reduced fractional anisotropy on diffusion tensor magnetic resonance imaging after hypoxic-ischemic encephalopathy. Pediatrics 2006;117(4):e619-630.

Weissenbacher A, Kasess C, Gerstl F, Lanzenberger R, Moser E, Windischberger C. Correlations and anticorrelations in resting-state functional connectivity MRI: a quantitative comparison of preprocessing strategies. Neuroimage 2009;47:1408–1416.

Welch EB, Manduca A, Grimm RC, Ward HA, Jack CR Jr. Spherical navigator echoes for full 3D rigid body motion measurement in MRI. Magn Reson Med 2002;47:32–41.

Welin AK, Svedin P, Lapatto R, Sultan B, Hagberg H, Gressens P, Kjellmer I, Mallard C. Melatonin reduces inflammation and cell death in white matter in the mid-gestation fetal sheep following umbilical cord occlusion. Pediatr Res 2007;61:153-8.

Wechsler D. Wechsler Pre-school and Primary Scale of Intelligence–Revised. Kent: The Psychological Corporation, 1990.

Westbrook C, Roth CK, Talbot J. MRI in practice. 3rd edition. 2008 Blackwell Publishing Inc.

Wezel-Meijler G, Leijser LM, de Bruïne Francisca T, Steggerda SJ, van der Grond J, Walther SJ. Magnetic resonance imaging of the brain in newborn infants: practical aspects. Early Human Development 2009; 85(2): 93-99

Wilke M, Holland SK, Myseros JS, Schmithorst VJ, Ball WS Jr. Functional magnetic resonance imaging in pediatrics. Neuropediatrics. 2003;34(5):225-33. Review.

Williams GD, Palmer C, Heitjan DF, Smith MB. Allopurinol preserves cerebral energy metabolism during perinatal hypoxia-ischemia: a 31P NMR study in unanesthetized immature rats. Neurosci Lett 1992;144:103-6.

Wimberger DM, Roberts TP, Barkovich AJ, Prayer LM, Moseley ME, Kucharczyk J. Identification of "premyelination" by diffusion-weighted MRI. J Comput Assist Tomogr. 1995;19(1):28-33.

Winter JD, Lee DS, Hung RM, Levin SD, Rogers JM, Thompson RT, Gelman N. Apparent diffusion coefficient pseudonormalisation time in neonatal hypoxic-ischemic encephalopathy. Pediatr Neurol 2007;37(4):255-62.

Winter JD, Tichauer KM, Gelman N, et al. Changes in cerebral oxygen consumption and high-energy phosphates during early recovery in hypoxiceischemic piglets: a combined near-infrared and magnetic resonance spectroscopy study. Pediatr Res 2009;65:181-7.

Wolf RL, Zimmerman RA, Clancy R, Haselgrove JH. Quantitative apparent diffusion coefficient measurements in term neonates for early detection of hypoxic-ischemic brain injury: initial experience. Radiology 2001;218(3):825-33.

Woods RP, Cherry SR, Mazziotta JC. Rapid automated algorithm for aligning and reslicing PET images. J Comput Assist Tomogr 1992;16:620–633.

Woods RP, Grafton ST, Watson JDG, Sicotte NL, Mazziotta JC. Automated image registration: II. Intersubject validation of linear and nonlinear models. J Comput Assist Tomogr 1998;22:153–65.

Woolrich MW, Ripley BD, Brady JM, Smith SM. Temporal autocorrelation in univariate modelling of fMRI data. NeuroImage. 2001;14(6):1370–1386.

Wu Q, Butzkueven H, Gresle M, Kirchhoff F, Friedhuber A, Yang Q, Wang H, Fang K, Lei H, Egan GF, Kilpatrick TJ. MR diffusion changes correlate with ultra-structurally defined axonal degeneration in murine optic nerve. Neuroimage. 2007;1;37(4):1138-47.

Wu YW, Bauer LA, Ballard RA, Ferriero DM, Glidden DV, Mayock DE, Chang T, Durand DJ, Song D, Bonifacio SL, Gonzalez FF, Glass HC, Juul SE. Erythropoietin for neuroprotection in neonatal encephalopathy: safety and pharmacokinetics. Pediatrics. 2012;130(4):683-91.

Wyatt JS, Cope M, Delpy DT, Richardson CE, Edwards AD, Wray S, Reynolds EO. Quantitation of cerebral blood volume in human infants by near-infrared spectroscopy. J Appl Physiol. 1990;68(3):1086-91.

Wylie GR, Genova H, DeLuca J, Chiaravalloti N, Sumowski JF. Functional Magnetic Resonance Imaging Movers and Shakers: Does Subject-Movement Cause Sampling Bias? Human Brain Mapping. 2014;35(1):1-13

Wyss M, Smeitink J, Wevers RA, Wallimann T. Mitochondrial kreatine kinase: a key enzyme of aerobic metabolism. Biochimica et Biophysica Acta 1992;1102:119-66.

Xu L, Yenari MA, Steinberg GK, Giffard RG. Mild hypothermia reduces apoptosis of mouse neurons in vitro early in the cascade. J Cereb Blood Flow Metab. 2002;22(1):21-8.

Xue H, Srinivasan L, Jiang S, Rutherford M, Edwards AD, Rueckert D, Hajnal JV. Automatic segmentation and reconstruction of the cortex from neonatal MRI. Neuroimage. 2007;15;38(3):461-77

Yakovlev PI. Pathoarchitectonic studies of cerebral malformations. III. Arrhinencephalies (holotelencephalies). J Neuropathol Exp Neurol. 1959;18(1):22-55.

Yakovlev PI, Lecours AR. The myelogenetic cycles of regional maturation of the brain. In: Minkowski, A (Ed.), Regional Developmentof the Brain Early in Life. 1967 Blackwell Scientific Publications Inc., Boston pp. 3–70. Massachusetts.

Yamada H, Sadato N, Konishi Y, Kimura K, Tanaka M, Yonekura Y, Ishii Y. A rapid brain metabolic change in infants detected by fMRI. NeuroReport 1997;8: 3775–3778.

Yamada H., Sadato N., Konishi Y., Muramoto S., Kimura K., Tanaka M. Yonekura Y, Ishii Y, Itoh H. A milestone for normal development of the infantile brain detected by functional MRI. Neurology 2000; 55:218–223.

Yang G, Iadecola C. Glutamate microinjections in cerebellar cortex reproduce cerebrovascular effects of parallel fiber stimulation. Am J Physiol. 1996;271(6 Pt 2):R1568-75.

Yang G, Iadecola C. Obligatory role of NO in glutamate-dependent hyperemia evoked from cerebellar parallel fibers. Am J Physiol. 1997;272(4 Pt 2):R1155-61.

Yang G, Zhang Y, Ross ME, Iadecola C. Attenuation of activity-induced increases in cerebellar blood flow in mice lacking neuronal nitric oxide synthase. Am J Physiol Heart Circ Physiol. 2003;285(1):H298-304.

Yarowsky P, Kadekaro M, Sokoloff L. Frequency-dependent activation of glucose utilization in the superior cervical ganglion by electrical stimulation of cervical sympathetic trunk. Proc Natl Acad Sci U S A. 1983;80(13):4179-83.

Yeo BT, Sabuncu MR, Vercauteren T, Ayache N, Fischl B, Golland P. Spherical demons: Fast diffeomorphic landmark-free surface registration. IEEE Trans Med Imaging 2010;29:650-668.

Yokochi K. Clinical profiles of subjects with subcortical leukomalacia and border-zone infarction revealed by MR. Acta Pediatr 1998;87, 879–883.

Yu Q, Allen EA, Sui J, Arbabshirani MR, Pearlson G, Calhoun VD. Brain connectivity network in schizophrenia underlying rsting state functional magnetic resonance imaging. Curr Top Med Chem. 2012;12(2):2415-25

Yue T, Xian K, Hurlock E, Xin M, Kernie SG, Parada LF, Lu QR. A critical role for dorsal progenitors in cortical myelination. J Neurosci. 2006 25;26(4):1275-80.

Zacharopoulos NG, Narayana PA. Selective measurement of white matter and gray matter diffusion trace values in normal human brain. Med Phys. 1998;25(11):2237-41.

Zappe AC, Uludag K, Oeltermann A, Ugurbil K, Logothetis NK. The Influence of Moderate Hypercapnia on Neural Activity in the Anesthetized Nonhuman Primate. Cereb Cortex. 2008;18(11):2666-73

Zhang D, Snyder AZ, Fox MD, Sansbury MW, Shimony JS, Raichle ME. Intrinsic functional relations between human cerebral cortex and thalamus. J Neurophysiol 2008;100:1740–1748.

Zhang, D, Johnston JM, Fox MD, Leuthardt EC, Grubb RL, Chicoine MR, Smyth M D, Snyder AZ, Raichle ME, Shimony JS. Preoperative sensorimotor mapping in brain tumor patients using spontaneous fluctuations in neuronal activity imaged with functional magnetic resonance imaging: initial experience. Neurosurgery 2009;65, 226–236.

Zhang D, Raichle ME. Disease and the brain's dark energy. Nat Rev Neurol 2010;6:15–28.

Zhang H, Schneider T, Wheeler-Kingshott CA, Alexander DC. NODDI: practical in vivo neurite orientation dispersion and density imaging of the human brain. Neuroimage. 2012;16;61(4):1000-16.

Zhang J, Wang Q, Xiang H, Xin Y, Chang M, Lu H. Neuroprotection with erythropoietin in preterm and/or low birth weight infants. J Clin Neurosci. 2014; S0967-5868(14)00046-0.

Zhang Y, Brady M, Smith S. Segmentation of brain MR images through a hidden Markov random field model and the expectation-maximization algorithm. IEEE Trans Med Imag, 2001;20(1):45-57.

Zhou Y, Milham MP, Lui YW, Miles L, Reaume J, Sodickson DK, Grossman RI, Ge Y. Default-mode network disruption in mild traumatic brain injury. Radiology. 2012;265(3):882-92.

Zhu C, Wang X, Cheng X, Qiu L, Xu F, Simbruner G, Blomgren K. Post-ischemic hypothermia-induced tissue protection and diminished apoptosis after neonatal cerebral hypoxia-ischemia. Brain Res. 2004;16;996(1):67-75.

Zhu C, Kang W, Xu F, Cheng X, Zhang Z, Jia L, Ji L, Guo X, Xiong H, Simbruner G, Blomgren K, Wang X. Erythropoietin improved neurologic outcomes in newborns with hypoxic-ischemic encephalopathy. Pediatrics 2009;124(2):e218-26.

Zifman E, Mouler M, Eliakim A, Nemet D, Pomeranz A. Subcutaneous fat necrosis and hypercalcemia following therapeutic hypothermia--a patient report and review of the literature. J Pediatr Endocrinol Metab. 2010;23(11):1185-8. Review.

Zonta M, Angulo MC, Gobbo S, Rosengarten B, Hossmann KA, Pozzan T, Carmignoto G. Neuron-to-astrocyte signaling is central to the dynamic control of brain microcirculation. Nat Neurosci. 2003;6(1):43-50.

Zuo XN, Kelly C, Adelstein JS, Klein DF, Castellanos FX, Milham MP. Reliable intrinsic connectivity networks: test-retest evaluation using ICA and dual regression approach. Neuroimage 2010;1;49(3):2163-217.